Design, Technology and Evaluation of a Microfluidic Chip for Point-of-Care Diagnosis of Bone Turnover Biomarkers

Ontwerp, technologie en evaluatie van een microfluïdische chip voor 'point of care'-diagnose van biomarkers voor het botmetabolisme

Patricia Khashayar

Promotors: Prof. J. Vanfleteren, PhD, Prof. G. Amoabediny, PhD, Prof. B. Larijani, MD, R. Verplancke, PhD
Doctoral thesis submitted in order to obtain the academic degrees of Doctor of Biomedical Engineering (Ghent University) and Doctor in Nanobiotechnology (University of Tehran)

Department of Electronics and Information Systems
Head of Department: Prof. R. Van de Walle, PhD
Faculty of Engineering and Architecture

UNIVERSITEIT GENT

Department of Life Science Engineering
Head of Department: Prof. A. H. Rezayan, PhD
Faculty of New Sciences and Technologies

Academic year 2015 - 2016

ISBN 978-90-8578-919-2
NUR 954, 870
Wettelijk depot: D/2016/10.500/51

Universiteit Gent
Faculteit Ingenieurswetenschappen en Architectuur, Centrum voor Microsysteemtechnologie (CMST)

Universiteit van Teheran
Faculteit Nieuwe Wetenschappen en Technologie, Departement Biologische Wetenschappen

Promotoren: Prof. J. Vanfleteren, PhD
Prof. G. Amoabediny, PhD
Prof. B. Larijani, MD
R. Verplancke, PhD

Universiteit Gent
Faculteit Ingenieurswetenschappen en Architectuur
Centrum voor Microsysteemtechnologie (CMST)
914 Technologiepark, B-9052 Zwijnaarde, België

Tel.: +32-9-264.53.60
Fax.: +32-9-264.53.74

Dit werk kwam tot stand in het kader van een specialisatiebeurs van de Universiteit Gent als een gezamenlijk doctoraat met de Universiteit Teheran.

Proefschrift ingediend tot het behalen van de graad van
Doctor in de ingenieurswetenschappen: biomedische ingenieurstechnieken (Universiteit Gent) & Doctor in Nanobiotechnology (Universiteit van Teheran)
Academiejaar: 2015-2016

Acknowledgment

"To be a doctor is to be an intermediary between man and God," Felix Marti-Ibanez said famously in his "To Be a Doctor" book. This realization struck a chord with me and made me study medicine. Thanks to my family, I had learned that "One of the essential qualities of the clinician is interest in humanity, for the secret of the care of the patient is in caring for the patient," so I dedicated my life to help patients.

As time passed, I struggled with the idea that I could not help all my patients no matter how hard I tried. I imagined that in months and years to come, I would stand by their bedside as patients experienced complications due to late diagnosis or deferred treatment. I couldn't help but strive to seek a solution that would come to their aid.

Adopting the motto "Science is knowing and Technology is doing. Science focuses on understanding the natural phenomena, while Technology focuses on understanding the made environment," I realized that bioengineering would provide the perfect blend and present me with the remedy to my internal struggle. My final goal was to incorporate my medical knowledge into developing new devices that would fill the gaps in modern medicine, and thus help people around the world.

In order to improve my grasp of the engineering world, and develop a better understanding of the options available, I started my PhD and this was a new beginning and a life changer.

I would like to express my sincere gratitude to the Osteoporosis Research Center and Endocrinology and Metabolism Research Institute of Tehran University of Medical Sciences, the Research Center for New Technologies in Life Science Engineering and the Electrochemistry Institute of the University of Tehran for their continued support.

I feel thankful to all present and former colleagues in CMST for making my working days pleasant. My special thanks go to Nuria Teigell Benéitez and Jindrich Windels for always being there for me and making my stay in Ghent pleasing.

It is an honor for me to thank Parviz Norouzi and Annemie Adriaens and their team who provided me an opportunity to join their team, and who gave access to the laboratory and research facilities. And my sincere thanks also goes to Farideh Razi, Tom Fiers and Stefan Goemaere for providing us with the serum samples. Without their precious support it would not be possible to conduct this research.

It is also a pleasure to thank those who made this thesis possible. I am grateful to Steven Van Put, Peter Geerinck, Filip Thielemans and Filip Vermeiren for helping me with my samples, no matter how busy they were and how late I had submitted my run tracker. I would like to thank Dieter Cuypers, Lothar Mader, Kristof Dhaenens, Tom Sterken, An-

dres Desmet, Bart Plovie and Ann Monté.
I owe my deepest gratitude to David Schaubroeck for helping me with scientific consult and contact, whenever everything was just wrong. My special thanks to Nadine Carchon and Katrien Vanneste for taking care of all administrative issues. I would like to express my special appreciation and thanks to Frederik Leys, who has been a tremendous help.
I am heartily thankful to my supervisor, Bagher Larijani, whose encouragement, guidance and support from the initial to the final level enabled me to develop an understanding of the subject. This thesis would have remained a dream had it not been for my Professor, Ghassem Amoabediny. He introduced me to the Ghent University and his guidance and persisted help made this thesis possible. It is with immense gratitude that I acknowledge the support and help of my Professor, Jan Vanfleteren for his insightful comments and encouragement, but also for the ideas which incented me to widen my research from various perspectives. I am indebted to Rik Verplancke who helped me out, especially in the first months when I literally had no idea what to do. His guidance helped me in all the time of research and writing of this thesis. I wish to thank the rest of my committee members who were more than generous with their expertise and precious time.
I would also like to thank my uncle Manoochehr and uncle Khosrow and his family. They have made available their support in a number of ways, especially for their love, their efforts to cheer me up when I was sad and lonely, and offering me a safe haven to escape to when nothing was working out.
And finally, a special thanks to my family. Words cannot express how grateful I am to my mom, my dad, my sister Paria and my brother Pouria, for all of the sacrifices that you've made on my behalf. Your prayer for me was what sustained me thus far. Thank you for always taking care of me, for your love and your patience, for supporting me all through my life and incenting me to strive towards my goals. You always encourage me to be a better person."

Gent, July 8, 2016
Patricia Khashayar

Table of Contents

List of Figures

List of Tables

List of Acronyms

A

Ab	Antibody
ACA	Anisotropic conductive adhesive
ADC	Analog-to-digital converter
AFM	Atomic-force microscopy
Ag	Antigen
AuNP	Gold Nanoparticles
AUX	Counter/Auxiliary electrode

B

BALP	Bone Alkaline Phosphatase
BMD	Bone Mineral Density
BSA	Bovine Serum Albumin
BSP	Bone Sialoprotein
BTM	Bone Turnover Marker

C

CA	Chronoamperometry
CatK	Cathepsin K
CE	Capillary electrophoresis
CFD	Computational Fluid Dynamics
CL	Chemilunescence
CLIA	Chemiluminescent Immunoassay
CNT	Carbon Nanotube
COC	Cyclic olefin copolymer
Cr	Creatinine
CRF	Chronic Renal Failure

CTX	Cross-linked Telopeptides of type I collagen
CV	Cyclic Voltammetry
C.V.	Coefficient of Variation

D

DLS	Dynamic light scattering
Dpd	Deoxypyridinoline
DPV	Differential Pulse Voltammetry
DTT	Dithiothreitol
DXA	Dual-energy X-ray absorptiometry

E

ECA	Enzymatic Colorimetric Assay
ECLIA	Electrochemiluminescence Immunoassay
ECV	Electrodeposition using cyclic voltammetry
EDC	b-1-ethyl-3-(3-dimethylamonipropyl) carbodiimide
EIA	Enzyme Immunoassay
EIS	Electrochemical Impedance Spectroscopy
ELISA	Enzyme-linked Immunosorbent Assay

F

Fab	Fragment antigen-binding region
FET	Field-effect Transistor
FITC	Fluorescein isothiocyanate
FTIR	Fourier transform infrared spectroscopy
FRAX	Fracture Risk Assessment Tool
FRF	Frequency Response Function
Fx	Fracture

G

GnRH	Gonadotropin-releasing hormone
GSH	Glutathione

H

HPLC	High-Performance Liquid Chromatography
HRT	Hormone Replacement Therapy
Hyp	Hydroxyproline

I

ICMA	Immunochemiluminescence Assay
IOF	International Osteoporosis Foundation
IRMA	Immunoradiometric Assay

L

LBL	Layer-by-layer
LLD	Lower Limits of Detection
LoD	Limit of Detection
LoQ	Limit of Quantification
LSC	Least Significant Change

M

MEMS	Microelectromechanical Systems

N

NP	Nanoparticle
NHS	N-Hydroxysuccinimide
NTX	N-Terminal Crosslinking Telopeptide of type I collagen

O

Oc	Osteocalcin
OPG	Osteoprotegerin

P

PBS	Phosphate buffered saline
PCB	Printed Circuit Board
PDDA	Poly(diallyldimethylammonium chloride) solution
PDMS	Polydimethylsiloxane
PEG	Polyethylene glycol
P1NP	Procollagen type 1 Nterminal propeptide
P1CP	Procollagen type 1 C-terminal propeptide
PMMA	Poly(methyl methacrylate)
POC	Point of Care
PPV	Positive Predictive Value
PTH	Parathyroid hormone
PZT	Piezoelectric Transducer

Q

QCM	Quartz Crystal Microbalance

R

RAI	Radioimmunoassay
REF	Reference Electrode
RSD	Relative Standard Deviation

S

S/N	Signal-to-noise ratio
SAM	Self-assembled monolayer
SD	Standard deviation
SEM	Scanning electron microscopy
SPE	Screen-printed Electrode
STEM	Scanning transmission electron microscopy

T

TEM	Transmission electron microscopy
Tg	Glass Transition temperature
Ti	Titanium
TRAP	Tartrate-Resistant Acid Phosphatase

U

ULD	Upper Limits of Detection
UV	Ultraviolet

W

WE	Working Electrode
WHO	World Health Organization

Glossary

Absorbance	When a beam of light passes through the sample, the light absorption occurs because of the atoms or molecules taking away the energy from the light. In general, the absorbance of a sample is directly proportional to the optical path length of the sample holder and the concentration of the sample.
Anabolics	Anabolic osteoporosis agents such as Teriparatide (human parathyroid hormone [1-34]) reduce fracture incidence by improving other bone qualities in addition to increasing bone mass by directly stimulating bone formation.
Antibody	Antibody is a large, Y-shaped protein produced mainly by plasma cells that is used by the immune system to identify and neutralize pathogens such as bacteria and viruses. The antibody recognizes a unique molecule of the harmful agent, called an antigen. Antibody and antigen interact by spatial complementarity (lock and key).
Antigen	An antigen is any substance that causes the immune system to produce antibodies against it. Each antibody is specifically produced by the immune system to match an antigen.
Antiresorptives	Antiresorptive osteoporosis agents limit bone loss by decreasing the rate of absorption by osteoclasts, which are cells that absorb bone. By reducing how quickly osteoclasts work, antiresorptives may prevent further loss of bone mass. There are a number of classes of antiresorptives, including bisphosphonates, calcitonin, estrogen therapy or hormone therapy, and estrogen agonists/antagonists.
Biomarker	A biomarker is any substance, structure or process that can be measured in the body or its products and influence or predict the incidence of outcome or disease.

Bone Turnover Marker	Bone turnover markers are bone tissue proteins or their fragments/enzymes released from bone cells during bone turnover. These markers include collagen breakdown products and other molecules released from osteoclasts and osteoblasts during the process of bone resorption and formation.
Calibration curve	A calibration curve is a general method for determining the concentration of a substance in an unknown sample by comparing the unknown to a set of standard samples of known concentration. It shows how the instrumental response, the so-called analytical signal, changes with the concentration of the analyte (the substance to be measured).
Chemiluminescence	CL is the light produced by a chemical reaction. The CL intensity is directly proportional to the concentration of a limiting reactant involved in the CL reaction. As a principle, in CL, reactants A and B react with an excited intermediate to form a product and emit the light which can be detected and analyzed by an optical detection system.
Conjugated Antibody	A conjugated antibody is a monoclonal or polyclonal antibody linked to a label and used for detection in a diverse range of assay techniques.
FET	FET is a transistor that uses an electric field to control the shape and electrical conductivity of a charge carrier channel in a semiconductor material. FET's conductivity is regulated by the voltage applied to the gate contact. This voltage imposes an electric field into the device, which in turn attracts or repels charge carriers to or from the region between the source and drain contacts.
Fluorescence	Fluorescence is the emission of certain wavelength of visible light from a substance by the absorption of an excitation light of different wavelengths. Fluorescence detection is the most commonly observed form of optical detection, because of its high sensitivity and the ease of integrating a label.
Glutathione	GSH is a thiol-containing aminoacid with high affinity towards gold nanoparticles through the formation of Au-S bond.
Immunoassay	An immunoassay is a biochemical test that measures the presence or concentration of an analyte (usually proteins) in a solution (biological liquids such as

	serum or urine for medical and research purposes) through the use of an antibody or an antigen.
Limit of Detection	LoD is the lowest quantity of a substance that can be distinguished from the blank value within a stated confidence limit (generally 1 %). It is estimated from the mean of the blank, the SD of the blank and some confidence factor. Another consideration that affects the LoD is the accuracy of the model used to predict concentration from the raw analytical signal.
Limit of Quantification	LoQ is the lowest concentration at which the analyte can not only be reliably detected but at which some predefined goals for bias and imprecision are met. The LoQ may be equivalent to the LoD or it could be at a much higher concentration.
Molecular Pathway	A biological/molecular pathway is a series of actions among molecules in a cell that leads to a certain product or a change in a cell. Such a pathway can trigger the assembly of new molecules, such as a fat or protein. Pathways can also turn genes on and off, or spur a cell to move.
Nanoprobe	Nanoprobe refers generically to any chemical or biological technique that deals with nanoquantitles. In other words, that is introducing nanoparticles in aqueous solution to serve in the detection, diagnosis, and treatment of various diseases.
Positive Predictive Value	PPV is the probability that subjects with a positive screening test truly have the disease. In other words, it is the ability of the test to correctly label people who test positive. It is calculated in two ways: ■ PPV = (# true positives) / (# true positives + # false positives) ■ PPV = sensitivity x prevalence / sensitivity x prevalence + (1-sensitivity) x (1-prevalence)
Proteomics	Proteomics is a rapidly growing field of molecular biology that is concerned with the systematic, high-throughput approach to protein expression analysis of a cell or an organism. Typical results of proteomics studies are inventories of the protein content of differentially expressed proteins across multiple conditions.
Relative Standard Deviation	

	RSD is a special form of SD calculated using $\frac{100*SD}{\bar{x}}$, where SD is the sample standard deviation and $\bar{x}$ is the sample mean.
Surrogate Marker	A surrogate marker is an event or a laboratory value that researchers hope can serve as a reliable substitute for an actual disease. A common example of this is blood cholesterol levels. These levels are surrogates, or substitutes, for heart disease.
Surface plasmon resonance	When a polarized light hits a prism covered with a thin film of metal at a specific (resonance) angle, SPR occurs. SPR effect is sensitive to the binding of analyte because the increase in mass causes a proportional increase in the refractive index at the interface between a thin metal film and an ambient medium. For an immunoassay, before an antigen binds to an immobilized antibody, the refractive index of the prism is constant. After the binding event, the refractive index changes. In this way, it is possible to monitor the biomolecular interaction on the metal film. Therefore, SPR provides a non-invasive, label-free approach for detecting the concentration of analytes, kinetics, and affinity in real time.
T-score	T-score is the comparison of a person's bone density with that of a healthy 30-year-old of the same sex. at -1.0 and above.
Theranostics	Theranostics is used to define ongoing efforts in clinics to develop more specific, individualized therapies for various diseases, and to combine diagnostic and therapeutic capabilities into a single agent.
	ULD limit is the largest intrinsic intensity that the source can have and yet have a given probability of remaining undetected.
Voltammetry	Voltammetry is an electroanalytical method used in analytical chemistry. In voltammetry, a time-dependent potential is applied to an electrochemical cell and the resulting current is measured as a function of that potential. The technique provides quantitative and qualitative information about the species involved in the oxidation or reduction reaction.

چکیده

تشخیص پوکی استخوان، که امروزه با استفاده از سنجش تراکم مواد معدنی استخوان (BMD) صورت می گیرد، از محدودیت های متعددی رنج می برد. به همین دلیل به نظر می رسد استفاده از مارکرهای استخوانی (BTMs) می توانند در بهبود تشخیص پوکی استخوان کمک کننده باشند. استفاده از BTMs در مقایسه با BMD و ابزار ارزیابی ریسک بالینی، نه تنها در پایش روند درمان بلکه در شناسایی افراد در معرض خطر شکستگی، از مزایای متعددی برخوردار است. این در حالی است که ارزش تشخیصی BTMs در پیش بینی پوکی استخوان پایین بوده و به این ترتیب اندازه گیری همزمان چند BTMs با دقت بالا برای غلبه بر این محدودیت لازم می باشد.

با وجود پیشرفت های اخیر در پروتئومیکس و پزشکی فردی (personalized medicine)، فن آوری های موجود برای اندازه گیری BTM، مانند سنجش ایمونوسوربنت متصل به آنزیم (ELISA) و الکتروکمی لومینسنس (ECLIA)، نه تنها وقت گیر و پر زحمت بوده بلکه به برچسب های خاص و ابزار گران نیاز دارد. با توجه به این محدودیت های آشکار، تمرکز مطالعات مرتبط با سلامت در سالهای اخیر به سمت توسعه و ساخت حسگرهای زیستی نقطه مراقبت (POC) بدون برچسب، قابل حمل، قابل استفاده مجدد و در عین حال قابل استفاده برای اندازه گیری همزمان چند مارکر به ویژه برای تشخیص و نظارت بیماریهای مختلف می باشد. این دستگاه ها که همچنین به عنوان دستگاه های تشخیصی در محل (on-the-spot) نیز شناخته می شوند، باید ساده، حساس، سریع، اختصاصی، ارزان و با قابلیت تفسیر آسان باشند.

به همین صورت، تقاضا برای ساخت حسگرهای زیستی ارزان قیمت و مینیاتوری جهت ارزیابی روند بازسازی استخوان با دقت بالا رو به رشد می باشد. با توجه به بررسی های انجام شده، تاکنون، هیچ یک از حسگرهای زیستی استخوان موجود در این زمینه موفق نبوده اند.

یک بیوسنسور کارآمد به اتصال انتخابی/اختصاصی ماده شناساگر با آنالیت هدف و همچنین مبدل مناسب برای نشان دادن فرآیند اتصال براساس زمان پاسخ، نسبت سیگنال به نویز (S/N) و حد پایین تشخیص (LOD) نیاز دارد.

در این پروژه، گزارش ساخت یک میز پروتئومیک میکروسیالی که به راحتی قابل تبدیل به یک دستگاه تشخیص برای هر نشانگری (biomarker) می باشد ارائه شده است. این پلت فرم حاصل ادغام تکنولوژی میکروسیالی با سیستم سنجش الکتروشیمیایی بوده و از یک محفظه واکنش/تشخیص برای اندازه گیری سطح سرمی نشانگرهای زیستی متفاوت تشکیل شده است. طراحی منحصر به فرد این پلت فرم امکان اندازه گیری نشانگرها با حساسیت بالا را فراهم می آورد و ساختارهای میکروسیالی و الکتروشیمیایی به طور مستقل قابل بهینه سازی می باشند.

در گام نخست، از طریق تعامل میان نانوذرات طلا (AuNPs) و مولکولهای زیستی آنتی بادی، یک نانوکاوشگر (nanoprobe) طلا برای اندازه گیری الکتروشیمیایی غیرآنزیمی نشانگرها ساخته شد. این روش نه تنها متدی ساده برای بارگذاری حجم بالایی از آنتی بادی بر روی نانوذرات را فراهم آورد بلکه تا حد زیادی تکرارپذیری فرآیند تولید این کاوشگر را نیز بهبود بخشید. این نانوکاوشگر، به همراه یک الکترود یکبار مصرف، می تواند برای اندازه گیری الکتروشیمیایی یک یا چند نشانگر بکار برده شود. به عبارت دیگر، این نانوکاوشگر می تواند ابزاری (تک/ تسهیم شده) دقیق با توان بالا برای اندازه گیری غلظت های مختلف نشانگرهای مختلف ایجاد نماید.

گام بعدی نشاندن این کاوشگر بر روی سطح الکترود با حفظ ساختار و کارکرد آنتی بادی موجود در آن بود. در این راستا، رسوب نانوذرات طلا بر روی سطح الکترود طلا به منظور بهبود ویژگی های الکتروشیمیایی سطح صورت گرفت. به عبارت دیگر، نسبت بالاتر سیگنال به نویز بدنبال نشاندن AuNP فرآیند کوچک سازی سیستم را بهبود بخشیده و از طرف دیگر با افزایش سطح باعث تقویت سیگنال پاسخ می شود. مرور مطالعات نشان داد که نشاندن طلا برروی الکترود طلا به روشهای مختلف امکان پذیر است و به همین دلیل در این پروژه روشهای رسوب لایه به لایه (LBL)، روش خود مونتاژ تک لایه (SAM) و آبکاری مقایسه شدند. نتایج نشان داد که آبکاری AuNPs به روش ولتامتری باعث افزایش قابل مشاهده در پیک جریان شده و بدین ترتیب کینتیک الکترود را بهبود می بخشد. الکترودهای اصلاح شده به این روش همچنین پایداری و تکرارپذیری بیشتری را از خود نشان دادند.

استئوکلسین (Oc) و کلاژن کراس لینک C ـ تلوپپتید نوع ۱ (CTX) بواسطه پیوند کووالانسی و از طریق کراس لینکرها برروی الکترودهای طلای اصلاح شده با AuNP نشانده شدند و غلظتهای مختلف آنتی ژن های مربوطه توسط آنها اندازه گیری شد.

امروزه استفاده از فن آوری میکروسیالی در ساخت دستگاه های تشخیصی نقطه مراقبت و برای مبارزه با مسائل بهداشت جهانی به طور گسترده ای در حال توسعه می باشد. این به دلیل مزایای بالقوه این سیستمها شامل نیاز به حجم کم نمونه و معرف، توان و حساسیت بالا، نسبت بالای سطح به حجم، و همچنین توانایی کوچک سازی می باشد. به همین دلیل در این پروژه تصمیم به ادغام تراشه الکتروشیمیایی با سیستم میکروسیالی شد. ساخت کانالهای میکروسیالی معمولا پرهزینه بوده و نیاز به فرآیندهای پاکسازی متعدد در آزمایشگاه، لیتوگرافی نوری، قلم زنی و یا پخت در محیط های اتاق تمیز داشته و به همین دلیل اصلاح و یا تغییر طرح معمولا دشوار می باشد. علاوه بر این، بستن مناسب محوطه کانال بدون تغییر طرحهای کوچک و یا انسداد کانال در حین فرایند اتصال چالش برانگیز است. بنابراین ما از یک روش ارزان، قابل اعتماد و سریع برای ساخت کانال میکروسیالی با استفاده از نوارچسب دو طرفه بهره جستیم. با کمک این روش نه تنها ساخت کانال با ابعاد مقطعی یکنواخت بلکه امکان ایجاد سیستم های ترکیبی، متشکل از لایه های مختلف، با توجه به چسبندگی مناسب بین لایه ها امکان پذیر بود.

در مرحله آخر تراشه الکتروشیمیایی و ساختار های میکروسیالی برای ساخت سیستم استئوکیت ادغام شدند. در این پلت فرم مبتنی بر واکنش آنتی بادی و آنتی ژن کلیه مراحل معرفی نمونه، انکوباسیون و اندازه گیری الکتروشیمیایی در کانالهای میکروسیالی اتفاق می افتاد. الکترودهای طلای موجود در محفظه میکروسیالی برای نشاندن آنتی بادیهایی که در مراحل بعدی بصورت انتخابی با آنتی ژن مربوطه واکنش می دادند عاملدار شده بودند. روش کرونوآمپرومتری در دمای اتاق برای اندازه گیری غلظت محلول آنتی ژن استفاده شد.

نتایج نهایی نشان داد که استئوکیت دقت، حساسیت و اختصاصی بودن لازم برای سنجش سطح سرمی استئوکلسین و CTX را دارد. حد پایین تشخیص برای استئوکلسین ۱/۹۴ ng/mL و برای CTX معادل ۲/۷۷ pg/mL بود. این دستگاه همچنین برای اندازه گیری سطح سرمی نشانگرهای Oc و CTX مورد استفاده قرار گرفت و نتایج با مقادیر حاصله از ECLIA مقایسه شد. این نتایج حاکی از تطابق قابل قبول میان نتایج داشت.

سنسور ساخته شده برای اندازه گیری غلظت Oc سرمی حساس و اختصاصی بوده و می تواند سطح سرمی نشانگر را در طیف وسیعی از ۲/۵ تا ۷۵ نانوگرم/میلی لیتر تشخیص دهد که با توجه به مرجع نرمال این نشانگر (۹ تا۴۲ نانوگرم/میلی لیتر) قابل قبول است. به طور مشابه، سطح CTX با موفقیت از ۱ تا۲۵۰۰

pg/mL قابل اندازه گیری بود که با توجه به مرجع نرمال نشانگر (۵۰ تا۴۵۰ pg/mL) قابل قبول است. از طرف دیگر، سنسور ساخته شده هیچ واکنش متقاطعی برای سایر نشانگرها (کراس لپ بتا و هورمون پاراتیروئید برای سنسور Oc و استئوکلسین و هورمون پاراتیروئید برای سنسور CTX) نشان ندادند. ارتباط قابل قبول میان نتایج ECLIA و هر دو نشانگر Oc و CTX برروی سرم خون بیماران نشان داد که سنسور ساخته شده قابلیت اندازه گیری سطح سرمی نشانگرها در محدوده بالینی را داشته و سایر مولکولهای موجود در سرم، در نتایج تغییر قابل ملاحظه ای ایجاد نمی کنند. با این حال، این واقعیت که آنتی ژن استئوکلسین مورد استفاده برای رسم منحنی کالیبراسیون در واقع پپتید کامل انسانی بود، در حالی که کیتهای ECLIA برای اندازه گیری زنجیره میانی Oc طراحی شده ممکن است نتایج ما را تحت تاثیر قرار داده باشد.

می توان نتیجه گرفت که در مقایسه با روش های مرسوم، دستگاه الکتروشیمیایی ساخته شده برای اندازه گیری نشانگرهای پیشنهاد شده انتخابی و حساس بوده و از دیگر مزایای این سیستم تشخیصی ساده می توان به کاهش زمان اندازه گیری و نیاز به مقدار کمتر نمونه و ثبات بالا اشاره نمود.

نتایج نشان دهنده دقت، حساسیت، اختصاصی بودن و ثبات تراشه الکتروشیمیایی ساخته شده با این روش و در نتیجه امکان استفاده از آن برای برنامه های کاربردی بالینی در آینده بود. کل مدت اندازه گیری برای این سنسور (شامل بارگذاری آنتی ژن، انکوباسیون، شستشو و اندازه گیری غلظت) حدود ۱۰ دقیقه است، این در حالی است که ECLIA به زمان بیشتری برای این اندازه گیری نیاز دارد.

با توجه به مطالعات ما، این اولین دستگاه میکروسیالی ساخته شده برای اندازه گیری BTM می باشد. همچنین نتایج موجود نشان دهنده حساسیت قابل قبول استئوکیت برای اندازه گیری این نشانگرها در مقایسه با روشهای مرسوم مورد استفاده یعنیELISA و الکتروکمیلومینسانس می باشد. در این کار، تنها دو BTM مورد مطالعه قرار گرفتند اما سیستم ساخته شده قابلیت استفاده برای اندازه گیری سایر نشانگرهای زیستی را نیز دارا می باشد. این نتایج نیاز به اعتبار بخشی داشته اما نشان می دهد که سیستم ساخته شده همراستا با تحقیقات در ساخت دستگاه های تشخیصی برای بیومارکرها می باشد.

Samenvatting

Diagnose van osteoporose wordt hedendaags gedaan op basis van metingen van de mineraaldichtheid van beenderen “bone mineral density“ (BMD), deze methode heeft echter beperkingen. Er wordt aangenomen dat “bone turnover markers“ (BTM) kunnen helpen bij het detecteren van osteoporose. Hoewel het gebruik van BTMs in het diagnosticeren van osteoporose verschillende voordelen heeft over BMD, niet alleen in het monitoren van de behandeling maar ook in het identificeren van risico’s, blijft de diagnostische waarde in het voorspellen van osteoporose laag, en dus worden er verschillende BTMs gebruikt op hetzelfde moment wat leidt tot een hogere nauwkeurigheid en een lagere variantie om deze limitatie te overwinnen.
Ondanks recente vooruitgang in proteomics en gepersonaliseerde geneeskunde blijven beschikbare technologieën voor BTM metingen, namelijk enzyme-linked immunosorbent assays (ELISA) en elektrochemiluminescentie (ECLIA), tijdrovend en arbeidsintensief, ze vereisen ook speciale labels, dure instrumenten. Met deze duidelijke beperkingen, is de focus van gezondheid gerelateerde studies verschoven naar de ontwikkeling van draagbare, herbruikbare en multiplex, vrij van labels, Point-of-Care (PoC) biosensoren vooral voor het diagnosticeren en monitoren van verscheidene ziektes.
Er is dus een groeiende vraag naar het ontwikkelen van verschillende types biosensoren die geminiaturiseerde platformen aanbieden om het remodelleringsproces van beenderen beter weer te geven. Voor zover wij weten, is er geen enkele bestaande biosensor die slaagt op dit vlak.
Een efficiënte biosensor is sterk afhankelijk van selectieve binding van het herkenningselement met de doel analyten en de transducer voor het signaleren van de binding in termen van responsietijd, signaal-ruisverhouding “signal-to-noise ratio“ (S/N) en detectiegrenzen “limits of detection“ (LoD).
In deze studie, melden wij een microfluïdisch proteomics platform dat gemakkelijk gebruikt kan worden voor de diagnose van biomarkers. Dit platform integreert microfluïdische technologie met elektrochemische detectie en belichaamt een reactie/detectie kamer die serumniveaus van verschillende biomarkers kan opmeten. Het unieke ontwerp van dit platform biedt de mogelijkheid voor grotere gevoeligheid omdat zowel de microfluïdische als elektrochemische structuren onafhankelijk van elkaar geoptimaliseerd kunnen worden.
Als eerste stap, door de inherente interactie tussen gouden nanodeeltjes (AuNPs)

en antilichamen, werd een nieuwe gouden nanoprobe ontwikkeld voor gebruik in niet-enzymatische elektrochemische immuno-assays. Deze één-pot methode biedt niet alleen een eenvoudige methode voor het voorzien van een hooge gehalte van antilichaamen aan de nanodeeltjes maar verbeterd ook aanzienlijk de herhaalbaarheid en controleerbaarheid van de nanoprobe voorbereiding. Met andere woorden, door het gebruiken van deze nanoprobe kan een hoge throughput methode (single/multiplex sensors) ontwikkeld worden om verschillende en grote hoeveelheden keuze markers te screenen.
De volgende stap was de immobilisatie van de probe op het elektrodeoppervlak met behoud van zowel de structuur en functionaliteit van de antilichamen. De afzetting van gouden nanodeeltjes (AuNPs) op het oppervlak van de gouden electrode zorgt voor betere elektrochemische eigenschappen van het oppervlak. Met andere woorden, de hoge signaal-ruisverhouding verbeterd de miniaturisatie van de sensor-elementen, terwijl het oppervlak, dat hoge specificiteit vertoont, ideaal is om het signaal antwoord te versterken. Volgens bestaande literatuur kan dit gebeuren op verscheidene manieren. Wij vergeleken de laag per laag "layer-by-layer" depositie, self-assembled monolayer techniek en elektrodepositie methoden. Onze resultaten toonden aan dat cyclische voltammetrie elektrodepositie van AuNPs zorgen voor een observeerbare toename in de piekstroom, waardoor de elektrode-kinetiek verbeterd. Deze gemodificeerde elektroden toonde ook een aantal voordelen met betrekking tot stabiliteit en reproduceerbaarheid.
Osteocalcine (Oc) en collageen type 1 cross-linked C-telopeptide (CTX) werden vervolgens covalent geïmmobiliseerd op de AuNP gemodificeerde gouden elektrodes door crosslinkers en verschillende concentraties van overeenkomstig antigeen werden aangebracht voor directe bepaling.
Tegenwoordig worden microfluïdische technologieën op grote schaal gebruikt in het ontwikkelen van point-of-care diagnostiek om globale gezondheidsaspecten aan te kaarten omwille van hun potentiële voordelen van lage sample en reagens consumptie, hoge throughput en gevoeligheid, groot oppervlak-volume ratio en andere voordelen gerelateerd met miniaturisatie. Om deze redenen besloten wij onze elektrochemische chip te integreren in een microfluidïsch systeem. Het maken van microfluidïsche kanalen is meestal kostelijk en vergt laboratium-intensieve schoonmaking, fotolithographie en etching of baking stappen in cleanroom omgeving, wat het moeilijk maakt om dit proces te modificeren. Ook is het voldoende insluiten van de kanalen zonder het vervormen van de kleinere features of zonder het verstoppen van de kanalen gedurende het bonding proces een hele uitdaging. Daarom hebben wij een goedkope, betrouwbare en snelle methode ontworpen om microfluidïsche kanalen te maken gebruik makend van dubbelzijdige tapes, wat het mogelijk maakt om niet alleen de doorsnede hoog uniform te houden over het gehele kanaal maar ook voldoende hechting geeft voor hybride systemen, bestaande uit verschillende lagen.
Daarna werden de elektrochemische sensor en de microfluidïsche chips geïntegreerd om een osteokit systeem te ontwikkelen. De sensing-interface fabrica-

tie, sample incubatie en elektrochemische detectie in dit antilichaam-antigeen-gebaseerd platform zijn allemaal uitgevoerd d.m.v. het gebruik van microfluidïsche kanalen. Microgefrabiceerde Au electrodes, die in een microfluidïsche kamer waren ingebracht, werden gefunctionaliseerd om antilichamen te immobiliseren, die op hun beurt selectief de overeenkomstige antigenen vastleggen. Chronoamperometrische technieken op kamertemperatuur werden gebruikt om de concentratie van antigeen-oplossingen op te meten. De omvang van de respons stroom varieerde lineair met de logaritmische concentratie van de relatieve biomarker, en werd dus gebruikt om de concentratie van de relatieve biomarker in de serum samples te kwantificeren.
We hebben de implementatie, haalbaarheid en specificiteit van dit platform (Osteokit) aangetoond door het meten van serum niveaus van Oc en CTX. De detectie limiet van Oc was 1.94 ng/mL, waar die van CTX 2.77 pg/mL was. Het toestel werd ook gebruikt om de serum niveaus van Oc en CTX op te meten en de resultaten werden vergeleken met dat van ECLIA, waarvan het resultaat aanvaardbare gelijkenis toonde.
De ontwikkelde sensor was gevoelig en specifiek voor serum Oc en kan serumniveaus van de marker detectereen in een bereik van 2.5 tot 100 ng/mL. De normale referentie van de marker is 9 tot 42 ng/mL, wat suggereert dat de sensor OC kan detecteren. Op een gelijkaardige manier als hierboven beschreven werden CTX niveaus succesvol gemeten in een bereik van 1 tot 2500 pg/mL. Dit is terwijl de normale referentie van de marker 50 tot 450 pg/mL is, wat aantoont dat de sensor CTX op een acceptabele manier kan detecteren.
Onze sensor vertoonde geen kruisreactiviteit voor andere biomarkers (voor b-CrossLaps en parathyroïd hormoon (PTH) in Oc sensor en voor Oc en PTH in CTX sensor). De goede correlatie tussen ECLIA en Osteokit toont aan dat onze sensor gebruikt kan worden in een klinisch relevant bereik en dat andere macromolecules in het serum onze resultaten niet verstoren. Het feit dat Oc antigeen, dat gebruikt werd om onze calibratie curve op te stellen, een volle lengte proteïne is, terwijl ECLIA ontwikkeld werd om N-mid Oc op te meten, kan onze resultaten beïnvloed hebben.
De ontwikkelde elektrochemische chips toonden hoge gevoeligheid, specificiteit, stabiliteit en betrouwbaarheid, wat veelbelovend is voor klinische toepassingen. De totale responsietijd van de sensor is ongeveer 10 minuten (belading van antigeen, incubatietijd, spoelen met PBS en testen), terwijl ECLIA enkele uren duurt. Er werd geconcludeerd dat in vergelijking met conventionele methodes de elektrochemische sensor de voorgestelde marker kan detecteren met hoge selectiviteit, gevoeligheid, gereduceerde interferentie, korte meet-tijd, nood aan minder samples en een beter stabiliteit in een eenvoudig detectie systeem.
Voor zover wij weten, is dit het eerste toestel dat gefabriceerd werd om BTMs te meten. Onze resultaten toonden aan dat de gevoeligheid van Osteokit vergelijkbaar zijn met de “state-of-art“-methodes van dit moment, ELISA en elektrochemiluminescentie. Slechts twee belangrijke BTMs zijn onderzocht in deze studie,

maar het detectie systeem kan gemakkelijk aangepast worden voor andere biomarkers in de toekomst. Deze resultaten hebben verdere validatie nodig maar kunnen wijzen op de richting waarin het veld van de diagnostische biomarkers evolueert.

Summary

Osteoporosis diagnosis, which is nowadays generally made based on bone mineral density (BMD) measurements, suffers from certain limitations. Thus it is believed that bone turnover markers (BTMs) can help improve osteoporosis detection. While the use of BTMs in osteoporosis diagnosis has certain advantages over BMD and clinical risk assessment tools, not only in monitoring treatment but also in identifying those at-risk, the diagnostic value of BTMs in predicting osteoporosis is low, and thus several BTMs are used at the same time with higher accuracy and lower variability to overcome this limitation.

Despite recent advancements in proteomics and personalized medicine, available technologies for BTM measurement, enzyme-linked immunosorbent assays (ELISA) and electrochemiluminescence (ECLIA), are time consuming, laborious, require special labels and expensive instruments. With these apparent limitations, the focus of health-related studies has shifted towards the development of portable, reusable and at the same time multiplex, label-free Point-of-Care (PoC) biosensors particularly for diagnosis and monitoring of different diseases. Also known as on-the-spot diagnostic devices, these PoC biosensors should be simple, sensitive, rapid, specific, cheap, and easy to interpret.

Thus, there is a growing demand to fabricate different types of biosensors to provide low cost miniaturized platforms to assess bone remodeling process more accurately. To our knowledge, none of the existing bone biosensors have succeeded in this regard.

An efficient biosensor relies heavily on selective/specific binding of the recognition element with the target analytes as well as the transducer for signaling the binding event in terms of response time, signal-to-noise (S/N) ratio, and limits of detection (LoD).

In this work, we report a microfluidic proteomic platform that can easily be translated into a biomarker diagnostic. This platform integrates microfluidic technology with electrochemical sensing and embodies a reaction/detection chamber to measure serum levels of different biomarkers. The unique design of the platform offers the potential for greater sensitivity as the microfluidic and electrochemical structures can be independently optimized.

As the first step, through the inherent interaction between gold nanoparticles (AuNPs) and antibody biomolecules, a novel gold nanoprobe was developed to be used in the non-enzymatic electrochemical immunoassay. This one-pot

method not only provides a simple method for loading high-content antibody on nanoparticles but also greatly improves the repeatability and controllability of the nanoprobe preparation. Combined with a disposable electrode, it could be used for a single/multiplexed electrochemical immunosensing method. In other words, using this nanoprobe, high throughput instrumentation applying (single/multiplexed sensors) could be developed to screen a variety and vast quantities of samples for choice markers.
The next step was the immobilization of this probe on the electrode surface while saving the structure and functionalization of the antibodies. The deposition of gold nanoparticles (AuNPs) on the surface of gold electrode is believed to enhance the electrochemical characteristics of the surface. In other words, their high signal to noise ratio improves miniaturization of the sensor elements, whereas their high surface area makes them ideal for amplifying the signal response. According to the existing literature, this could be performed in various ways. We thus compared the layer-by-layer deposition, self-assembled monolayer technique and electrodeposition methods. Our results showed that cyclic voltammetry electrodeposition of AuNPs causes an observable increase in the peak current, causing improved electrode kinetics. These modified electrodes also showed several advantages with respect to stability and reproducibility.
Osteocalcin (Oc) and collagen type 1 cross-linked C-telopeptide (CTX) were then covalently immobilized on the AuNP-modified gold electrodes by cross linkers and different concentrations of corresponding antigens were applied for direct determination.
As nowadays, microfluidic technologies are widely employed in developing point-of-care diagnostics to address global health issues because of their potential advantages of low sample and reagent consumption, high throughput and sensitivity, large surface-to-volume ratio, and other benefits related to miniaturization, we decided to integrate our electrochemical chip into a microfluidic system. The fabrication of microfluidic channels is commonly costly and requires laboratory-intensive cleaning, photolithography, and etching or baking steps in cleanroom environments, making it difficult to modify. Besides, proper channel enclosure without deforming small features or without clogging of the channel during the bonding process is challenging. We therefore developed a cheap, reliable and rapid method for the fabrication of microfluidic channels using double-sided tapes, enabling not only highly uniform cross-sectional dimensions along the channels but also proper adhesion in hybrid systems, composed of different layers.
As the last step, the electrochemical ssystem and the microfluidic chips were integrated to develop the Osteokit system. The sensing interface fabrication, sample incubation, and electrochemical detection in this antibody-antigen-based platform were all performed using microfluidic channels. Microfabricated Au electrodes encased in a microfluidic chamber were functionalized to immobilize the antibodies, which can selectively capture the corresponding antigen. Chronoam-

perometry technique at room temperature was used to measure the concentration of the antigen solutions. The magnitude of the response current varied linearly with the logarithmic concentration of the relative biomarker, and thus was used to quantify the concentration of the relative biomarker in serum samples.
We demonstrated the implementation, feasibility and specificity of this platform (Osteokit) in assaying serum levels of Oc and CTX. The detection limit of Oc was 1.94 ng/mL, whereas that of CTX was 2.77 pg/mL. The device was also used to measure serum levels of the both Oc and CTX and the results were compared to that of ECLIA. The results of which showed acceptable concordance.
The developed system was sensitive and specific for serum Oc and could detect serum levels of the marker within the range of 2.5 - 100 ng/mL. This is while the normal reference of the marker is 9 - 42 ng/mL, suggesting that the system can acceptably detect Oc. Similarly, CTX levels were successfully measured from 1 - 2500 pg/mL. This is while the normal reference of the marker is 50-450 pg/mL, suggesting that the system can acceptably detect CTX.
Our system showed no cross-reactivity for other biomarkers (b-CrossLaps and parathyroid hormone (PTH) for Oc system and Oc and PTH for CTX system). The good correlation between the ECLIA and Osteokit showed that they can be used in the clinically relevant range and other macromolecules available in serum do not affect our results. However, the fact that the Oc antigen used to develop our calibration curve was a full-length protein, while ECLIA was designed to measure N-mid Oc may have affected our results.
The developed electrochemical chips showed ultrahigh sensitivity, specificity, stability and reliability, thus providing a highly promising potential for clinical applications. The total assay time for this system is about 10 min (loading of antigen, incubation time, flushing with PBS and testing), while ECLIA needs several hours to be performed.
It was concluded that compared to conventional methods, the proposed electrochemical device resulted in selective and sensitive measurement of the proposed BTM levels with reduced interference reactions, reduced measurement time, need for less amount of sample and better stability in a simplified detection system.
To our knowledge, this is the first such device fabricated to measure BTMs. Our results also showed the sensitivity of Osteokit to be comparable with the current state of art, ELISA and electrochemiluminescence. In this work, only two major BTMs were studied, but the assay system could easily be adapted to other biomarkers in future experiments. These results require further validation but may suggest a direction towards which the field of diagnostic biomarkers is moving.

1 Introduction

1.1 Importance of Point-of-Care Testing in Osteoporosis Management

1.1.1 The Concept of Bone Remodeling

Bone is a dynamically and metabolically active organ that is continuously subjected to resorption and formation by the coordinated action of the two different categories of bone cells, namely osteoclasts (cells responsible for resorbing bone), and osteoblasts (cells responsible for building bone) and their descendants osteocytes. These two processes are collectively called bone turnover or bone remodeling and they are coupled in time and space [1]. (Figure 1.1) After middle age, bone loss occurs as resorption exceeds formation. This process is also known as osteoporosis [2].

1.1.2 What is Osteoporosis?

Osteoporosis, literally meaning 'porous bone', is the most frequently found metabolic bone disease. (Figure 1.2) The systemic skeletal disease is characterized by

- Low bone mass
- Micro-architectural deterioration of the bone

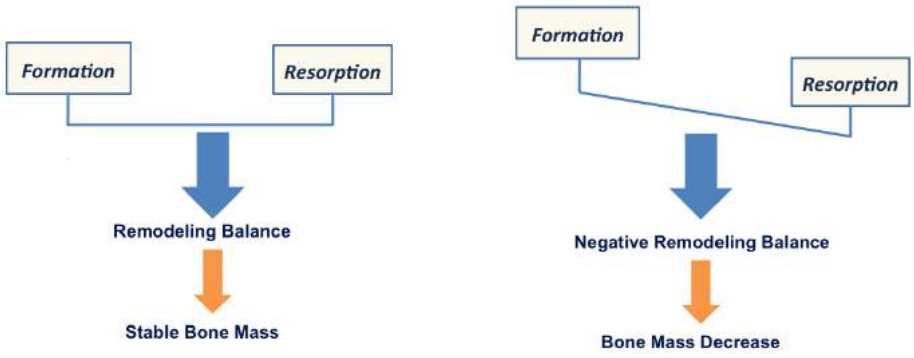

(a) (b)

Figure 1.1: a) Formation and resorption status leading to stable bone mass. b) Formation and resorption status leading to bone loss.

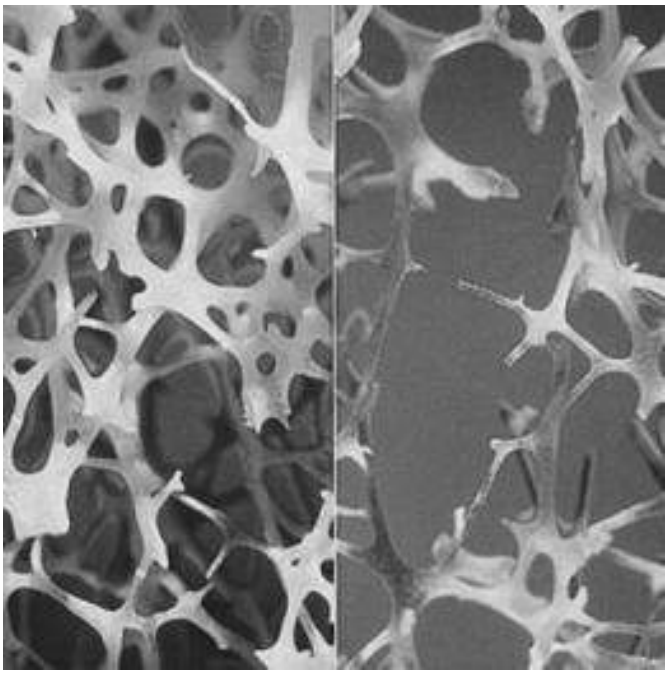

Figure 1.2: Healthy (L) and osteoporotic (R) bone (Same scale).

- Increased bone fragility and fracture risk

Osteoporosis has been operationally defined on the basis of bone mineral density (BMD) assessment. Using the operational definition of the World Health Organization (WHO) based on BMD measurement at the spine, hip or forearm by Dual X-ray absorptiometry (DXA) devices [3]:

- Normal: BMD lies within 1 standard deviation (SD) of the average value for young healthy adult (T-score at -1.0 and above).
- Low bone mass ("osteopenia"): BMD lies between 1.0 and 2.5 SD below that of the average value for young healthy adult (T-score between -1.0 and -2.5).
- Osteoporosis: BMD lies 2.5 SD or more below that of the average value for young healthy adult (T-score at or below -2.5).

Epidemiology of Osteoporosis

Osteoporosis is a multifactorial systemic disease that affects a large number of people in different parts of the world. (Figure 1.3) It is more prevalent than breast and prostate cancer, which are considered as the most common tumors in each gender.
Osteoporosis is currently considered as a serious global public health concern, with over 200 million people suffering from the disease worldwide. According to the WHO criteria, osteoporosis affects 30% of postmenopausal white women in the US (9.4 million women) [4].
The prevalence of osteoporosis in the EU is estimated at 27.6 million in 2010 [5]. In Belgium, 120,695 men aged over 50 (6.5%) and 476,875 women of the same age group (22.4%) were reported to suffer from osteoporosis in 2010.
Latest figures show that 25,969,046 and 3,024,798 Iranians suffer from osteopenia and osteoporosis, adding that the rate would experience a rapid surge and reach 40,303,730 and 3,592,708 by 2020 [6]. (Figure 1.4)

Osteoporosis Risk Factors

Despite the common misperception that osteoporosis is always the result of bone loss due to aging, reports have shown that failing to reach optimal (i.e., peak) bone mass during childhood and adolescence may result in osteoporosis in the absence of accelerated bone loss [7]. Hence sub-optimal bone growth in childhood and adolescence is as important as bone loss due to the development of osteoporosis.
A number of factors can increase the likelihood of developing osteoporosis; these factors are divided into two main groups: (Table 1.1)

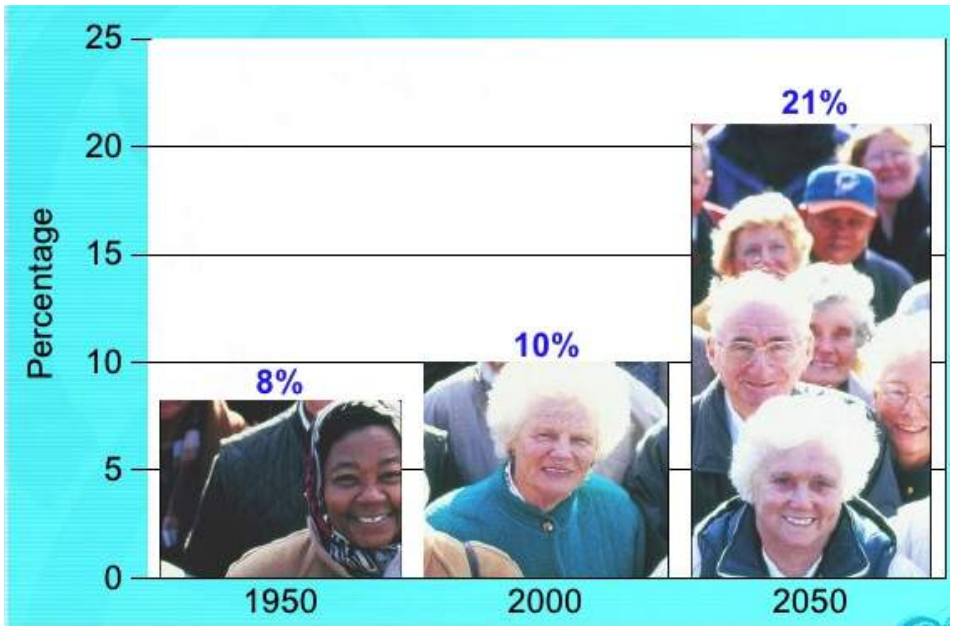

Figure 1.3: Worldwide risk of developing osteoporosis in different decades.

Table 1.1: Risk factors attributed to osteoporosis

Major Risk Factors	Minor Risk Factors
Age ≥ 65 years	Rheumatoid arthritis
Family history of osteoporotic fracture	Past history of clinical hyperthyroidism
Fragility fracture after age 40	Chronic anticonvulsant therapy
Vertebral compression fracture	Low dietary calcium intake
Apparent osteopenia on X-ray film	Smoking
Malabsorption syndrome	Excessive alcohol intake
Primary hyperparathyroidism	Excessive caffeine intake
Propensity to fall	Weight < 57 kg
Systemic glucocorticoid therapy for > 3 months	Weight loss > 10% of weight at age 25
Hypogonadism	Chronic heparin therapy
Early menopause (before age 45)	

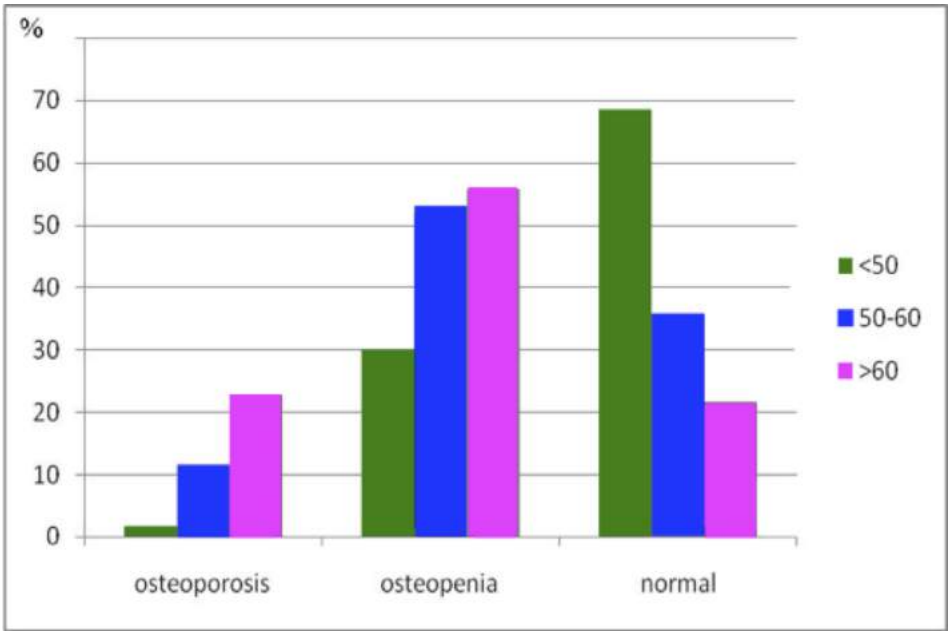

Figure 1.4: Number of Iranians suffering from different degrees of bone loss.

Complications of Osteoporosis

Osteoporosis is often called a 'silent disease' as bone loss occurs without any symptoms. The affected individual, therefore, would not become aware of having the condition until his/her bones become so weak that a sudden strain or fall causes fracture or vertebral collapse.The end-stage of osteoporosis and its major complication, fracture, is associated with diminished life-quality, shortened life-span and heavy health care costs [8]. In addition to morbidity, osteoporotic fractures also increase mortality risk in affected patients [9].
After the age of 50, nearly 40% of women and 13% of men in western countries will sustain a fragility fracture [4]. (Figure 1.5)This is while fractures, particularly hip fractures, impose a heavy burden on a country's healthcare system. Healthcare expenditure attributed to osteoporotic fractures in the US in 1995 was estimated to be USD 13.8 billion [10].
A study conducted by Hernlund et al showed that hip fractures only account for 17% of all osteoporotic fractures in Europe in 2013 but comprise 54% of the direct cost of fracture [5]. In Belgium, with 10 million inhabitants, 13,150 hospital stays per year for hip fractures have generated an annual cost of 118,047,194 USD [11].
Iran accounts for 0.85% of the global burden of hip fractures and 12.4% of the burden of hip fractures in the Middle East [13]. Based on existing reports, a large

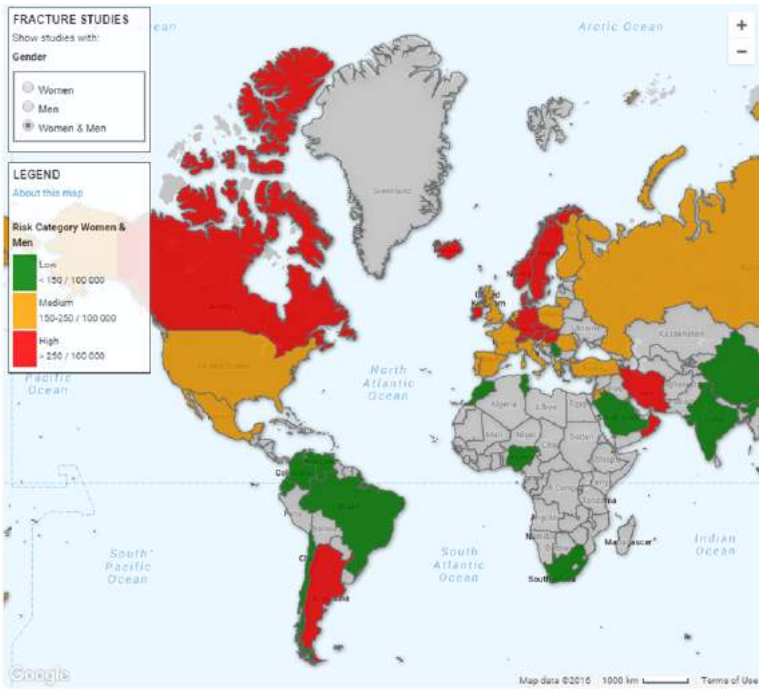

(a)

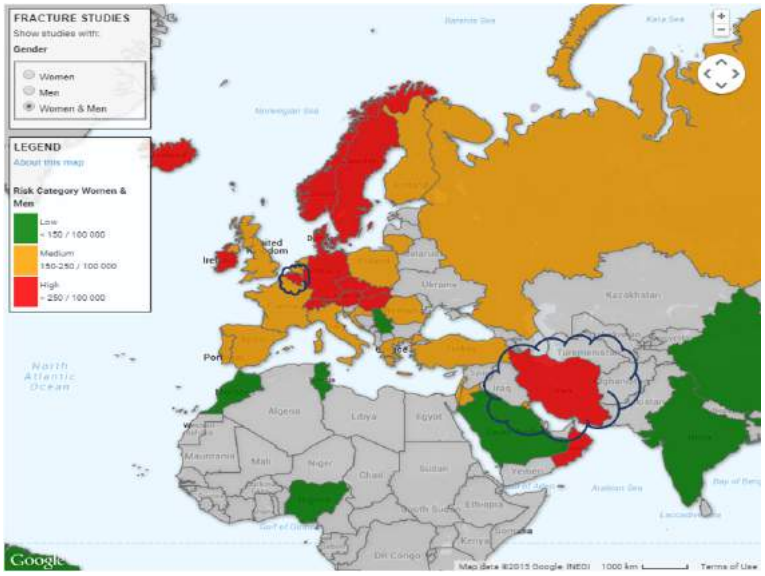

(b)

Figure 1.5: a) Hip fracture world map b) Iran and Belgium have a high risk for hip fracture in both genders.
adopted from International Osteoporosis Foundation (IOF) Map[12]

number of the Iranian population, mainly elderly, experience at least one fracture in their life [14]. About 472.1 fractures per 100,000 (individuals aged more than 50) population occur in the country [15] [16].

1.1.3 Osteoporosis Detection Techniques

Assessment of the bone micro-architecture requires bone biopsy, which is invasive and thus not routinely used in clinical practice. Therefore, BMD assessment remains the gold standard to diagnose osteoporosis.

Dual-energy X-ray absorptiometry (DXA)

Dual energy x-ray absorptiometry (DXA) is the widely available noninvasive method for assessing BMD with the aim of identifying individuals with osteoporosis and, possibly, those at- risk for fracture [17][18]. (Figure 1.6)

DXA Setbacks Although osteoporosis is one of the strongest risk factors for fracture, only about half of the fractures occur in women with BMD values lower than the diagnostic threshold for the disease. This is mainly because previous studies have shown that BMD can only detect osteoporosis when a large amount of bone is lost [19].
In other words, BMD represents one important, but not exclusive, dimension of bone strength and therefore can provide an estimation of the likelihood of a future fracture. Moreover, DXA is incapable of assessing bone quality, which consists of its micro- and macro-architecture and turnover, and its results depend on many factors such as the presence of lumbar osteoarthritis [20].
On the other hand, while BMD changes are considered as a valid end point for verifying the efficacy of osteoporosis treatments, BMD changes and fracture risk reduction rate following medication is not measurable at early stages [21]. It takes more than two years for DXA to be able to detect changes in bone mass and thus possible response to treatment [22].
In addition, there have been major advances in the number and range of agents available for osteoporosis treatment, all with proven anti-fracture efficacy [23]. These agents have differing modes of action in protecting against fracture and these need to be taken into account when developing monitoring strategies. Ideally, only those individuals who are at high risk of sustaining a fracture should receive anabolic or anti-resorptive medication and treatment should be targeted on the basis of risk assessment rather than the BMD measurement alone. Furthermore, BMD alone is incapable of diagnosing patients suffering from secondary osteoporosis, caused by certain underlying medical conditions or the use of medications that may cause bone loss [7]. In other words, bone loss could be secondary to an increase in bone resorption (due to postmenopausal state, secondary hyperparathyroidism, high inflammatory status, ...) or de-

Figure 1.6: Dual-energy X-ray absorptiometry (DXA) device.

crease in bone formation (due to steroid use, adynamic bone disorders due to hypoparathyroidism and/or vit-D deficiency etc.). Osteoporosis management in these patients is therefore based on the treatment of the underlying cause and mostly requires additional measurement of certain markers including bone turnover markers (BTMs).

Other Imaging Modalities

Quantitative computerized tomography (QCT) QCT measures volumetric bone density of the spine and hip and analyzes cortical and trabecular bone separately [24].
It is however not recommended for screening (application of T-scores to predict the risk of fracture has not been validated with QCT). Moreover, it is more costly and results in greater exposure to radiation than DXA.

Peripheral measurements The most commonly used techniques in this category are the following, all of which have their pros and cons [25]:

- Ultrasonography

- Peripheral Dual-energy X-ray Absorptiometry (pDXA)
- Peripheral Quantitative Computed Tomography (pQCT) of the heel, radius, or hand
- High-Resolution Peripheral Quantitative Computed Tomography (HR-pQCT), which provides a virtual biopsy of the bone

Fracture Risk Assessment Tool (FRAX)

In an attempt to better estimate fracture risk even when BMD measurement is not available, WHO developed the FRAX tool, which can calculate the 10-year probability of osteoporotic fracture based on clinical risk factors [26]. The introduction of the multivariate algorithm-based fracture risk assessment tool has evolved the definition of the disease and based the treatment decisions on absolute risk of fracture threshold. The application of the tool in clinical practice has resulted in a higher positive predictive value (PPV), reduced number of individuals needed to be treated to prevent one fracture and more importantly enhanced sensitivity [27].
There are, however, a number of general and methodology-specific limitations for FRAX, as the tool only evaluates nine of the many risk factors related to osteoporosis and more importantly does not consider all the medications which influence fracture risk. Moreover, in this model, risk factors are quantified in a binary approach.
QFracture and Garvan are among other existing fracture risk assessment tools [28]. QFracture includes a larger number and wider variety of clinical risk factors compared with FRAX and GARVAN, and is reported to be more accurate than them. This is while FRAX is considered as the most validated instrument.

1.1.4 Early Diagnosis in Osteoporosis Detection

Osteoporosis, once thought to be a natural part of ageing among women, is no longer considered age or gender-dependent. It is largely preventable due to the remarkable progress in the scientific understanding of its causes, diagnosis, and treatment [29]. Optimization of bone health is a process that must occur throughout the lifespan in both males and females. Factors that influence bone health at all ages are essential to prevent osteoporosis and its consequences [30].
Many osteoporosis guidelines recommend intervention to be considered for men and women who have sustained a fragility fracture, stressing that these individuals are at increased risk of a second fracture [31].
Despite recent advances in diagnosis of osteoporosis, assessment of fracture risk, development of interventions that reduce risk of fractures, and the development of practical guidelines, surveys indicate that only a minority of men and women at high fracture risk actually receive treatment [32]. Recent statistics show that

less than 20% of patients who sustain a fragility fracture receive therapies to reduce the risk of future fracture within the year following the fracture [33]. The therapeutic care gap is even wider in the elderly in whom the importance and impact of treatment is well-known. Studies have shown that as few as 10% of older women with fragility fractures receive any osteoporosis therapy (estrogens not considered) [31].
Many studies therefore have expressed the importance of prevention and therefore early detection before any fracture has happened in reducing the burden of the disease [9]. According to these studies, in view of the fact that the restoration of diminished bone volume seems quite difficult, early diagnosis of osteoporosis is the most valuable strategy for preventing osteoporotic fractures.
Early diagnosis can help to not only identify those who would benefit from intervention but also determine the optimal manner in which response to treatment should be monitored.

1.2 Current Work

1.2.1 Application field of current work

Current trends towards theranostics and provision of personalized diagnostic therapy tailored to an individual has emphasized the need for inexpensive point-of-care (PoC) devices, capable of performing rapid analysis, with small volumes of sample, minimum number of assay steps, and no need for highly skilled personnel for routine check up and patient screening. PoC diagnostics are analytical testing platforms that can be used both in a clinical laboratory and in the vicinity of a patient using portable equipment [34].
Therefore, the entire clinical diagnosis and treatment community is witnessing a paradigm shift from conventional diagnostic devices to the miniaturized and PoC devices [35]. These devices can fulfill the increasing demand of the medical sector for fully automated instruments that can directly use unprocessed specimens and that require minimal electronic or mechanical maintenance [36].
PoC diagnostics have the potential to provide rapid and accurate results, at reasonable costs. An ideal diagnostic device should provide a suitable environment for interaction of the analyte to be tested in a given sample with the biorecognition molecule (e.g.protein, lipid, nucleic acid, whole cell), which is immobilized onto the sensor surface.
PoC diagnostics are critically dependent on the combination of the analytical tools and the rapidly emerging knowledge on molecular biomarkers. They can be used to identify both physiological and biological entities associated with diseases, and have evolved from simple single physiological parameters to novel markers that span fields from genomics to metabolomics.
As mentioned above, the restoration of diminished bone volume seems difficult to achieve and thus early diagnosis of osteoporosis is the most valuable strategy

for preventing osteoporotic fractures. Prevention of fracture starts by early identification of fracture prone individuals [37]. However, the prediction of rapid bone loss, incidence of osteoporosis, and osteoporotic fracture remains difficult. The identification of individuals who would best benefit from intervention and for those on treatment, the optimal manner in which response to treatment should be monitored are therefore important gaps in the clinical armamentarium in osteoporosis management.
Recent studies have pointed out the importance of BTMs in this regard [38]. BTMs are bone tissue proteins or their fragments/enzymes released from bone cells during bone turnover.
Bone remodeling rate therefore can be assessed by measuring BTMs in serum or urine. A more detailed explanation of BTMs and their characteristics could be found in Chapter 3. Biochemical markers of bone turnover have been investigated in osteoporosis for three main purposes:

- to monitor anabolic or anti-resorptive therapy
- to predict potential bone loss and the risk of developing osteoporosis
- to improve assessment of fracture risk in individuals

Although BTMs have shown clinically interesting associations with the rate of bone loss, the routine use of BTMs in clinical practice is not generally recommended, as these tests vary in sensitivity and specificity and their appropriate role in patient management is not yet known [39].
This is while Enzyme-Linked Immunosorbent Assay (ELISA), Electrochemiluminescence immunoassay (ECLIA) and other prevailing laboratory techniques in the current state of the art for biomarker quantification do not lend themselves well to miniaturized automated systems for application at PoC [40]. Moreover, they are time consuming, expensive, labor intensive, require highly trained personnel and lack consistency in laboratory accuracy. Thus performing rapid multiplexed measurements to monitor several biochemical parameters at the same time to reach a rapid and accurate medical decision still remains a largely unmet challenge.
Biosensors on the other hand can help determine reaction kinetics of marker interaction in real-time. The technique needs only one step (reaction) and can thus be used for point of care screening. As a result, several biosensors were developed during the past years to improve measurement of some of these markers, none of them are routinely used in practice. Detailed explanation of these sensors is discussed in Chapter 3.
In this context, multiplexed detection of different biomarkers integrated with microfluidic systems has potential to play a very influential role in diagnostics; and advances in microfluidics, arrays, sensors, and naomaterials have paved the way for the development of lab-on-a-chip instruments [41]. Microfluidics is an extremely attractive technology because of its ability to manipulate small volumes

of fluid (micro- to nanoliters) within given spatial dimensions, and the ease of multiplexing and integrating this system into low-cost,compact and portable devices for on-chip testing [42]. It, therefore, provides a very promising way to miniaturize immunoassays, which has played an important role in the diagnosis of different diseases in the past 50 years. Such devices also provide added benefits such as portability, increased reliability, improved sensitivity, decreased analysis time, minimal reagent consumption and parallel processing [43][44]. Among different techniques used to generate a signal in these platforms, the electrochemical method has shown the most suitable results because of its simple instrumentation and easy signal quantification [45]. A clear challenge resides in the integration and operation of such microfluidic platforms for measurement of different biomarkers, such as BTMs.
In this thesis, we describe a microfluidic proteomic platform that can easily be translated into a biomarker diagnostic. This platform integrates microfluidic technology with electrochemical sensing and embodies a reaction/detection chamber to measure serum levels of different biomarkers. The unique design of the platform offers microfluidic and electrochemical structures to be independently optimized.
We demonstrated the implementation, feasibility and specificity of this platform (Osteokit) in assaying serum levels of BTMs using osteocalcin (Oc) and Cross-linked Telopeptides of type I collagen (CTX). It was concluded that the whole platform is simple in design, inexpensive and easy to manufacture whilst offering accurate measurements. The use of microfluidic components together with electrochemical detection, suggests that the proposed device could be operated as a hand-held device in future.
This work serves as the basis for a clinical diagnostic that can be used by healthcare providers to identify patients at-risk of osteoporotic fracture, those who may benefit more from treatment and monitor treatment effectiveness.

1.2.2 Structure of the thesis

Upon the development of a 'New Biomarker Assay' and before the device enters the market, several steps are executed: Assay Development, Analytical Validation, Clinical Utility Validation, Clinical Implementation. (Figure 1.7) The first two steps are discussed in this PhD.

- Chapter 1 consists of an introduction, explaining the importance of Point-of-Care (PoC) testing in osteoporosis management and the application field of this PhD work followed by the scientific goals and strategy.
- Chapter 2 consists of a literature overview on BTMs and existing bone biosensors. In the next section, special attention is paid to methods used to deposit gold nanoparticles on a gold electrode, and protein immobilization techniques.

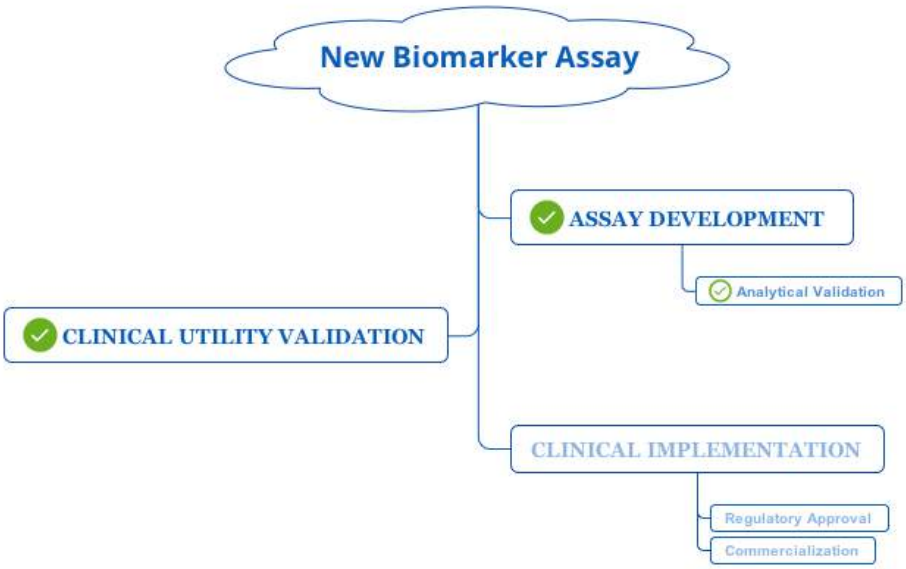

Figure 1.7: New Biomarker Assay Development Steps.

- The third chapter provides scientific information and background of the major scientific subjects of this thesis. The first part, focuses on biosensors and then basic principles of electrochemistry and microfluidic devices are provided.
- Chapter 4 includes the verification of the conjugated AuNP-antibody nanoprobe fabricated for electrochemical biosensors.
- Chapter 5 explains the fabrication process of the electrodes used in this thesis. Different modification methods to deposit AuNPs on gold electrodes are also compared in this chapter.
- Chapter 6 discusses characteristics and validation process of the Oc and CTX biosensors.
- Chapters 7 and 8 discuss the Osteokit prototype fabrication technology and experiment results, respectively.
- Chapter 9 consists of general conclusions and future prospects of the performed research.

Additional information on BTMs and their characteristics are listed in Appendix A. All the information regarding the 'materials and reagents' as well as the 'apparatus' used in this work is provided in Appendix B.

1.2.3 Scientific Goals

Regarding osteoporosis, the goal of this work was to develop a reliable, cost-effective, powerful detection and monitoring tool for fracture risk indication and treatment monitoring so that the patient can receive the most appropriate therapy and that physicians can monitor the disease progression.
In this regard we decided to develop a microfluidic platform capable of measuring serum levels of several biomarkers with high accuracy. The plan was to develop a unique architecture which enabled low sample volume requirements, short assay time, simplicity of fabrication and use, and low-cost instrumentation and at the same time portability, high sensitivity and specificity for the biomarkers. (Figure 1.8) Furthermore, we wanted our measurement results to be comparable in sensitivity with the current gold standard ECLIA.
Here, we propose the development of a functional conjugated AuNP-antibody nanoprobe to be used to modify the surface of the electrode for sensing purposes as the first step. This nanoprobe was directly reacted with antigen following their pre-incubation in solution or the probe was assembled onto the electrode to bind with antigen, by so-caled 'in-solution' or 'on-chip' methods, respectively.

- A detailed description of the characteristics of the in-solution nanoprobe is provided in Chapter 4.
- Stable immobilization of the nanoprobe on the electrode, while keeping the antibodies' bioactivity in microreactor environment, and thus supporting high quality and low-background noise in electrochemical sensing was our next goal. In this work, gold electrodes were coated with AuNPs by electrodeposition using cyclic voltammetry (Chapter 5). This goal is not limited to the development of the modified surface but also includes characterization of the modified surfaces using advanced chemical surface analysis techniques including XPS, STEM and AFM.
- One of the most crucial steps in biosensor fabrication is assessing the sensitivity and selectivity of the system. In this work a calibration curve was plotted for each of the measured markers and the final results were compared with that of the current state-of-art ECLIA.
- The application of micro-manufacturing technology and development of microfluidic chips allowed considerable throughput portability and the capacity for a high level of integration, and thus fulfilled the requirements of fluidic sample-based point-of-care diagnostics. This also lowered the consumed reagent and sample volume as well as the analysis time without compromising the detection limit of the device, which are required for PoC devices.
- In the final stage, the parameters which were taken into account to improve the sensitivity and specificity of the microfluidic platform are studied.

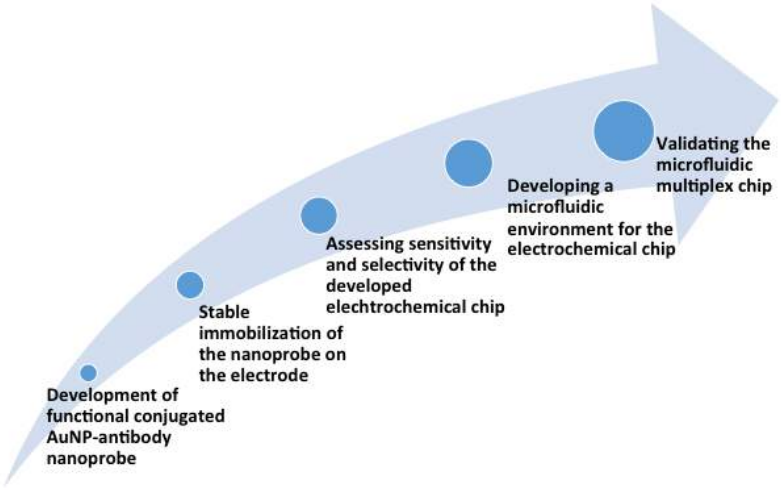

Figure 1.8: Thesis Workflow.

Hence, the reproducibility of the measurements were investigated through comparing the results with ECLIA.

References

[1] M. S. Calvo, D. R. Eyre, and C. M. Gundberg, "Molecular basis and clinical application of biological markers of bone turnover," *Endocr Rev*, vol. 17, no. 4, pp. 333–368, 1996.

[2] R. Recker, J. Lappe, K. M. Davies, and R. Heaney, "Bone remodeling increases substantially in the years after menopause and remains increased in older osteoporosis patients," *J Bone Miner Res*, vol. 19, no. 10, pp. 1628–1633, 2004.

[3] J. A. Kanis, L. J. r. Melton, C. Christiansen, C. C. Johnston, and N. Khaltaev, "The diagnosis of osteoporosis," *J Bone Miner Res*, vol. 9, no. 8, pp. 1137–1141, 1994.

[4] L. Melton, "How many women have osteoporosis now?" *J Bone Miner Res*, vol. 10, pp. 175–177, 1995.

[5] E. Hernlund, A. Svedbom, M. Ivergård, J. Compston, C. Cooper, J. Stenmark, E. McCloskey, B. Jönsson, and J. Kanis, "Osteoporosis in the european union: medical management, epidemiology and economic burden," *Arch. Osteoporos.*, vol. 8, no. 1-2, 2013.

[6] B. Larijani, H. Resch, J. Bonjour, H. Aghai Meybodi, and M. Mohajery Tehrani, "Osteoporosis in iran, overview and management," *Iranian J Public Health*, vol. A Supplementary issue on Osteoporosis, pp. 1–13, 2007.

[7] K. D. Harper and T. J. Weber, "Secondary osteoporosis. diagnostic considerations," *Endocrinol Metab Clin North Am*, vol. 27, no. 2, pp. 325–348, 1998.

[8] C. Cooper, G. Campion, and L. J. Melton, "Hip fractures in the elderly: a world-wide projection," *Osteoporos Int*, vol. 2, pp. 285–289, 1992.

[9] "Clinical practice guidelines for the diagnosis and management of osteoporosis. scientific advisory board, osteoporosis society of canada," *CMAJ*, vol. 155, no. 8, pp. 1113–33, 1996.

[10] N. Ray, J. K. Chan, M. Thamer, and L. Melton, "Medical expenditures for the treatment of osteoporotic fractures in the united states in 1995: Report from the national osteoporosis foundation," *J Bone Miner Res*, vol. 12, pp. 24–35, 1997.

[11] J. Reginster, P. Gillet, S. W. Ben, G. Brands, O. Ethgen, C. de Froidmont, and C. Gosset, "Direct costs of hip fractures in patients over 60 years of age in belgium," *Pharmacoeconomics.*, vol. 15, no. 5, pp. 507–514, 1999.

[12] "http://www.iofbonehealth.org/facts-and-statistics/hip-fracture-incidence-map."

[13] S. Ahmadi-Abhari, A. Moayyeri, and F. Abolhassani, "Burden of hip fracture in iran," *Calcif Tissue Int.*, vol. 80, no. 3, pp. 147–153, 2007.

[14] F. Hadaegh, H. Harati, A. Ghanbarian, and F. Azizi, "Prevalence of coronary heart disease among tehran adults : Tehran lipid and glucose study," *East. Mediterr. Health J.*, vol. 15, no. 1, pp. 157–166, 2009.

[15] S. Ghafoori, A. Keshtkar, P. Khashayar, M. Ebrahimi, M. Ramezani, Z. Mohammadi, F. Saeidifard, N. Nemati, M. Khoshbin, S. Azizian, F. Zare, S. Shirazi, and B. Larijani, "The risk of osteoporotic fractures and its associating risk factors according to the frax model in the iranian patients: a follow-up cohort," *J Diabetes Metab Disord.*, vol. 13, p. 93, 2014.

[16] I. Salehi, S. Khazaeli, S. Najafzadeh, H. Ashraf, and M. Malekpour, "High prevalence of low bone density in young iranian healthy individuals," *Clin Rheumatol*, vol. 28, pp. 173–177, 2009.

[17] J. Kanis, O. Johnell, C. De Laet, B. Jonsson, A. Oden, and A. Ogelsby, "International variations in hip fracture probabilities: Implications for risk assessment," *J Bone Miner Res*, vol. 17, no. 7, pp. 1237–1244, 2002.

[18] K. Briot and C. Roux, "What is the role of dxa, qus and bone markers in fracture prediction, treatment allocation and monitoring?" *Best Pract Res Clin Rheumatol*, vol. 19, no. 6, pp. 951–964, 2005.

[19] S. Schuit, M. van der Klift, A. Weel, C. de Laet, H. Burger, E. Seeman, A. Hofman, A. Uitterlinden, J. van Leeuwen, and H. Pols, "Fracture incidence and association with bone mineral density in elderly men and women: the rotterdam study," *Bone.*, vol. 34, no. 1, pp. 195–202, 2004.

[20] C. A. Cefalu, "Is bone mineral density predictive of fracture risk reduction?" *Curr Med Res Opin*, vol. 20, no. 3, pp. 341–349, 2004.

[21] S. L. Bonnick and L. Shulman, "Monitoring osteoporosis therapy: bone mineral density, bone turnover markers, or both?" *Am J Med*, vol. 119, no. 4 Suppl 1, pp. S25–31, 2006.

[22] E. Siris, Y. Chen, T. Abbott, E. Barrett-Connor, P. Miller, L. Wehren, and M. Berger, "Bone mineral density thresholds for pharmacological intervention to prevent fractures," *Arch Intern Med.*, vol. 164, no. 10, pp. 1108–1112, 2004.

[23] V. Elliot-Gibson, E. Bogoch, S. Jamal, and D. Beaton, "Practice patterns in the diagnosis and treatment of osteoporosis after a fragility fracture: a systematic review," *Osteoporos Int*, vol. 15, no. 10, pp. 767–778, 2004.

[24] G. Guglielmi, "Quantitative computed tomography (qct) and dual x-ray absorptiometry (dxa) in the diagnosis of osteoporosis," *Eur J Radiol.*, vol. 20, no. 3, pp. 185–187, 1995.

[25] G. Guglielmi, S. Muscarella, and A. Bazzocchi, "Integrated imaging approach to osteoporosis: State-of-the-art review and update," *RadioGraphics*, vol. 31, no. 5, pp. 1343–1364, 2011.

[26] J. A. Kanis, O. Johnell, A. Oden, H. Johansson, and E. McCloskey, "Frax and the assessment of fracture probability in men and women from the uk," *Osteoporos Int*, vol. 19, no. 4, pp. 385–397, 2008.

[27] H. Johansson, J. A. Kanis, A. Oden, O. Johnell, and E. McCloskey, "Bmd, clinical risk factors and their combination for hip fracture prevention," *Osteoporos Int*, vol. 20, no. 10, pp. 1675–1682, 2009.

[28] A. Marques, R. J. O. Ferreira, E. Santos, E. Loza, L. Carmona, and J. A. P. da Silva, "The accuracy of osteoporotic fracture risk prediction tools: a systematic review and meta-analysis," *Annals of the Rheumatic Diseases*, vol. 74, no. 11, pp. 1958–1967, 2015.

[29] J. T. Lin and J. M. Lane, "Osteoporosis: A review," *Clin Orthop Relat Res*, vol. 425, pp. 126–134, 2004.

[30] N. Zethraeus, F. Borgström, O. Ström, J. Kanis, and B. Jönsson, "Cost-effectiveness of the treatment and prevention of osteoporosis—a review of the literature and a reference model," *Osteoporos Int*, vol. 18, no. 1, pp. 9–23, 2007.

[31] J. A. Kanis, A. Svedbom, N. Harvey, and E. McCloskey, "The osteoporosis treatment gap," *J Bone Miner Res*, vol. 29, no. 9, pp. 1926–8, 2014.

[32] L. Jennings, A. Auerbach, J. Maselli, P. Pekow, P. Lindenauer, and S. Lee, "Missed opportunities for osteoporosis treatment in patients hospitalized for hip fracture," *J Am Geriatr Soc*, vol. 58, no. 650-657, 2010.

[33] A. Diez-Perez, F. H. Hooven, J. D. Adachi, S. Adami, F. A. Anderson, S. Boonen, R. Chapurlat, J. E. Compston, C. Cooper, P. Delmas, S. L. Greenspan, A. Z. Lacroix, R. Lindsay, J. C. Netelenbos, J. Pfeilschifter, C. Roux, K. G. Saag, P. Sambrook, S. Silverman, E. S. Siris, N. B. Watts, G. Nika, and S. H. Gehlbach, "Regional differences in treatment for

osteoporosis. the global longitudinal study of osteoporosis in women (glow)," *Bone*, vol. 49, no. 3, pp. 493–498, 2011.

[34] J. Wang, "Electrochemical biosensors: Towards point-of-care cancer diagnostics," *Biosens Bioelectron*, vol. 21, no. 10, pp. 1887–1892, 2006.

[35] S. Kumar, V. Agrawal, R. John, and M. B, "Microfluidic-integrated biosensors: Prospects for point-of-care diagnostics," *Biotechnology Journal*, vol. 8, pp. 1267–79, 2013.

[36] C. Holland and F. Kiechle, "Point-of-care molecular diagnostic systems - past, present and future," *Curr Opin Microbiol*, vol. 8, pp. 504–9, 2005.

[37] World Health Organization (WHO), "Prevention and management of osteoporosis.report of a who scientific group," WHO Technical Report Series No. 921. Geneva, Switzerland, Tech. Rep., 2003.

[38] P. Khashayar, H. Aghaei Meybodi, G. Amoabediny, and B. Larijani, "Biochemical markers of bone turnover and their role in osteoporosis diagnosis: A narrative review," *Recent Pat Endocr Metab Immune Drug Discov.*, vol. 9, no. 2, pp. 79–89, 2015.

[39] N. A. M. Society, "Management of osteoporosis in postmenopausal women: 2010 position statement of the north american menopause society," *Menopause*, vol. 17, no. 1, pp. 25–54, 2010.

[40] A. Vasudev, A. Kaushik, Y. Tomizawa, N. Norena, and S. Bhansali, "An ltcc-based microfluidic system for label-free, electrochemical detection of cortisol," *Sensors and Actuators B: Chemical*, vol. 182, pp. 139–46, 2013.

[41] P. Auroux, D. Iossifidis, D. Reyes, and A. Manz, "Micro total analysis systems. 2. analytical standard operations and applications," *Anal Chem*, vol. 74, no. 12, pp. 2637–52, 2002.

[42] V. Goral and P. Yuen, "Microfluidic platforms for hepatocyte cell culture: New technologies and applications," *Ann Biomed Eng*, vol. 40, pp. 1244–54, 2012.

[43] A. Bange, H. B. Halsall, and W. R. Heineman, "Microfluidic immunosensor systems," *Biosens Bioelectron*, vol. 20, no. 12, pp. 2488 – 2503, 2005.

[44] D. Erickson and D. Li, "Integrated microfluidic devices," *Analytica Chimica Acta*, vol. 507, no. 1, pp. 11–26, 2004.

[45] W. Zimmerman, "Electrochemical microfluidics," *Chemical Engineering Science*, vol. 66, no. 7, pp. 1412–25, 2011.

2
Literature Overview

2.1 Introduction

This chapter focuses on:

1. Biochemical markers of bone turnover and their role in osteoporosis diagnosis
2. Bone biosensors: knowing the present and predicting the future
3. Protein immobilization strategies for biosensing purposes

2.2 Bone Turnover Markers and osteoporosis

2.2.1 Introduction

In the last decade, proteome analytical techniques have made a quantum leap forward and became powerful tools in addressing a broad variety of clinical problems through improving the prediction, diagnosis and prognostication of diseases and elucidating underlying molecular pathways [1]. Accurate assessment of the biomarkers of these diseases are prerequisites to achieving these goals.

2.2.2 What are biomarkers

The definition of biomarkers has evolved over the past decade, with WHO suggesting that "A biomarker is any substance, structure or process that can be measured in the body or its products and influence or predict the incidence of outcome or disease" [2][3].
Qualified biomarkers are valuable tools to diagnose patients earlier in the clinical course of disease, to predict outcomes and guide interventional approaches, to stratify participants in clinical trials, and to monitor response to therapy, and even in personalized medicine. Besides providing useful information in guiding clinical decision making, these biomarkers are increasingly linked to specific molecular pathway deregulations and/or pathogenesis to justify application of certain therapeutic/interventional strategies [4].
In other words, biomarkers are key molecular, chemical or cellular characteristics that can be objectively measured and evaluated as an indicator for a normal biological or pathogenic process such as the onset, manifestation, or progression of a disease as well as pharmacological response to a therapeutic intervention [5]. Regarding the context of use, biomarkers can be either disease- or therapy-related.

- Disease-related biomarkers are diagnostic (used to establish the disease state), prognostic (provide information regarding potential clinical outcome irrespective of the treatment), or predictive (provide information regarding potential clinical outcome in response to specific treatment).
- Therapy-related biomarkers provide information regarding the effectiveness of a particular drug in treating or managing a disease.

The Biomarkers and Surrogate End Point Working Group, alternatively, has classified biomarkers as [6]:

- Type 0 biomarkers: Markers of natural history of the disease that correlate with clinical indices (e.g., Complete blood count)
- Type I biomarkers: They represent the effects of a therapeutic intervention in accordance with drug mechanism of action (e.g., Decrease in urokinase-type plasminogen activator (uPA) gene expression upon dasatinib treatment in prostate cancer)
- Type II biomarkers: They are surrogate end points as a change in these markers indicate clinical benefit (e.g., Decrease in blood/urine glucose level).

Concerning their origins, biomarkers are categorized as following: (Figure 2.1)

- Protein biomarkers [1]: Proteins are vital biomolecules that function as the working unit for activities, ranging from the storage and metabolism of energy to the regulation of cellular functions. An abnormal expression of proteins or expression of unique proteins is often associated with specific disease.
  Protein biomarkers are primarily found in the blood or urine [7]. Most of them serve multiple clinical purposes during early or late disease progression. They can also be used to monitor treatment response and/or detect recurrence during follow-ups.
  Analyzing protein biomarkers involves several challenges, mainly because they are sensitive to their ambient environment, including temperature, ionic strength and pH. Moreover, the direct analysis of traces of proteins in crude or complex biological samples against the high background of other proteins in high abundance is difficult.
- Enzyme biomarkers
- Nucleic acids-based biomarkers (DNA and RNA)
- Small chemical products of cellular metabolism
- Direct analysis of cells

For a biomarker to become accepted for clinical application it has to have the following characteristics:

- Readily and consistently detectable in biological fluids, tissues, or other biological specimens.
- Rapidly detectable and stable.
- High sensitivity and specificity.
- Strong correlation with the phenotype or outcome of interest.
- Detectable via a simple, noninvasive, and cost-effective test.
- Consistent across genders.

2.2.3 Bone turnover markers (BTMs)

An important determinant of bone strength that cannot be assessed using BMD or clinical risk factor assessment tools is bone turnover [8]. BTMs can be useful in determining the number and the activity of bone cells. More specifically in terms of clinical utility, BTMs can help predict the risk of developing osteoporosis or experiencing fracture or potential response to therapy. They are also used in the assessment of early postmenopausal status [9].

[1] Considering the concept of this thesis, only the first category is briefly explained

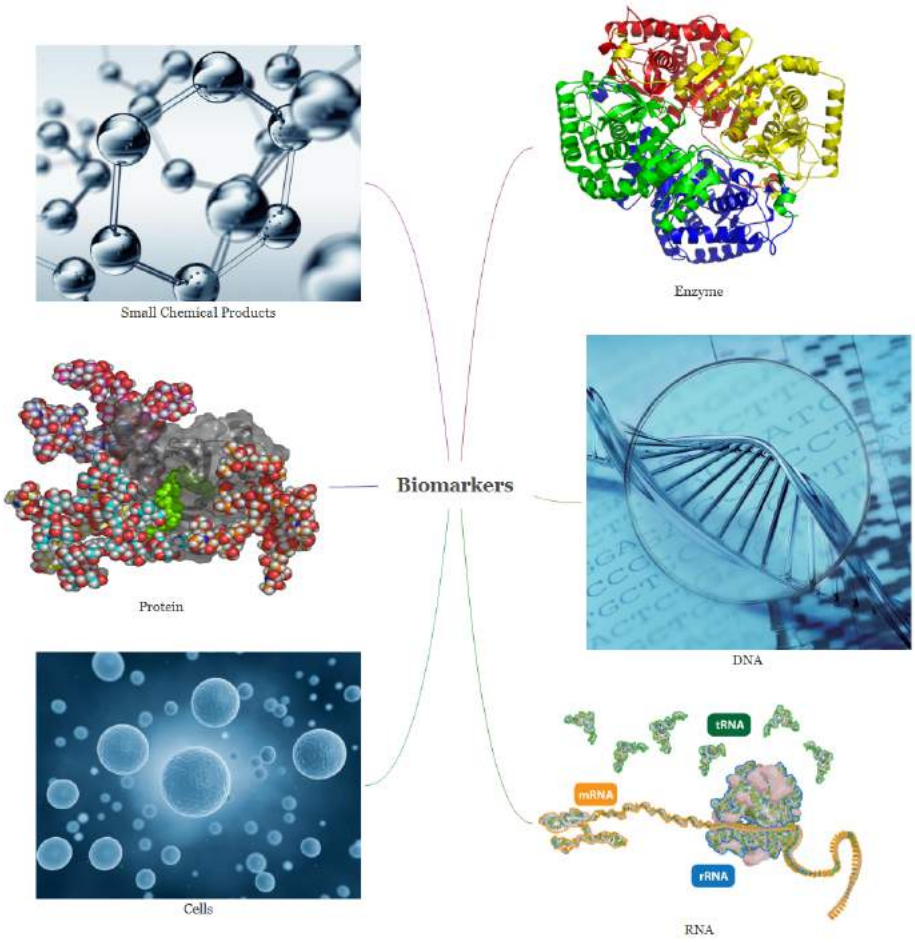

Figure 2.1: Different origins of biomarkers.

As a result, biochemical markers of bone turnover have been investigated for three main purposes [10]:

- to monitor anabolic or anti-resorptive therapy
- to predict potential bone loss and the risk of developing osteoporosis
- to improve assessment of fracture risk in individuals

Advantages of using BTMs

DXA is the widely available noninvasive and accepted method for assessing BMD to identify individuals with osteoporosis and, possibly, those at-risk for fracture [3]. While BMD changes are considered as a valid end point for verifying the efficacy of osteoporosis treatments, BMD changes and fracture risk reduction rate following medication is not measurable at early stages [4]. Moreover, DXA is incapable of assessing bone quality, which consists of its micro- and macro-architecture and turnover and its results are affected with advancing age, bone conditions such as osteoarthritis [5].
BTMs have shown promising results in osteoporosis care, such as:

- Samples of blood and urine are easily collected.
- They have a relative specificity for bone resorption or formation
- They provide complementary information to BMD
- Changes in BTMs occur earlier than that of BMD

Fig 2.2 compares the impact of various risk factors (low BMD, a prior fracture or high urinary CTX) on ten-year probability of hip fracture in Swedish women (women aged 65 years and over in OFELY study, and those of 80 years and over in EPIDOS study) according to age and relative risk. The difference in the impact of each of these risk factors alone on hip fracture probability is rather negligible. However, the combination of these risk factors improves the relative risk. In other words, the presence of two of these risk factors increases the risk of hip fracture probability by 2.0- to 2.6- fold, whereas with all these risk factors, a 3-fold increase is noted. Combination of these risk factors also enlarge the range of risk stratification and permit the identification of individuals above a threshold risk.

Moreover, BMD alone is incapable of diagnosing patients suffering from secondary osteoporosis, caused by certain underlying medical conditions or treatments that may interfere with the attainment of peak bone mass and thus result in bone loss. The treatment process in these patients may include treating the underlying cause of the disease which is based on additional tests including BTM assessment [12]. BTM measurements may also help to diagnose certain bone pathologies characterized by high bone turnover

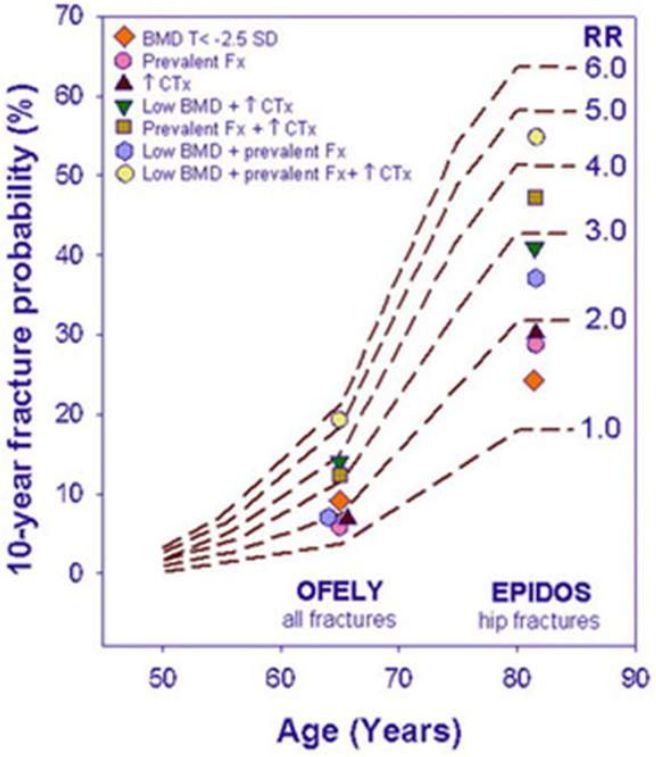

Fx = Fracture

RR= Relative Risk

Figure 2.2: Sensitivity of BMD and different bone markers in predicting hip fracture [11].

such as Paget disease, osteomalacia, multiple myeloma, and bone metastases.
Furthermore, since bone biopsy is invasive and cannot be repeated in clinical practice and because bone histomorphometry is less available due to the lack of specialized laboratories, the use of BTMs has gained momentum.
BTMs reflect whole-body rates of bone resorption and formation as they provide a more representative index of the overall bone loss than that obtained by BMD values measured at specific skeletal sites containing different ratios of cancellous to cortical components with different metabolic rates [8].
In view of the rapid and considerable changes noted in BTM values during the course of osteoporosis treatment, these markers can also be used to assess compliance and treatment response [13]. In other words, the better the compliance, the greater would be the decrease noted in BTM values, and the lower would be the fracture incidence.
The most effective antiresorptive treatments lower BTM values to a drug- and dose-dependent plateau within a few weeks or months (3 - 6 months), providing a surrogate marker with adequate sensitivity and specificity to BMD which needs a 2-year time to show the changes [14]. Bone resorption decreases significantly after 3 weeks of anti-resorptive treatment, whereas at least 6 weeks are needed for a significant decrease to be noticeable in the bone formation markers' values. At the same time considering BMD's short-term precision error (1± 1.5 %), a two-year period is needed before at least a 3 ± 5 % change, suggestive of an acceptable response to a potent bisphosphonate, is noted on the new BMD [15].
BTMs can also help identify patients who benefit more from anti-resorptive drugs [16]. It has been reported that baseline bone turnover values can predict treatment response, suggesting a higher increase in BMD values in patients with higher turnover rate after the use of anti-resorptive medication. Desai Meena et al showed increasing levels of bone resorption markers (Cross-linked Telopeptides of type I collagen (CTX) and Deoxypyridinoline (Dpd)) during the aging process, suggestive of a negative correlation between these markers and BMD [17]. The increase noted in levels of CTX and Dpd was significantly higher than the changes reported in the BMD values at femur and spine. Women with marker values of at least two standard deviations greater than the mean are reported to be at a 75 - 80 % risk of experiencing rapid bone loss [18].
Dresner-Pollak et al reported that N-telopeptide crosslinks (NTX), Oc, and serum parathyroid hormone explained 43% of the bone loss variability at hip in women [19]. Such a relation was not found in men. Similarly, Drake et al suggested that it is not possible to identify osteoporotic men who would be good candidates for alendronate therapy based on biochemical or hormonal markers [20]. In another study, fracture risk was reported to

be higher in men with increased P1NP or beta CTX levels but not TRAP5b [21].
Several studies have shown that biochemical markers of bone-remodeling are independent predictors of fracture, especially in spine and hip [16]. This is mainly explained by the fact that high rate of bone loss is a risk factor for fracture, independent of BMD values.

Disadvantage of using BTMs

Recent national guidelines from different countries have also adopted different roles for BTMs in the diagnosis and monitoring of osteoporosis treatments, revealing differing opinions regarding the utility of BTMs in the diagnosis and management of osteoporosis [22]. Despite all, the routine use of BTMs in the clinical practice is not recommended. This is mainly because BTM values depend not only on the bone turnover rate, but also on factors including age, gender and many more. Moreover the strength of the association between BTMs and the rate of bone loss largely depends on the accuracy of the measurement techniques [23]. Analytical variability, to be discussed later in this section, is also an important limitation in this regard.

2.2.4 BTM Classification

In order to provide a list of existing BTMs, and their pros and cons in assessing bone loss, more than 950 scientific communications were reviewed. In brief, the articles were gathered in following steps:

- Designing the search protocol
- Designing a quality assessment form
- Designing the data extraction form
- Searching electronic databases
- Hand searching
- Data extraction
- Data imputation and analysis

Data Sources International databases, including PubMed/MEDLINE, Web of Science, and Embase as well as congress abstracts conference proceedings, theses, and reports in related databases were assessed for related Mesh terms including all subheadings:
('Osteoporosis'[MeSH] OR 'Bone' [MeSH]) AND ('Biological Markers' [MeSH])

Inclusion criteria All studies conducted between January 1985 and December 2011 on the accuracy of bone turnover markers in predicting osteoporosis and its complications as well as those on new methods to study BTMs in this regard were included. There was no restriction on the language of the publication.

Exclusion criteria Studies conducted on children and secondary osteoporosis (chronic renal failure (CRF)) were excluded.

A list of most important BTMs and a short description on them is provided in Appendix A.
Considering the various results reported in these studies, the IOF, the International Federation of Clinical Chemistry and Laboratory Medicine (IFCC) and National Bone Health Alliance (NBHA) formed a committee of experts in 2011 to examine the efficacy of BTMs and to make clear recommendations on their use in clinical practice [24]. They concluded that CTX and P1NP are defined as the reference analytes for studying osteoporosis in clinical practice.

2.2.5 Biomarker Setbacks (with focus on BTMs)

The inevitable biological challenges for biomarker detection have encouraged researchers to continuously devote great effort in this field. As for osteoporosis, these challenges include:

Marker Limitations

Serum or Urine Serum-based assays are better than urine, because of their lower imprecision and day-to-day variation (within person reliability), better reproducibility (variable ionic strength of urine samples and need for creatinine (Cr) excretion correction).

Resorption or Formation Markers Changes in resorption marker values occur earlier than that of formation markers.

Single or Multiple Markers Osteoporosis is a multifactorial disease and a single biomarker has only a limited ability to predict bone loss and fracture risk with high specificity and sensitivity [25]. Moreover, to avoid false positives, arising from population variations in the expression of a single biomarker, simultaneous evaluation of a panel of biomarkers is typically

important and required.
In addition, no biomarker has been reported as an ideal screening tool that can meet the diagnostic, prognostic, and predictive requirements simultaneously. A model developed by Cosman et al showed that urine Hydroxyproline (Hyp), serum CTX, serum Bone Alkaline Phosphatase (BALP), and calcium intake predicts 42% of BMD change at lumbar spine in untreated postmenopausal women [17]. Together, the measurement of pyridinium cross-links and BALP or Oc is also reported as an index of bone turnover rate, which can help identify fast losers at high risk of osteoporosis or those in need of aggressive therapy [19].

Measurement Technique Limitations

Similar to other analytes, BTMs have their specific technical and analytical limitations. The relatively poor quality assurance of the measurement techniques along with their large coefficient of variation (C.V.) and assay variability are other factors limiting the use of BTMs in clinical practice. Thus assay sensitivity and specificity need to be improved, and the techniques must be standardized and validated. Thus, the validation of new techniques to measure biomarkers for efficient osteoporosis diagnosis is quite necessary and challenging. In addition, many questions have been raised regarding how new tests will be developed, evaluated, and integrated into clinical practices.
The main limitations in BTM measurements are categorized in two main groups:

Analytical variability Recent improvements in technology, particularly the introduction of automated immunoassays, has reduced the analytical C.V. of BTMs to about 5–15% [26]. However, considering the lack of a uniform standardization technique, it would be difficult to compare values obtained by dissimilar methods in different laboratories. The intra-individual reproducibility of BTMs is still a concern, especially when therapeutic approaches should be chosen based on a single measurement.
Studies have shown an intra-individual variability of around 10% and between 15- 25% for serum and urine markers, respectively [27]. This suggests that a least significant change (LSC) of at least 25–30% and 40–70% must be observed so that a significant change is considered for each of these markers, correspondingly. Compared with urinary resorption markers, this index is reported to be lower for serum bone formation markers. Moreover, it is preferable to measure a marker in serum as no correction for creatinine excretion would be needed and the ionic strength would be less variable in this case. It should also be kept in mind that some markers are sensitive

to thermo-degradation, UV radiation, hemolysis and other ambient influences.
Immunoassays, particularly, ELISA, have been extensively used in routine clinical diagnostics and are still the gold standard for the detection of proteins in physiological samples [28]. The same is true for BTMs.
Even though universally available, the use of ELISA has its limitations, especially in terms of sensitivity, dynamic range, and sample volume. On the other hand, ELISAs are best suited when only a few biomarkers are needed to be verified/validated on a large number of samples. They could also be a very tedious, expensive and time-consuming process. ELISAs require antibodies against each targeted protein/peptide and thus it is possible that high-quality assays would be unavailable for proteins of interest [29]. In addition, ELISA assays have limited multiplex capability and the cross reactivity is always a cause for concern. (Figure 2.3)
Continuous efforts have been devoted to further optimize these standard methods or to find new and better techniques for the measurement of biomarkers. The new techniques are often fluorescence or chemiluminescence based.
More recent studies thus have focused on developing newer technologies to overcome these setbacks. Next section would provide a detailed explanation of the developed bone biosensors. Although robust and highly efficient, most of these methods still suffer from lack of accuracy, sensitivity, and specificity for clinical diagnostic applications.

Pre-Analytical variability The BTMs' pre-analytical variability should also be taken into account during their clinical interpretation [30]. This variability is broadly divided into two categories: (Table 2.1)

- Uncontrollable factors such as age, gender, renal function, menopausal status, disease or recent fracture. The use of appropriate reference ranges or suitable adjustments can help overcome this variability to some extent.
- Controllable factors such as circadian rhythm, menstrual or physical activity status. The effects of these factors can be minimized by standardizing the timing and conditions under which the samples are collected.

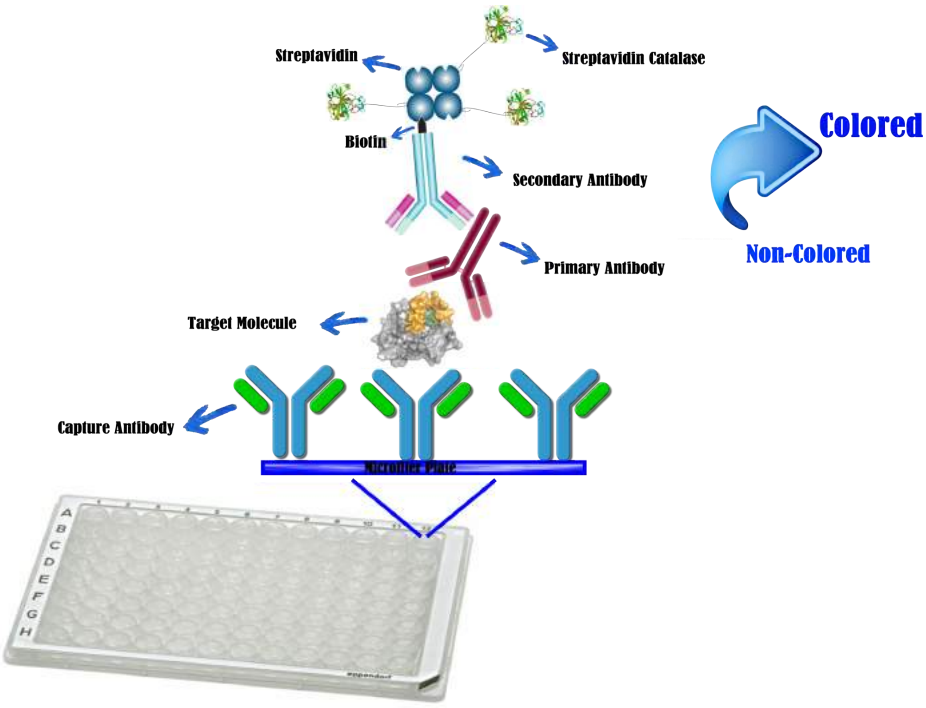

Figure 2.3: Schematic view of the sandwich ELISA format.

Table 2.1: Sources of biological variability

Source	Nature of effect
Uncontrollable Sources	
Age	BTM increase with age in men and women
Menopausal status	BTM increase within a few months after the last menstrual period
Gender	BTM are higher in older women than older men
Fracture	BTM increase after a fracture (maximal at 2 to 12 weeks, but effect lasts for up to 52 weeks)
Pregnancy and lactation	BTM are increased during pregnancy; highest levels during third trimester, even higher postpartum
Drug	BTM may be decreased (glucocorticoids) or increased (anticonvulsants)
Underlying Diseases	BTM often increased (thyrotoxicosis, chronic kidney disease)
Immobility	Bone formation markers decrease and resorption markers increase
Geography	Minor changes amongst countries, usually explained by differences in lifestyle
Ethnicity	Minor changes, such as lower Oc in African Americans vs. Caucasians
Controllable Sources	
Circadian	Most striking for bone resorption markers; highest values in second half of night and on waking; lowest values in afternoon and evening
Fasting status	Feeding results in a decrease in BTM; for example, s-CTX decreases by 20% after breakfast
Exercise	Changes occur but depend on type of exercise and age of subjects
Menstural	Minor decreases in bone resorption and increases in bone formation during luteal phase
Seasonal	Minor decreases in BTM over winter
Diet	Small reduction in BTM immediately following calcium supplementation

Uncontrollable Sources of Biological Variability

- Age and Renal Function
  BTM levels are significantly higher in children, particularly in the first year of life and during puberty [31]. After mid-puberty, BTM levels decrease but it is not until the fourth decade of life when they reach the baseline values. Thereafter, the majority of BTMs remain constant in men. In women however a marked increase is noted at the menopause. In the elderly, an increase in the levels of Oc as well as other markers metabolized and/or excreted by the kidney (pyridinoline crosslinks and related peptides) is noted due to gradual renal impairment which occurs during aging.
- Gender
  Compared with their female counterparts, BTM levels are higher in men in their third and fourth decades. As for older ages, however, the levels are higher in postmenopausal women [32].
- Ethnicity
  Bone resorption markers are lower in black youngsters compared with their white counterparts. Though, this difference only becomes apparent in women after menopause [32].
- Fractures
  The levels of BTMs vary throughout the fracture healing process. These changes are dependent on various factors, including the size of the fracture and the time needed for it to heal [33]. During the first 4 weeks of fracture, bone resorption and formation markers both increase by 20±50% and remain elevated for 6 months to one year.
- Pregnancy and Lactation
  During pregnancy and lactation, the maternal skeleton is required to provide the growing fetus and infant with more calcium [34]. Thus, bone turnover ratio (Dpd/Oc) rises during pregnancy. This is mainly because of placental clearance of Oc during this time. At term, bone resorption (NTX) and formation markers (P1NP) are increased by some 200% and 60%, respectively.
  After delivery, urinary NTX and CTX levels decrease but the levels of less bone-specific markers such as Pyd still continue to increase. During the first months of lactation, there is an elevation in BTM levels, which based on the results of some studies is about twice the level noted in aged- matched non-lactating subjects.
- Drugs
  Antiresorptive treatments for osteoporosis and other metabolic bone diseases such as HRT, selective estrogen receptor modulators and bisphosphonates, rapidly reduce BTMs by up to 70% [35]. Corticosteroids

promptly inhibit bone formation [36]. This is reported as a significant and rapid fall in Oc levels followed by a delayed and mild decrease in P1CP, P1NP and BALP values. Anti-convulsants and GnRH agonists both increase markers of bone turnover significantly. Thiazide diuretics, however, have a decreasing effect on bone turnover. Oral contraceptives are believed to increase serum and urinary calcium, Oc and urinary levels of Pyd and Dpd [37]. This effect is reported to be age-dependent.

- Diseases
  Apart from metabolic bone diseases, certain non-skeletal diseases such as liver or kidney disorders may also affect markers of bone turnover. Certain metabolic bone diseases such as Paget's disease, primary hyperparathyroidism, thyrotoxicosis, and acromegaly are responsible for increased levels of both bone formation and resorption markers [38]. This is while Cushing's disease or multiple myeloma may cause an increase in bone resorption and a decrease in bone formation markers. Mild decrease in bone formation and resorption markers at the same time is reported in patients with diseases such as hypoparathyroidism or hypopituitarism.
- Immobility
  Resting is associated with a very rapid increase in the values of bone resorption markers [39]. Urinary excretion of Pyd and Dpd are significantly increased after only 2 days of resting. Non- significant or no change is reported for the markers of bone formation during bed rest or immobility.
- Between-day variability
  The day-to-day variation in BTMs ranges between 16–26% for the urinary excretion of Pyd and Dpd, 7–25% for free pyridinoline, 13–35% for NTX, 12–35% for CTX, and 10–12% for TRAP [40].

Controllable Sources of Biological Variability

- Circadian rhythm
  In adults, circadian rhythm is the main source of undesirable but controllable biological variability. Controlling the time of sample collection therefore is of great importance. Except for alkaline phosphatase, which has a long half-life, the highest values of the markers are measured in the early morning hours and the lowest are noted late in the afternoon [41].
  As for BALP, the peaks are measured between 11:00 and 14:00 and another at 23:30. Compared with formation markers, resorption markers have a significantly greater amplitude of change during the circadian cycle [42]. The steepest morning decline has been described for

serum CTX. Bisphosphonate treatment and calcium supplementation, if taken at night, can suppress the circadian rhythm of bone resorption markers.

- Menstrual status
  A 10-20% variability is noted in BTM levels across the menstrual cycle [43]. Several studies have shown higher bone formation markers during the luteal phase, and higher bone resorption markers during the mid -follicular, late-follicular and early luteal phases.
- Seasonal effects
  While overall seasonal changes are reported to be responsible for only up to 12% of the variability in BTM levels, some studies consider the fluctuations of vitamin D repletion as the reason behind the higher difference between BTM levels measured in summer and winter [44]. High serum levels of Oc is reported during winter and spring; this is while BALP has an inverse rhythm with the lowest amounts reported in the winter and spring. On the contrary, no significant seasonal rhythm is reported for P1CP. Most bone resorption markers, on the other hand, are higher during the winter time. A single study however has shown high urinary Pyd excretion during the summer time.
- Physical activity
  Exercising has both long-term and acute effects on the variability of bone turnover markers [45]. Moderate intensity resistance training is reported to reduce bone resorption in short time, improving the overall bone turnover rate.
- Diet
  Except for HYP and CTX, diet, particularly collagen ingestion has no effect on serum/urinary levels of most BTMs [46]. The effect of the fasting–eating pattern on BTMs is however stronger than that of the physical activity. Fasting greatly affects the urinary and serum levels of CTX [47].

2.2.6 Conclusion

Considering the above mentioned facts, it is considered that the combination of several biomarkers and BMD at the same time could be useful in improving the identification of individuals at high risk for fracture [48].
As the existing BTMs could also be classified into two groups, as following, the selection of biomarkers should be made based on the final goal of the measurement system.

- BTMs that predict Bone Loss
  - Bone Formation Markers: P1NP, BALP, Oc

    - Bone Resorption Markers: Dpd, CTX, NTX
- BTMs that predict Fracture
    - Bone Formation Markers: BALP, P1CP, P1NP, Oc
    - Bone Resorption Markers: TRAP, CTX, NTX

2.3 Bone biosensors: knowing the present and predicting the future

2.3.1 Current approaches to assess bone remodeling

As mentioned in Chapter 1, bone health depends on how the cellular mechanisms in the body create balance in the remodeling process [49]. Over the past few decades, research has been conducted in the field of biosensors to study bone-cell mechanosensation and detect the concentration of BTMs in biological samples for robust diagnosis.
Technological developments have greatly enhanced assay performance producing reliable, rapid, non-invasive cost effective biosensors with improved sensitivity and specificity which can help improve Point-of-Care (POC) through real-time and remote health monitoring; the use of these devices is still limited to research and cannot be deployed in clinical practice because of their limitations and setbacks. In the following, the latest advancements in the field of bone biosensing technologies are provided.
Based on the existing literature, bone biosensors can be classified in three main categories (Table 2.2):

Table 2.2: Existing bone biosensors

Device	Characteristics	Pros & Cons
IMPACT3500 [50]	**Technology:** Strain gauge **Measures:** Strain (Elastic range, fatigue limit, occurrence of fractures **Usage:** Monitoring implant strain **Location:** Implant **LoD:** Elastic range: 300 μs (100-400 μs), fatigue limit: 150 μs	**Pros:** Real-time study **Cons:** Invasive, non-biodegradable, dependency of sensor response substantially on the position of the neutral axis
Biomechanical bone sensor [51][52]	**Technology:** Piezoelectric transducers **Measures:** Frequency response function (FRF) **Usage:** Monitor structural dynamic parameters of bones **Location:** Healing of critical bones after surgery **LoD:** Damping ratio: 0.035	**Pros:** Direct evaluation **Cons:** Invasive, non-biodegradable

Continued on next page

Table 2.2 – *Continued from previous page*

Device	Characteristics	Pros & Cons
Multi-axial bone sensor	**Technology:** Piezoresistive shear stress sensor **Measures:** Stress, resolution, response to tensile and bending loads **Usage:** Monitor healing process at fracture/graft site **Location:** Injured Bone **LoD:** Sensitivity: 0.13 $\frac{mV}{(mA.MPa)}$ for 1.4 N full scales shear force range, mean hysteresis Error: 3.5% [53] Resolution to 100 Pa, in 1 s- Response to tensile and bending loads up to 250 kPa [54]	**Pros:** Direct evaluation **Cons:** Invasive, non-biodegradable
Sirivisoot biosensor [55]	**Technology:** CNT **Measures:** Changes in CNT conductivity, osteoblast adhesion **Usage:** Release bone growth factor-Monitoring bone remodeling **LoD:** 20% increase in osteoblast adhesion	**Pros:** Biodegradable, improved bone growth **Cons:** Invasive

Continued on next page

Table 2.2 – *Continued from previous page*

Device	Characteristics	Pros & Cons
Nanofet sensor [56]	**Technology:** Label-free nanowire field effect transistor **Measures:** Proteins released by osteocytes under mechanical stress **Usage:** Studying load-induced remodeling process **Location:** Serum **LoD:** 10 fg/mL	**Pros:** Non-invasive, Label-free **Cons:** Indirect evaluation
Automated assay	**Technology:** Automated assay [57] **Measures:** P1NP **Usage:** Assessing serum P1NP levels (useful in osteoporosis) **Location:** Serum **LoD:** 5 μg/L	**Pros:** Fully automated **Cons:** Single marker
Multiplex Automated Assay	**Technology:** Automated assay **Measures:** P1NP, CTX, Oc, PTH [58] **Usage:** Assessing several biomarkers (useful in osteoporosis) **Location:** Serum **LoD:** 0.26g/L, 0.002g/L, 0.51g/L, 0.39 ng/L	**Pros:** Multiple markers, Fully automated **Cons:** Trained staff, laboratory equipment
Multiplex Automated Assay	**Technology:** Automated assay **Measures:** CTX, Oc, PTH [59] **Usage:** Assessing several biomarkers (useful in osteoporosis) **Location:** Serum	**Pros:** Multiple markers, Fully automated **Cons:** Trained staff, laboratory equipment

Continued on next page

Table 2.2 – *Continued from previous page*

Device	Characteristics	Pros & Cons
Calcium microchip [60]	**Technology:** Reflectance measurements from arsenazo III **Measures:** Calcium ions **Usage:** Assessing serum calcium levels (useful in different diseases) **Location:** Serum **LoD:** 2.68×10^{-5} M	**Pros:** Non-invasive **Cons:** Single marker
TRAP sensor [61]	**Technology:** Electrochemical cantilever **Measures:** TRAP, TRAP 5a, TRAP 5b **Usage:** Assessing Serum TRAP levels (useful in osteoporosis) **Location:** Serum	**Pros:** Non-invasive, high accuracy, low blood sample **Cons:** Single marker
CTX sensor [62]	**Technology:** Label-free electrochemical **Measures:** CTX **Usage:** Assessing Serum CTX levels (useful in osteoporosis) **Location:** Serum **LoD:** 50 ng/mL	**Pros:** Non-invasive, Label free, High accuracy, low blood sample **Cons:** Single marker

2.3.2 Biomechanical Sensors

In early 1892, Wolff suggested that stress plays an important role in determining bone structure, adding that this effect becomes more prominent during overload and disuse scenarios [63]. Moreover, currently used x-ray imaging systems cannot provide the accurate information needed about the biomechanical quality of bone regeneration at the bone graft or implant site. Thereafter more attention was focused on mechanically-induced adaptation of bones [64]. During the past decades, different sensors were therefore developed to non-invasively assess bone growth and strength [65][66][67][68]. While strain gauges are the gold-standard for in-vivo measurement of bone strain, their use in humans is limited because of the need for surgery to implant the sensors and cyanoacrylate adhesives to bond the sensors on the bones. Numerous extracellular sensors are fabricated for bone-cell mechanosensation in live subjects [69]. When bone is stressed in a succession of load-unload cycles, repeated microscopic damage to the bone occurs. The slow and overtime bone deformation process also known as strain in the "fatigue zone," may lead to fracture [70]. The IMPACT 3500 project showed that monitoring the deformation of femoral implants is a powerful tool for identifying dangerous overloads, anticipating implant failures and observing the healing process [50]. In this technique, the implant strain was measured using a resistive 5 kΩ strain gauge bonded to the floor of the implant cavity.
Yang et al similarly developed a flexible, implantable sensor array for measuring surface strain on live bones. They reported that the Polydimethylsiloxane (PDMS)-based strain gauge with piezoresistive readout could be used as part of an implantable, wireless array for real-time monitoring of bone remodeling process [66].
Vibrational analysis of bones has also been used to assess the diseased and fractured bones in research. Lack of reliability and reproducibility of the results however has limited its use in clinical practice. In this regard, OsteosonicTM was built by NASA to monitor bone fractures through analyzing the vibration response of bone tissue [71]. In 2003, Nogata et al, similarly estimated bone quality using ultrasound [72]. The method was based on the difference in the speed of ultrasound propagation through a two-dimensional area fraction of cancellous bone. Considering the good correlation between BMD values measured by DXA and the bone area fraction assessed by ultrasound, the technique is believed to be helpful in diagnosing osteoporosis.
Later, scientists developed a mechanical pressure sensor that could be embedded within orthopedic implants, to monitor the bone healing process at the fracture site [73]. The ultrasonic device measured the mechanical loading on the implant through studying the fluid level in the spirals.

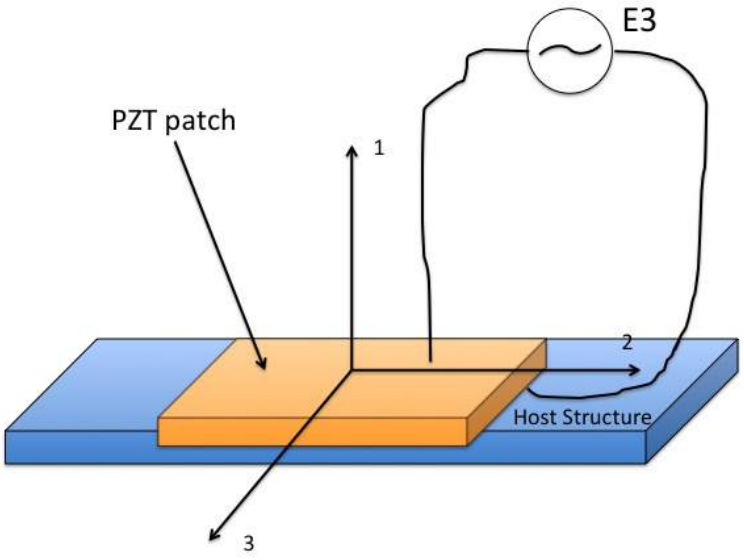

Figure 2.4: PZT patch bonded to a 1D slender structure.[2]

Piezoelectric sensors are shown to provide reproducible response regarding the changes in the mechanical properties of bones. Bhalla et al therefore used piezoelectric ceramic (PZT) transducers to evaluate mechanical and structural dynamic properties of bones, including modal frequencies and corresponding damping ratios derived from frequency response function (FRF) [51]. They reported that the technique could be used for monitoring the bone healing process after surgery as well as the diagnosis of ailments such as osteoporosis. (Figure 2.4)
Bender et al also used piezoelectric sensors to monitor capsule formation through studying the changes in mechanical properties of the tissue surrounding the implant. The sensor helped provide the surgeon with post-operative status of the implant [52].

Hsieh et al developed a contact-type micro piezoresistive sensor to measure shear stress at the knee prosthesis site using Micro-electro-mechanical system (MEMS) technology [53]. The fabricated sensor exhibited a sensitivity of 0.13mV/mA-MPa for a 1.4N full-scale shear force range and the overall mean hysteresis error of 3.5%. Alfaro et al also developed a MEMS

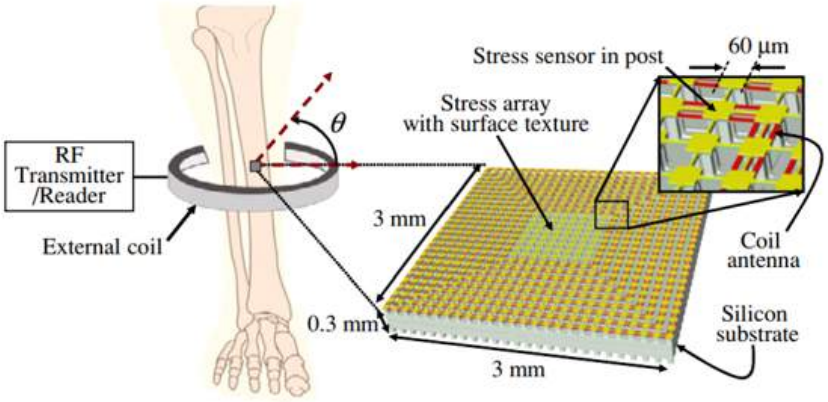

Figure 2.5: Envisioned implantable CMOS-MEMS multiaxis stress sensor.[3]

stress sensor to detect shear stress at a microstrain scale in bone [54]. The ultra-miniature wireless sensor was comprised of an array of piezoresistive sensors that could be permanently implanted within bone to assess new cell growth. (Figure 2.5)

The scientists later investigated the idea of making biodegradable versions of such devices to overcome the need for a second surgery to remove the device from the healed fracture site. Sirivisoot et al developed a biosensor composed of a conductive, biodegradable polymer layer that could sense and control bone regrowth near the newly implanted orthopedic material [55]. The biosensor released bone growth factor to help improve bone formation and thus the regeneration of the tissue needed for the success of the orthopedic implant. The polypyrrole and poly-lactic-co-glycolic acid polymer layers also degraded following sufficient bone grew, resulting in changes in conductivity that can be measured by the carbon nanotubes (CNTs) grown out of the anodized titanium (Ti) on the sensor. This was also used to inform the surgeon regarding the amount of bone formed around the implant at different stages. Li et al fabricated a sensitive Nano-field-effect transistor (FET) biosensor to study osteocyte mechanotransduction [56]. The novel nanomanipulation-based label free sensor was designed to assess the amount of proteins released from the mechanically-stimulated osteocytes. A novel microbend optical biosensor, inspired by Brain Neural Network, was also developed to improve the performance of biosensors in detecting early osteoporosis [74]. The sensor was used to detect and measure surface displacement, pressure and strain on live bones.
Later Umbrecht et al developed a wireless implantable passive strain sen-

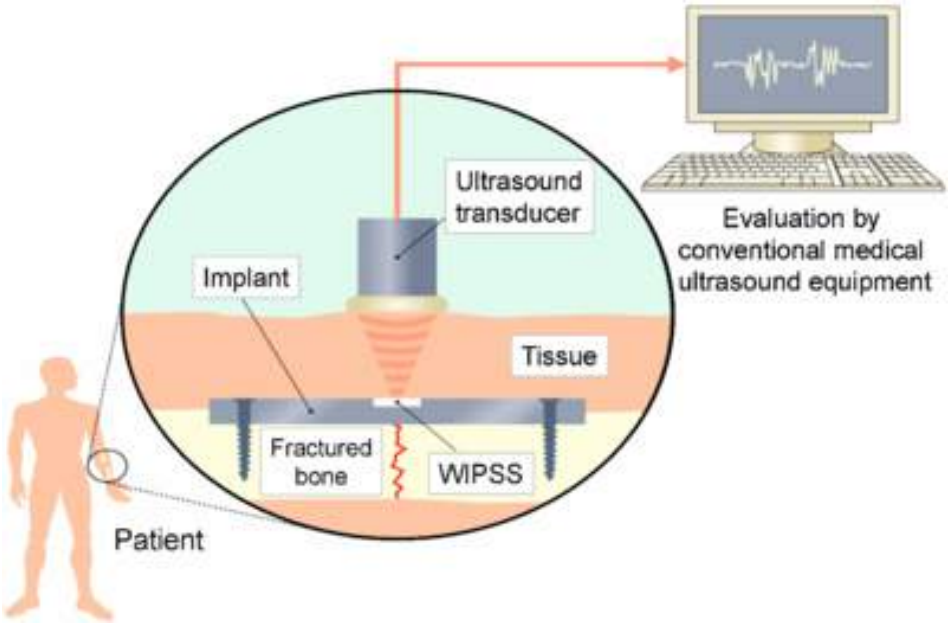

Figure 2.6: Schematic of the WIPSS sensor concept.[4]

sor (WIPSS) for monitoring the deformation of orthopedic implants based on a hydro-mechanical amplification effect [75]. (Figure 2.6) The biocompatible ultrasound-based sensor had a strain resolution of 1.7 ± 0.2e-5 over dynamic inputs of 0.1-5 Hz.

2.3.3 Multiplex Automated Assays

While the biomechanical sensors mentioned above can provide the scientists with information on pressure and strain levels on live bones, BTMs (Appendix A) can describe the status of the cellular and extracellular components of the skeletal matrix, reflecting bone metabolism. When applied and interpreted correctly, these inexpensive and comparatively non-invasive tools can help with the diagnosis and treatment of metabolic bone diseases [76].
Currently, BTMs are measured individually by manual or automated immunoassays. These assays were first confined to urine samples; newer techniques, however, measure serum levels of the markers, overcoming the need for correction for urinary creatine levels. Single assay methods have several limitations, including limited precision and need for large sample volumes of 50 to 300 μL in both techniques and significant labor time in the

manual assays.
Multiplex protein arrays, which enable simultaneous detection of multiple analytes, have overcome some of these problems [77][78]. Compared to traditional techniques, multiplex assays are miniaturized, have higher sensitivity, and need less sample and reagent volume [79]. Schafer et al reported great improvement in short and long-term assay variability using automated immunoassay techniques compared with ELISA [80].
Claudon et al developed an automated multiplex assay to assess CTX-1, P1NP, Oc, and intact PTH simultaneously in 20 μL of serum [58]. They reported that the automated protein – array chip demonstrated similar analytical precision compared with single assay methods. The new technique, however, needed less sample volume and showed improved analytical sensitivity.

2.3.4 Label–free biosensors

The majority of techniques mentioned above or currently used to detect biomarkers need certain radio-, enzymatic- or fluorescent-labeling to report the binding event. There are novel technologies, also known as label-free biosensors, which do not require labeling and thus allow complexes to be screened with minimal assay development [81]. Several label-free bone biosensors were developed during the past years, none of them are routinely used in clinical practice as they were designed to assess a single marker and many studies have reported that studying the alteration of the serum/urine levels of a single marker is not sufficient for assessing bone health as their changes are not disease-specific [82].
A microchip-based sensor was developed by Caglar et al for determining calcium ion levels [60]. The technique measured reflectance index of arsenazo III immobilized on the surface of polymer beads. They reported that the microfluidic sensor showed good agreement with other tools used for calcium ion measurement over a physiological range, adding that its results were less influenced by competing ions in the samples.
In another biosensor, the concentration or activity of tartrate-resistant acid phosphatase (TRAP) in blood was assessed using a quartz crystal microbalance (QCM) sensor [61]. In this biosensor, osteoclast function was studied through measuring the position deflection of a cantilever beam modified with antibodies against total TRAP, TRAP 5a or TRAP 5b using an optic detection plate.
Yun et al developed an electrochemical biosensor for quantitative POC measurement of CTX [62]. The label-free immunosensor, based on Electrochemical Impedance Spectroscopy (EIS), had a detection limit of 50 ng/mL and a dynamic range of up to 3 μg/mL. (Figure 2.7)
The sensors mentioned in this category have shown promising results in

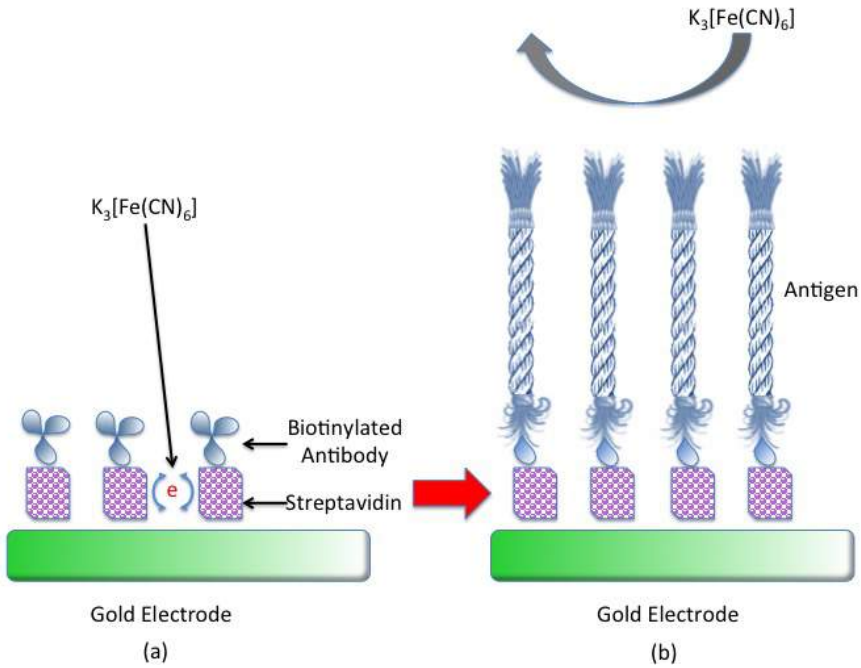

Figure 2.7: Schematic representation of a label-free immunosensor for bone maker detection. a) A self-assembled monolayer of dithiodipropionic acid deposited on a gold surface with streptavidin immobilized next as a self-assembled monolayer. Then the biotinylated antibody was bound to the streptavidin. b) Antigen-antibody binding reaction and how it hinders the interfacial electron transfer reaction of $K_3[Fe(CN)_6]$.adapted from Yun et al[62]

measuring serum levels of a certain biomarker. As mentioned earlier, measuring a single bone turnover marker is not sufficient in identifying individuals at-risk of fracture or for monitoring the osteoporosis treatment process, suggesting that development of a multiplex biosensor could be valuable [83].

2.3.5 Conclusion and Future Directions

This section seeks to provide an insight into the current state-of-the-art in the bone biosensor field, stressing that new strategies must be considered to bring this important technology into clinical practice.
Bone densitometry and other noninvasive imaging methods, currently used

to assess bone quantitatively and qualitatively, tell us little about changes in bone material composition and biomechanical design during the healing process [49]. According to the above mentioned explanation and Table 2.2, sensors categorized in group one (biomechanical sensors) provide valuable information about shear stress and biomechanical quality of bone regeneration at the graft or implant site. The poor bone quality at the fracture site is associated with increased mechanical stress on the implant as well as fracture movement under loading, resulting in fixation failure and increased fracture displacement [84].
Then again, monitoring of bone fracture healing is often performed based on complex imaging techniques and thus it is not possible to observe the patient during physiotherapy and outpatient visits [85]. As a result monitoring the biomechanics of the fractured bone and its remodeling process could be of great importance for clinicians to establish appropriate clinical treatment principles to minimize complications and enhance the patient's quality of life [86].
In other words, this group can help physicians to monitor the healing process of the live bone after the surgery but there are still concerns about their biodegradability over time. We are expecting the next generation of these biodegradable biomechanical sensors to be less invasive and provide physicians with more evidence about the quality of live bone.
PZT patches are believed to have several advantages over similar technologies used for this purpose, the most important of which is their low-cost and negligible weight [87]. However, their bio-compatibility (as the most popular is lead zirconate titanate) and the acquisition of the signatures has limited their use. It could be possible that in the near future nano-sized biodegradable PZT patches will be implanted on bones to monitor their mechanical properties, utilizing advanced wireless telemetry to further facilitate remote signature acquisition.
Sensors classified under the second and third group, on the other hand, are used to gather information on the metabolic status of the bone through measuring serum or urine levels of different BTMs. As mentioned in the previous section, BTMs are useful in understanding bone physiology during the modeling and remolding phases, predicting fracture risk, and monitoring bone response to treatment. The sensors in these groups are non-invasive. The sensors in the second group (Multiplex Automated Assays), can assess several markers at the same time but require expensive equipment and skilled technicians and thus are not always available.
In order to overcome these concerns, the sensors in the third group were developed. At the time being, the developed label–free biosensors, which work without the need for skilled technicians, can only assess a single marker at a time. But considering the fact that a single molecular marker cannot provide sufficient information to assist the clinicians in monitoring

the bone remodeling process, further studies are needed to develop label-free miniaturized sensors that can detect several markers simultaneously [26].

2.4 Protein immobilization strategies for biosensing purposes

Protein immobilization strategies can be classified based on their selectivity, ranging from nonspecific binding with low control on protein orientation (random adsorption), to more complex methods with high controllability, reproducibility, and stability (site-specific functionalization) [88]. An overview is provided in Table 2.3.

2.4.1 Physisorption

The most simple and inexpensive approach to immobilizing proteins on a surface is physisorption (physical adsorption), where proteins can be adsorbed to various surfaces via non-covalent interactions/intermolecular forces (such as van der Waals, hydrogen bonding interactions, or combination of those) [89]. Although physical adsorption offers some advantages (simplicity, no need for toxic reagents or sophisticated chemical protocols and possible reusability of the substrate), it generally leads to a surface coated with proteins in a random orientation or via multiple binding sites which can give rise to many disadvantages (reducing the accessibility to its functional sites or conformational changes influencing the proteins activity) [90][91].
An additional drawback is that physisorption is generally weak, and thus the adsorbed layer is not stable and highly dependent on environmental conditions such as pH, ionic strength and temperature. Immobilization density depends on protein size, as well as physicochemical surface properties; thus spacers such as polyethylene glycol (PEG) are widely used to reduce steric hindrance particularly when the immobilization density is too high [92].

2.4.2 Electrostatic interaction

Electrostatic or ionic interactions provide a stronger binding of immobilized molecules and thus are more frequently exploited in biochemical assays [93]. Ionic interactions generally occur between the negatively charged gold

surface and the positively charged terminals on the protein. Typical positively charged functional groups such as protonated amine (R-NH_3^+) and quaternary ammonium cations (NR_4^+) as well as negatively charged carboxylate (R-COO^-) and sulfonate (R-SO_3^-) ones are mainly involved in the electrostatic interactions.
While this method does not change protein conformation in a substantial extent, the usage of highly charged supports, which can interact with charged substrates or products can limit its use [94]. Moreover, despite its simplicity and reversibility, it is difficult to find suitable conditions under which the enzyme/antibody remains both strongly bound and fully active.

2.4.3 Covalent binding

Immobilization of proteins based on the formation of covalent bonds is among the most widely used techniques, mainly because of the stable nature of the formed bonds [95]. However, covalent linkage may suffer from reduced activity of proteins (by forming linkage on active sites), toxic reagents, long incubation times, and complicated chemistry [96].
The activation processes are generally designed to generate electrophilic groups on the support, which in the coupling step, react with the strong nucleophiles from the proteins. In other words, for covalent binding, the immobilization surface is activated via reactive reagents and then reacts with amino acid residues on the protein, not involved in the reaction mechanism, and forms an irreversible linkage. The most frequently used reactions involve lysine (ϵ-amino group), cysteine (thiol group), and aspartic and glutamic acids (carboxylic acid group) as the side chains of the amino acids. Bifunctional spacer molecules are commonly used in this approach.

Amine Chemistry

The amino groups of proteins (-NH_2) are the most commonly used moieties for covalent immobilization.

N-Hydroxysuccinimide (NHS) NHS s are the most commonly used agents that react with protein amine groups, with the formation of stable peptide bonds [97][98]. NHS is also often used as an activating reagent for carboxylic acids. Activated acids (basically esters with a good leaving group) can react with amines to form amides [99]. (Figure 2.8)

1-ethyl-3-(3-dimethylamonipropyl) carbodiimide (EDC) - amide EDC, the most frequently used carbodiimide, reacts with carboxylic acid to form

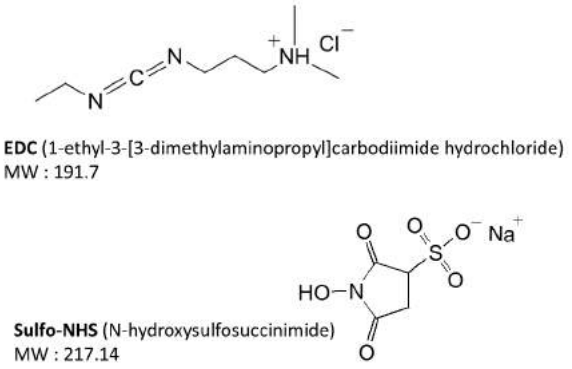

(a)

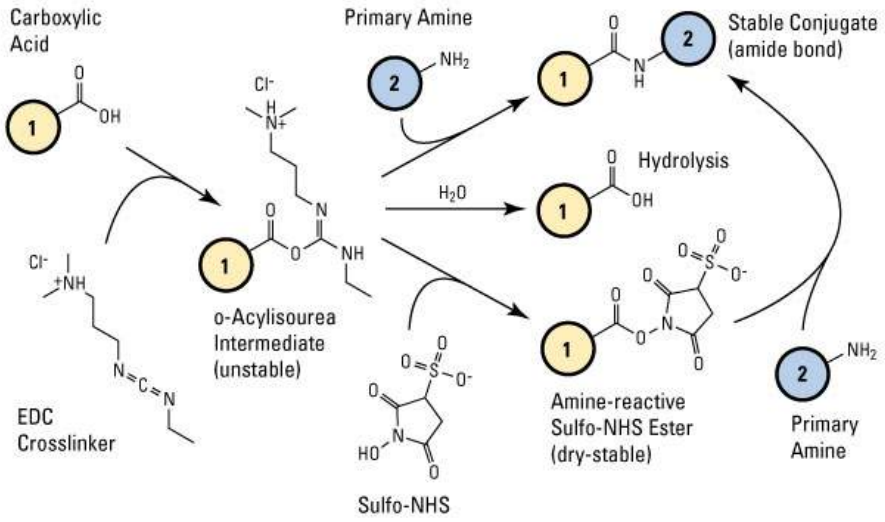

(b)

Figure 2.8: a) Chemical structure of EDC & sulfo-NHS, b) EDC & sulfo-NHS crosslinking reaction scheme. Molecules (1) and (2) can be peptides, proteins or any chemicals that have respective carboxylate and primary amine groups.

an o-acrylisourea intermediate, which subsequently reacts with primary amines to form amide bonds [100][101]. Reaction of o-acrylisourea with amines is slow and can be hydrolyzed in aqueous solution. Thus, EDC is usually used with NHS. (Figure 2.8)

Carboxylate-EDC+NHS-amine NHS esters can be formed using carbodiimide (EDC), NHS, and carboxylates to immobilize proteins [102]. The carboxylic group would later be activated with the NHS ester, and then covalently linked to the amine groups of antibodies. (Figure 2.8)
Other chemistries used to immobilize proteins via the exposed amine groups include sulfhydryl (epoxide), iso(thio)cyanate, azlactone, p-nitrophenyl ester, glutaraldehyde, sulfonyl chlorides, and cyanogen bromide [103].

Carboxyl Chemistry

The immobilization of proteins using the carboxylic side chains is of great interest, as the amino acids glutamic and aspartic acid constitute a major fraction of the surface exposed amino acids [104]. The carboxylic acid function of these amino acids, along with the C-terminus, can react with amines using the routine coupling chemistry also used for solid phase peptide synthesis. This coupling reaction is activated by a carbodiimide like N,N'-dicyclohexyl carbodiimide (DCC) or EDC and results in a rapid and quantitative formation of a peptide bond.

Thiol Chemistry

Free cysteines have a relatively low natural abundance in proteins and thus are an interesting tag for immobilization reactions as random orientations or multiple contact points are less a problem [105]. They contain a reactive thiol (SH) group, which is more nucleophilic than a primary amino group. In proteins with no free cysteines, the aminoacids can be inserted at a site of interest by site-directed mutagenesis. Maleimides and vinyl-sulfone groups are the most commonly used chemical groups to selectively modify surfaces toward covalent protein coupling via the free thiols [106] .
A covalent bond can also be established to substrates functionalized with disulfide probes via a thiol-disulfide exchange under oxidative conditions. This reaction is selective for cysteines, but similar to natural disulfide bonds, these couplings are not resistant to reducing agents like mercaptoethanol or Dithiothreitol (DTT) [107].

Tyrosine and Tryptophan

Tyrosine and tryptophan are relatively the rarest amino acids on protein surfaces and can be genetically introduced without changing the overall charge state or redox sensitivity [108]. They, however, are often overrepresented near active sites of proteins and thus targeting them for modification or immobilization needs careful consideration and specific conditions (acidic environment), which may have undesirable affects on the protein's structure and function [109].

2.4.4 Bioaffinity immobilization

The bioaffinity interaction or biospecific adsorption is based on the principle of complementary biomolecules interactions, which represents its biggest advantages, high selectivity, high specificity, and oriented protein immobilization [110]. Additionally, bioaffinity immobilization can be reversed using chemical treatment, pH change, or heat treatment [111]. Avidin-biotin, protein A/G-antibody, genetically engineered protein affinity ligands, DNA hybridization, and aptamers are common approaches in this strategy.

Avidin-biotin

One of the well-established affinity-based immobilization technique is based on the strong interaction between (strept)avidin (66-69 kDa tetrameric glycoprotein) and biotin (water-soluble vitamin B), and biotinylated proteins [112]. Avidin binds to biotin via an exceptionally strong noncovalent interaction, which is rapid and nearly insensitive to pH, temperature, proteolysis, and denaturing agents. It is also stable, showing no significant loss of activity over time. One downside of using the avidin-biotin system is the high cost of the proteinaceous-binding reagent.

Protein A/G-antibody

Protein A and G are both popular antibody (Immunoglobulin G (IgG)) immobilizing reagents, extracted from bacteria. They specifically bind to the constant fragment crystallizable region (Fc region) of IgG. Thus, the variable Fragment antigen-binding (Fab) region of IgG is accessible to Ag binding [113]. An additional benefit of using protein A/G is that antibody can be detached by acid treatment and the surface made reusable.

Site-Specific, Covalent Immobilization

Site-Specific covalent immobilization, an oriented covalent coupling of a protein to a substrate is performed in a controllable way via a unique chemical group or sequence introduced in the protein at a site-specific location [114]. Several bioorthogonal chemistries, also known as 'click' reactions such as, copper or ring-strain catalyzed azide-alkyne cyclo-additions, Staudinger-ligations, Diels-Alder cyclo-additions, thiol-ene additions, and oxime formation are commonly used in this regard.

Affinity tags

One of the most important advantages of fusion proteins (chimeric proteins), also known as affinity tags, is the possibility to attach a generating recombinant fusion part, the preparation of which can sometime be very expensive or complicated, for immobilization of various proteins [115]. Polyhistidine tags, in which the C- or N-terminus of proteins are genetically engineered to have an oligohistidine (His) segment that specifically reacts with metal ions immobilized on the matrix, are of the most common applications of this technique [116].
Although the affinity of these tags is much weaker than that of the streptavidin-biotin linkage, the immobilization could be reversed by adding competing chelating agents such as ethylenediaminetetraacetic acid (EDTA), and the controlled orientation of immobilized proteins is another benefit. The interference of large number of metal-binding proteins or additional interactions between the immobilized protein and affinity support, on the other hand, is a serious limitation.

2.4.5 Conclusion

As described above, each immobilization mechanism has its drawbacks and advantages with relative importance depending on fabrication constraints and application requirements. Thus, attempts have been made to address the limitations of individual mechanisms, aiming for better protein activity, more control for protein orientation, less steric hindrance, more protein patterning density, and less nonspecific protein adsorption using a combined method.

Table 2.3: Most common immobilization techniques, their pros and cons

Technique		Pros	Cons
Physisorption		Inexpensive; simple; no need for toxic reagents or sophisticated chemical protocols; possible reusability of the substrate	Random orientation of the antibody or multiple binding sites, reduced accessibility to the functional sites or conformational changes influencing protein activity, weak attachment
Electrostatic Interaction		Simplicity, reversibility, stronger binding and less conformational change compared with physisorption	Limited use because of need for highly charged support and suitable condition for antibody/enzyme to remain both strongly bound and fully active
Covalent binding	NHS EDC-amine Carboxylate- EDC+NHS-amine Carboxyl Chemistry Thiol Chemistry Tyrosine & Tryptophan	Stable nature	Reduced activity of proteins (because of linkage on active sites), need for toxic reagents, long incubation times, complicated chemistry
Bioaffinity immobilization	Avidin- Biotin Protein A/G-Ab Site-specific, covalent immobilization Affinity tags	High selectivity, high specificity, oriented protein immobilization, reversibility	High cost, complicated protocols

References

[1] A. Patel, E. Puzas, and J. Baumhauer, "Practical osteoporosis management: topical review," *Foot Ankle Int.*, vol. 31, no. 4, pp. 354–360, 2010.

[2] A. Morrison, T. Fan, S. Sen, and L. Weisenfluh, "Epidemiology of falls and osteoporotic fractures: a systematic review," *Clinicoecon Outcomes Res.*, vol. 5, pp. 9–18, 2013.

[3] K. Briot and C. Roux, "What is the role of dxa, qus and bone markers in fracture prediction, treatment allocation and monitoring?" *Best Pract Res Clin Rheumatol*, vol. 19, no. 6, pp. 951–964, 2005.

[4] S. L. Bonnick and L. Shulman, "Monitoring osteoporosis therapy: bone mineral density, bone turnover markers, or both?" *Am J Med*, vol. 119, no. 4 Suppl 1, pp. S25–31, 2006.

[5] C. A. Cefalu, "Is bone mineral density predictive of fracture risk reduction?" *Curr Med Res Opin*, vol. 20, no. 3, pp. 341–349, 2004.

[6] M. Buyse, D. Sargent, A. Grothey, A. Matheson, and A. de Gramont, "Biomarkers and surrogate end points—the challenge of statistical validation," *Nat Rev Clin Oncol*, vol. 7, pp. 309–317, 2010.

[7] H. Johansson, J. A. Kanis, A. Oden, O. Johnell, and E. McCloskey, "Bmd, clinical risk factors and their combination for hip fracture prevention," *Osteoporos Int*, vol. 20, no. 10, pp. 1675–1682, 2009.

[8] R. K. McCormick, "Osteoporosis: integrating biomarkers and other diagnostic correlates into the management of bone fragility," *Altern Med Rev*, vol. 12, no. 2, pp. 113–145, 2007.

[9] T. Bhattarai, K. Bhattacharya, P. Chaudhuri, and P. Sengupta, "Correlation of common biochemical markers for bone turnover, serum calcium, and alkaline phosphatase in post-menopausal women." *Malays. J. Med. Sci.*, vol. 21, no. 1, pp. 58–61, 2014.

[10] J. Lenora, K. K. Ivaska, and P. Gerdhem, "Use of bone turnover markers in osteoporosis," *Clin Rev Bone Miner Metab*, vol. 8, no. 1, pp. 1–14, 2010.

[11] O. Johnell, A. Odén, C. De Laet, P. Garnero, P. D. Delmas, and J. A. Kanis, "Biochemical indices of bone turnover and the assessment of fracture probability," *Osteoporos Int*, vol. 13, no. 7, pp. 523–526, 2002.

[12] K. D. Harper and T. J. Weber, "Secondary osteoporosis. diagnostic considerations," *Endocrinol Metab Clin North Am*, vol. 27, no. 2, pp. 325–348, 1998.

[13] J. A. Clowes, N. F. A. Peel, and R. Eastell, "The impact of monitoring on adherence and persistence with antiresorptive treatment for postmenopausal osteoporosis: a randomized controlled trial," *J Clin Endocrinol Metab*, vol. 89, no. 3, pp. 1117–1123, 2004.

[14] D. J. Baylink, "The diagnosis and management of osteoporosis," *Z Rheumatol*, vol. 59 Suppl 1, pp. 42–44, 2000.

[15] N. Yoshimura and World Health Organization, "Absolute risk for fracture and who guideline. bone turnover markers as predictive factors for osteoporotic fractures," *Clin Calcium*, vol. 17, no. 7, pp. 1049–1057, 2007.

[16] P. Garnero, E. Hausherr, M. C. Chapuy, C. Marcelli, H. Grandjean, C. Muller, C. Cormier, G. Bréart, P. J. Meunier, and P. D. Delmas, "Markers of bone resorption predict hip fracture in elderly women: the epidos prospective study," *J Bone Miner Res*, vol. 11, no. 10, pp. 1531–1538, 1996.

[17] P. Desai Meena, M. Khatkhatay, K. Bhanu Prakash, L. Savardekar, R. Shah, and Z. Ansari, "Hormonal profiles and biochemical indices of bone turnover in indian women," *Osteoporos Int.*, vol. 18, no. 7, pp. 923–929, 2007.

[18] K. J. L. Bell, A. Hayen, L. Irwig, M. C. Hochberg, K. E. Ensrud, S. R. Cummings, and D. C. Bauer, "The potential value of monitoring bone turnover markers among women on alendronate," *J Bone Miner Res*, vol. 27, no. 1, pp. 195–201, 2012.

[19] R. Dresner-Pollak, R. Parker, M. Poku, J. Thompson, M. Seibel, and S. Greenspan, "Biochemical markers of bone turnover reflect femoral bone loss in elderly women," *Calcif Tissue Int*, vol. 59, no. 5, pp. 328–333, 1996.

[20] W. M. Drake, D. L. Kendler, C. J. Rosen, and E. S. Orwoll, "An investigation of the predictors of bone mineral density and response to therapy with alendronate in osteoporotic men," *J Clin Endocrinol Metab*, vol. 88, no. 12, pp. 5759–5765, 2003.

[21] N. B. Watts, "Clinical utility of biochemical markers of bone remodeling," *Clin Chem*, vol. 45, no. 8, pp. 1359–1368, 1999.

[22] P. Glendenning, "Markers of bone turnover for the prediction of fracture risk and monitoring of osteoporosis treatment: a need for international reference standards," *Clin Biochem Rev*, vol. 32, no. 1, pp. 45–47, 2011.

[23] G. Wheater, M. Elshahaly, S. P. Tuck, H. K. Datta, and J. M. van Laar, "The clinical utility of bone marker measurements in osteoporosis," *J Transl Med*, vol. 11, p. 201, 2013.

[24] D. C. Bauer, P. Garnero, S. L. Harrison, J. A. Cauley, R. Eastell, K. E. Ensrud, E. Orwoll, and for the Osteoporotic Fractures in Men (MrOS) Research Group, "Biochemical markers of bone turnover, hip bone loss, and fracture in older men: The mros study," *J Bone Miner Res*, vol. 24, no. 12, pp. 2032–2038, 2009.

[25] F. Cosman, J. Nieves, C. Wilkinson, D. Schnering, V. Shen, and R. Lindsay, "Bone density change and biochemical indices of skeletal turnover," *Calcif Tissue Int*, vol. 58, no. 4, pp. 236–243, 1996.

[26] S. Vasikaran, C. Cooper, R. Eastell, A. Griesmacher, H. A. Morris, T. Trenti, and J. A. Kanis, "International osteoporosis foundation and international federation of clinical chemistry and laboratory medicine position on bone marker standards in osteoporosis," *Clin Chem Lab Med*, vol. 49, no. 8, pp. 1271–1274, 2011.

[27] C. Popp-Snijders, P. Lips, and J. Netelenbos, "Intra-individual variation in bone resorption markers in urine," *Ann Clin Biochem.*, vol. 33, no. 347-348, 1996.

[28] M. Seibel, M. Lang, and W. Geilenkeuser, "Interlaboratory variation of biochemical markers of bone turnover," *Clin Chem.*, vol. 47, pp. 1443–1450, 2001.

[29] R. Lequin, "Enzyme immunoassay (eia)/enzyme-linked immunosorbent assay (elisa)," *Clin Chem.*, vol. 51, no. 12, pp. 2415–2418, 2005.

[30] R. Hannon and R. Eastell, "Preanalytical variability of biochemical markers of bone turnover," *Osteoporos Int.*, vol. 11, no. Suppl 6, pp. S30–44, 2000.

[31] M. Midtby, J. Magnus, and R. Joakimsen, "The tromso study: a population-based study on the variation in bone formation markers with age, gender, anthropometry and season in both men and women," *Osteoporos Int.*, vol. 12, no. 835-843, 2001.

[32] Y. Henry and R. Eastell, "Ethnic and gender differences in bone mineral density and bone turnover in young adults: effect of bone size," *Osteoporos Int*, vol. 11, no. 512-517, 2000.

[33] G. Cox, T. Einhorn, C. Tzioupis, and P. Giannoudis, "Bone turnover markers in fracture healing," *J Bone Joint Surg Br*, vol. 92-B, no. 3, pp. 329–334, 2010.

[34] C. More, H. Bhattoa, P. Bettembuk, and A. Balogh, "The effects of pregnancy and lactation on hormonal status and biochemical markers of bone turnover," *Eur J Obstet Gynecol Reprod Biol.*, vol. 106, no. 2, pp. 209–213, 2003.

[35] P. D. Delmas, P. Eastell, P. Garnero, M. J. Seibel, J. Stepan, and for the Committee of Scientific Advisors of the International Osteoporosis Foundation., "The use of biochemical markers of bone turnover in osteoporosis," *Osteoporos Int*, vol. 11, no. Suppl 6, pp. S2–S17, 2000.

[36] A. Dovio, L. Perazzolo, G. Osella, M. Ventura, A. Termine, E. Milano, A. Bertolotto, and A. Angeli, "Immediate fall of bone formation and transient increase of bone resorption in the course of high-dose, short-term glucocorticoid therapy in young patients with multiple sclerosis," *J Clin Endocrinol Metab*, vol. 89, no. 10, pp. 4923–4928, 2004.

[37] V. Gargano, M. Massaro, I. Morra, C. Formisano, C. Di Carlo, and C. Nappi, "Effects of two low-dose combined oral contraceptives containing drospirenone on bone turnover and bone mineral density in young fertile women: a prospective controlled randomized study," *Contraception*, vol. 78, no. 1, pp. 10–15, 2008.

[38] R. Civitelli, R. Armamento-Villareal, and N. Napoli, "Bone turnover markers: understanding their value in clinical trials and clinical practice," *Osteoporos Int.*, vol. 20, no. 6, pp. 843–51, 2009.

[39] M. Heer, N. Baecker, C. Mika, A. Boese, and R. Gerzer, "Immobilization induces a very rapid increase in osteoclast activity," *Acta Astronaut*, vol. 57, no. 31-6, 2005.

[40] A. Blumsohn, R. Hannon, A. al Dehaimi, and R. Eastell, "Short-term intraindividual variability of markers of bone turnover in healthy adults," *J Bone Miner Res.*, vol. 9, no. Suppl 1, p. S153, 1994.

[41] R. Eastell, M. Calvo, M. Burritt, K. Offord, R. Russell, and B. Riggs, "Abnormalities in circadian patterns of bone resorption and renal calcium conservation in type i osteoporosis," *J Clin Endocrinol Metab.*, vol. 74, pp. 487–494, 1992.

[42] A. Schlemmer, C. Hassager, S. Jensen, and C. Christiansen, "Marked diurnal variation in urinary excretion of pyridinium cross-links in

premenopausal women," *J Clin Endocrinol Metab.*, vol. 74, pp. 476–480, 1992.

[43] A. Schlemmer, C. Hassager, J. Risteli, L. Risteli, S. Jensen, and C. Christiansen, "Possible variation in bone resorption during the normal menstrual cycle," *Acta Endocrinol (Copenh)*, vol. 129, pp. 388–392, 1993.

[44] H. Woitge, C. Scheidt-Nave, C. Kissling, G. Leidig-Bruckner, K. Meyer, and A. Grauer, "Seasonal variation of biochemical indexes of bone turnover: Results of a population-based study," *J Clin Endocrinol Metab*, vol. 83, pp. 68–75, 1998.

[45] T. Whipple, B. Le, L. Demers, V. Chinchilli, M. Petit, N. Sharkey, and N. Williams, "Acute effects of moderate intensity resistance exercise on bone cell activity," *Int J Sports Med.*, vol. 25, no. 7, pp. 496–501, 2004.

[46] M. Lang, P. Haag, H. Schmidt-Gayk, R. Ziegler, and M. Seibel, "Influence of ambient storage conditions and of diet on the measurement of biochemical markers of bone metabolism," *Calcif Tissue Int*, vol. 55, p. 497, 1995.

[47] A. Schlemmer and C. Hassager, "Acute fasting diminishes the circadian rhythm of biochemical markers of bone resorption," *Eur J Endocrinol.*, vol. 140, no. 4, pp. 332–337, 1999.

[48] O. Löfman, P. Magnusson, G. Toss, and L. Larsson, "Common biochemical markers of bone turnover predict future bone loss: a 5-year follow-up study," *Clin Chim Acta*, vol. 356, no. 1-2, pp. 67–75, 2005.

[49] E. Seeman and P. D. Delmas, "Bone quality–the material and structural basis of bone strength and fragility," *N Engl J Med.*, vol. 354, no. 21, pp. 2250–2261, 2006.

[50] F. Burny, M. Donkerwolcke, F. Moulart, R. Bourgois, R. Puers, K. Van Schuylenbergh, M. Barbosa, O. Paiva, F. Rodes, J. B. Bégueret, and P. Lawes, "Concept, design and fabrication of smart orthopedic implants," *Med Eng Phys*, vol. 22, no. 7, pp. 469–479, 2000.

[51] S. Bhalla and S. Bajaj, "Bone characterization using piezotransducers as biomedical sensors," *Strain*, vol. 44, no. 6, pp. 475–478, 2008.

[52] J. W. Bender, H. I. Friedman, V. Giurgiutiu, C. Watson, M. Fitzmaurice, and M. L. Yost, "The use of biomedical sensors to monitor capsule formation around soft tissue implants," *Ann Plast Surg*, vol. 56, no. 1, pp. 72–77, 2006.

[53] M. Hsieh, Y. Fang, M. Ju, J. Ho, and S. Ting, "Development of a new contact-type piezoresistive micro-shear-stress sensor," *Proc. SPIE 4755, Design, Test, Integration, and Packaging of MEMS/MOEMS*, no. 285, 2002.

[54] A. Fernando, W. Lee, C. Phil, M. Mark, and K. F. Gary, "Design of a multi-axis implantable mems sensor for intraosseous bone stress monitoring," *J. Micromech Microeng*, vol. 19, no. 8, 2009.

[55] S. Sirivisoot, C. Yao, X. Xiao, W. Sheldon, Brian, and J. Webster, Thomas, "Developing biosensors for monitoring orthopedic tissue growth," *MRS Proceedings*, vol. 950, 2006.

[56] J. Li, "Fabrication and characterization of nano-fet biosensors for studying osteocyte mechanotransduction," Master's thesis, Department of Mechanical and Industrial Engineering Institute of Biomaterials and Biomedical Engineering University of Toronto, 2011.

[57] P. Garnero, P. Vergnaud, and N. Hoyle, "Evaluation of a fully automated serum assay for total n-terminal propeptide of type i collagen in postmenopausal osteoporosis," *Clin Chem*, vol. 54, no. 1, pp. 188–196, 2008.

[58] A. Claudon, P. Vergnaud, C. Valverde, A. Mayr, U. Klause, and P. Garnero, "New automated multiplex assay for bone turnover markers in osteoporosis," *Clin Chem*, vol. 54, no. 9, pp. 1554–1563, 2008.

[59] H. Schmidt-Gayk, E. Spanuth, J. Kötting, R. Bartl, D. Felsenberg, J. Pfeilschifter, F. Raue, and H. Roth, "Performance evaluation of automated assays for beta-crosslaps, n-mid-osteocalcin and intact parathyroid hormone (biorose multicenter study)," *Clin Chem Lab Med.*, vol. 42, no. 1, pp. 90–95, 2004.

[60] P. Caglar, S. A. Tuncel, N. Malcik, J. P. Landers, and J. P. Ferrance, "A microchip sensor for calcium determination," *Anal Bioanal Chem*, vol. 386, no. 5, pp. 1303–1312, 2006.

[61] Y. Chung and Y. Liu, "Biosensor and method for bone mineral density measurements," US Patent 20050059875, Tech. Rep., 2005.

[62] Y.-H. Yun, A. Bhattacharya, N. B. Watts, and M. J. Schulz, "A label-free electronic biosensor for detection of bone turnover markers," *Sensors (Basel)*, vol. 9, no. 10, pp. 7957–7969, 2009.

[63] J. Wolff, *Das Gesetz der Transformation der Knochen*, Hirschwald, Ed. Berlin, Germany, 1892.

[64] D. A. Hoey, J. C. Chen, and C. R. Jacobs, "The primary cilium as a novel extracellular sensor in bone," *Front Endocrinol (Lausanne)*, vol. 3, p. 75, 2012.

[65] G. Bergmann, F. Graichen, J. Siraky, H. Jendrzynski, and A. Rohlmann, "Multichannel strain gauge telemetry for orthopaedic implants," *J Biomech.*, vol. 21, no. 2, pp. 169–176, 1988.

[66] G. Y. Yang, V. J. Bailey, Y.-H. Wen, G. Lin, W. C. Tang, and J. H. Keyak, "Fabrication and characterization of microscale sensors for bone surface strain measurement," *IEEE Sensors*, pp. 1355–1358, 2004.

[67] S. J. Hoshaw, D. P. Fyhrie, Y. Takano, D. Burr, and C. Milgrom, "A method suitable for in vivo measurement of bone strain in humans," *J. Biomech.*, vol. 30, pp. 521–524, 1997.

[68] N. Elvin, A. Elvin, and M. Spector, "Implantable bone strain telemetry sensing system and method," US Patent 6034296, Tech. Rep., 2000.

[69] G. J. Pratt, "Apparatus for establishing in vivo, bone strength," US Patent 4421119, Tech. Rep., 1983.

[70] A. Chamay, "Mechanical and morphological aspects of experimental overload and fatigue in bone," *J Biomech*, vol. 3, no. 3, pp. 263–270, 1970.

[71] F. Gattiker, F. Umbrecht, J. Nevenschwander, U. Sennhauser, and C. Hierold, "Novel ultrasound read-out for a wireless implantable passive strain sensor system," *Proc IEEE Sensors*, pp. 20–23, 2008.

[72] F. Nogata, A. Shimamoto, and T. Habu, "Estimation of in-vivo bone strength using ultrasound signals," *Int J of Modern Physics B*, vol. 17, no. 8, 9, pp. 1381–1387, 2003.

[73] "Mechanical sensor teams up with ultrasound for bone monitoring," 2008. [Online]. Available: http://www.medgadget.com/2008/11/mechanical_sensor_teams_up_with_ultrasound_for_bone_monitoring.html

[74] P. Singh, H. M. Rai, and Z. Singh, "Effect of neurons on the performance of microbend optical biosensor," *IJEIT*, vol. 1, no. 6, pp. 233–236, 2012.

[75] F. Umbrecht, P. Wagli, S. Dechand, F. Gattiker, J. Neuenschwander, U. Sennhauser, and C. Hierold, "Wireless implantable passive strain sensor: design, fabrication and characterization," *J. Micromech. Microeng.*, vol. 20, no. 085005, 2010.

[76] D. J. Leeming, P. Alexandersen, M. A. Karsdal, P. Qvist, S. Schaller, and L. B. Tankó, "An update on biomarkers of bone turnover and their utility in biomedical research and clinical practice," *Eur J Clin Pharmacol*, vol. 62, no. 10, pp. 781–792, 2006.

[77] M. J. Seibel, H. W. Woitge, I. Farahmand, H. Oberwittler, and R. Ziegler, "Automated and manual assays for urinary crosslinks of collagen: which assay to use?" *Exp Clin Endocrinol Diabetes*, vol. 106, no. 2, pp. 143–148, 1998.

[78] C. Wingren and C. A. K. Borrebaeck, "Antibody microarrays: current status and key technological advances," *OMICS*, vol. 10, no. 3, pp. 411–427, 2006.

[79] R. Eastell, P. Garnero, C. Audebert, and D. L. Cahall, "Reference intervals of bone turnover markers in healthy premenopausal women: results from a cross-sectional european study," *Bone*, vol. 50, no. 5, pp. 1141–1147, 2012.

[80] A. L. Schafer, E. Vittinghoff, R. Ramachandran, N. Mahmoudi, and D. C. Bauer, "Laboratory reproducibility of biochemical markers of bone turnover in clinical practice," *Osteoporos Int*, vol. 21, no. 3, pp. 439–445, 2010.

[81] B. E. Rapp, F. J. Gruhl, and K. Länge, "Biosensors with label-free detection designed for diagnostic applications," *Anal Bioanal Chem*, vol. 398, no. 6, pp. 2403–2412, 2010.

[82] M. J. Seibel, "Biochemical markers of bone turnover: part i: biochemistry and variability," *Clin Biochem Rev*, vol. 26, no. 4, pp. 97–122, 2005.

[83] P. Khashayar, H. Aghaei Meybodi, G. Amoabediny, and B. Larijani, "Biochemical markers of bone turnover and their role in osteoporosis diagnosis: A narrative review," *Recent Pat Endocr Metab Immune Drug Discov.*, vol. 9, no. 2, pp. 79–89, 2015.

[84] A. Leonidou, M. Moazen, P. Lepetsos, S. Graham, G. Macheras, and E. Tsiridis, "The biomechanical effect of bone quality and fracture topography on locking plate fixation in periprosthetic femoral fractures," *Injury*, vol. 46, no. 2, pp. 213–217, 2015.

[85] C. Moß, N. Weinrich, K. Seide, and J. Müller, "Wireless recording system for long-term monitoring of bone fracture healing," in *IFMBE Proceedings*, vol. 25/7. Munich, Germany: World Congress on Medical Physics and Biomedical Engineering, 2009, pp. 446–448.

[86] E. Chao, N. Inoue, T. Koo, and Y. Kim, "Biomechanical considerations of fracture treatment and bone quality maintenance in elderly patients and patients with osteoporosis," *Clin Orthop Relat Res.*, vol. 425, pp. 12–25, 2004.

[87] S. Bhalla, *Smart Materials in Structural Health Monitoring, Control and Biomechanics*. Springer, 2012, ch. Bone Characterization Using Piezo-Transducers as Bio-Medical Sensors.

[88] R. E. Steen, D. Ta, D. Cortens, B. Billen, W. Guedens, and P. Adriaensens, "Protein engineering for directed immobilization," *Bioconjug Chem.*, vol. 24, no. 11, pp. 1761–1777, 2013.

[89] A. Ansari and Q. Husain, "Potential applications of enzymes immobilized on/in nano materials: a review," *Biotech Adv.*, vol. 30, pp. 512–523, 2012.

[90] K. Nakanishi, T. Sakiyama, Y. Kumada, K. Imamura, and H. Imanaka, "Recent advances in controlled immobilization of proteins onto the surface of the solid substrate and its possible application to proteomics," *Curr. Proteomics*, vol. 5, p. 161, 2008.

[91] C. Mateo, J. Palomo, G. Fernandez-Lorente, J. Guisan, and R. Fernandez-Lafuente, "Improvement of enzyme activity, stability and selectivity via immobilization techniques," *Enzyme Microb Technol*, vol. 40, pp. 1451–1463, 2007.

[92] J. Yakovleva, R. Davidsson, A. Lobanova, M. Bengtsson, S. Eremin, T. Laurell, and J. Emnéus, "Microfluidic enzyme immunoassay using silicon microchip with immobilized abs and chemiluminescence detection," *Anal. Chem.*, vol. 74, p. 2994, 2002.

[93] D. Kim and A. Herr, "Protein immobilization techniques for microfluidic assays," *Biomicrofluidics.*, vol. 7, no. 4, 2013.

[94] E. Benešová and B. Králová., *Affinity Interactions as a Tool for Protein Immobilization, Affinity Chromatography*. InTech, 2012.

[95] B. Brena, P. González-Pombo, and F. Batista-Viera, *Immobilization of Enzymes and Cells. Methods in Molecular Biology*. Springer, 2013, vol. 1051, ch. Immobilization of Enzymes: A Literature Survey.

[96] J. Křenková and F. Foret, "Immobilized microfluidic enzymatic reactors," *Electrophoresis*, vol. 25, p. 3550, 2004.

[97] J. Guisán, "Agarose-aldehyde gels as supports for immobilization-stabilization of enzymes," *Enzyme Microb Technol*, vol. 10, pp. 375–382, 1998.

[98] B. Wang, C. Guo, M. Zhang, B. Park, and B. Xu, "High-resolution single-molecule recognition imaging of the molecular details of ricin-aptamer interaction," *J. Phys. Chem. B*, vol. 116, pp. 5316–5322, 2012.

[99] Z. Pei, H. Anderson, A. Myrskog, G. Dunér, B. Ingemarsson, and T. Aastrup, "Optimizing immobilization on two-dimensional carboxyl surface: ph dependence of antibody orientation and antigen binding capacity," *Anal. Biochem.*, vol. 398, pp. 161–168, 2010.

[100] Y. Wang, H.-H. Lai, M. Bachman, C. E. Sims, L. G.P, and A. N. L., "Covalent micropatterning of poly (dimethylsiloxane) by photografting through a mask," *Anal. Chem.*, vol. 77, pp. 7539–7546, 2005.

[101] D. Bartczak and A. Kanaras, "Preparation of peptide-functionalized gold nanoparticles using one pot edc/sulfo-nhs coupling," *Langmuir.*, vol. 27, no. 16, pp. 10 119–23, 2011.

[102] T. Didar, A. Foudeh, and M. Tabrizian, "Patterning multiplex protein microarrays in a single microfluidic channel," *Anal. Chem.*, vol. 84, p. 1012, 2012.

[103] T. Boller, C. Meier, and S. Menzler, "Eupergit. oxirane acrylic beads: how to make enzymes fit for biocatalysis," *Org Process Res Dev*, vol. 6, pp. 509–519, 2002.

[104] L. Cao, "Immobilised enzymes: science or art?" *Curr Opin Chem Biol*, vol. 9, pp. 217–226, 2005.

[105] E. Basle, N. Joubert, and M. Pucheault, "Protein chemical modification on endogenous amino acids," *Chem. Biol.*, vol. 17, pp. 213–227, 2010.

[106] G. Hermanson, *Bioconjugate Techniques*, 2nd ed. Academic Press, Rockford., 2008, ch. 2.7: The chemistry of reactive groups: Vinylsulfone Derivatives.

[107] Y. Kim, S. Ho, N. Gassman, Y. Korlann, E. Landorf, F. Collart, and S. Weiss, "Efficient site-specific labeling of proteins via cysteines," *Bioconjugate Chem.*, vol. 19, pp. 786–791, 2008.

[108] N. Joshi, L. Whitaker, and M. Francis, "A three-component mannich-type reaction for selective tyrosine bioconjugation," *J. Am. Chem. Soc.*, vol. 126, pp. 15 942–15 943, 2004.

[109] M. Gauthier and H. Klok, "Peptide/protein-polymer conjugates: synthetic strategies and design concepts," *Chem. Commun.*, vol. 23, pp. 2591–2611, 2008.

[110] B. Brena and F. Batista-Viera, *Immobilization of enzymes and cells*, 2nd ed. Humana Press Inc., New Jersey, 2006, ch. Immobilization of enzymes.

[111] S. Laib and B. MacCraith, "Immobilization of biomolecules on cycloolefin polymer supports," *Anal. Chem.*, vol. 79, p. 6264, 2007.

[112] K. Holland-Nell and A. Beck-Sickinger, "Specifically immobilised aldo/keto reductase akr1a1 shows a dramatic increase in activity relative to the randomly immobilised enzyme," *Chem Bio Chem*, vol. 8, pp. 1071–1076, 2007.

[113] J. Yakovleva, R. Davidsson, M. Bengtsson, T. Laurell, and J. Emnéus, "Microfluidic enzyme immunosensors with immobilised protein a and g using chemiluminescence detection," *Biosens. Bioelectron.*, vol. 19, p. 21, 2003.

[114] R. Blanco, J. Calvete, and J. Guisán, "Immobilization-stabilization of enzymes. variables that control the intensity of the trypsin (amine)-agarose-(aldehyde) -multipoint attachment," *Enzyme Microbial Technol*, vol. 11, pp. 353–359, 1989.

[115] J. Arnau, C. Lauritzen, G. E. Petersen, and J. Pedersen, "Current strategies for the use of affinity tags and tag removal for the purification of recombinant proteins," *Protein Expr Purif*, vol. 48, no. 1, pp. 1–13, 2006.

[116] S. Knecht, D. Ricklin, A. N. Eberle, and B. Ernst, "Oligohis-tags: mechanisms of binding to ni2+-nta surfaces," *J Mol Recognit*, vol. 22, no. 4, pp. 270–279, 2009.

3
Scientific Background

3.1 Introduction

This chapter aims to introduce the scientific and technical principles applied in the experimental chapters of this work. Three major subjects will be discussed.

- The first subject is an overview on biosensors and its types. A special focus is dedicated to electrochemical sensors.
- The second part deals with different electrochemical techniques. The definition of these techniques will be described.
- The last section embraces main principles of microfluidic devices.

3.2 Overview on Immunosensors

3.2.1 Introduction

The concept of using immunological components as sensing agents was first described within an immunoassay for plasma insulin in human subjects [1]. The ELISA test, developed based on the high dissociation constants (K_d) with which antibodies bind to their target antigen, has since

then been seen the gold standard for comparison against all newly developed immunoassays and immunosensors [2]. Briefly, ELISAs involve the immobilization of a reactant (an antibody or antigen) onto a solid surface, with enzymes being used as markers for the presence and abundance of a specific antibody-antigen (Ab/Ag) interaction [3].
The widespread use of antibodies regardless of their high cost, variable affinity, and short shelf life arises from their exceptional specificity and sensitivity toward their binding partners, i.e. the antigens (Ag). Immunoassays, therefore, make use of the sensitivity and specificity of the antibody-antigen interaction [4]. Several methods exist to transduce a signal created by the binding of antibody and analyte, each with associated advantages and disadvantages, leading to a wealth of research into fabrication of immunosensors and immunoassays [5].
Most clinical analyses are carried out by specialized staff in laboratories using desktop instruments, thus assuring the highest possible confidence in the obtained results. However, there are many cases in which a critical clinical analysis cannot be performed in those optimal conditions because of the lack of trained analysts or the required facilities, as is often the case in underdeveloped or isolated areas. In those cases, biosensors can be the only option to make a trustworthy medical diagnosis.(Figure 3.1)

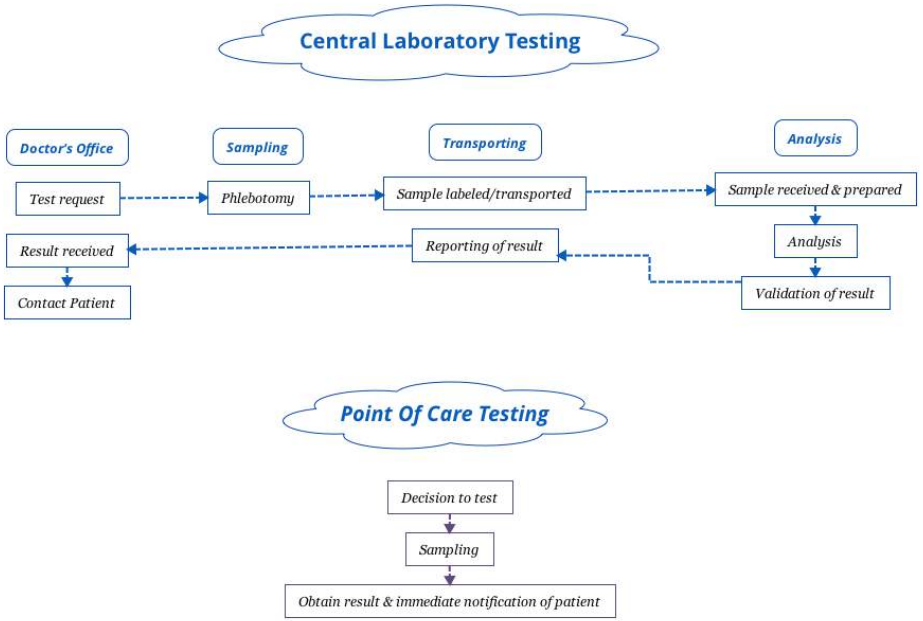

Figure 3.1: Process of clinical testing in outpatient situations using central laboratory versus POC methods. The processes are shown in a simplified format and may sometimes contain additional steps [6].

3.2.2 What is a Biosensor

The first biosensor was described in 1962 by Clark and Lyons [7]. They immobilized glucose oxidase (GOD) on a semipermeable dialysis membrane on an amperometric oxygen electrode surface to quantify glucose concentration directly.
According to the International Union of Pure and Applied Chemistry (IUPAC), 'A biosensor is a self-contained integrated device which is capable of providing specific quantitative or semi-quantitative analytical information using a biological recognition element (biochemical receptor) which is in direct spatial contact with a transducer element. A biosensor should be clearly distinguished from a bioanalytical system, which requires additional processing steps, such as reagent addition. Furthermore, a biosensor should be distinguished from a bioprobe which is either disposable after one measurement, i.e. single use, or unable to continuously monitor the analyte concentration [8].
In other words, biosensors permit the analysis of analytes with great specificity and sensitivity in a short time [9]. These techniques have the capability to be used in POC systems and portable devices [10].
PoC testing is an 'on site' test, detailed within a large proportion of research. However, none of the existing immunosensors offer a complete set of the necessary characteristics for a good POC sensor including full automation, portability, precision, accuracy and sensitivity, low cost and ease of use [11]. Non-invasiveness is another important characteristic when considering POC sensor design, preferably using samples such as urine, sweat or saliva are used. Minimizing the pain associated with blood sampling is also possible by reducing needed sample volume [11].
The detection process in a biosensor is mainly based on the specific interaction between the analyte of interest and the recognition element (such as an electrode). As a result of this specific interaction, changes in one or several physicochemical properties (pH, electron transference, heat transfer, change of potential or mass, variation of optical properties, etc.) occur, which later on are detected and measured by a specific transducer.
It therefore could be concluded that a biosensor is composed of two main parts: (Figure 3.2)

- A bioreceptor or an immobilized sensitive biological element (enzyme, DNA probe, antibody) recognizing the analyte (enzyme substrate, complementary DNA, antigen).
- A transducer used to convert (bio)chemical signal resulting from the interaction of the analyte with the bioreceptor into an electronic one. The intensity of the generated signal is directly or inversely proportional to the concentration of the analyte [12].

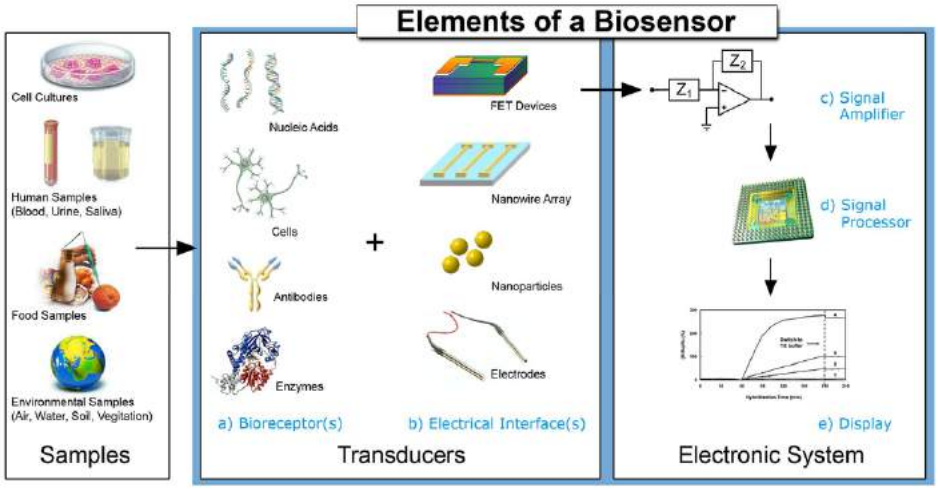

Figure 3.2: Different types of biosensors based on their structure.

3.2.3 Main Types of Immunoassays

Immunosensors could be divided into 'direct' or 'indirect' assays, meaning that the detection mechanism operates either directly via the Ab/Ag interaction, or a further label, such as an enzyme or fluorescent molecule, is used in order to detect whether a binding event has occurred. (Figure 3.3) The principal challenge for many label-free assays of protein biomarkers is the occurrence of a relatively less significant change in properties upon target binding and that the acquired responses are highly specific [13].

In another classification, immunoassays are divided into 'competitive' and 'noncompetitive'. In competitive assays, the analyte competes in proportion to its concentration with labeled analyte for a limiting number of antibody binding sites. As the analyte concentration increases, more labeled analyte is displaced, giving a decrease in signal if antibody-bound labeled analyte is detected, or an increase in signal if the free labeled analyte is detected. In a noncompetitive assay, such as a sandwich immunoassay, which will be discussed in more detail in the following paragraphs, the signal increases in proportion to the analyte concentration [14].
On the other hand, there are two main types of immunoassays:

Heterogeneous immunoassays In heterogeneous immunoassays, the antibody (or in some cases antigen) is immobilized on a solid support [15][16]. The most commonly used heterogeneous immunoassay is the sandwich as-

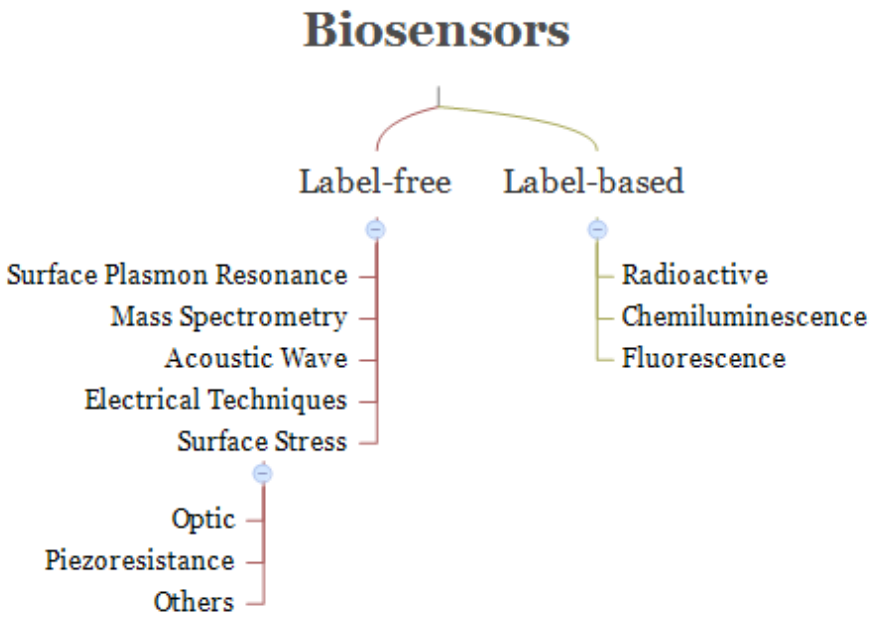

Figure 3.3: Different types of biosensors based on the detection technique.

say. The procedure usually consists of a capture step with a primary antibody followed by a second binding reaction between the captured antigen and a labeled second antibody. An advantage of this technique is the enhanced specificity obtained from two separate recognition steps provided by the two antibodies that are generally selected to recognize two different epitopes on the antigen. This is usually the preferred assay format when the application demands the highest degree of sensitivity and selectivity. A limitation of the sandwich assay is the requirement that the analyte should be able to bind with two antibodies simultaneously, which generally restricts its use to molecules with a molecular weight of greater than about 1000 Da.

Homogenous immunoassays Homogeneous immunoassays take place entirely in the solution phase. They rely on the formation of the antigen-antibody complex causing a change in the intensity of the label's signal. Distinguishing between the bound and unbound states enables the immunoassay to be done without a separation step. This simplifies the assay, removing the antibody immobilization and rinsing steps. An advantage is that there is no solid phase that can be affected by non-specific binding [17]. Homogeneous assays are more difficult to develop and generally have poorer limits of detection and selectivity than heterogeneous assays. They are commonly used for detecting therapeutic drugs that have a relatively high concentration in blood.

3.2.4 Immunosensor components

The most commonly used components in immunosensor technology are as following:

Carbon nanotubes

The importance of single-walled (SWNT's) and multi-walled (MWNT's) CNTs in the development of the immunochemical devices was first reported in 1991 [18]. This was mainly due to their role in enhancing detection sensitivity compared to sensors incorporating other carbon platforms (possibly due to increased surface area, their electrocatalytic effects, lower levels of fouling, being mechanically strong and flexible and excellent electrical and thermal conductivity) [19].

Nanoparticles

Over the past decade, more and more research has been performed on the use of nano-sized metal particles, particularly noble metal nanoparticles

with controlled size, morphology, and crystal orientation, as their physical and chemical properties differ from that of the bulk material [20].[21]. The inherent benefit of nanoparticles is their ability to significantly enhance sensitivity and lower detection limits of sensors, possibly due to the increased surface area onto which antibodies can be immobilized, or affecting the refraction of light in SPR-based sensors [22]. These noble metal nanoparticles are becoming more popular in electrochemical sensing devices, as many studies have suggested that the use of modified electrodes can improve the performance of an electrochemical sensor [23].
Among the noble metal nanoparticles, gold nanoparticles (AuNPs) are of particular interest not only because of their stability, but also because of their specific physicochemical properties, including the enhanced diffusion of electroactive species based on their high effective surface area, improved selectivity, catalytic activity, and higher signal-to-noise ratio and conductivity [24] [25]. Important here, AuNPs provide a stable surface for protein immobilization and overcome the need for external electron-transfer mediators in electrochemical sensing [26] [27] [28]. The use of AuNPs in this work is going to be discussed later on in Chapters 4 and 5.

3.2.5 Detection Techniques

As mentioned earlier, biosensors could also be categorized based on their detection techniques [29]:

- Optical [30]
  - Direct detection by monitoring the light properties: fluorescence, absorbance, and luminescence/chemiluminescence.
  - Light property modulation detections: surface plasmon resonance (SPR), evanescent waves, interferometry, Raman spectrometry, fiber optics, and optical waveguides [31].
- Non-optical
  - Electrochemical: The electrochemical detection can be used to measure the concentration of the analyte by converting the analyte's chemical signal into the electrical signal via the electrodes [32].
    - Amperometry: Amperometric sensors measure the current signal generated by the redox reaction on the electrode while a constant potential is applied [33]. Amperometric detection is based on the fact that the applied voltammetric potential between the reference and working electrode would cause the oxidation or reduction of the electroactive species in the vicinity, and induce an electrical current. The change of the current

is related to the concentration of the analyte. (Figure 3.4)
Such sensors consume a small percentage of analytes during measurement, and thus either the analyte must be redox active or use of a redox active label will be necessary. Consumption of the analyte creates concentration gradients, thereby rendering responses are stir - dependent.
The sensitivity of amperometric immunosensors can be improved using a layer-by-layer (LBL) construction approach utilizing AuNPs or methylene blue to form a uniform and stable base [34]. This is mainly because increasing the surface area onto which capture agents are immobilized increases binding events and sensitivity. Cross-linking also prevents conformational change and unfolding of the antibodies allowing markedly enhanced sensitivity when compared with similar constructs, longer storage times and higher resistance to extremes of pH and temperature. The first technique is to be discussed later on in Chapter 5 and the latter is already discussed in Chapter 2.

- Potentiometry: In potentiometric detection, analyte is assessed by monitoring the potential of an ion-selective electrode (usually a membrane/surface sensitive to an analyte) against a reference electrode. The reaction between the surface and the analyte generates a potential proportional to the logarithm of the electrochemically active material concentration. (Figure 3.5)
  A sensor design which transduces the potential across a membrane into a digitized signal or field-effect transistors (FETs) whose semi-conductive surface potential changes upon a change in analyte concentration are examples of potentiometric sensors [36].
- Conductometry: Conductometric biosensors can measure the changes of the electrical conductivity of a medium between electrodes. Most reactions involve a change in the composition of the solution. The detection involves measuring the conductivity at a series of frequencies, both in conventional contacted and capacitively coupled contactless conductivity detection (C4D) methods such as potential gradient detection.
- Impedimetry: Impedimetric detection method is similar to the amperometric detection method. The difference between them is that the AC is used in the impedimetric detection, and thus the electrolysis of the electrodes can be eliminated. However, like the conductometric detection method, the sensitivity depends on the difference of the impedance between the back-

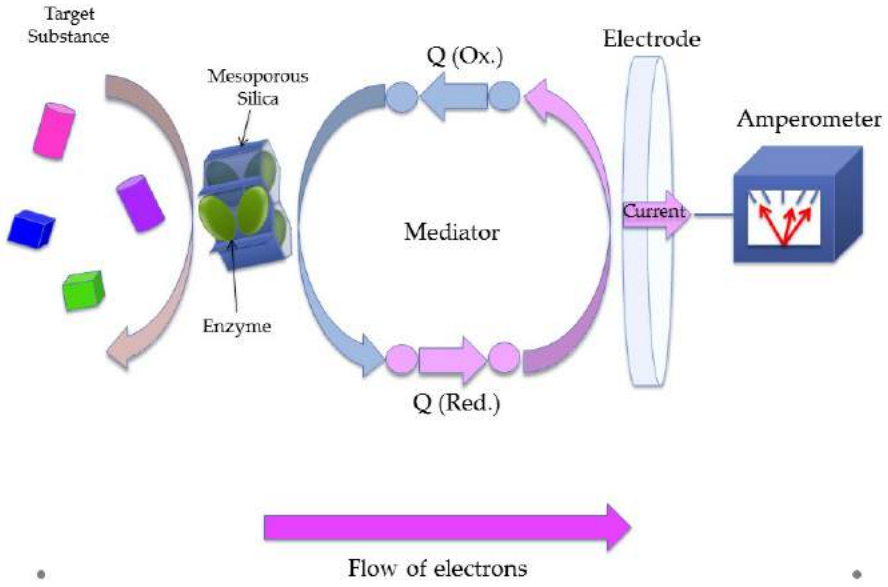

Figure 3.4: Schematic diagram of detection mechanism in a sample enzymatic amperosensor [35].

.

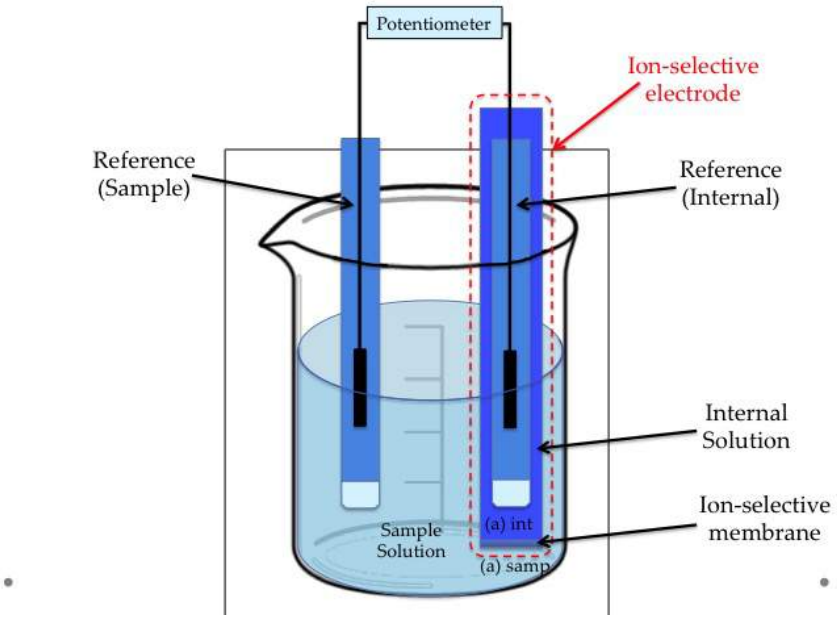

Figure 3.5: Schematic diagram showing a typical potentiometric cell with an ion-selective electrode. The ion-selective electrode's membrane separates the sample, which contains the analyte from an internal solution containing the analyte.[1]

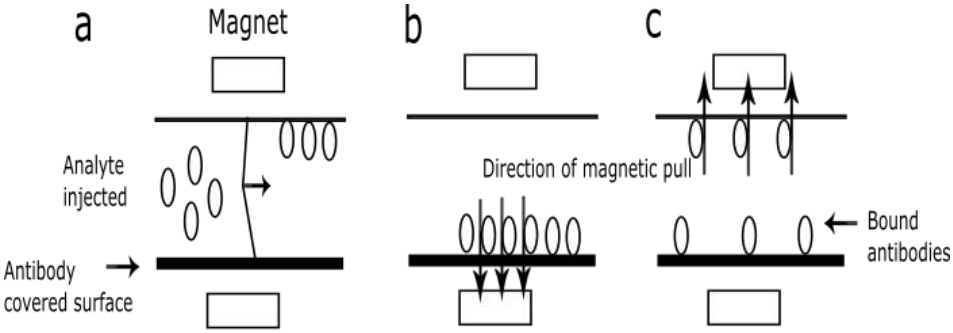

Figure 3.6: (a) The microchamber is filled with analyte in solution and the antibodies are redispersed into the solution, some bind with the analyte. (b) Magnetic particles are attracted to the lower surface. (c) The free and weakly bound immunosensors which are not bound to analyte are removed from the lower surface when the upper magnet is switched on.

ground and the analyte.

- Magnetic immunosensors: There has been a recent surge of interest in the use of magnetic particles within biosensors [38][39]. Electromagnets can pull immuno-substituted beads towards a binding site and then weakly bound species can be removed by an oppositely located electromagnet. This allows a higher level of control [40]. There are no extra wash stages, giving a simple one-step measurement once the sample fluid has been added, allowing simplicity and rapid procurement of results necessary for POC. (Figure 3.6)
- Piezoelectric: Piezoelectric devices convert a physical or mechanical change into electrical energy and vice versa. The commonest piezoelectric sensor is the quartz crystal microbalance (QCM), which exploits the change in the resonance of quartz crystals upon changes in their mass, allowing binding of antigen to antibody (when one of these is immobilized on the crystal surface) to be measured electrically [41] [42].
- Mass-Spectrometry
- Others such as nuclear magnetic resonance (NMR) spectroscopy, magneto-resistive, and acoustical

3.3 Electrochemistry: Principles

One key issue to take into consideration in biosensing platform integration is the increasing demand for higher sensitivity and selectivity at minimal costs, and the possibility to monitor biosensing in real-time, especially for point-of-care platforms, for which simplicity should also be considered [43]. Considering this, calorimetric and electrochemical approaches are the most promising due to their simplicity, high sensitivity and specificity, in addition to the fact that in most cases they simply do not require expensive and complex instrumentations to achieve a sample-in/answer-out biosensing platform. Moreover, such approaches allow for multiplexing biosensing enabling their application in a range from low- to high-throughput diagnostics.
Electrochemistry combines an oxidation-reduction chemical reaction that occurs in a liquid phase with an electrical circuit that is completed by solid conductive materials. Depending on the type of the analysis, either potential or current may be measured. In this way the kinetics of the reaction occurring on the electrode is described by the signal produced from electron transfer through the system [44].
As mentioned earlier, electrochemistry provides powerful analytical techniques encompassing the advantages of instrumental simplicity, moderate cost and portability. Another advantage to electrochemical assays is that they are highly sensitive to very low concentrations. The biological component in the sensor recognizes its analyte bioselectivity, resulting in a catalytic or binding event that ultimately produces an electrical signal monitored by a transducer that is proportional to analyte concentration [45] [46]. Considering these advantages, an electrochemical biosensor was designed to fulfill the final objective of this work.

In the following, some basic electrochemistry principles are discussed.
A standard electrochemical experiment, referred to as a three-electrode setup, uses a reference electrode (REF), working electrode (WE), and counter/auxiliary electrode (AUX). (Figure 3.7)

- Working electrode: A polarizable electrode is used for the working electrode on which an electrochemical reaction takes place.
- Reference electrode: The reference electrode is a potential standard to supply a constant potential for introducing the electrochemical reaction on the working electrode. The ideal reference electrode provides a stable, known potential so that any change in E_{cell} is attributed to the analyte's effect on the potential of the metal indicator electrode.[2]

[2]Metal indicator electrodes are paired with a reference electrode and can be used to determine the concentrations of targeted analytes in a solution. In other words, the cell potential will be directly

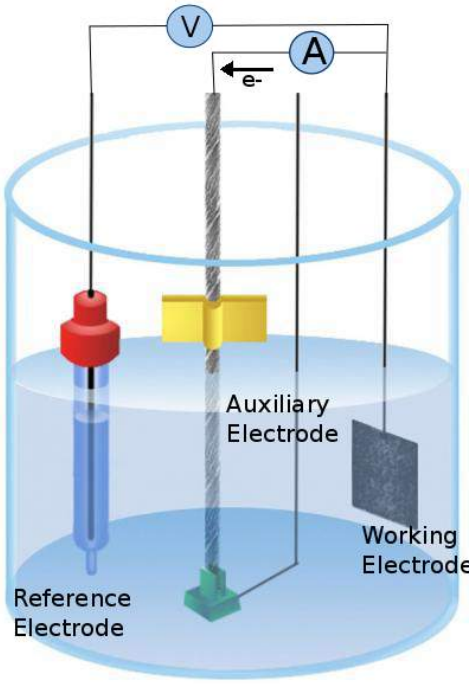

Figure 3.7: Schematic representation of a three-electrode system.

(Equation (3.1))

$$E_{cell} = E_{ind} - E_{ref} + E_j \tag{3.1}$$

Where E_{ind} refers to the metal indicator potential and E_j to the junction potential.
Since no current passes through the reference electrode, its potential remains constant at the value specified by the analyst. This is a theoretical model and in reality there is a drop in potential between the working and reference electrodes, since they cannot be placed infinitely close to each other [44]. In addition, the ideal reference electrode should be easy to make and to use. Common reference electrodes are 'Standard Hydrogen Electrode', 'Calomel Electrode', and 'Silver/Silver Chloride Electrode'.

- Auxiliary electrode: The AUX is distinct from the REF, which establishes the electrical potential against which other potentials may be measured, and the WE, at which the cell reaction takes place. When a certain potential is applied to the WE with respect to the REF, the redox reaction occurs. The reaction generates the current that can be measured between the WE and the AUX electrodes. The current is proportional to the concentration of the analyte.

The appeal of potentiostatic techniques is that the thermodynamics of the system can be controlled by adjusting the potential. For a general electrochemical reaction, this relationship is described by the Nernst equation [47]. In other words, the Nernst equation describes the relationship between the potential applied to an electrode and the concentration of the redox species on the electrode surface [32]. If an electrode is at equilibrium with the solution in which it is immersed, the electrode will have a potential, invariant with time, which is thermodynamically related to the composition of the solution. In solution, the 'Oxidant' is capable of being reduced to the 'Reductant' on the electrode by the following reversible electrochemical reaction.(Equation (3.2))

$$Oxidant + ne^- \leftrightarrows Reductant \tag{3.2}$$

The Nernst equation relates the potential E, which is applied to the electrode and the concentration of the Oxidant and Reductant on the electrode surface: (Equation (3.3), (3.4))

$$E = E_0 - (\frac{RT}{nF})lnQ \tag{3.3}$$

influenced by the target analyte concentration.

also written as,

$$E = E_0 - \frac{0.0592V}{n} log[Q] \tag{3.4}$$

where E is the potential difference between the electrodes (V); E_0 is the standard reduction potential (V); R is the universal gas constant (R = 8.314 J/mol.K); T is the temperature (K); n is the number of electrons transferred in the half reaction; F is the Faraday's constant (F = 96,484.6 C/mol); Q is the reaction quotient, which is the ratio of activities of the species (Q = $\frac{[R]}{[O]}$, where [R] is the surface concentration of the reductant species and [O] is the surface concentration of the oxidant species).
Cyclic voltammetry (CV) and linear sweep voltammetry (LSV) have received great interest as they can be used for the elucidation of electrode processes and redox mechanisms. Differential pulse voltammetry (DPV) and square wave voltammetry (SWV) are particularly useful in the determination of trace amounts of electroactive compounds in pharmaceuticals and biological fluids. Stripping voltammetry has also been widely utilized due to its ability to pre-concentrate analytes for ultra-sensitive detection [48].

3.3.1 Cyclic Voltammetry

CV is a direct current (DC) potentiostatic technique where potential is swept between two limits at a constant rate and the current at the working electrode is monitored during the potential scan. The limits are chosen such that they flank the potential at which the species is expected to oxidize/reduce. The relationship between potential and time is described by a triangular waveform. (Figure 3.8).

The voltammogram is a display of current versus potential. (Figure 3.8) After the initial non-faradaic region, the neutral species starts to get oxidized as the potential becomes more positive. As oxidization occurs on the electrode, the mass transfer rate of neutral species towards the electrode increases, and so does the current. This current reaches a maximum peak, after which the surface concentration of the neutral species starts to decline due to depletion from the solution, resulting in a reduced oxidation current. (Equation (3.5))The process is then repeated in the same manner for the reverse scan to obtain the reduction behavior. (Equation (3.6))

$$[Fe^{II}(CN)_6]^{3-} + e^- \rightarrow [Fe^{III}(CN)_6]^{4-} \tag{3.5}$$

$$[Fe^{III}(CN)_6]^{4-} \rightarrow [Fe^{II}(CN)_6]^{3-} + e^- \tag{3.6}$$

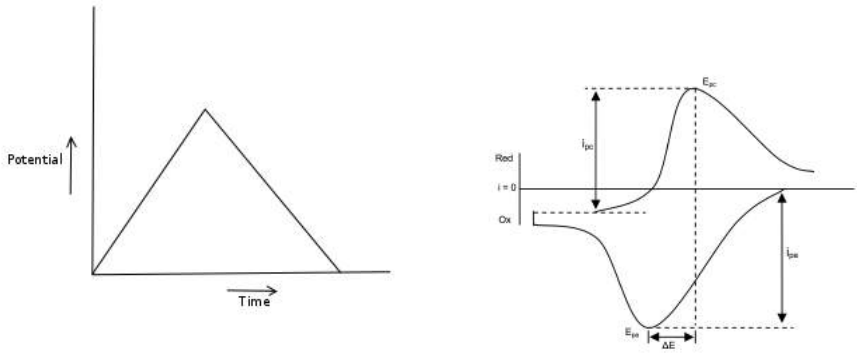

(a) (b)

Figure 3.8: a) Typical excitation waveform for analog CV, b) Theoretical CV for a reversible reaction of 1mM $K_3Fe(CN)_6$ in 1M NaCl.

Activation potentials are the range of potentials at which the reactants oxidize/reduce without influences associated with diffusion/transport. Within this range, there is a steep increase in current due to the conversion of the reactants at the electrode surface. This current, also known as the 'faradaic current', is the result of direct electron transfer to or from the analyte. Eventually the reaction is limited by the diffusion of reactants toward the surface or products away from the surface, so the current reaches a maximum and then tails off.
The peak current (i_p) is measured relative to the baseline extrapolated from the baseline signal so as not to include charging current in the analysis. The current is measured in ampere (A). Potential is measured in volts (V).
The formal reduction potential E_0 for an electrochemically reversible couple (Equation (3.7)) can be found at the value that corresponds to 85% of the peak potential and the thickness of the diffusion layer [3] can be estimated from $(Dt)^{1/2}$, where D is the diffusion coefficient and t is time in seconds [49].

$$E_0 = E_{pa} + E_{pc} \tag{3.7}$$

[3]The diffuse-layer model depicts the distribution of net charge near the electrode surface which diminishes as the interfacial region stretches toward the bulk. The random motion of ions results in a diffuse layer of charge in which the concentration of counter ions is greatest next to the electrode surface and decreases progressively until a homogenous distribution appears in bulk electrolyte. Specific adsorption of desolved ions at the electrode is weak and therefore the adsorbed inner layer of negative charge only partially shields the positive charge at the electrode. As a result, a layer of solvated anions is present adjacent in the diffuse layer.

Where E_{pa} is the anodic peak potential and E_{pc} is the cathodic one. For a reversible redox couple, the number of electrons transferred in the electrode reaction can be determined by the separation between the peak potentials: (Equation(3.8))

$$\Delta E = E_{pa} - E_{pc} \cong \frac{0.059}{n} \tag{3.8}$$

CV has the capability for rapidly observing redox behavior over a wide potential range. The potential cycle may be repeated to obtain additional information about system stability. The step, or scan rate, at which the potential is varied can also be used to extract further information pertaining to mass transfer profile near the electrode as the thickness of the diffusion layer can be adjusted by the scan rate.
It should be noted that the choice of the electrolyte affects the intrinsic behavior of the redox couple. The activity of the reactants also changes depending on the electrolyte concentration.
In a system where the electron transfer occurs much faster than the diffusion of an electroactive species to the electrode, the peak current, i_p (A) for the forward sweep of the first cycle, can be calculated from the Randles-Sevcik relationship. (Equation (3.9)) Therefore, CV is useful for quantitative experiments because the current signal is directly proportional to the concentration of the analyte being measured.

$$i_p = k.n^{3/2}.A.D^{1/2}.C.v^{1/2} \tag{3.9}$$

where k is a constant; n is the number of moles of electrons transferred; A (cm^2) is the area of the electrode; D (cm^2/s) is the diffusion coefficient; C (mol/cm^3) is the solution concentration and v (V/s) is the scan rate.
This relationship can be used to determine if a reaction is diffusion limited by simply plotting the peak current versus the square root of the scan rate. If a linear plot is obtained then the reaction is mass transfer limited. The slope of the resulting line is also proportional to the diffusion coefficient, as shown in the Randles-Sevcik equation. (Equation (3.9)) Moreover, the peak potentials at varying scan rates can be compared to find out if a reaction is reversible. In a reversible reaction where the electron transfer rate is fast, all peaks should appear at the same potential at different scan rates. (Figure 3.9).

3.3.2 Differential Pulse Voltammetry

In order to increase speed and sensitivity, many forms of potential modulation (other than just a simple staircase ramp) have been tried over the

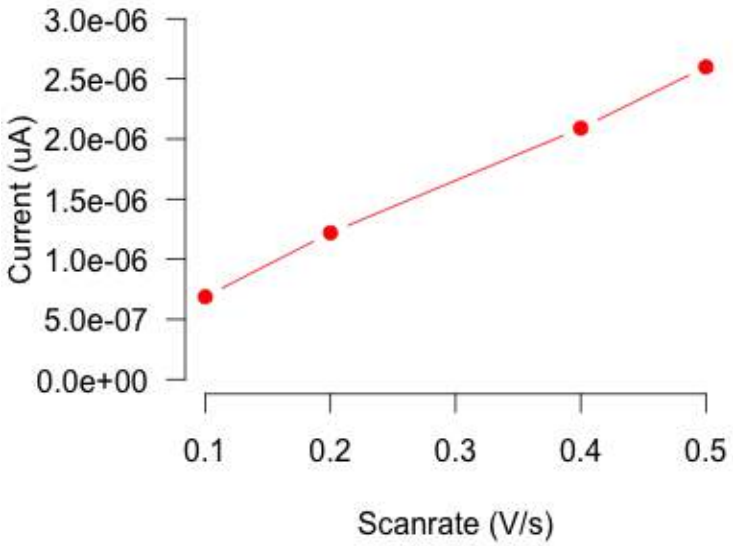

Figure 3.9: Plot of peak height for $K_3[Fe(CN)_6]$ reduction at different scan rates.

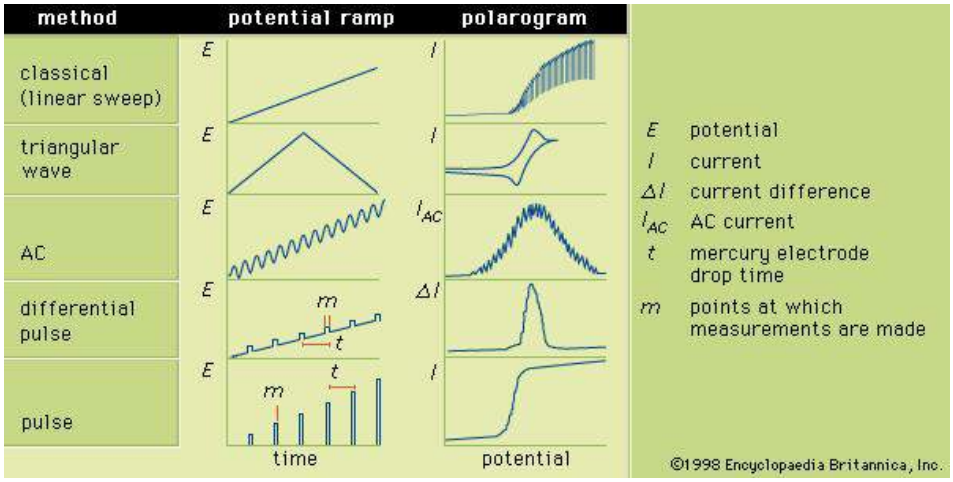

Figure 3.10: The potential ramps applied to the auxiliary electrode during selected forms of voltammetry and the corresponding voltammograms. E is the potential; I, the current; ΔI, the current difference; IAC, the AC current; t, the electrode drop time; and m, the points at which measurements are made.

years. DPV is an electrochemical technique where the current is measured as a function of time and as a function of the potential between the auxiliary and reference electrodes. It can be considered as a derivative of linear sweep voltammetry or staircase voltammetry, with a series of regular voltage pulses superimposed on the potential linear sweep or stair-steps. The current is measured immediately before each potential change, and the current difference is plotted as a function of potential. By sampling the current just before the potential is changed, the effect of the charging current can be decreased.(Figure 3.10)

3.3.3 Chronoamperometry

Chronoamperometry (CA) is a useful tool for determining diffusion coefficients and for investigating kinetics and mechanisms. Unlike the CV technique, CA can yield this information in a single experiment. (Figure 3.11)

When a potential step large enough to cause an electrochemical reaction is applied to an electrode, the current changes with time (t). The study of this current response as a function of time is called CA and is studied using the Cottrell equation: (Equation(3.10))

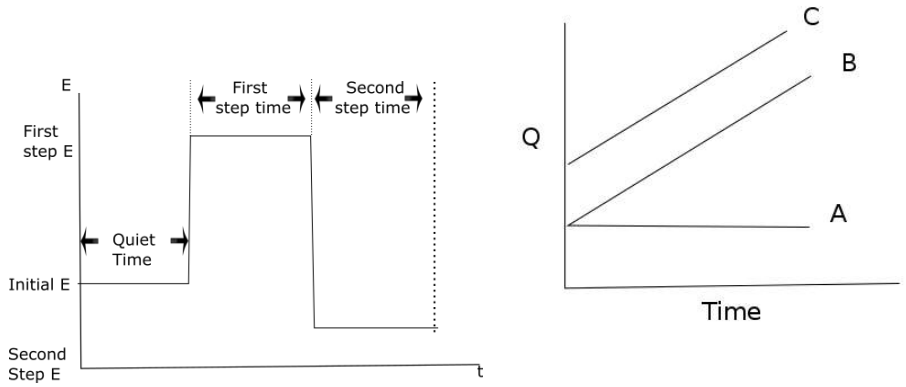

Figure 3.11: a) Potential wave form for chronoamperometry and chronocoulometry, b) Theoretical Anson plots for a blank (A), a redox system (B), and a system showing adsorption (C).

$$i = \frac{n.F.A.D^{1/2}.C^{b}}{(\pi.t)^{1/2}} \tag{3.10}$$

where n represents number of electrons; F, the Faraday's constant; D, the diffusion coefficient; C^b, the concentration of the bulk; and A, the surface area of the electrode.
Simply stating, the Cottrell equation shows that the current is proportional to $\frac{1}{t^{1/2}}$. It also helps calculating the diffusion coefficient by simply rearranging the equation, providing the number of electrons obtained from the CV experiment and providing values for the other variables. Another useful parameter to calculate is the 'true' area of the electrode, where the geometric area of an electrode is not the same as the electrochemically active area due to surface roughness.

3.3.4 Chronocoulometry

Chronocoulometry (CC) is an outgrowth of the chronoamperometric technique with two main advantages:

- It helps determine the kinetic rate constant more accurately

- It helps detect adsorption of a species on an electrode surface more easily

In a CC experiment, the charge used in an oxidation or reduction process is measured and then plotted with respect to time. The excitation waveform is the same as that used for CA, but the resulting curve shows an increase of charge with time, rather than the decrease seen in CA.
Like the CA response curve, the CC curve shows that in most reactions the diffusion of the reacting species to the electrode takes some time. This implies that at the start of the experiment (time zero) the only charge measured is due to the charging of the double layer of the electrode. In cases where a species is adsorbed on the surface of the electrode, the reaction of this material can take place at time zero. This reaction gives rise to current and to a larger value of charge at the initial point than would be expected for a non-adsorbed species. The technique is therefore also used to calculate adsorption layer thickness.
Since CC is based on the same assumptions as CA, the charge at any time can be calculated by simply integrating the Cottrell equation and adding corrections for the charge due to the double layer and any interfacial interactions (for example, adsorption). The resulting equation is: (Equation(3.11))

$$Q = \frac{2n.F.A.C_{\mathrm{b}}.D^{1/2}.t^{1/2}}{\pi^{1/2}} + Q_{d1} + Q_1 \tag{3.11}$$

where Q is charge; n represents number of electrons in the reaction; F, the Faraday's constant; A, the electrode surface area; C_b, the bulk concentration; D, diffusion coefficient; Q_{d1}, charge due to double layer; and Q_1, charge due to interfacial interaction.
If Q is plotted versus $t^{1/2}$ the result is the Anson plot. The slope of the plot would be $\frac{2n.F.A.C_{\mathrm{b}}.D^{1/2}}{\pi^{1/2}}$ if no adsorption is assumed to occur and the intercept is the double layer charge. If adsorption does occur, the line in this plot would be offset by the charge due to this interfacial phenomenon. It is easy to differentiate between the charge due to the double layer and that due to adsorption. (Figure 3.11)

3.3.5 Electrochemical Impedance Spectroscopy (EIS)

Originally developed by Sluyters et al., EIS techniques allow for the characterization of complex processes and interfaces by observation of a system's impedance response to a small periodic alternating perturbation at steady state or a voltage perturbation [50]. In other words, EIS is highly

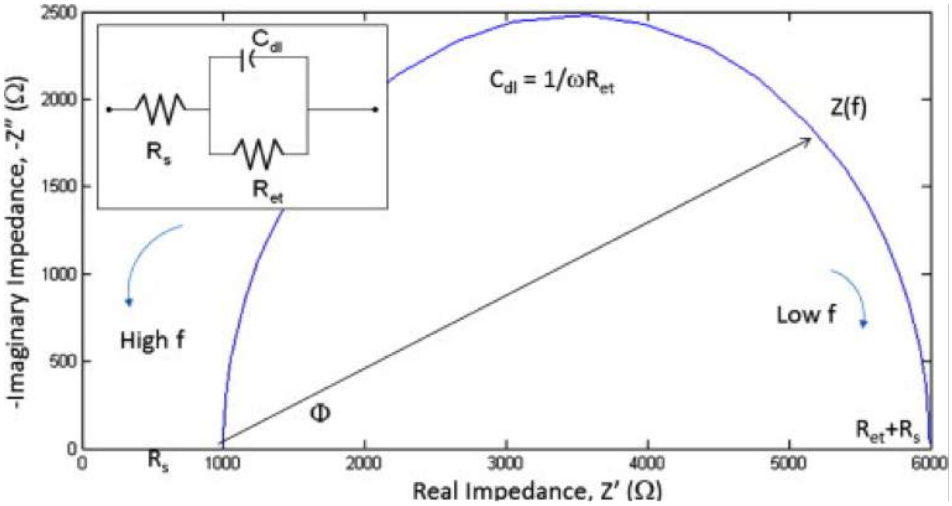

Figure 3.12: Impedance spectra, Nyquist curve, a plot of the real impedance versus imaginary impedance. The graph is semicircular with higher frequencies associated near the origin and lower ones away from the origin.

sensitive for measuring electrode surface changes, and allows complex biorecognition events to be probed with a simple, label-free, and mediator-free strategy.

During an impedance measurement, a small amplitude AC signal is imposed to excite the surface and the current with respect to the polarizing potential is monitored with the capacitive (imaginary (Z")) and faradaic (real (Z')) components of impedance being identified, quantified and displayed as Nyquist plots to determine the resistive, capacitive and inductive behavior of the surface at that particular frequency [51]. (Figure 3.12)

From these Nyquist curves, several key parameters and system operations are deduced. Namely, solution resistance, double layer capacitance (or constant phase elements formation) and electron transfer resistance were calculated to measure solution stability, surface properties or diffusion issues. Since this plot also contains the frequency information associated with a particular impedance measurement, it is widely used in impedance analysis.

Impedance changes between electrode surfaces and a surrounding solution upon a binding event can be transduced into an electrical signal, using a frequency response analyzer. There are several theories as to how this binding event affects changes in real and imaginary components of the system, although it is difficult to identify the origin of these changes. One theory hypothesizes that binding of larger antigens forms a resistive bar-

rier, causing the impedance to increase whilst binding of smaller antigens can facilitate a charge transfer and lower impedance [52]. Another theory is that when the Ab/Ag complex is formed, the binding events between the hyper-variable loop regions mean that conformational changes occur and potential changes are introduced into the system.
During EIS, a signal in the form below is applied: (Equation(3.12))

$$V_{(t)} = V_m.sin(\omega.t) \tag{3.12}$$

where $V_{(t)}$ is the overall signal with an amplitude (V_m) and an angular frequency (ω). The resulting current response is measured through Equation (3.13).

$$i_{(t)} = I_m.sin(\omega.t + \theta) \tag{3.13}$$

The impedance at a particular frequency is then calculated simply by the following relationship: (Equation(3.14))

$$Z_\omega = \frac{V(t)}{i(t)} \tag{3.14}$$

3.4 Basic Concepts in Microfluidic devices

3.4.1 Introduction

In the past 10 years, microfluidic technology has evolved from an intriguing concept to a vigorous growth industry that produces numerous publications and patents per year and yet can still be considered in its infancy. Despite impressive laboratory results, microfluidic immunoassay devices have yet to make a major impact on the commercial market. A reason for this is that all of the necessary technologies such as fabricating structures, modifying surfaces, integrating detection, and the chemistry of the immunoassay need to be combined and optimized in order to compete with existing methods that have been perfected over decades [53].
A microfluidic device can be identified by the fact that it has one or more channels with at least one dimension less than 1 mm. Common fluids used in microfluidic devices include blood samples, bacterial cell suspensions, protein or antibody solutions and various buffers. Microfluidic technology in general seeks to improve analytical performance by reducing the consumption of reagents, decreasing the analysis time, increasing reliability and sensitivity through automation, and integrating multiple processes

in a single portable device. These features are particularly suitable for immunoassay applications.
Microfluidic systems for biosensing normally consist of a set of fluidic operation units that allow different biomolecules to be detected and assayed in an easy and flexible manner. Overall, the chip-based platform which has good integration with micro/nano-fluidic components is capable of sampling, filtration, preconcentration, separation, restacking, and detection for biomolecules.
Based on their flow type, microfluidic systems can be categorized into two main types, continuous and discrete.

- Continuous microfluidic systems: Continuous-flow microfluidic operation is a promising approach for many well-defined and simple biochemical applications or even chemical separation, because it is easy to implement and less sensitive to protein fouling problems. They, however, are less suitable for tasks requiring a high degree of flexibility or complicated fluid manipulations. These closed-channel systems are inherently difficult to integrate and scale because the parameters that govern the flow field vary along the flow path making the fluid flow at any one location dependent on the properties of the entire system.
- Discrete microfluidic systems: Droplet-based microfluidic systems are currently an emerging area of microfluidic research. One of the most popular means is to inject multiple laminar streams of aqueous reagents into an immiscible carrier fluid and therefore to induce flow instability instantly for forming the droplets [54].
  There are several distinctive advantages based on droplet-based microfluidic systems. First, the systems promise a new high-throughput technology that enables the generation of microdroplets in excess of several thousand per seconds. In addition, parallel and serial in-vitro compartmentalization is possible with this technology. The reagents are confined inside the droplets in water-in-oil (w/o) emulsions and reagent transport occurs with no dispersion. This unique feature enables chemical reaction indexing, thereby facilitates many chemical reactions in a highly organized manner. Furthermore, fast mixing can occur within minute volumes of microdroplets (nanoliter to femtoliter range) due to the short diffusion distance and chaotic mixing within droplets with the use of twisting channel geometries by stretching, folding, and reorienting fluid. Another feature is that the variation of the channel dimensions can regulate the droplet volumes. With a control of flow rate, the reagent concentrations can be modified accordingly.

While heterogeneous immunoassays benefit from the high surface area/volume ratio in the microchannel, homogeneous assays typically take

advantage of the multiplexing and very fast electrophoretic separations made possible by the microchip format.
Microfluidic devices can be used to obtain a variety of interesting measurements including molecular diffusion coefficients, fluid viscosity, pH, chemical binding coefficients and enzyme reaction kinetics. Other applications for microfluidic devices include capillary electrophoresis, isoelectric focusing, immunoassays, flow cytometry, sample injection of proteins for analysis via mass spectrometry, polymerase chain reaction (PCR) amplification, DNA analysis, cell manipulation, cell separation, cell patterning and chemical gradient formation. Many of these applications have utility for clinical diagnostics. In pursuit of these goals, special interest should be focused on the following areas [55]. It should be noted that considering the final goal of this work, this section is focused on microfluidic immunoassays.

- Materials. In addition to practical considerations for fabrication, the nature of the exposed surface in the channel can be especially important because of the large surface area to volume ratios associated with these dimensions. Given the cost advantage of plastics, which is especially important in disposable devices, the search for improved plastic materials for the microfluidic chip will continue.
- Surface modification. A problem that will continue to be faced when working in the microscale is non-specific adsorption. Modification of the surface of the channels is often necessary to prevent adsorption of the sample and key reagents, which degrades assay performance. Non-specific adsorption of biological components of an assay, especially on plastic, can also create a background signal that determines the detection limit for an assay. Surface modification will also be used to improve electroosmotic flow, which requires a charged surface, in channels made of plastic for Capillary electrophoresis(CE)-based immunoassays.[4]
- Introducing sample/reagent and moving fluid within the microfluidic. A strategy must be devised to interface the macroscale of the traditional laboratory to the microscale of the device.
  The capability for simultaneous multianalyte analysis will grow, prob-

[4]Microchip CE-based immunoassays: Miniaturized devices using electrophoresis to perform immunoassays have been reported where the assay relies on a difference in the electrophoretic mobilities of the immunocomplex of antigen and labeled antibody from either of the two components [56]. Thus, microchip CE assays use a separation step, electrokinetically separating the immunocomplex from the free antibody. Chip-based microfluidic immunoassays have several advantages over conventional CE assays. The channel is very small relative to the bulk of the chip, so heat is dissipated much faster than capillary-based systems. This allows higher field strengths to be used, resulting in faster separations and higher resolution. The faster separations, combined with greater capability for integrated sample preparation and the potential for multiplexing, make chip-based CE a valuable tool for high throughput applications such as combinatorial chemistry that only supply small sample volumes.

ably through more complicated multipath microfluidic systems, by integration with microarrays, or by coded microbeads that carry a number of different capture antibodies.

- Microfluidic design. Design is critical to the device performance characteristics, particularly in accommodating or exploiting the properties of fluid water on the microscale.
- Detection. Detection on small volumes will improve. This is while different assay techniques use various signal transduction pathways to recognize an antibody/antigen binding event, and these must be adapted to the very small volumes.
- Integration and miniaturization. The lack of full integration of on-chip components such as detection has limited the implementation of microfluidics technology for application outside the laboratory or research facility. Common detection strategies involve microscopes, potentiostats, photomultiplier tubes, lasers, and other hardware that is bulky, expensive, and requires a trained technician to maintain. Only one completely on-board system has been reported [57].
  On-chip components include miniature pumps and valves, electrochemical detectors, and electromagnets to capture beads for a sandwich heterogeneous assay.
- Reagent stability. As portable devices for use in the field appear, issues of reagent stability and storage will be dealt with. This is especially important since the key bio-reagents are fragile.

Some of these specific areas are discussed in detail below:

3.4.2 Materials for the microfluidic devices

The materials used to construct microfluidic immunoassay devices vary depending on the application, but the vast majority of such devices are constructed of glass, silicon, or polymers [58]. Each of these materials has its own advantages and limitations.
The glass materials were preferred partly for the biocompatibility toward the biomedical related applications and the ideal surface characteristics where high temperature or strong solvents should appear [59]. However, lack of optical transparency at wavelengths of interest (for silicon), micromachining difficulties, and comparably high expenses for both silicon and glass materials have hampered their wider applications in microfluidics. Tremendous effort has been made to find alternative materials that are more cost-effective and easier for micromachining.
With the development of related fabrication techniques in recent years,

the polymer/plastic-based microfluidic systems have garnered more interest than its conventional competitors [60]. In spite of comparatively weak bonding and structure deformation during device packaging processes, polymer materials still seem attractive due to the facts that: they are more economic compared to silicon and glasses, easier to be fabricated in/on, avoidance of high-temperature annealing and stringent cleaning, more system integration friendly (e.g., interconnections), and there exists a wider range of materials to be chosen for characteristics that are required for each specific application, such as good optical transparency, biocompatibility, and chemical or mechanical properties. Another important reason for the interest from both academia and industry on polymer microfluidic devices is the possibility of disposable microfluidic chips toward biomedical and clinical applications.

One particular polymer that is extensively used in this regard is PDMS. PDMS is a transparent, elastomeric polymer that can be fabricated rapidly with features having dimensions as small as 10 nm [61]. The elastomeric nature of PDMS makes it seal well, and often the adhesion due to conformal surface contact with a smooth, flat surface is enough to seal microchannels for low pressure applications. Alternatively, PDMS can be bonded irreversibly to itself, glass, or silicon by treating both bonding surfaces with plasma treatment. Another significant advantage of PDMS over glass, silicon, and many other polymers is that the PDMS fabrication process can be done under normal laboratory conditions, as opposed to the confines of a clean room that can be expensive to maintain or difficult to access [62]. The principal limitations of PDMS for immunoassay applications are due to its hydrophobic surface properties. Thus, proteins and other molecules tend to adsorb to an untreated PDMS surface, and the surface is poorly wetted and prone to forming bubbles in aqueous systems. These limitations can be reduced or eliminated through chemical or plasma treatment of the surface [63].

Although PDMS now has an established role in prototyping new designs for microfluidic devices, its usefulness for commercial applications is limited because the fabrication process does not lend itself to the mass production accessible to injection molded or embossed hard plastics [64]. Also, PDMS is not as durable as the more rigid plastics and polymers such as polystyrene, polycarbonate, and polymethyl methacrylate (PMMA) that are often used in commercial devices.

Thermoplastic polymers, including PMMA and cyclic olefin copolymer (COC), possess low surface free energy and thus tend to be hydrophobic or weakly hydrophilic, limiting the strength of bonds which may be formed between mating substrates [65].

Thermoplastic polymers have several advantages including the low material cost, availability of range of material properties tailored for specific need, and amenability for high- throughput fabrication. They are receiving attention for their structural strength, optical clarity, and biocompatibility.
COC is a comparatively new thermoplastic material, and has been gaining esteem in LOC (Lab-on-chip) fabrication due to its better chemical properties [66]. COC is a copolymer consisting of ethylene and norbornene that is synthesized using a metallocene catalyst [60]. Through its characteristic molecular structure and tailored catalyst technology, COC offers a wide range of grade variations, in terms of flow properties and heat resistance, such as:

- Topas-8007 (Tg = 78°C)
- Topas-5013 (Tg = 130°C)
- Topas-6015 (Tg = 160°C)
- Topas-6017 (Tg = 178°C).

As a result, depending on the specific application, an appropriate substrate material can be selected for the microdevice. Moreover, due to the olefinic character, COC has good resistance towards hydrolysis, acids and alkalis, and most organic polar solvents such as acetone, methanol, and isopropyl alcohol [67]. It can be soluble in organic solvents such as toluene and naphtha. It is characterized as having high purity, good biocompatibility and excellent optical properties. It has higher transparency in visible and near ultraviolet regions compared to PMMA. The refractive index of COC is higher than that of PMMA, making COC ideally suited for applications that use optical detection methods. COC is easier to emboss, which is especially important when using soft PDMS tools because the density of COC is lower than that of PMMA. The water absorption of COC is 0.01% which is ten times less than that of PMMA. Thus, the relative humidity changes in the environment will not significantly affect devices replicated in COC.
Current methods for fabrication of microfluidic devices include prototyping techniques (includes hot embossing, injection molding, and soft lithography) and direct fabrication techniques such as laser photoablation or laser micromachining, photolithography/optical lithography and x-ray lithography [68] [69]. In fact, during the past decade photolithography techniques have progressed to achieve smaller feature patterning ability and have been coupled to various plastic/polymer-based techniques to better suit lab-on-a-chip applications. To date, most of the current soft lithography processes still rely on modern photolithography techniques for master template/mask fabrication. Consequently, the low resolution ability of soft lithography can be gradu-

ally improved with the high quality masks by modern photolithography. Sub-100-nm fabrication resolution can also be achieved by composite layers of stamps [70].
Bonding can also be enhanced through the generation of electrostatic interactions, and surfaces possessing high specific energy in the form of polar functional groups, which can produce hydrogen or covalent bonds across the interface, are capable of providing bond strengths exceeding that of the bulk polymer [71].

3.4.3 Surface modification

In the microscale environment, the high surface area/volume ratio magnifies the effects of non-specific binding. This is especially important in immunoassays where key reagents such as antibodies and enzyme labels can adsorb to hydrophobic surfaces, seriously degrading the assay performance. To address this, different strategies have been applied to block or modify the surface of the microchannel, the most common of which has been the use of a blocking agent such as bovine serum albumin (BSA) to pre-coat the surface. While sufficient for many applications, the surface modification is not permanent, and the resulting surface is somewhat heterogeneous [72].
As mentioned earlier, heterogeneous assays are distinguished by attaching the primary antibody to a solid support, and a separation step that isolates the desired analyte from any other potential source of signal. The majority of heterogeneous immunoassay applications use antibodies immobilized on the surface of the device or particles such as beads as the solid phase. Devices that use the microchannel surface for antibody immobilization have the advantage of a higher surface area to volume ratio than a standard well format.
This is while the antibodies that are directly adsorbed on a hydrophobic surface by the hydrophobic effect may be partially or completely denatured due to the conformation changes associated with the adsorption process. A further limitation of immobilization on a hydrophobic surface is that blocking steps are usually necessary to limit the non-specific binding of proteins and small molecules that could reduce the effectiveness of the assay. Different strategies to immobilize antibodies on the surface are discussed earlier in Chapter 2.

3.4.4 Introducing sample/reagent and moving fluid within the microfluidic.

A strategy must be devised to interface the macroscale of the traditional laboratory to the microscale of the device. Reagents are typically

introduced by way of pressure-, electrokinetic-, or capillary-driven flow.

Pressure Driven Flow In pressure driven flow, the fluid is pumped through the device via positive displacement pumps, such as syringe pumps. One of the basic laws of fluid mechanics for pressure driven laminar flow, the so-called no-slip boundary condition, states that the fluid velocity at the walls must be zero. This produces a parabolic velocity profile within the channel. The parabolic velocity profile has significant implications for the distribution of molecules transported within a channel. Pressure driven flow can be a relative inexpensive and quite reproducible approach to pumping fluids through microdevices. With the increasing efforts at developing functional micropumps, pressure driven flow is also amenable to miniaturization.

Electrokinetic Flow Another common technique for pumping fluids is that of electro-osmotic pumping. In devices that use electrokinetic flow, reagents are typically pipetted or otherwise transferred into a reservoir on the device, at which point flow is controlled by applying electric potentials. Similarly, samples introduced by capillary flow are typically loaded into a reservoir connected to the microchannel.
If the walls of a microchannel have an electric charge, as most surfaces do, an electric double layer of counter ions will form at the walls. When an electric field is applied across the channel, the ions in the double layer move towards the electrode of opposite polarity. This creates motion of the fluid near the walls and transfers via viscous forces into convective motion of the bulk fluid. If the channel is open at the electrodes, as is most often the case, the velocity profile is uniform across the entire width of the channel. However, if the electric field is applied across a closed channel (or a backpressure exists that just counters that produced by the pump), a recirculation pattern forms in which fluid along the center of the channel moves in a direction opposite to that at the walls. In closed channels, the velocity along the centerline of the channel is 50% of the velocity at the walls.
One of the advantages of electrokinetic flow is that the blunt velocity profile avoids many of the diffusion nonuniformities that occur with pressure driven flow. However, sample dispersion in the form of band broadening is still a concern for electro-osmotic pumping. Another advantage to electrokinetic flow is that it is straight forward to couple other electronic applications on-chip. However, electrokinetic flow often requires very high voltages, making it a difficult technology to miniaturize without off-chip power supplies. Another significant disadvantage of electrokinetic flow is the variability in surface properties.

Capillary flow Capillary forces result from the interaction of liquid, gas and solid surfaces, at the interface between them. In the liquid phase, molecules are held together by cohesive forces. In the bulk of the liquid, the cohesive forces between one molecule and the surrounding molecules are balanced. However, for the same molecule at the edge of the liquid, the cohesive forces with other liquid molecules are larger than the interaction with air molecules. As a result, the liquid molecules at the interface are pulled together towards the liquid. The overall effect of these forces is to minimize the free surface of the liquid that is exposed to air. The proportionality between the decrease in energy of the surface that results from decreasing the surface is described by the surface tension.
The flow of a fluid through a microfluidic channel can be characterized by the Reynolds number, defined as Equation (3.15), where v is the maximum velocity of the object relative to the fluid (m/s); L is a characteristic linear dimension (traveled length of the fluid) (m); μ is the dynamic viscosity of the fluid (Pa.s or N.s/m^2 or kg/(m.s)); ν is the kinematic viscosity ($\nu = \frac{\mu}{\rho}$) (m^2/s); ρ, is the density of the fluid (kg/m^3) [73].
For many microchannels, L is equal to 4A/P where A is the cross sectional area of the channel and P is the wetted perimeter of the channel. Due to the small dimensions of microchannels, the Re is usually much less than 100, often less than 1.0. In this Reynolds number regime, flow is completely laminar and no turbulence occurs. Laminar flow provides a means by which molecules can be transported in a relatively predictable manner through microchannels. The transition to turbulent flow generally occurs in the range of Reynolds number 2000.

$$Re = \frac{inertial forces}{viscous forces} = \frac{\rho.v.L}{\mu} = \frac{v.L}{\nu} \tag{3.15}$$

3.4.5 Detection

Different assay techniques use different signal transduction pathways to recognize an antibody/antigen binding event. Most applications use a label to increase the sensitivity of detection. Current labels include metals, redox labels, optical labels and enzymes. The majority of detection techniques mentioned in the biosensor section can similarly be adopted in microfluidic devices.
In recent years, microfluidic systems fabricated using micromanufacturing techniques integrated with electrochemical sensing electrodes and microfluidic control devices have attracted considerable interest and shown their great potential for chemical analysis and

biomedical applications.
Electrochemical detection strategies commonly have an innate high sensitivity and simplicity that can be effectively married to miniaturized hardware. As such, they constitute, arguably, the most practical, quantifiable, and saleable of all low cost diagnostic assessments of a protein's presence.
From among different types of electrochemical techniques mentioned in the previous section, amperometry is a simple technique and thus miniaturization and integration can be easily achieved by creating a three-electrode system in the microfluidic chip [74]. Amperometric detection method has some advantages including simple, low background noise. It is the most popular electrochemical detection method in the microfluidic immunoassay system. However, it is not the universal method. It requires the analyte to have the electrochemical activity; otherwise some additional substances with the electrochemical activity must be introduced to the immunoassay system for the indirect detection.
Potentiometric detection method has the specificity because it uses the ion-selective membrane to achieve charge separation. However, the selective membrane is hard to integrate into the microfluidic system, which greatly limits the application of this method in the microfluidic immunoassay. Conductometric detection method is a universal detection method but lacks the specificity. According to the principle, the conductivity between the background solution and the analyte must be sufficiently different. If there are two kinds of the analytes which have the similar conductivity, then this method cannot distinguish them.
A significant advantage of voltammetry for detection in a microfluidic system is the improvement in performance that accompanies the reduction of electrode size into the low micrometer range. As the electrode diameter is decreased into the low micrometer range, a shift to nonplanar diffusion (e.g., hemispherical) occurs, causing an increase in the collection efficiency of the electroactive species at the surface [75]. The practical result is an increase in the signal to noise ratio, which generally translates into a lower detection limit [76].

3.4.6 Design

The materials, shape, and complexity of different microfluidic systems vary depending on the intended application. Some devices consist of a single channel, while others are complex patterns with multiple integrated components. While the on-chip integration of such components as mixers, valves and detectors has the advantage of increased porta-

bility, the complexity of the fabrication process increases dramatically, and the reliability of the device diminishes.
This is while, adding multiple channels or other more complex two-dimensional designs does not significantly affect the time or difficulty of fabrication, and so many high-throughput multiplexing applications can be efficiently addressed using microfluidics [56].

References

[1] R. Yalow and S. Berson, "Assay of plasma insulin in human subjects by immunological methods," *Nature*, vol. 184, pp. 1648–1649, 1959.

[2] E. Engvall and P. Perlmann, "Enzyme-linked immunosorbent assay (elisa) quantitative assay of immunoglobulin g," *Immunochemistry*, vol. 8, no. 9, pp. 871–874, 1971.

[3] J. Butler, "Enzyme-linked immunosorbent assay," *J Am Geriatr Soc Immunoassay*, vol. 21, no. 2-3, pp. 165–209, 2000.

[4] J. Vaitukaitis, G. Braunstein, and G. Ross, "A radioimmunoassay which specifically measures human chorionic gonadotropin in the presence of human luteinizing hormone," *Am J Obstetrics and Gynecology*, vol. 113, no. 6, pp. 751–758, 1972.

[5] S. Centi, S. Laschi, and M. Mascini, "Strategies for electrochemical detection in immunochemistry," *Bioanalysis*, vol. 1, no. 7, pp. 1271–1291, 2009.

[6] P. von Lode, "Point-of-care immunotesting: Approaching the analytical performance of central laboratory methods," *Clin Biochem*, vol. 38, no. 7, pp. 591–606, 2005.

[7] A. Sassolas, L. J. Blum, and B. D. Leca-Bouvier, "Immobilization strategies to develop enzymatic biosensors," *Biotechnol Adv*, vol. 30, no. 3, pp. 489–511, 2012.

[8] D. R. Thévenot, K. Toth, R. A. Durst, and G. S. Wilson, "Electrochemical biosensors: recommended definitions and classification," *Biosens Bioelectron*, vol. 16, no. 1-2, pp. 121–131, 2001.

[9] F. Faridbod, V. K. Gupta, and H. A. Zamani, "Electrochemical sensors and biosensors," *Int J Electrochem*, 2011.

[10] H. Nassef, L. Civit, A. Fragoso, and C. O'Sullivan, "Amperometric immunosensor for detection of celiac disease toxic gliadin based on fab fragments," *Anal. Chem.*, vol. 81, no. 13, pp. 5299–5307, 2009.

[11] A. Warsinke, "Point-of-care testing of proteins," *Anal Bioanal Chem*, vol. 393, no. 5, pp. 1393–1405, 2009.

[12] A. Koyun, E. Ahlatcioglu, and Y. Koca Ipek, *A Roadmap of Biomedical Engineers and Milestones*. InTech, 2012, ch. Biosensors and Their Principles.

[13] G. Zheng, F. Patolsky, Y. Cui, W. Wang, and C. Lieber, "Multiplexed electrical detection of cancer markers with nanowire sensor arrays," *Nat Biotechnol.*, vol. 23, no. 10, pp. 1294–1301, 2005.

[14] D. S. Hage, "Immunoassays," *Analytical Chemistry*, vol. 67, no. 12, pp. 455–462, 1995. [Online]. Available: http://dx.doi.org/10.1021/ac00108a030

[15] J. Wang, A. Ibáñez, M. P. Chatrathi, and A. Escarpa, "Electrochemical enzyme immunoassays on microchip platforms," *Anal. Chem.*, vol. 73, no. 21, pp. 5323–5327, 2001.

[16] D. L. Stokes, G. D. Griffin, and T. Vo-Dinh, "Detection of e. coli using a microfluidics-based antibody biochip detection system," *Fresen J Anal Chem*, vol. 369, no. 3-4, pp. 295–301, 2001.

[17] A. Hatch, A. E. Kamholz, K. R. Hawkins, M. S. Munson, E. A. Schilling, B. H. Weigl, and P. Yager, "A rapid diffusion immunoassay in a t-sensor," *Nat Biotechnol*, vol. 19, no. 5, pp. 461–465, 2001.

[18] S. Iijima, "Helical microtubules of graphitic carbon," *Nature*, vol. 354, no. 6348, pp. 56–8, 1991.

[19] H. Ke-Jing, N. De-Jun, X. Wan-Zhen, and W. Wei, "A disposable electrochemical immunosensor for carcinoembryonic antigen based on nano-au/multi-walled carbon nanotubes–chitosans nanocomposite film modified glassy carbon electrode," *Anal Chem Acta*, vol. 659, no. 1-2, pp. 102–108, 2010.

[20] M. Daniel and D. Astruc, "Gold nanoparticles: assembly, supramolecular chemistry, quantum-size-related properties, and applications toward biology, catalysis, and nanotechnology," *Chem. ReV.*, vol. 104, pp. 293–346, 2004.

[21] T. Sreeprasad and T. Pradeep, *Springer Handbook of Nanomaterials*. Springer Berlin Heidelberg, 2013, ch. Noble Metal Nanoparticles.

[22] L. Hirsch, J. Jackson, A. Lee, N. Halas, and J. West, "A whole blood immunoassay using gold nanoshells," *Anal. Chem.*, vol. 75, no. 10, pp. 2377–2381, 2003.

[23] J. Svarc-Gajic, Z. Stojanovic, Z. Suturovic, N. Marjanovic, and S. Kravic, "Direct mercury determination in natural waters by chronopotentiometric stripping analysis in macroelectrode process vessel," *Desalination*, vol. 249, pp. 253–259, 2009.

[24] T. Hezarda, K. Fajerwerge, D. Evrardc, V. Collièree, P. Behraa, and P. Grosc, "Influence of the gold nanoparticles electrodeposition method on hg(ii) trace electrochemical detection," *Electrochim Acta*, vol. 73, pp. 15–22, 2012.

[25] W. Vastarella, L. Della Seta, A. Masci, J. Maly, M. De Leo, L. Maria Moretto, and R. PIlloton, "Biosensors based on gold nanoelectrode ensembles and screenprinted electrodes," *Int J Environ An Ch*, vol. 87, no. 10-11, pp. 701–714, 2007.

[26] Y. Lia, H. Schluesenerb, and S. Xua, "Gold nanoparticle-based biosensors," *Gold Bull*, vol. 43, no. 1, pp. 29–41, 2010.

[27] G. Lai, F. Yan, and H. Ju, "Dual signal amplification of glucose oxidase-functionalized nanocomposites as a trace label for ultrasensitive simultaneous multiplexed electrochemical detection of tumor markers," *Anal. Chem.*, vol. 81, no. 23, pp. 9730–9736, 2009.

[28] J. Pingarron, P. Yanez-Sedeno, and A. Gonzalez-Cortes, "Gold nanoparticle-based electrochemical biosensors," *Electrochim Acta*, vol. 53, pp. 5848–5866, 2008.

[29] T. R. Holford, F. Davis, and S. P. Higson, "Recent trends in antibody based sensors," *Biosens Bioelectron*, vol. 34, no. 1, pp. 12 – 24, 2012.

[30] X. Fan, I. M. White, S. I. Shopova, H. Zhu, J. D. Suter, and Y. Sun, "Sensitive optical biosensors for unlabeled targets: A review," *Anal Chem Acta*, vol. 620, no. 1–2, pp. 8 – 26, 2008.

[31] D. Shankaran, K. Gobi, and N. Miura, "Recent advancements in surface plasmon resonance immunosensors for detection of small molecules of biomedical, food and environmental interest," *Sens Actuator B*, vol. 12, pp. 158–177, 2007.

[32] J. Bard and L. Faulkner, *Electrochemical methods: fundamentals and applications*, 2nd ed. Wiley, New York, 2001.

[33] J. Zhu, Z. Zhu, Z. Lai, R. Wang, X. Guo, X. Wu, G. Zhang, Z. Zhang, Y. Wang, and Z. Chen, "Planar amperometric glucose sensor based on glucose oxidase immobilized by chitosan film on prussian blue layer," *Sensors*, vol. 2, pp. 127–136, 2002.

[34] R. Chai, R. Yuan, Y. Chai, C. Ou, S. Cao, and X. Li, "Amperometric immunosensors based on layer-by-layer assembly of gold nanoparticles and methylene blue on thiourea modified glassy carbon electrode for determination of human chorionic gonadotrophin," *Talanta*, vol. 74, no. 5, pp. 1330–1336, 2008.

[35] T. Shimomura, T. Sumiya, M. Ono, T. Ito, and T.-a. Hanaoka, "A novel, disposable, screen-printed amperometric biosensor for ketone 3-b-hydroxybutyrate fabricated using a 3-b-hydroxybutyrate dehydrogenase-mesoporous silica conjugate," *Anal Bioanal Chem*, vol. 405, no. 1, pp. 297–305, 2013.

[36] P. B. Luppa, L. J. Sokoll, and D. W. Chan, "Immunosensors—principles and applications to clinical chemistry," *Clin Chim Acta*, vol. 314, no. 1-2, pp. 1–26, 2001.

[37] *The Dynamic Chemistry E-textbook*. UCDAVIS, 2014, ch. Potentiometric Methods.

[38] J. Haun, T.-J. Yoon, H. Lee, and R. Weissleder, "Magnetic nanoparticle biosensors," *Wiley Interdisciplinary Reviews: Nanomedicine and Nanobiotechnology*, vol. 2, no. 3, pp. 291–304, 2010.

[39] N. Teigell Beneitez, J. Missinne, E. W. A. Visser, L. J. van IJzendoorn, M. W. J. Prins, J. J. H. B. Schleipen, J. L. Vinkenborg, G. Rietjens, M. A. Verschuuren, G. Krishnamoorthy, J. G. Orsel, and G. Van Steenberge, "Evanescent field biosensor using polymer slab waveguide-based cartridges for the optical detection of nanoparticles," *IEEE J. Sel. Top. Quantum Electron.*, vol. 22, no. 3, pp. 1–8, 2016.

[40] D. Bruls, T. Evers, J. Kahlman, P. Van Lankvelt, M. Ovsyanko, E. Pelssers, J. Schleipen, F. De Theije, C. Verschuren, T. Van Der Wijk, J. Van Zon, W. Dittmer, A. Immink, J. Nieuwenhuis, and M. Prins, "Rapid integrated biosensor for multiplexed immunoassays based on actuated magnetic nanoparticles," *Lab Chip*, vol. 9, no. 24, pp. 3504–3510, 2009.

[41] A. Washburn, M. Luchansky, A. Bowman, and R. Bailey, "Quantitative, label-free detection of five protein biomarkers using multiplexed arrays of silicon photonic microring resonators," *Anal. Chem*, vol. 82, no. 1, pp. 69–72, 2010.

[42] V. Mecea, "From quartz crystal microbalance to fundamental principles of mass measurements," *Anal Lett*, vol. 38, pp. 753–767, 2005.

[43] A. M. Coto-Garcia, E. S. Sotelo-Gonzalez, M. T. Fernandez-Arguelles, R. Pereiro, J. M. Costa-Fernandez, and A. Sanz-Medel, "Nanoparticles as fluorescent labels for optical imaging and sensing in genomics and proteomics," *Anal Bioanal Chem*, vol. 399, no. 1, pp. 29–42, 2011.

[44] E. Gileadi, *Electrode Kinetics for Chemists, Chemical Engineers, and Materials Scientists*. New York: Wiley-VCH, Inc., 1993.

[45] A. I. Mohammed, S. Gupta, and S. Hussaini, "A review on electrochemical biosensors: Principles and applications," *Advances in Bioresearch*, vol. 3, no. 4, pp. 158–163, 2012.

[46] N. J. Ronkainen, H. B. Halsall, and W. R. Heineman, "Electrochemical biosensors," *Chem Soc Rev*, vol. 39, no. 5, pp. 1747–1763, 2010.

[47] M. Thompson and L. Kateley, "The nernst equation: Determination of equilibrium constants for complex ions of silver," *J Chem Edu*, vol. 76, no. 1, pp. 95–96, 1999.

[48] P. Kissinger and W. R. Heineman, "Cyclic voltammetry," *J Chem Edu*, vol. 60, no. 9, pp. 702–706, 1983.

[49] R. Greef, R. Peat, L. Peter, D. Pletcher, and J. Robinson, *Instrumental Methods in Electrochemistry*. New York: John Wiley and Sons, 1985.

[50] B. Chang and S. Park, "Electrochemical impedance spectroscopy," *Annu Rev Anal Chem (Palo Alto Calif)*, vol. 3, pp. 207–229, 2010.

[51] S. Grant, F. Davis, K. A. Law, A. C. Barton, S. D. Collyer, S. P. Higson, and T. D. Gibson, "Label-free and reversible immunosensor based upon an ac impedance interrogation protocol," *Anal Chem Acta*, vol. 537, no. 1-2, pp. 163–168, 2005.

[52] E. Tully, S. P. Higson, and R. O'Kennedy, "The development of a 'labeless' immunosensor for the detection of listeria monocytogenes cell surface protein, internalin b," *Biosens. Bioelectron.*, vol. 23, no. 6, pp. 906–912, 2008.

[53] A. Bange, H. B. Halsall, and W. R. Heineman, "Microfluidic immunosensor systems," *Biosens Bioelectron*, vol. 20, no. 12, pp. 2488 – 2503, 2005.

[54] J. Tice, H. Song, A. Lyon, and R. Ismagilov, "Formation of droplets and mixing in multiphase microfluidics at low values of the reynolds and the capillary numbers," *Langmuir*, vol. 19, pp. 9127–9133, 2003.

[55] C.-Y. Liu, J. Rick, T.-C. Chou, H.-H. Lee, and G.-B. Lee, "Integrated microfluidic system for electrochemical sensing of urinary proteins," *Biomed Microdevices*, vol. 11, no. 1, pp. 201–211, 2009.

[56] A. Bromberg and R. Mathies, "Multichannel homogeneous immunoassay for detection of 2,4,6-trinitrotoluene (tnt) using a microfabricated capillary array electrophoresis chip," *Electrophoresis*, vol. 25, no. 12, pp. 1895–1900, 2004.

[57] J.-W. Choi, K. W. Oh, J. H. Thomas, W. R. Heineman, H. B. Halsall, J. H. Nevin, A. J. Helmicki, H. T. Henderson, and C. H. Ahn, "An integrated microfluidic biochemical detection system for protein analysis with magnetic bead-based sampling capabilities," *Lab Chip*, vol. 2, pp. 27–30, 2002.

[58] J. Wu and M. Gu, "Microfluidic sensing: state of the art fabrication and detection techniques," *J Biomed Opt*, vol. 16, no. 8, 2011.

[59] P. Vulto, T. Huesgen, B. Albrecht, and U. G. A., "A full-wafer fabrication process for glass microfluidic chips with integrated electroplated electrodes by direct bonding of dry film resist," *J. Micromech. Microeng.*, vol. 19, no. 077001, 2009.

[60] R. K. Jena and C. Y. Yue, "Cyclic olefin copolymer based microfluidic devices for biochip applications: Ultraviolet surface grafting using 2-methacryloyloxyethyl phosphorylcholine," *Biomicrofluidics.*, vol. 6, no. 1, p. 12822, 2012.

[61] S. Sia and G. Whitesides, "Microfluidic devices fabricated in poly(dimethylsiloxane) for biological studies," *Electrophoresis*, vol. 24, no. 21, pp. 3563–3576, 2003.

[62] J. McDonald, D. Duffy, J. Anderson, D. Chiu, H. Wu, O. Schueller, and G. M. Whitesides, "Fabrication of microfluidic systems in poly(dimethylsiloxane)," *Electrophoresis*, vol. 21, no. 1, pp. 27–40, 2000.

[63] H. Makamba, J. Kim, K. Lim, K. Park, and J. Hahn, "Surface modification of poly(dimethylsiloxane) microchannels," *Electrophoresis*, vol. 24, no. 21, pp. 3607–3619, 2003.

[64] R. Mukhopadhyay, "When pdms isn't the best," *Anal. Chem.*, vol. 79, pp. 3248–3253, 2007.

[65] C. Tsao, L. Hromada, J. Liu, P. Kumar, and D. D.L, "Low temperature bonding of pmma and coc microfluidic substrates using uv/ozone surface treatment," *Lab Chip*, vol. 7, pp. 499–505, 2007.

[66] T. Nielsen, D. Nilsson, F. Bundgaard, P. Shi, P. Szabo, O. Geschke, and A. Kristensen, "Nanoimprint lithography in the cyclic olefin copolymer, topas, a highly ultraviolet-transparent and chemically

resistant thermoplast," *J Vac Sci Technol B: Microelectron Nanometer Struct*, vol. 22, pp. 1770–5, 2004.

[67] "http://www.topas.com/sites/default/files/files/optical_e.pdf."

[68] H. Becker and U. Heim, "Hot embossing as a method for the fabrication of polymer high aspect ratio structures," *Sens. Actuators A*, vol. 83, pp. 130–135, 2000.

[69] U. Attia, S. Marson, and J. Alcock, "Micro-injection moulding of polymer microfluidic devices," *Microfluid. Nanofluid.*, vol. 7, pp. 1–28, 2009.

[70] T. W. Odom, J. C. Love, D. B. Wolfe, K. E. Paul, and G. M. Whitesides, "Improved pattern transfer in soft lithography using composite stamps," *Langmuir*, vol. 18, pp. 5314–5320, 2002.

[71] W. Niles and P. Coassin, "Cyclic olefin polymers: Innovative materials for high-density multiwell plates," *ASSAY and Drug Development Technologies*, vol. 6, 2006.

[72] V. Linder, E. Verpoorte, W. Thormann, N. de Rooij, and H. Sigrist, "Surface biopassivation of replicated poly(dimethylsiloxane) microfluidic channels and application to heterogeneous immunoreaction with on-chip fluorescence detection," *Anal. Chem.*, vol. 73, no. 17, pp. 4181–4189, 2001.

[73] H. Bruus, *Theoretical Microfluidics*. Oxford University Press., 2007.

[74] Y. S. Choi, Y. Ding, C. H. Ahn, H. B. Halsall, and W. R. Heineman, "A microchip electrochemical immunosensor fabricated using micromachining techniques," *Engineering in Medicine and Biology Society, 1997. Proceedings of the 19th Annual International Conference of the IEEE*, vol. 5, pp. 2264–2266 vol.5, 1997.

[75] A. Michael and R. Wightman, *Laboratory Techniques in Electroanalytical Chemistry*, 2nd ed. Dekker, 1996, ch. Microelectrodes.

[76] J. Marcus, W. Anderson, and S. Quake, "Parallel picoliter rt-pcr assays using microfluidics," *Anal. Chem*, vol. 78, pp. 956–958, 2006.

4

Conjugated AuNP-antibody nanoprobe Fabrication and Validation

4.1 Introduction

An electrochemical biosensor usually consists of three parts:

- A receptor biomolecule, which incorporates a biological or biomimetic recognition element (nucleic acid, enzyme, antibody, tissue, organelles or whole cells) and plays a key role in determining the sensitivity of the electrochemical biosensors.
- A transducer, a conductive phase, which converts biochemical signal into a measurable one based on the interaction between the analyte and the biological molecule associated with the transducer surface.
- An amplifier, a computerized apparatus/software used to boost/readout of signal.

An efficient biosensor, therefore, relies heavily on selective/specific binding of the recognition element with the target analytes as well as the transducer for signaling the binding event in terms of response time, signal-to-noise (S/N) ratio, and limits of detection (LoD) [1].

Therefore, designing sensors with higher efficacy depends on the development of novel materials to improve both the recognition and transduction steps.

Nanomaterials, more specifically noble metal nanoparticles (NPs) have played an important role in the development of new biosensors and/or in the enhancement of existing biosensing techniques to fulfill the demand for more specific and highly sensitive biomolecular diagnostics [2] [3]. They can measure between 1 to 100 nm in diameter, have different shapes and can be composed of one or more inorganic/metallic compounds. The majority of them exhibit size-related properties that differ significantly from those observed in micron-sized particles or bulk materials. Recent studies have shown that the labeling of biomolecules such as antibodies with noble metal NPs results in highly sensitive and specific bioassays, while maintaining the bioactivity of the biomarker [4]. The concentration of analytes can also be detected based on the signal detection of such NPs.

Gold nanoparticles (AuNPs) are the most often used labels in sensor studies because of their intriguing size dependent electrical, optical, magnetic, and chemical properties as well as their ease of synthesis, characterization and surface functionalization [5] [6]. Being redox active, AuNPs provide the possibility for the miniaturization of sensing devices to the nanoscale, offering excellent prospects for chemical and biological sensing. They also offer a suitable platform for multifunctionalization with a wide range of organic or biological ligands for the selective binding and detection of biomarkers [7]. This means that the functional activity of these molecules remain unaffected even after their immobilization on AuNPs.

Moreover, because of their high surface area to volume ratios, AuNPs serve as an excellent scaffold to immobilize large quantities of organic or biomolecules, thus increasing the chance of their interaction with a target analyte [8]. On the other hand, AuNPs (e.g., citrate capped) are mostly negatively charged, and can therefore be tailored to electrostatically interact with certain positively charged biomolecules that in turn can have a highly selective interaction exclusively with the target analyte of interest. Furthermore, biofunctionalized AuNPs also have the advantage of multiplexing in the detection of analytes. AuNPs offer size based signal amplification as one of the benefits and thus substantial increase in the size of these particles increases the sensitivity of the sensor.

In view of the above mentioned facts, broad potential of AuNPs for signal amplification of antibody–antigen recognition events on simple, ultrasensitive, multiplexed immunosensors becomes apparent [9]. Thus much attention should be devoted to the preparation and appli-

cation of antibody-AuNP conjugates with better operability and controllability in biomarker detection. With the developed and discussed technique herein, a simple, sensitive, and low cost solution has been modeled to be used for measuring serum levels of biomarkers later on in this work and in future in single and/or multiplexed sensor systems.

4.2 Synthesis of a conjugated AuNP-antibody nanoprobe

4.2.1 Synthesis of AuNPs

Ever since Faraday's work in 1857, several methods have been applied to synthesize AuNPs with a good level of homogeneity and provide fine control over size, shape and surface properties, in order to better take advantage of their unique physicochemical properties for biosensing [10]. These AuNPs, also known as colloidal gold, can be easily synthesized in sizes ranging between 3 and 200 nm in diameter and in different shapes, being the most common the quasi-spherical shape, mainly due to their surface energy that favors the formation of spherical particles.

One of the most common approaches for the preparation of AuNPs in aqueous solution was introduced by Turkevich, and subsequently improved by Frens [11] [12]. In order to synthesize 10–100 nm AuNPs, generally, tetrachloroauric acid ($HAuCl_4$) is reduced in the presence of different concentrations of trisodium citrate as a reducing agent. Briefly, in this work, 200 ml of 0.01 % $HAuCl_4$ solution was brought to boil with gentle stirring. Thereafter, 4.5 ml of 1 % trisodium citrate was rapidly added and boiling was pursued for an additional 15 min. The solution was stirred continuously after removing the beaker from the hot plate. Once mixing occurred, the color of the solution changed gradually from light yellow to wine red. The solution was then cooled down to room temperature. This solution was stored at 4° C for further use. (Figure 4.1)

The sodium citrate, in this procedure, not only behaves as a reducing agent but also provides the negative surface charge adsorbed around the AuNPs, which can repel the particles and restrain the formation of any aggregation. The concentrations of gold salt and trisodium citrate as well as temperature and mixing rate are main factors defining the size-distribution of the synthesized gold nanoparticles [13]. The strength of the observed color of solution is highly dependent on the quality as well as the size of the developed colloidal gold particles [14].

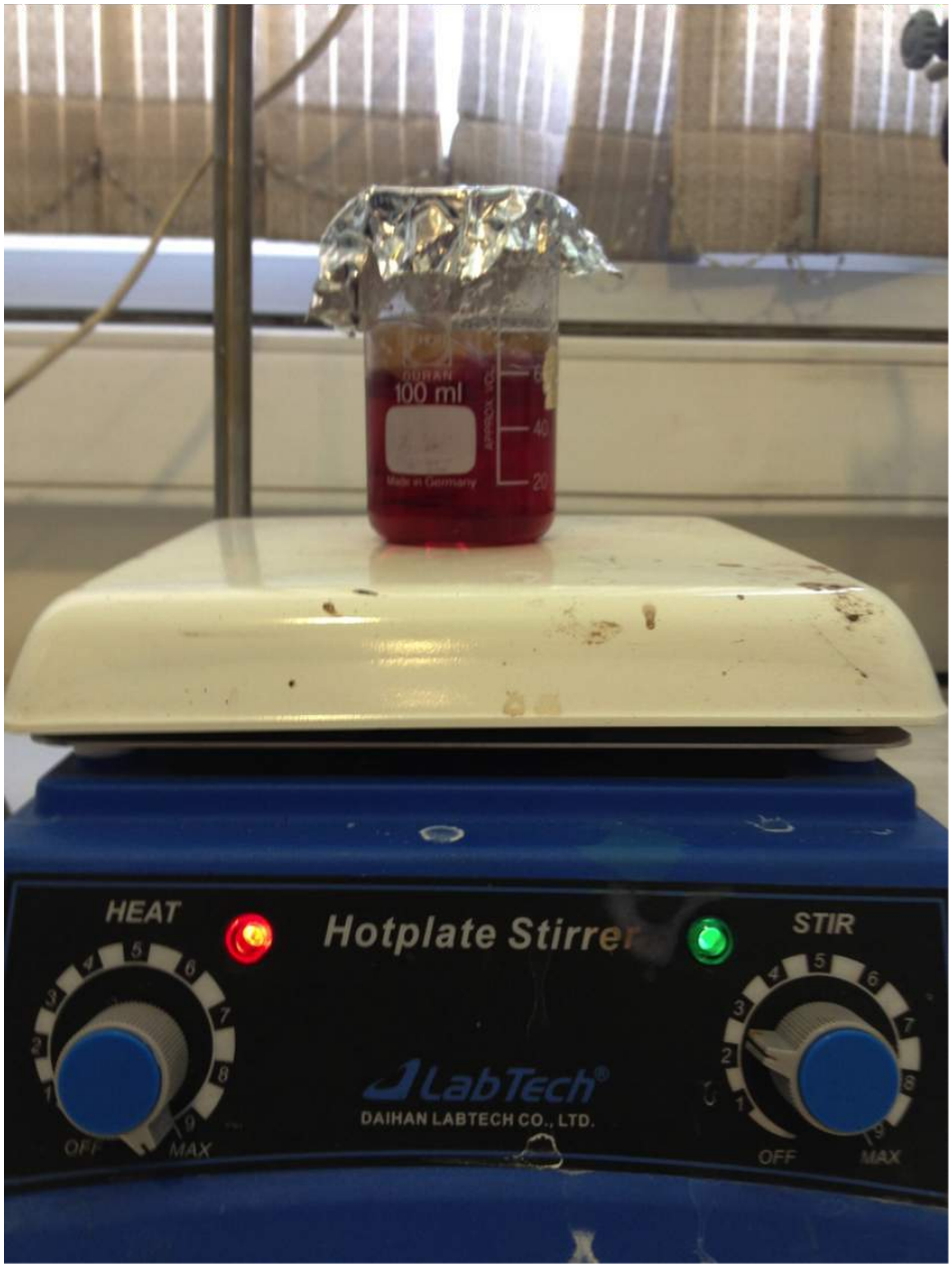

Figure 4.1: Colloid gold preparation process.

4.2.2 AuNP-antibody Conjugation

As mentioned in Chapter 2, conjugation of noble metal nanoparticles such as gold and silver with biomolecules has mainly been achieved by one of four major mechanisms: electrostatic adsorption, direct chemisorption of thiol derivatives, covalent binding through bifunctional linkers, and specific affinity interactions [15].
In view of these facts, the covalent binding through crosslinkers was used in this work. As the first step, Oc antibody (10 μg/mL) and sulfo-NHS (100 mM) were incubated for 2.5 hours at room temperature. The GSH solution (10mM) was then added to the complex and left to react for another hour. Thereafter the AuNP solution was added.

4.3 Characterization of conjugated AuNP-antibody nanoprobe

4.3.1 Characterization of AuNPs

In order to obtain information about structure, morphology and size of the synthesized AuNPs, UV-Vis spectroscopy, TEM analysis and zeta potential measurements were applied.
The UV–Vis spectrophotometer has been the first optical technique employed for the characterization of AuNPs. In this method, the width of the absorption spectra is related to the size distribution range of the nanoparticles and with increasing particle size, the absorption peak shifts to longer wavelengths [16]. Generally, gold nanospheres display a single absorption peak in the visible range between 510-550 nm, mainly at 520 nm due to surface plasmon resonance properties (SPR) of colloidal AuNPs prepared by the conventional citrate reduction method [17]. (Figure 4.2) Similarly, the UV-Vis spectrum of the as-prepared AuNP showed only one band with a maximum λ at 520 nm. Lack of a band at around 680 nm indicates the absence of aggregated gold particles [18].

The size and size-distribution of gold nanoparticles developed using the Turkevich and Frens method is reported to be dependent on the concentrations of gold salt, trisodium citrate, temperature and mixing rate. TEM was used to characterize the morphology and determine the size of the as-prepared AuNPs. According to the results, numerous uniformly distributed nanoparticles with size distribution of about 5-10 nm were observed in the solution with very few particles of higher and lower size distribution. These images also show that the majority

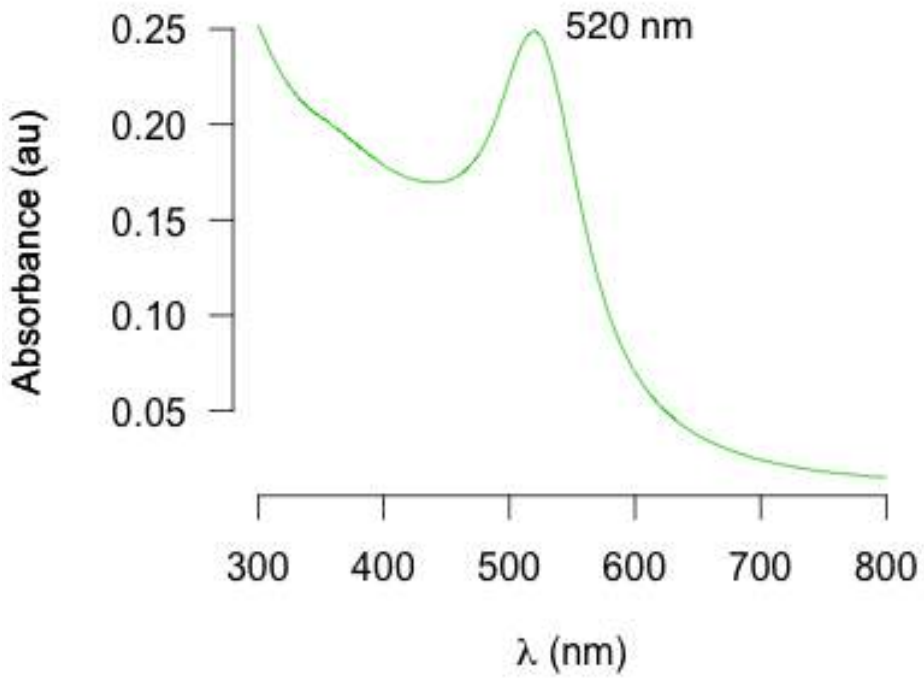

Figure 4.2: UV–Vis spectra of colloidal AuNPs.

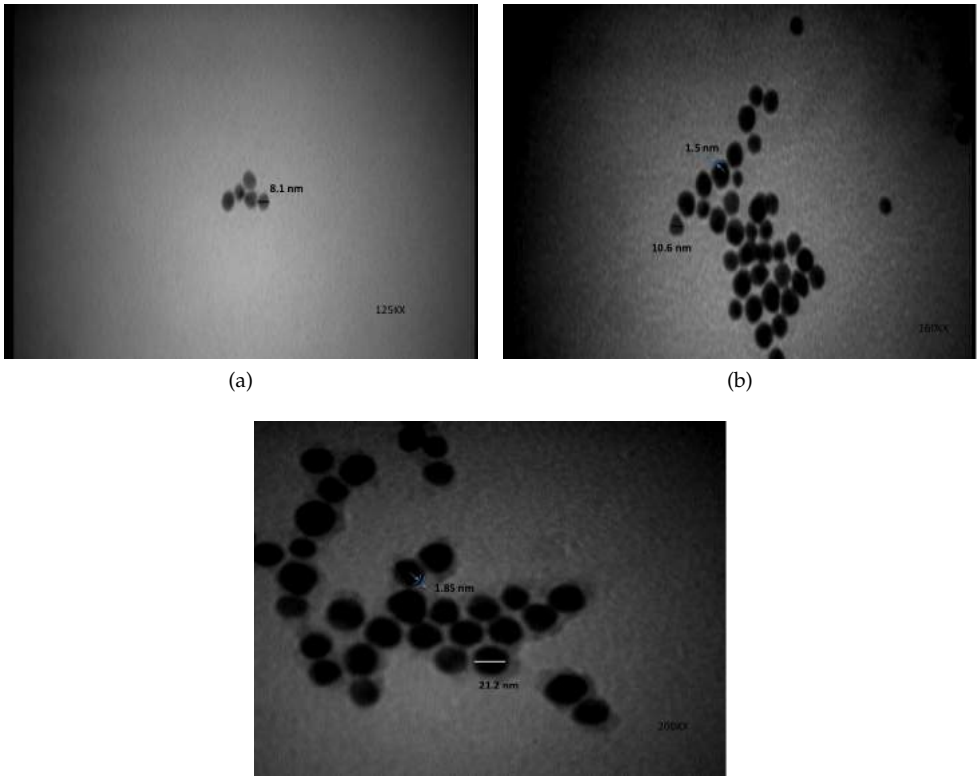

(a) (b)

(c)

Figure 4.3: TEM results of a) monodispersed gold nanoparticles, b) gold nanoparticles capped with GSH, c) antibody-conjugated gold nanoparticles. (For a, scale = 125 KX; for b, scale = 160 KX; for c, scale = 200 KX)

of the developed gold nanoparticles were spherical in shape.(Figure 4.3)

The hydrodynamic diameter of nanoparticles was measured using a zeta-sizer nano-ZS. (Figure 4.4) The peak mean, about 7.5 nm, shows the mean diameter of the majority of the particles according to intensity. The particles had a mean zeta potential of 97 mV.

4.3.2 Characterization of AuNP/Ab nanocomplex

AuNP conjugation with different proteins is well studied in the literature but the mechanisms behind the process are poorly understood.

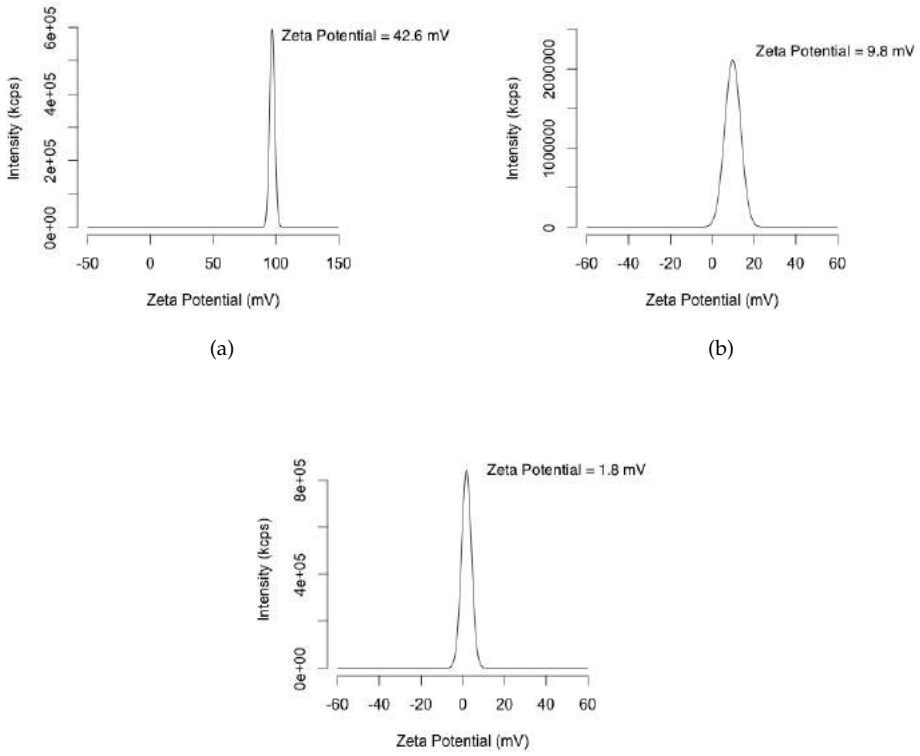

Figure 4.4: Zeta-potential results of a)gold nanoparticles, b) GSH-capped gold nanoparticles, c) antibody-conjugated gold nanoparticles.

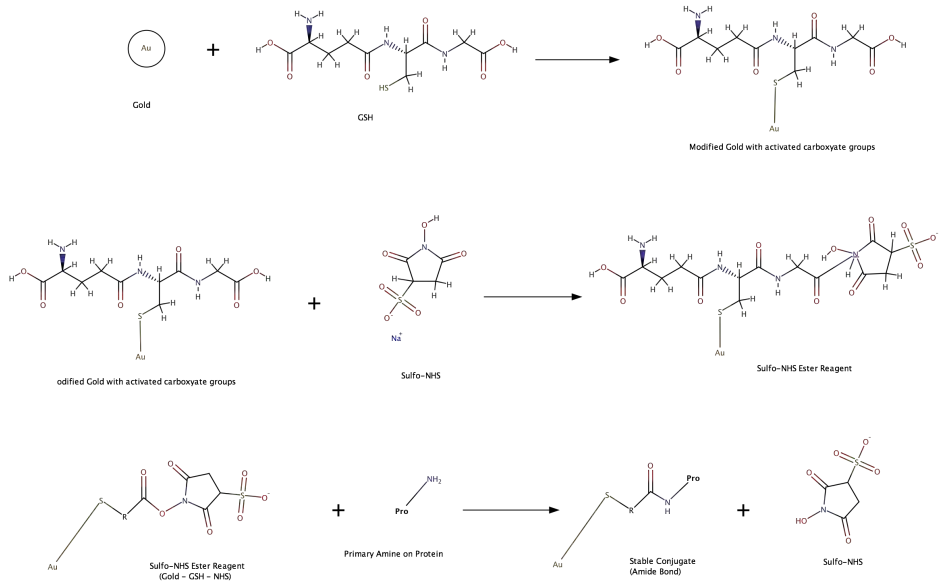

Figure 4.5: Chemical reactions occurring in different steps.

Therefore special care needs to be taken throughout the process to ensure the quality of the end product. The protocol used for conjugation of AuNPs to Oc antibody in this work relies on covalent and electrostatic attractions between constituents.

In this reaction, sulfo-NHS acts as a cross-linker facilitating the bonding of an amine group of the antibody to a carboxylic group of GSH. (Figure 4.5) GSH on the other end provides the thiol groups needed to bind the antibody complex to AuNPs. In other words, binding of antibody complex to gold atoms happened through thiol linkages, ionic interactions between the negatively charged gold surface and the positively charged terminals on the complex, and interactions originating from absorption of hydrophobic groups on AuNPs.

Another advantage of the above mentioned method is covalent coupling via a cross-linker being specific and controllable. The tertiary structure of the protein is maintained in this method and thus the antibody remains functional in the future steps.

The conjugates developed through direct absorption of the antibody on the surface of the nano-colloid particles using non-covalent bonds, such as London, van der Waals force and hydrophobic interactions were not stable. (Figure 4.6)

Characterization of the resulting conjugates was done promptly by

Figure 4.6: Representative schematic showing nanoconjugate formation steps.

TEM and FTIR measurements of freshly prepared solution. (Figure 4.3) According to these results, dispersed AuNPs became aggregated upon addition of GSH without significant alteration in particle morphology or size. This was also confirmed by DLS, which showed a slight increase in nanoparticle size from 3.88 to 7.48 nm after GSH addition. (Figure 4.7)

The attachment of the Ab to GSH-modified gold nanoparticles, on the other hand, resulted in a considerable increase in size and the core-shell structure, in accordance with previously reported Ab-conjugated-nanoparticles [19] [20]. According to DLS, the size of the antibody-conjugated nanoparticles was as high as 74.3 nm. (Figure 4.4) Adding GSH and Ab also considerably reduced the electro kinetic potential of the nanoparticles from 42.6 mV to 9.8 mV and 1.8 mV, respectively.

The conjugation of gold nanoparticles with antibodies, Oc in our case, was also verified by FTIR. (Figure 4.8) The FTIR spectrum of GSH-modified AuNP showed an obvious absorption peak corresponding to the N-H stretch at 3213/cm. The –COOH stretch vibration in GSH-AuNP remained unaltered at 1095/cm, indicating no hydrogen binding among GSH molecules. The characteristic GSH band seen at 2530/cm, due to –SH groups, was absent because of surface binding of GSH to AuNP through thiolate linkage.

After the addition of sulfo-NHS and Ab, as expected, the –COOH

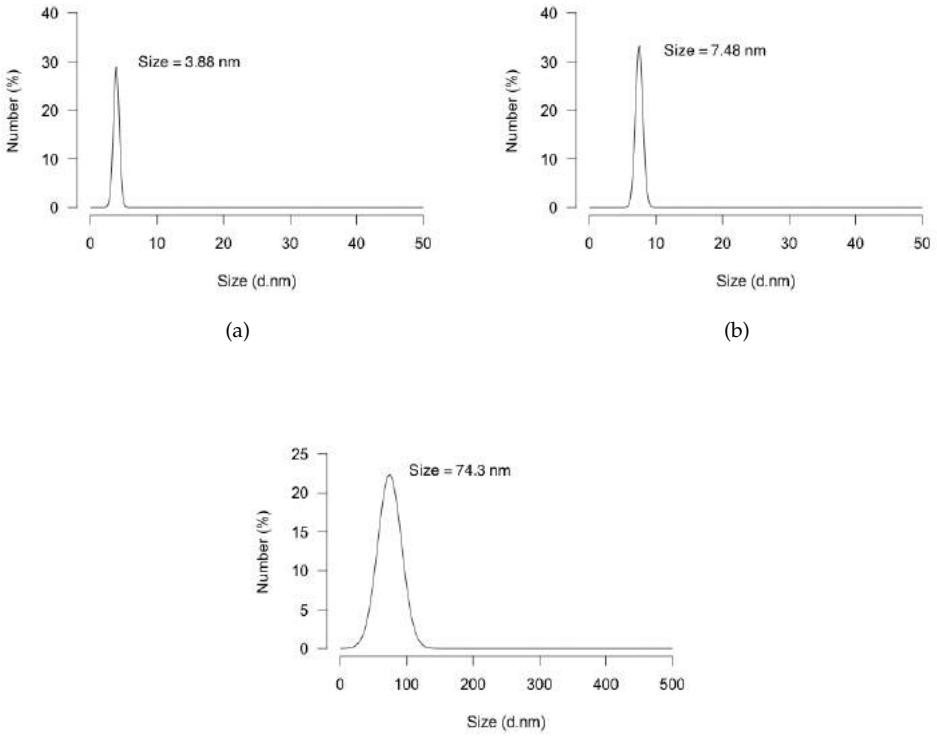

(a) (b)

(c)

Figure 4.7: DLS results of a) gold nanoparticles, b) GSH-capped gold nanoparticles, c) antibody-conjugated gold nanoparticles.

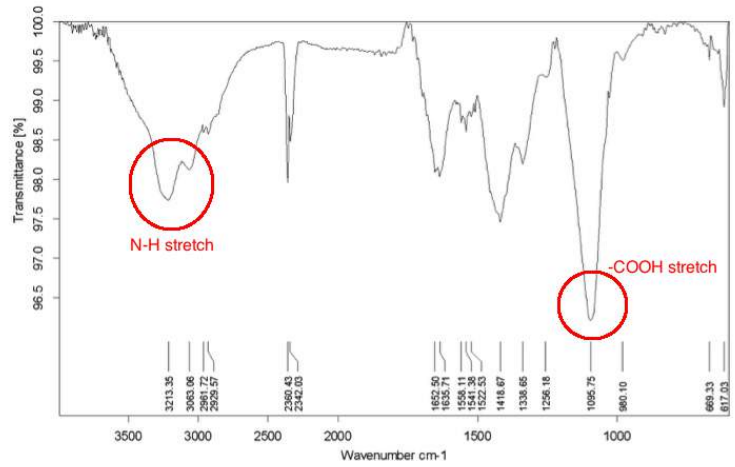

(a)

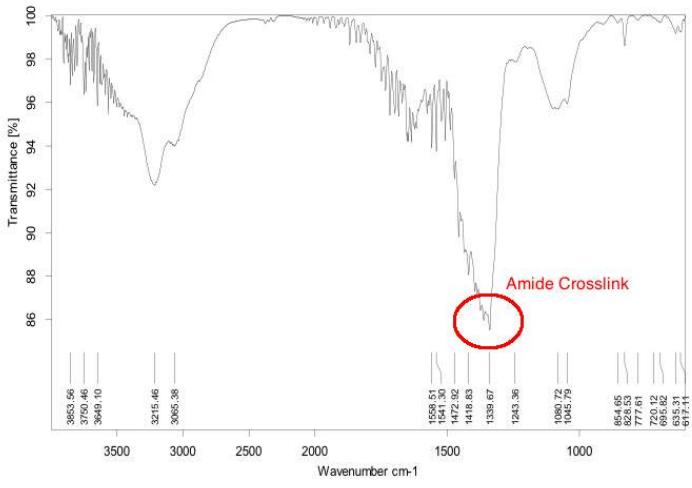

(b)

Figure 4.8: FTIR results of a) GSH-modified gold nanoparticles b) antibody-conjugated gold nanoparticles.

stretching vibration band at 1095/cm was reduced, indicating the conjugation of sulfo-NHS to GSH molecules through the –COOH linkage. Moreover, a visible band, assigned to the formation of amide crosslink between the antibody and the sulfo-NHS/GSH complex, appeared at 1339/cm.

4.4 Optimization of AuNP/Ab nanoconjugate preparation

The preparation of a well-dispersed nanoprobe with uniform size distribution and no aggregation is of great importance in immunoassay studies. Therefore lowest amount of antibody enough to stabilize the gold was determined by incubating 1 mL of colloid gold with antibody solutions at varying concentrations (1 - 50 μg/mL, 1 mL). After 5 min, 0.5 mL of 10% (w/v) NaCl was added and the color of the solution was noted. The concentration in which the color of the solution turned blue was considered the minimum required amount for stabilization.
Further tests while using the nanoprobe in an electrochemical sensor showed that lower concentrations of Ab in the nanoprobe produces small electrochemical response, suggesting that such low concentrations does not provide sufficient antibody to react completely with the antigen on the immunosensor surface. (Figure 4.9) Higher concentrations of the nanoprobe, on the other hand, improved the current while contributing to higher nonspecific adsorption.

4.4.1 Environmental Factors

As mentioned in the literature, environmental factors such as temperature and pH play an important role in the efficiency of the nanoconjugate. Previous studies have shown that the thermal optimum depends on the chemical nature of the protein, adding that hydrogen bonds are more stable at low temperature, whereas the strength of the hydrophobic bonds increases with temperature [21]. Antigen-Ab reactions are also expected to stabilize at lower temperatures.
According to our results, however, no significant change was reported when the incubation was performed at a temperature range of 4° C to room temperature. As a result, to simplify the process, all the processes were performed at room temperature and the optimized incubation time for this temperature was calculated to be 2.5 hours, indicating saturated binding of the immunoreaction.
The pH of the solution is another factor affecting the quality of the end product. The optimal reaction rate of NHS chemistry proceeds around

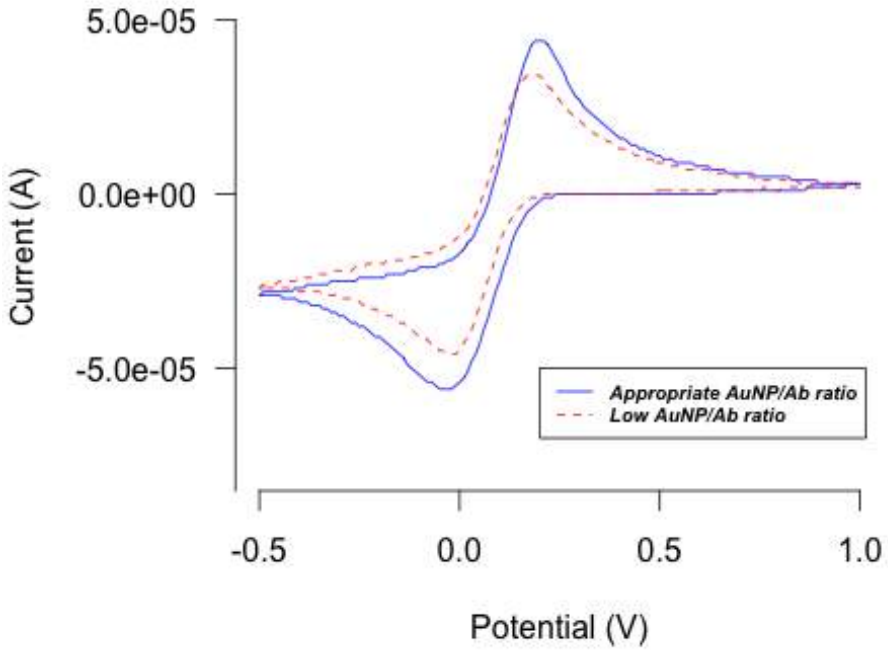

Figure 4.9: Cyclic voltammetry results of 2 different concentrations of Ab-conjugated gold nanoparticles.

pH 4.5 – 7.2. In other words, NHS-esters hydrolyze faster in higher pH, whereas no reaction will take place at pH values lower than 3.5 [22]. As for GSH, best results are achieved by adjusting the pH at values in which the carboxylic groups are in their protonated form. This occurs when GSH is as a zwitterion (pH=3-7) [23].
Moreover, extreme pH values induce marked conformational changes in the Ab molecule that probably may affect its complementarity with the antigen. On the other hand, since Oc, the Ab used in this work, has an isoelectric point (pI) of 4.4, at lower pH values it carries more positive charge and thus positively influences the electrostatic attraction between the oppositely charged surface carboxyl anions and the protonated amino group of the ligand [24]. As a result, no attempts were made to change the negative pH of the sulfo-NHS solution.

4.5 Conclusions

Through the inherent interaction between AuNPs and antibody biomolecules, a novel gold nanoprobe was developed to be used in nonenzymatic electrochemical immunoassay. This one-pot method not only provides a simple method for loading high-content antibody on nanoparticles but also greatly improves the repeatability and controllability of the nanoprobe preparation. Combined with a disposable electrode, it could be used for a single/multiplexed electrochemical immunosensing method.
Generally, these electrochemical sensors have the virtue of high sensitivity and selectivity, but it requires several fabrication steps. Current nanoprobe has overcome this problem as it provides direct electron transfer between biomolecules and electrode without any mediators after being immobilized on the surface. This method of detection will not only simplify the fabrication steps with better stability but also the high-content of AuNPs in the nanoconjugate results in accelerated electron transfer and greatly amplifies the detection signal.

References

[1] J. Ren-Der, C. Wei-Da, H. Meng-Hsuan, C. Fu-Hsuan, B. Jong-Shing, and L. Dean-Mo, "Highly electrostatically-induced detection selectivity and sensitivity for a colloidal biosensor made of chitosan nanoparticle decorated with a few bare-surfaced gold nanorods," *Biosens Bioelectron*, vol. 52, pp. 111–117, 2014.

[2] J. Zhang, B. Ting, M. Khan, M. Pearce, Y. Yang, Z. Gao, and J. Ying, "Pt nanoparticle label-mediated deposition of pt catalyst for ultrasensitive electrochemical immunosensors," *Biosens Bioelectron*, vol. 26, no. 2, pp. 418–423, 2010.

[3] T. R. Holford, F. Davis, and S. P. Higson, "Recent trends in antibody based sensors," *Biosens Bioelectron*, vol. 34, no. 1, pp. 12 – 24, 2012.

[4] B. Chikkaveeraiah, A. Bhirde, N. Morgan, H. Eden, and X. Chen, "Electrochemical immunosensors for detection of cancer protein biomarkers," *ACS Nano*, vol. 6, no. 8, pp. 6546–6561, 2012.

[5] J. Rusling, C. Kumar, J. Gutkinde, and V. Patele, "Measurement of biomarker proteins for point-of-care early detection and monitoring of cancer," *Analyst*, vol. 135, pp. 2496–2511, 2010.

[6] G. Laia, H. Zhanga, J. Yong, and J. Yu, "In situ deposition of gold nanoparticles on polydopamine functionalized silica nanosphere for ultrasensitive nonenzymatic electrochemical immunoassay," *Biosens Bioelectron*, vol. 47, pp. 178–183, 2013.

[7] A. Yakoh, C. Pinyorospathum, W. Siangproh, and O. Chailapaku, "Biomedical probes based on inorganic nanoparticles for electrochemical and optical spectroscopy applications," *Sensors*, vol. 15, pp. 21 427–21 477, 2015.

[8] F. Kurniawan, V. Tsakova, and V. M. Mirsky, "Analytical applications of electrodes modified by gold nanoparticles: Dopamine detection," *J Nanosci Nanotechnol*, vol. 9, no. 4, pp. 2407–2412, 2009.

[9] P. B. Luppa, L. J. Sokoll, and D. W. Chan, "Immunosensors—principles and applications to clinical chemistry," *Clin Chim Acta*, vol. 314, no. 1-2, pp. 1–26, 2001.

[10] M. Faraday, "Experimental relations of gold (and other metals) to light," *Proc. Roy. Soc. Lond.*, vol. 147, pp. 145–181, 1857.

[11] J. Turkevich, P. Stevenson, and J. Hillier, "A study of the nucleation and growth processes in the synthesis of colloidal gold," *Discuss. Faraday Soc.*, vol. 11, pp. 55–75, 1951.

[12] G. Frens, "Controlled nucleation for the regulation of the particle size in monodisperse gold suspensions," *Nature*, vol. 241, no. 105, pp. 20–22, 1973.

[13] H. Verma, P. Singh, and R. Chavan, "Gold nanoparticle: synthesis and characterization," *Vet. World*, vol. 72, no. 4, pp. 72–77, 2014.

[14] G. Hermanson, A. Mallia, and P. Smith, *Immobilized Affinity Ligand Techniques*. Academic Press, San Diego, 1992.

[15] A. M. Coto-Garcia, E. S. Sotelo-Gonzalez, M. T. Fernandez-Arguelles, R. Pereiro, J. M. Costa-Fernandez, and A. Sanz-Medel, "Nanoparticles as fluorescent labels for optical imaging and sensing in genomics and proteomics," *Anal Bioanal Chem*, vol. 399, no. 1, pp. 29–42, 2011.

[16] A. Zuber, M. Purdey, E. Schartner, C. Forbes, B. van der Hoek, D. Giles, A. Abell, T. Monro, and H. Ebendorff-Heidepriem, "Detection of gold nanoparticles with different sizes using absorption and fluorescence based method," *Sensors and Actuators B: Chemical*, vol. 227, pp. 117 – 127, 2016. [Online]. Available: http://www.sciencedirect.com/science/article/pii/S0925400515307711

[17] G. Lai, F. Yan, and H. Ju, "Dual signal amplification of glucose oxidase-functionalized nanocomposites as a trace label for ultrasensitive simultaneous multiplexed electrochemical detection of tumor markers," *Anal. Chem.*, vol. 81, no. 23, pp. 9730–9736, 2009.

[18] M. Hu, J. Chen, Z. Li, L. Au, G. Hartland, X. Li, M. Marquez, and Y. Xia, "Gold nanostructures: engineering their plasmonic properties for biomedical applications," *Chem Soc Rev*, vol. 35, pp. 1084–1094, 2006.

[19] Z. Guo, Z. Liu, X. Yao, K. Zhang, X. Chen, J. Liu, and X. Huang, "A molecular-gap device for specific determination of mercury ions," *Sci. Rep.*, vol. 3, p. 3115, 2013.

[20] E. Day, L. Bickford, J. Slater, N. Riggall, R. Drezek, and J. West, "Antibody-conjugated gold-gold sulfide nanoparticles as multifunctional agents for imaging and therapy of breast cancer," *Int J Nanomedicine*, vol. 5, pp. 445–454, 2010.

[21] R. Reverberi and L. Reverberi, "Factors affecting the ag-ab reaction," *Blood Transfus.*, vol. 5, no. 4, pp. 227–240, 2007.

[22] M. Fischer, "Amine coupling through edc/nhs: A practical approach," *Methods Mol Biol.*, vol. 627, pp. 55–73, 2010.

[23] M. Hormozi-Nezhada, E. Seyedhosseinia, and E. Robatjazia, "Spectrophotometric determination of glutathione and cysteine based on aggregation of colloidal gold nanoparticles," *Scientia Iranica*, vol. 19, no. 3, pp. 958–963, 2012.

[24] "http://web.expasy.org/cgi-bin/compute_pi/pi_tool1?P02818@52-100@average."

5
Electrochemical Chip Preparation

5.1 Introduction

Since most electrochemical reactions occur in close proximity of the electrode surface, the electrodes itself play a crucial role in the performance of electrochemical biosensors. In other words, a biosensor is created on a solid electrode surface by chemically or electrostatically attaching bio(macro)molecules such as proteins and nucleic acids. If the surface is chemically modified, the biochemical molecules bind in a layer such that they cover the electrode surface. This layer is also known as the 'recognition layer,' as its molecules are specific to a target in the analyte. When the electrode is placed into a sample solution, the analyte and recognition layer interact, and an electrical signal, characteristic of the analyte, is obtained [1].
The dynamic range of concentration that a biosensor can detect is determined by the maximum loading capacity of this layer. Moreover, based on the function of chosen material on the electrode, its surface modification or its dimensions greatly influence its sensing abilities.
According to the literature, electrochemical transducers are made of different materials including carbon-based matrices such as glassy carbon, graphite and nano-carbon, different metals such as platinum,

gold and silver, or polymers with electrical conductivity property. The desirable characteristics of the materials to be used for this purpose include:

- High versatility in shape and size
- Low cost
- Easy fabrication
- High signal-to-noise ratio
- Surface regeneration
- Suitable mechanic and conducting characteristics
- Long-term stability and lifetime
- Biocompatibility
- Large surface area

When an electrode is prepared, CV was used to study its properties. The electrodes were cycled twice in 0.1 mM $K_3[Fe(CN)_6]$, containing 0.01 M NACl solution from 0.0 V to +1.2 V, at 0.1 V/s scan rate in order to get stable CV responses suitable for comparison. The same setting was used all through this work, when a CV was performed.
It is also imperative that their reproducibility, reusability and stability is studied to guarantee a proper electrical conductivity without losing its properties over time.

- The reproducibility of the electrodes is generally tested by comparing the cyclic voltammograms of three prepared electrodes from different batches. Electrodes with less than 5% difference in the peak current are considered reproducible.
- The reusability of the prepared electrodes is assessed through evaluating current change during 10 successive CV cycles.
- The stability of the electrodes is studied by comparing the baseline CV and that recorded after continuously stirring the electrodes in water for 20 min. This process was repeated four times.
- As for the storage stability, the cyclic voltammograms of the electrodes preserved at room temperature for a week are compared with that of a freshly prepared electrode using the same method.

This chapter therefore explains the attempts made to develop the most appropriate electrode that fulfilled the above mentioned characteristics for our purposes and reports its reproducibility, reusability and stability characteristics.

5.2 Electrode Selection

5.2.1 Carbon Electrodes

Carbon is an ideal electrode material due to its wide anodic potential range, low residual current, chemical inertness, low cost, fast response time, and ease of fabrication in different configuration and size as well as suitability for various sensing and detection applications. Compared with platinum or gold, carbon electrodes allow scans to more negative potentials and better anodic potential windows [2]. Carbon is observed in several variants such as glassy carbon, graphite, fullerene, graphene and carbon nanotubes [3].

Pencil Electrodes

As the first step, pencil lead was used as the electrode because of the good electro-catalytic properties, abundance, high electrochemical reactivity, good mechanical rigidity, and low cost of the graphite [4]. Graphite, the dark gray, soft and porous material found particularly in the pencil, has high adsorption capacity, an electrical conductivity of 2 * 10^5 σ (S/m) at ambient temperature, electrical resistivity of 50 $\mu.\Omega$.m and density of 1.95-2.3 g/cm^3 [5].
The anisotropic nature of graphite is the result of two types of bondings acting in different crystallographic directions. In graphite, three out of four valence electrons of each carbon atom are used in bond formation with three other carbon atoms while the fourth electron of each carbon atom forms delocalized π-bonds which spread uniformly over all carbon atoms. The carbon atoms are arranged hexagonally in a planar condensed ring. The layers are stacked parallel to each other, with the atoms within the rings bonded covalently, whereas the layers are loosely bonded together by Van der Waals forces. Thus, the layers can easily slip off one to another.

Preparation Technique Pencil lead was extracted from more than 20 brands of regular and mechanical pencils with different rigidity (H1- H6- HB- B1- B8). A wire and the electrical contact made of a conductive material such as copper was attached to one end of the lead to make the first generation electrodes. A non-conductive cylindrical shaft was press-fitted to cover the lead, protecting it from chemical reactions while inserted in the probe. (Figure 5.1) In order to facilitate the fabrication process, the second generation electrodes were made by simply placing the pencil lead in a plastic tubing or pipette tips.

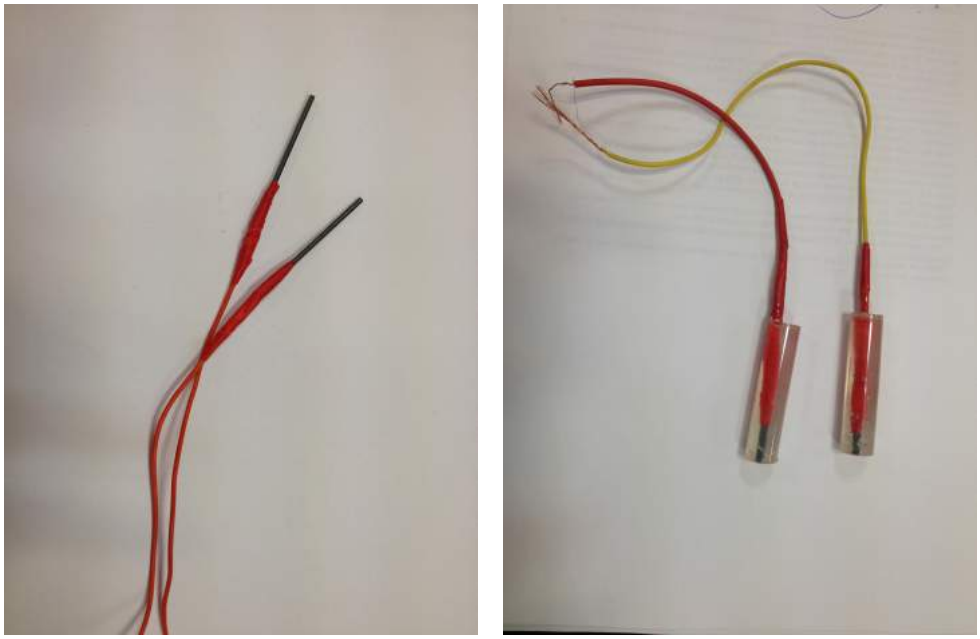

(a) (b)

Figure 5.1: First generation of pencil lead electrodes.

Considering the conductive properties of the graphite, the pencil lead was directly connected to the system. (Figure 5.2)

A combination of pretreatment methods, listed below, were applied to eliminate any possible impurities in the lead and thus to improve the reproducibility of the electrodes: (Figure 5.3)

- Pencil lead was baked in oven at 50 °C for 5 min.
- Pencil lead was polished with aqueous slurry of 0.3 - 0.5 μm alumina powder on a polishing cloth to a mirror finish.
- Pencil lead was placed in a cellulose thimble and then in a soxhlet extractor for 24 hrs of continuous reflux in methanol. Then it was washed with 0.1 M HCl, placed in an ultrasonic bath for 10 min and finally rinsed with water.
- Electrochemical cleaning by applying a conditioning potential of 1.4V for 60s, in a cell containing H_2SO_4 (50 mM).
- Electrochemical cleaning by applying a conditioning potential of 1.8V for 5 min, in a cell containing acetate buffer solution (ABS) (50 mM, pH= 4.8).

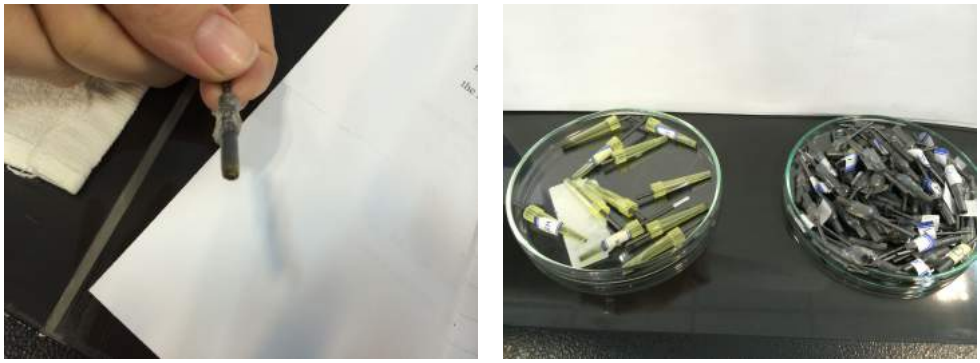

(a) (b)

Figure 5.2: Second generation of pencil lead electrodes.

- Electrochemical cleaning by applying 10 cycles in the potential range of -0.5V to 2V with scan rate of 0.5V/s, in a cell containing ABS Solution (50 mM, pH= 4.8).

Reproducibility Tests None of the electrodes, even those made from a single brand, and regardless of applied pretreatment procedures, produced similar CVs and thus the first and second generation of hand-made graphite electrodes were considered not reproducible. (Figure 5.4)

Patterned electrodes have garnered more attention these days because they offer advantages such as lower cost, disposability and miniaturization [3]. (Figure 5.5)

Unlike the hand-made electrodes, carbon screen printed electrodes (SPEs), used as standard, produced reproducible results. (Figure 5.6)

5.2.2 Gold Electrodes

The unique physicochemical properties of noble metals, particularly gold, such as high mechanical strength, rich electronic and catalytic properties, have been explored to design a new generation of electronic biosensor devices [6] [7]. These electrical and electrochemical approaches generally rely on the changes in the ohmic response of an electrical circuit or the flow of electrons arising from faradaic processes (i.e., oxidation or reduction) near the surface of an electrode, respectively. Although the direct electrical and electrochemical detection of biomolecules is possible, many have benefited from the electroactive

Figure 5.3: Pencil lead was placed in a cellulose thimble and then in a soxhlet extractor for 24 hrs of continuous reflux in methanol, as a pre-treatment procedure.

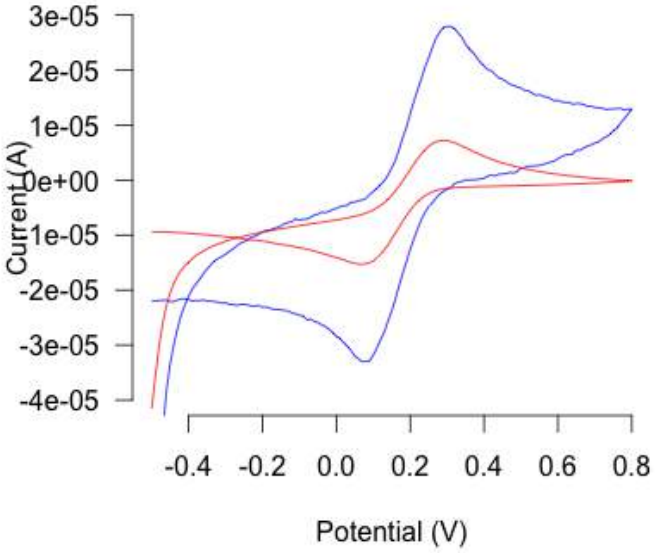

(a)

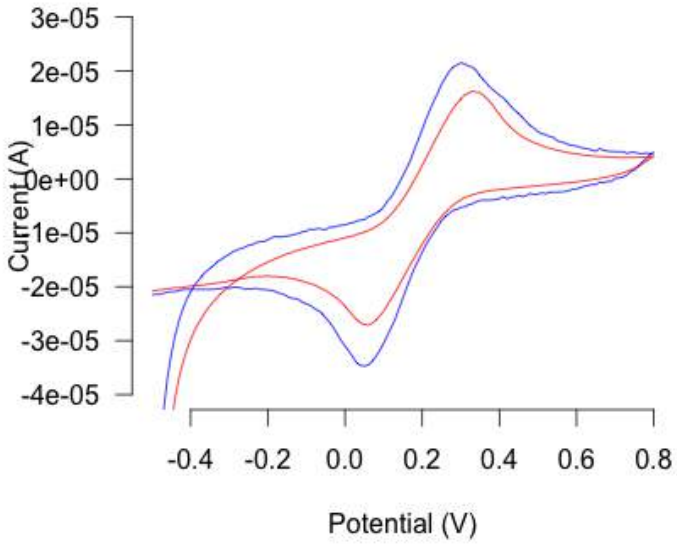

(b)

Figure 5.4: Reproducibility studies of the hand-made graphite electrodes a) first generation b) second generation.

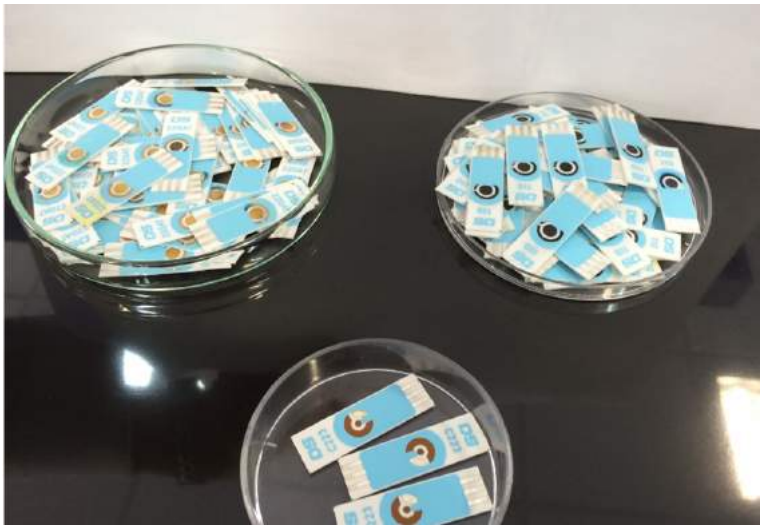

Figure 5.5: Sample Carbon and Gold SPEs.

or catalytic properties of noble metals as reporters for biosensing with unprecedented levels of sensitivity [8].

Glass-based Gold Electrodes

Preparation Technique White float glass substrates were thoroughly cleaned to remove organic residues. They were firstly soaked in RBS aqueous detergents which assure wetting and penetrating actions on the residues. The mechanical effect of an ultrasonic bath then permitted the removal and dispersion of the residues. The cleaned substrates were finally rinsed by soaking in isopropanol (IPA) and DI water, and dried. Next, a 50 nm titanium tungsten (TiW (10%/90%)) adhesion enhancement layer, followed by 500 nm copper, 50 nm titanium tungsten (TiW (10%/90%)) and a 50 nm gold film were sputtered within one vacuum cycle of an Alcatel SCM600 system.
Later, however, the Cu layer was eliminated as it was damaged by H_2SO_4 used for cleaning. The thickness of the Au layer was also increased to improve conductivity. In the final design, a 50 nm titanium tungsten (TiW (10%/90%)) adhesion enhancement layer and a 100 nm gold film were sputtered on the cleaned glass substrate. The metal films were subsequently patterned by photolithography and subsequent wet etching.
The electrode design was fabricated using common computer aided

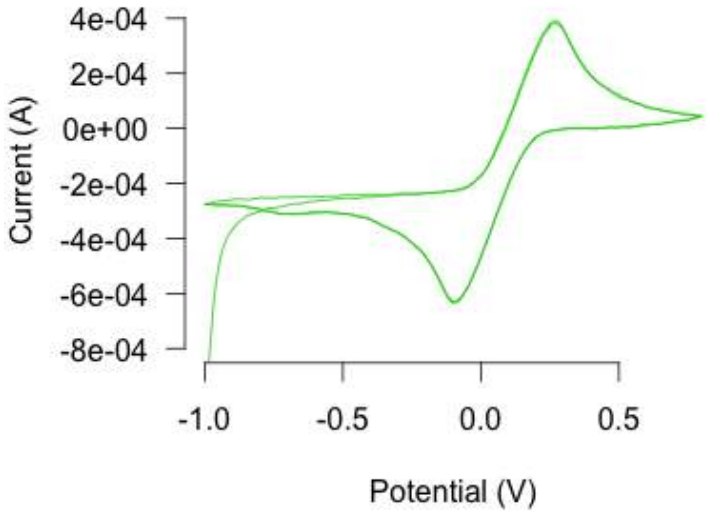

(a)

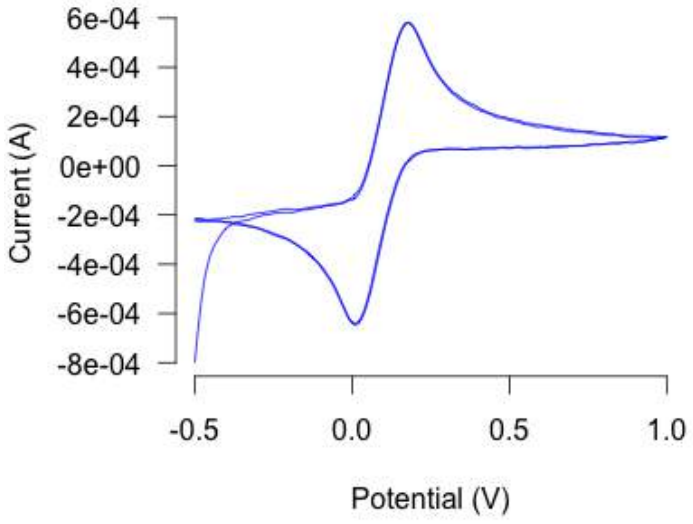

(b)

Figure 5.6: Reproducibility results of a) Carbon SPEs b) Gold SPEs.

drawing (CAD) software and printed onto a transparent foil by the JD photo-tools in the UK. The design followed several considerations:

- The primary consideration for the relative location of the three electrodes in a cell is the minimization of the solution resistance. This was accomplished by keeping the three electrodes as close together as feasible, while not interfering with the current paths between one another.
- The second important consideration involves the shape and size of the auxiliary electrode relative to the working electrode. The Aux should be at least as large in area as the WE, and positioned symmetrically with respect to the WE so that the current density and potential experienced along its entire length is constant.
- Close proximity of the Ref and WE electrodes is important.

To this end, positive photoresist S1818 was used as masking layer to wet etch both metal films. A 1.8 μm thick coating of S1818 was spin coated at 4000 rpm for 60 s and soft baked on a hot plate for 2 min at 90 °C. Next, the photoresist was UV exposed through the foil mask with the desired pattern for 7.5 s at 13 mW/cm^2, developed for 30 s in 50 % Microposit developer and hard baked for 30 min in a convection oven at 120 °C. The gold and titanium tungsten films were then wet etched using a solution of iodine (I_2) and potassium iodide (KI) (1:4 (1g I_2, 4g KI, 73ml H_2O)) at room temperature, and a 30 % H_2O_2 solution at 55 °C, respectively. Finally, acetone was used to strip the remaining photoresist from the electrode surface.

Since the connection lines between the electrodes and their connections points were all made of gold, SU-8 was used as an insulation layer to cover the whole surface, exposing just the electrodes to the electrolyte solutions. SU-8 was used because it was biocompatible and spectrophotometry results showed its negligible protein adsorption rate[1] [9].

In this regard, TI PRIME was first spin-coated on the substrate to improve the adhesion of SU-8 to the glass substrate. In the absence of TI PRIME, the SU-8 layer was delaminated easily. (Figure 5.7) 10-μm thick layer of the negative-tone photoresist SU-8 3010 was then spin-coated on the substrate. After the soft bake (65 °C for 1 min, followed by 95 °C for 3 min), the substrate was allowed to cool down to room temperature. Next, the coating was exposed to UV radiation (300 mJ/cm2) through a glass mask, using a double side mask aligner (EVG 620; Austria). A long pass filter was used to eliminate UV radiation below 350 nm. After the post-exposure bake (65 °C for 1 min, followed by 95 °C for 2 min), the SU-8 was developed (90 s in SU-8

[1]The process is explained in detail in Chapter 7

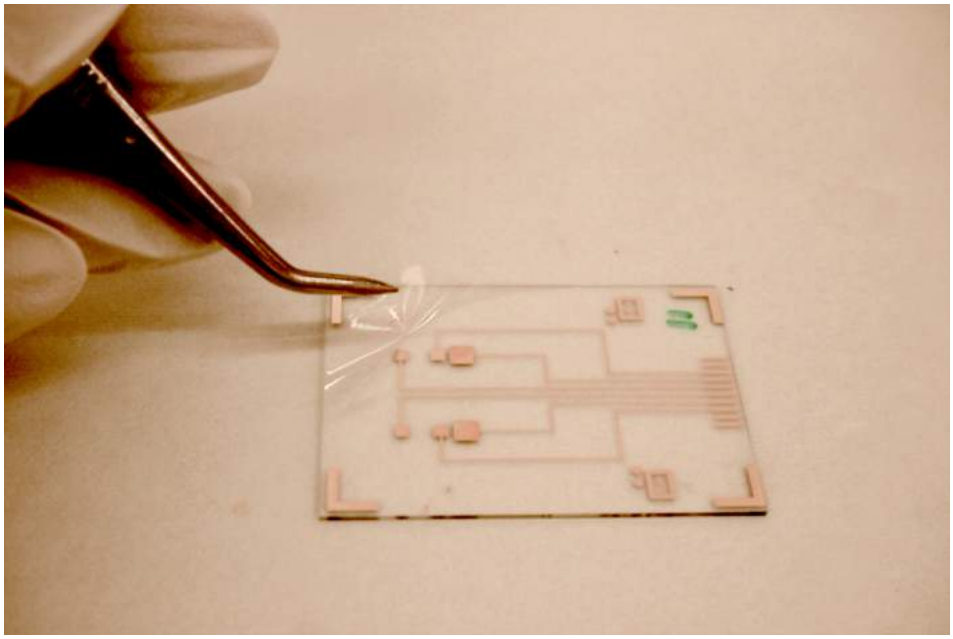

Figure 5.7: SU-8 delamination in the absence of TI PRIME.

developer), followed by a rinse in IPA. Finally, a hard bake was performed (120 °C for 90 min) to further cross-link the SU-8, after which the substrates were diced. (Figure 5.8)

In the final design, the electrochemical chip consisted of 6 gold electrodes arranged in 2 by 3 electrode arrays on a glass. The glass was 25.5*85.5 mm^2, leaving a 25.5*10 mm^2 uncovered area for the contact pads to be connected to the reader using a printed circuit board (PCB). The PCB with electrical connection leads and lines to the electrodes was used to connect the array to the potentiostat. Each gold working electrode (1.5*1.5 mm^2) was placed between one gold pseudo- reference (1.4*1.4 mm^2) and one gold counter electrode (2.5*2.5 mm^2). (Figure 5.9)
The gold electrodes were dried using N_2 and kept at 4 °C prior to use.

Cleaning Technique Upon exposure to a non-cleanroom laboratory environment, the gold surface is subject to numerous ambient contaminants (AuO, hydrocarbons, ...), affecting binding kinetics of thiols in addition to electrochemical effects. As a result, gold must be cleaned immediately before it is chemically modified for electrochemical uses.

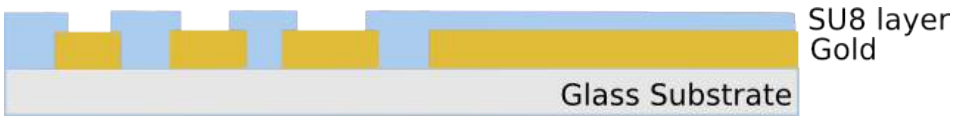

(a)

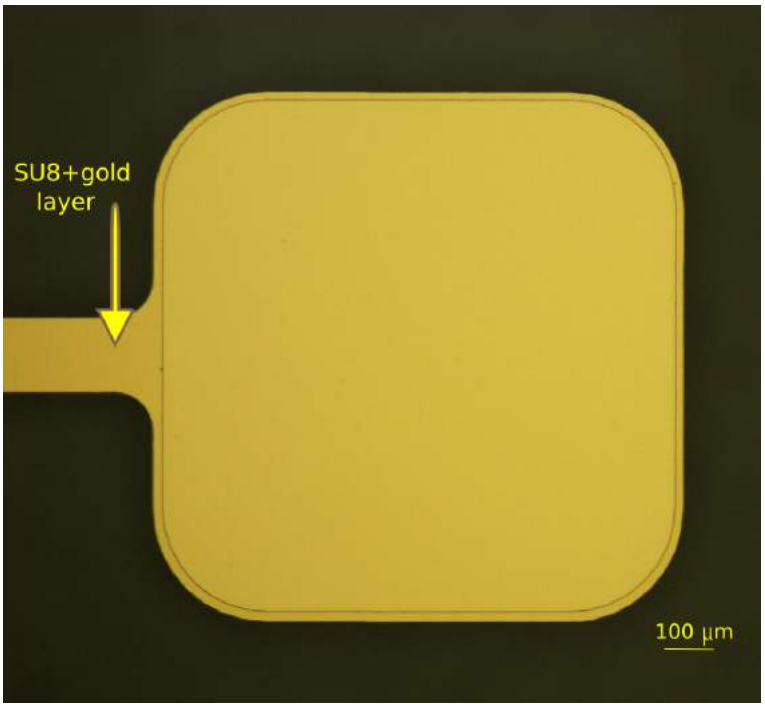

(b)

Figure 5.8: a) Schematic illustration of the cross-section of an electrochemical chip b) Optical microscope image of one of the electrodes on the electrochemical chip with SU-8 layer on its edges and connection line.

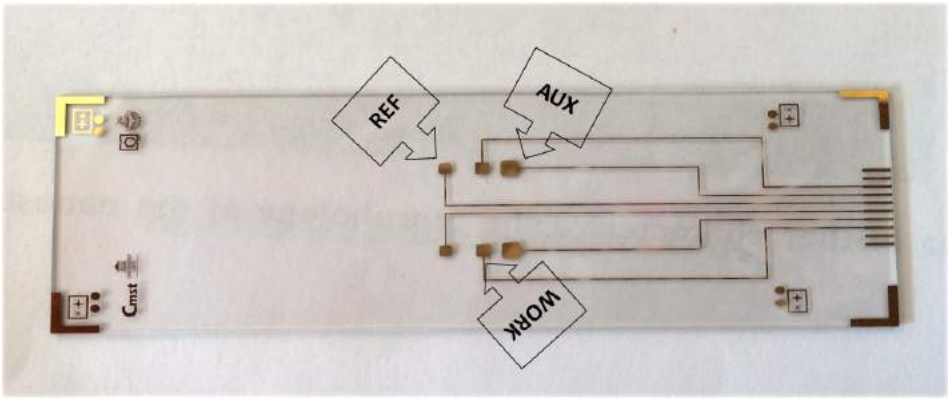

Figure 5.9: Structure of the electrochemical chip manifold.

Table 5.1: Common gold cleaning methods [10].

1	Ultraviolet ozone cleaning
2	Potassium hydroxide and hydrogen peroxide cleaning
3	Potassium hydroxide potential sweep
4	Sulfuric acid and hydrogen peroxide cleaning
5	Sulfuric acid potential cycling
6	Hydrochloric acid potential cycling
7	Reducing agent solutions cleaning
8	Aqua Regia cleaning

(Table 5.1)

Before storing the electrodes, they were etched by means of radicals, formed in the gas mixture plasma, chemically reacting on the surface of the substrate, and physically by means of ions bombarding the surface in the Reactive Ion Etching (RIE) machine. The goal was to remove possible contaminating material deposited on the surface of the electrodes.(Figure 5.10)

Upon usage, cleaning was performed using electrochemical pretreatment by cycling the electrode from large positive to negative potentials (+1.4 V to -0.4 V, scan rate 100 mV/s) in sulfuric acid solution (50 mM) multiple times and the process was continued until a stable CV was achieved [11]. The peak-current potential-differences obtained from cyclic voltammetry were used to compare the cleanliness of the gold electrodes.
At this potential range, gold oxide is formed, which upon reduction

(a) (b)

Figure 5.10: Microscope image of the gold electrodes a) before and b) after RIE.

can be stripped away, together with other surface contaminants and possible remnants of the photoresist on the electrode surface. We found that after approximately 20 cycles, the recorded CVs were reproducible and features characteristic of a clean gold surface became visible. Further CVs showed a remarkable repeatability of the as mentioned treated Au working electrode.

Performance Analysis Considering the fact that the electrochemical chip has all the working, auxiliary and reference electrodes all together, the accuracy of the system was checked as following.
First, as the voltage that is applied to the working electrode is controlled with respect to the reference electrode, the stability of the reference electrode was measured based on the consistency between cycles of the potential at which the peaks occurred, compared with an external reference electrode was used. The average, standard deviation and relative standard deviation (RSD) were calculated for the peak potentials within nine successive CV cycles of one measurement. A less than 5% variation was noted between cycles, suggesting not only the reference electrode was stable over the time period in which the measurement was collected, but also the difference between using an on-chip and external reference electrode were ignorable.
However, considering the slightly different potential and offsets between the working and reference electrodes, commonly reported in sensors using quasi-reference electrodes such as ours, we averaged all the electrochemical plots for each of the studied electrodes [12].
Moreover, as the current in the system passes between the working

and counter electrodes, the stability of these electrodes was determined by examining the variation in maximum current in each peak and comparing the results to that reported when using an external counter electrode. Similarly, a less than 5% reported variation suggested the difference between using an on-chip and external counter electrode to be ignorable.

Reproducibility Tests The as prepared gold electrodes were reported to be stable during successive CV analyses and reproducible. (Figure 5.11)

Again the results were compared with gold SPE as a standard. (Figure 5.5)

5.3 Surface modification of gold electrodes with AuNPs

The purpose of electrode modification with nanostructures is to improve the sensitivity and selectivity of the biosensor. The higher surface-to-volume ratio of nanostructure enhances the electrical properties, which makes the electrode susceptible to external influences. Since the dimension of nanostructure becomes similar to the size of the target biomolecules, measurement sensitivity will increase, and this will enhance higher capture efficiency [13].

In other words, these electrodes enhance the analytical performance of the sensor through providing a suitable microenvironment for biomolecule immobilization, their effects on increasing the surface area of the exposed gold and facilitated electron transfer between the immobilized proteins and electrode surfaces. As mentioned earlier, AuNPs are the most common nanostructures used in this regard.

According to the existing studies, AuNP deposition results in three-dimensional Au deposits, which have a higher desire to adsorb specific functional groups [14] [15]. The size, structure, and distribution of these structures, however, have a strong effect on the performance of the system and thus should be well controlled.

Diverse strategies have been reported to coat various working electrodes such as platinum, carbon and gold with a layer of AuNPs [16] [17]. These coating techniques include layer-by-layer (LBL) deposition of AuNPs, self assembled monolayer (SAM) development, sol–gel technique, impregnation, co-precipitation, metal organic-chemical vapor deposition, incipient wetness, electrodeposition and dip-coating [18] [19].

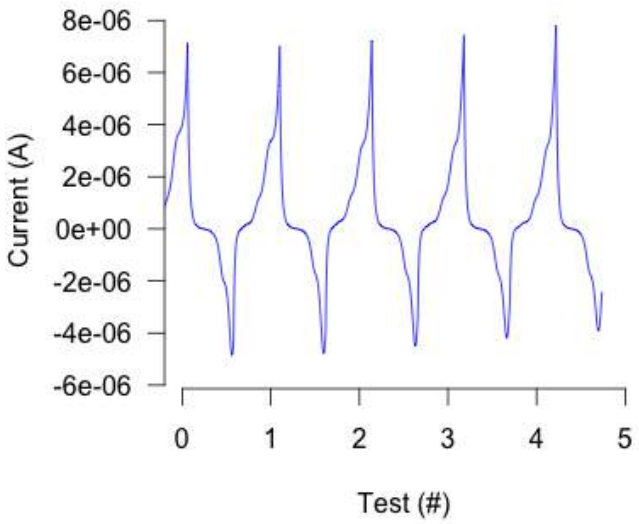

(a)

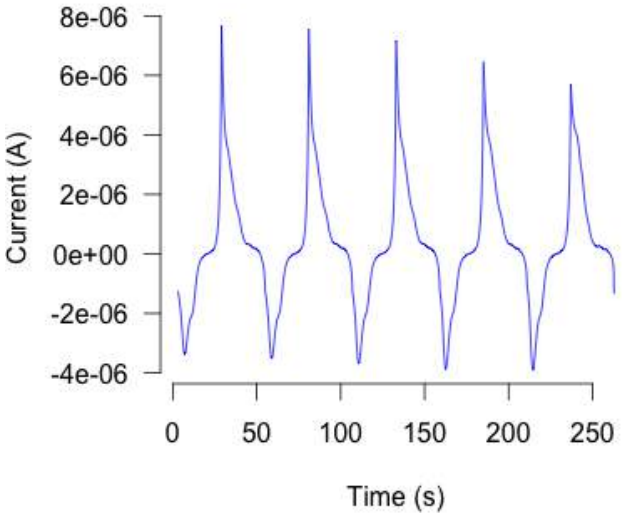

(b)

Figure 5.11: CV analyses showed the gold electrodes were a) reproducible b) stable during successive CVs.

Some of them, such as the fabrication of metal nanoparticles layers using electron-beam lithography (EBL) or nanotemplating, require expensive equipment or special templates and are thus less commonly used [20]. Many studies have also reported that the use of electrodeposition techniques is preferred, compared to physical vapor deposition (PVD) methods, because of their relatively low-cost and potentially higher deposition rate and film thickness [21] [22].
The aim of this section is to compare the most common existing methods for depositing gold nanoparticles on gold electrodes for electrochemical sensing purposes and present an optimized, adopted protocol to increase the surface area and analytical performance.

5.3.1 Gold Deposition Techniques

In this work, deposition of the gold nanostructures was performed through different methods. Some of them are simple modification of methods adopted from literature, whereas others are replications of techniques previously used for other purposes.

Method 1: Layer-by-layer deposition of AuNP

Previous studies have suggested that the interactions in the spherical electron density around the gold atoms are responsible for the gold-gold bond in a reliable way [23]. Moreover, some studies have shown the high binding affinity of the terminal functional groups on the periphery of the ligand shell of the gold nanoparticles and the gold electrode surface [24]. They have shown the occurrence of the ligand replacement reactions when this binding affinity exceeds that of the ligand to the particle. As a result, this kind of deposition could be performed in different ways:

(a) Multilayer AuNP-electrodes - 2 μl of the prepared aqueous solution of AuNP was deposited on the gold electrodes[2], and was subsequently dried at room temperature. This process was repeated three times. The electrodes were rinsed with deionized water and dried in a stream of nitrogen gas before the next layer deposition.

(b) In order to improve the results, the layer-by-layer (LBL) deposition technique was applied [25]. The LBL method is based on the alternate deposition of oppositely charged (bio-) polymers, in our case poly(diallyldimethylammonium chloride)(PDDA) [26]. PDDA is commonly used as a reducing and stabilizing agent to avoid AuNP aggregation. When deposited through LBL, the

[2]Preparation of AuNP is explained in Chapter 4

water-soluble, quaternary ammonium, cationic polyelectrolyte enables control over the total AuNP/polymer thickness. The negatively charged substrate also improves attachment of positive compounds.

(c) The same process as mentioned in method 1a was repeated using PDDA-protected AuNPs. The electrode was rinsed with deionized water and dried in a stream of nitrogen gas before the next layer deposition.

(d) According to another method in literature, the previous process was repeated on a GSH-modified gold electrode [27].

(e) The gold electrode was immersed in PDDA solution (20 % aq solution in 0.5 M NaCl) for 10 to 30 min. After drying, 2 μl of prepared aqueous solution of GSH-modified AuNP was deposited on the gold electrode and dried at room temperature [28]. This process was repeated three times. The electrode was rinsed with deionized water and dried in a stream of nitrogen gas before the next layer deposition.

(f) In another attempt, the PDDA-coated substrate was immersed into $HAuCl_4$ solution (10 mg/mL) for 15 min [29]. Thereafter, the electrode was rinsed with deionized water and dried under N_2 before the next layer deposition. Subsequently, the electrode was placed in 0.1 M KNO_3 solution and -0.4 V potential was applied for 60s. The process was repeated three times.

Preparation of PDDA-Protected AuNPs Hereof 250 μL of PDDA solution, 40 mL water, 200 μL 0.5 M NaOH and 100 μL $HAuCl_4$ (10 mg/mL) were mixed and subsequently heated to 100 °C with gentle stirring until the color changed to red. The UV-Vis spectrum showed that the band with a maximum λ at 520 nm in the colloid gold solution was shifted rightward to λ max = 523 nm. (Figure 5.12)

Preparation of GSH-modified AuNPs GSH is a tripeptide biomolecule (–Glu-Cys-Gly), containing a –SH group which can easily be adsorbed onto AuNP surface. There are functional groups ($–NH_2$, –COOH) which have strong affinity to metal ions in GSH (coordination bonds). A dense layer of GSH-AuNP enlarges the electroactive surface area and provides carboxylic groups on the surface of AuNP to covalently bind a dense layer of antibody/protein for detection. Best results are reported when GSH is available in zwitterion (pH = 3 - 7) as pH affects the -OH, -COOH, $-NH_2$ groups in the protein and the aggregation of GSH benefits from H-bonding, which is pH dependent (Acidic environment best results). The rate of

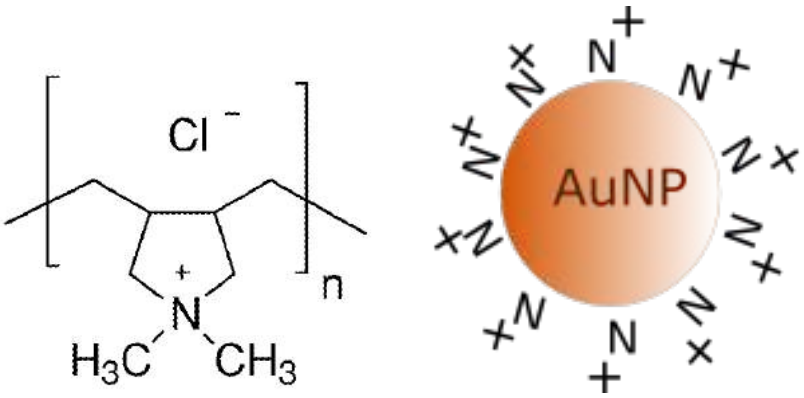

(a) (b)

Figure 5.12: a) PDDA structure, b) Schematic of PDDA-Protected AuNP.

aggregation decreases with an increase in NP concentration. (Figure 5.13, 5.14)

A stock solution of glutathione (10mM) was prepared. Dilute HCl solution (10 mM, 100 μL) was added to gold aqueous solution (3 mL) to lower the pH (~4) [30]. An aliquot of GSH solution (10 mM, 30 μL) was added to the acidic gold aqueous solution, until the color changed from deep red to blue, indicating formation of aggregates amongst AuNPs.

Method 2: Self assembled monolayer (SAM) development

SAM could be achieved after deposition of cysteamine, mercaptocarboxylic acid, 3,3–dithiodipropionic acid, 2-mercaptoethanesulfonate, 4-aminothiophenol, triazole and ultrafin polypyrolle tetradecyl sulfate as well as by the composite 11-mercaptoundecanoic acid-polyethylene glycol and many other options on gold electrodes [31] [32]. It has been proved that the three-dimensional monolayers of S-containing organic compounds facilitate the electron transfer in the redox reaction occurring at the electrode-solution interface, ensuring an easier access of reagents to the electrode surface [33].
A thiol molecule consists of (1) a sulfur head group, which forms a strong, covalent bond with the gold electrode, (2) a hydrocarbon chain of variable length, which stabilizes the SAM through van der Waals interactions, and (3) a terminal group, which has different functionalities. In our case, the -SH-terminated thiols of the dithiol used made the

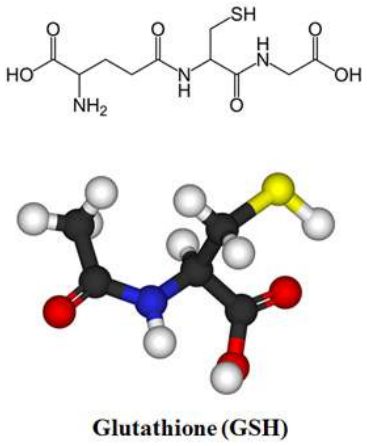

(a)

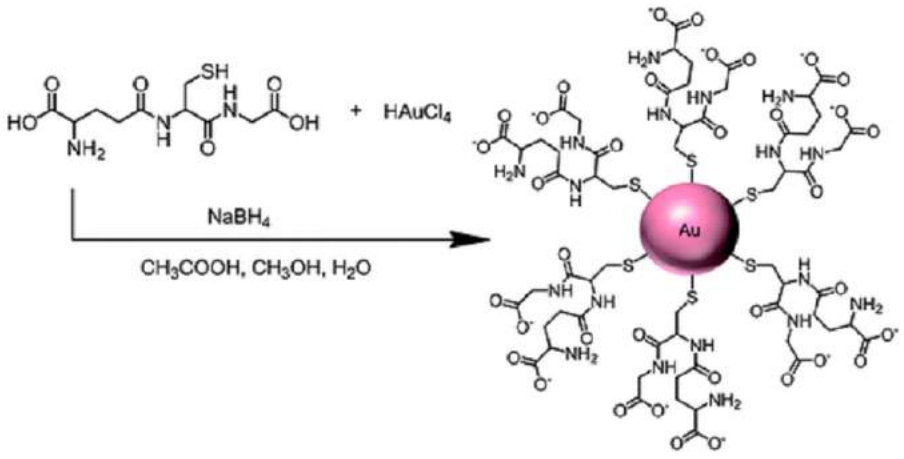

(b)

Figure 5.13: a) GSH structure, b) Schematic of GSH-decorated AuNP.

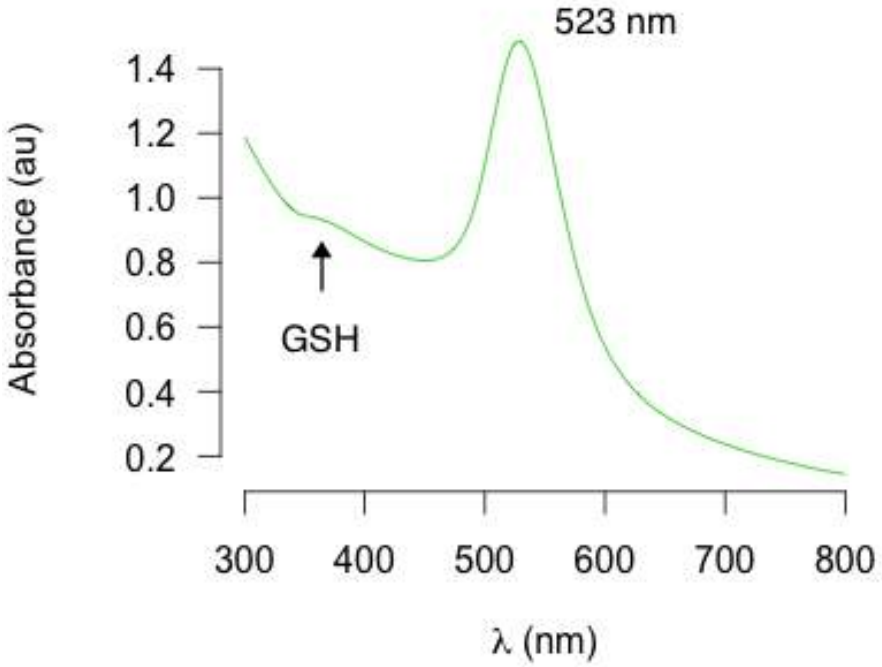

Figure 5.14: UV–Vis spectra of GSH-decorated AuNP solution.

binding of metallic ions of the gold electrode and gold nanoparticles to the SAM possible [34]. Studies have shown that the adsorption time depends on the nature of the molecule, adding that dithiol deposition from solution needs less time [35]. This is while long chain alkanethiols need 2 - 12 hrs compared with short chain alkanethiols or thiols with certain end groups different from -CH_3 that need at least 24 h to form a well-ordered SAM.
When using dithiols, the SAM is developed using the following reactions: (Equation (5.1), (5.2))

$$HS(CH_2)_nSH + Au \rightarrow (HS(CH_2)_nSH)_{phy}Au \tag{5.1}$$

$$(HS(CH_2)_nSH)_{phy}Au + Au \rightarrow Au - S(CH_2)_nSAu + H_2 \tag{5.2}$$

Moreover, dithiols provide a more stable SAM compared to alkanethiols because of the formation of two thiolate bonds per molecule in dithiols and their reductive peak potentials are more negative [36] [19]. On the other hand, these bonds can hinder the transition from the lying down to the standing up configuration, particularly in dithiols with short chain length, resulting in smaller chain-chain interactions, smaller gain in energy and thus higher stability.
Taking this all into account, we decided to use 1, 8–octanedithiol. In this regard, SAM was prepared by immersing gold electrodes into 1 mM 1, 8–octanedithiol in ethanol for 24 h in a dark environment at room temperature [37]. The modified electrodes were then taken out, soaked in distilled water and subsequently dried in a stream of nitrogen gas.

Method 3: Electrodeposition

Electrochemical deposition is an important technique as it not only involves simple instrumentation and operation but also is versatile and cost effective. It is generally performed through application of an electrical field to a solution containing the ions of the target material. Electrically-enhanced diffusion of the reactive ions towards the electrode followed by an electron transfer from or to the ion, results in oxidative or reductive deposition of the desired material on the electrode, respectively. Figure 5.15 shows a voltammogram of an electrodeposition process using CV. The reverse scan of the voltammogram in these experiments exhibits the reduction of Au(III) to Au(0), inducing the deposition of AuNPs onto the electrode surface according to the following reaction. (Equation (5.3))

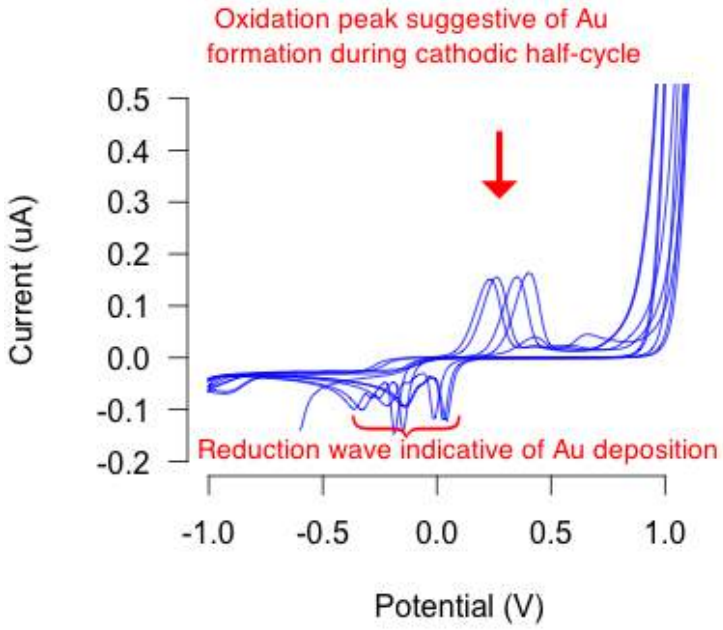

Figure 5.15: a) Voltammograms of the ECV process in 1.0 mM $HAuCl_4$ and 0.5 M H_2SO_4 in the presence of 0.1 mM NaCl.

$$H^+[AuCl_4]^-_{aq} + 3e^- \rightarrow Au^0_s + 4Cl^-_{aq} + H^+ \tag{5.3}$$

Different protocols have been proposed for gold electrodeposition on gold electrodes. Using them, various morphologies, including rod-like and dendritic gold nanoparticles, have been obtained in a one-step process. In this work, electrodeposition was performed in an aqueous solution of 1.0 mM $HAuCl_4$ and 0.5 M H_2SO_4 in the presence of 0.1 mM NaCl as the supporting electrolyte. For the electrodeposition step, external AgCl reference and Pt. gauze (Alfa Aesar Gmbh & Co, Germany) as auxiliary electrode was used.

(a) Cyclic voltammetry: Electrodeposition was performed by CV scanning the potential from - 0.5 V to + 0.5 V, + 1.0 V and + 1.5 V at a scan rate 0.1 V/s for a given number of scans [38]. The process was repeated until the CV became reproducibly stable. The sweeping potential, the scan rate and the number of cycles needed were then optimized based on the results. This method is called

ECV all throughout this work.
There was a broad reduction wave at 0.0 V suggestive of AuNP deposition. As the number of cycles increased, there was a sharp oxidation peak at 1.0 V. Throughout the electrodeposition process, the current read at this peak increased during each cycle, which is consistent with thermodynamics that predicts an easier growth of previously formed AuNPs than a nucleation of new AuNPs on the electrode. In addition, the peak area of the reduction of gold oxide suggests that a large amount of gold nanoparticles have been deposited onto the surface of the electrode. After 60 repeated scans, there was no more change in peak height or shape.

(b) Pulsed electrodeposition: The potential was stepped from - 0.5 V to + 0.5 V, + 1.0 V and + 1.5 V with a 5 s deposition time [39]. NP-like gold islands were generated on the electrode; the size and density of the islands increased with increasing number of pulsed electrodeposition cycles.

5.3.2 Performance Analysis

The comparison between the different protocols applied in this work is outlined in Table 5.2. Previous studies have suggested that not only the stability of the AuNP layer but also the density and size of the NPs are of great importance in the sensors' analytical performance, stressing that high density of rather small, spherical-shaped NPs are associated with best responses [40].
The results of the CV analysis showed that adding a layer of AuNP using method 1a did not affect the results significantly. (Figure 5.16)

While adding an AuNP-layer is believed to provide a larger surface area for the subsequent layers to bind, the unstable attachment between AuNPs and the electrode might be the reason behind the absence of any change in the results. Similar, results were noted for electrodes modified using method 1c. Despite the stronger attachment of PDDA-protected AuNPs to the underlying layers, their non-conductive nature was unfavorable in biosensing processes. This was shown based on a slight decrease in peak current in CV results, suggestive of reduced conductivity of the surface. (Figure 5.17)
CV analysis of the electrodeposited electrodes (method 3a) showed higher current compared with methods 1 and 2, indicating that gold nanoparticles have been successfully attached onto the surface of the electrode and thus improving the conductivity and surface area.

Figure 5.17 shows a considerable increase in the electrical response after SAM development. In comparison to LBL, the SAM technique pro-

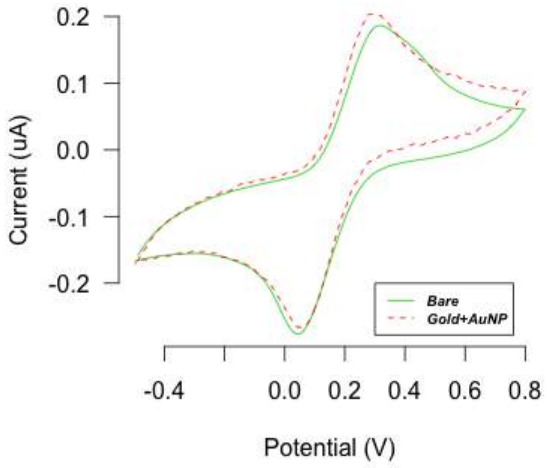

(a)

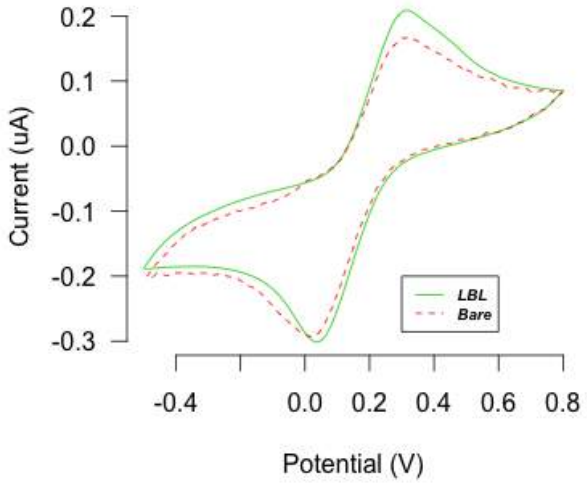

(b)

Figure 5.16: Comparison of voltammograms of bare electrodes and electrodes developed by a) method 1a and b) method 1b in 0.1 mM $K_3[Fe(CN)_6]$.

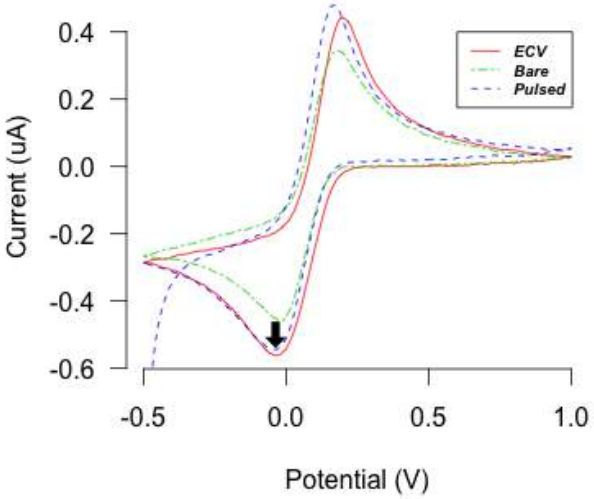

(a)

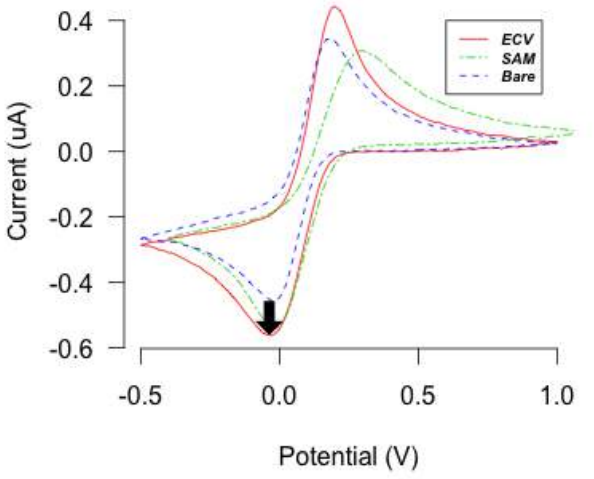

(b)

Figure 5.17: Comparison of voltammograms of bare electrodes and electrodes developed by each of the above-mentioned techniques in 0.1 mM $K_3[Fe(CN)_6]$.

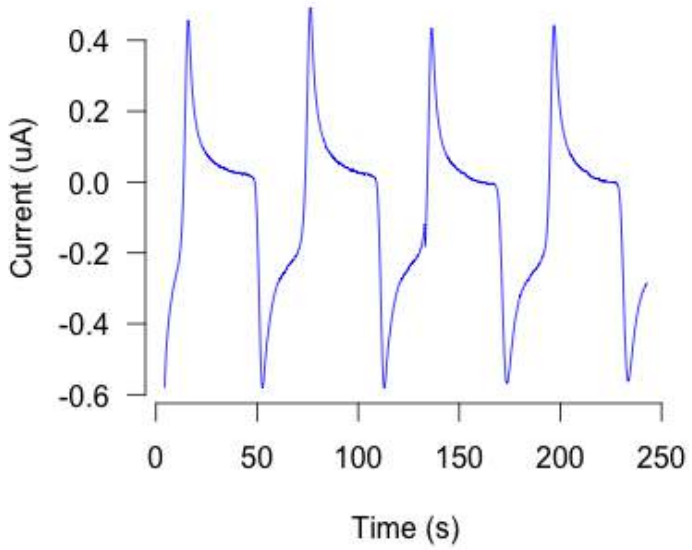

Figure 5.18: Voltammograms of electrodes prepared using method 2 in 0.1 mM $K_3[Fe(CN)_6]$ over time.

vided a more stable nanoparticle layer (less than 5% variability in peak currents after 10 CVs). (Figure 5.18)

CV analysis of the electrodeposited electrodes showed higher current compared with previous methods, causing improved electrode kinetics and a reduction in the oxidation potential (thermodynamically feasible reaction). This is attributed to the larger surface area of the modified electrodes and synergistic effects of electrical conductivity and electroactivity of AuNP.

5.3.3 Reproducibility, Reusability, and Stability Tests

The reusability of biosensors is also of great importance. The electrodes modified through LBL deposition were unstable and not reproducible. On the other hand, adding PDDA to the process did not improve the bonding of gold nanoparticles to the electrode surface significantly and thus no significant improvement was noted in the stability results (more than 5% variability in peak currents of 10 successive CVs). Similar results were noted after surface modification using methods 1d and 1e. This is while the nanostructures were firmly im-

mobilized on the gold electrode prepared using SAM and ECV techniques, resulting in an acceptable stability and reproducibility.
Similar to electrodes prepared using SAM techniques, there was no noticeable change of currents during the successive CV cycles (less than 5% variability in peak currents), which implies that the nanostructures, prepared using ECV technique, are firmly immobilized on the gold electrode. (Figure 5.19)

Our results suggested that while AuNPs deposited using both SAM and electrodeposition techniques provided a stable layer, the electrodes prepared using electrodeposition showed higher current and thus electron transfer rate and analytical performance. This is while many of the previous studies had suggested SAM techniques as an effective way for stable protein attachment [41]. (Table 5.2) It has been evidenced that several factors including the packing density as well as chain length of the SAM play an important role in surface coverage and electron transfer rate. In other words, if SAM is too densely packed, similar to our results, it would exhibit a blocking behavior due to its high resistance, a process which would decrease electron transfer rate and subsequently delay the sensing process [42].
The study of the storage stability of the ECV-modified electrodes showed a slight current change (less than 5% variability), showing their long-time stability. (Figure 5.19). This however was not true for the electrodes prepared using pulsed electrodeposition techniques.(Figure 5.20)

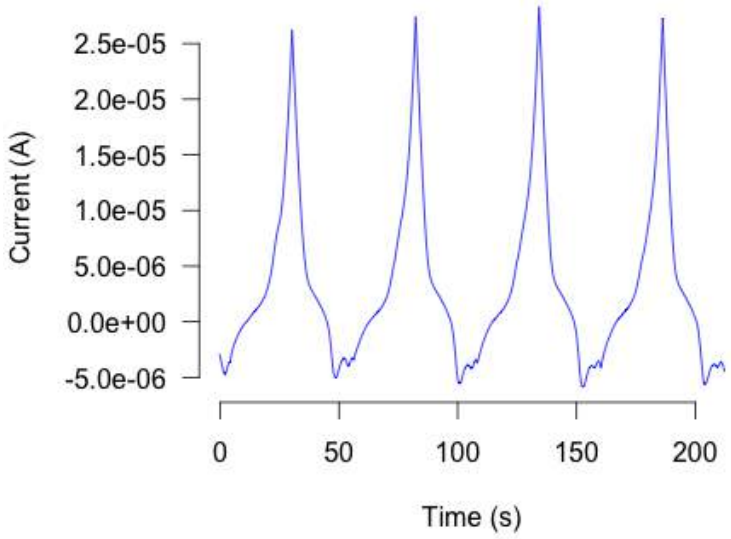

(a)

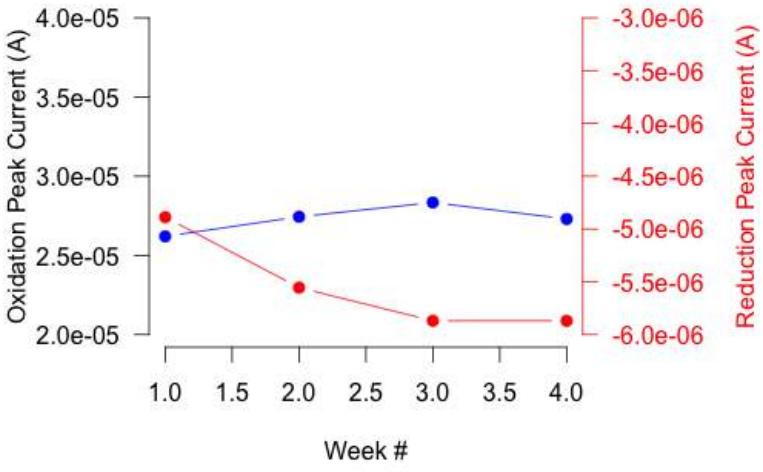

(b)

Figure 5.19: Comparison of voltammograms of electrodes prepared using method 3a in 0.1 mM $K_3[Fe(CN)_6]$ a) during successive CV cycles b) over several weeks.

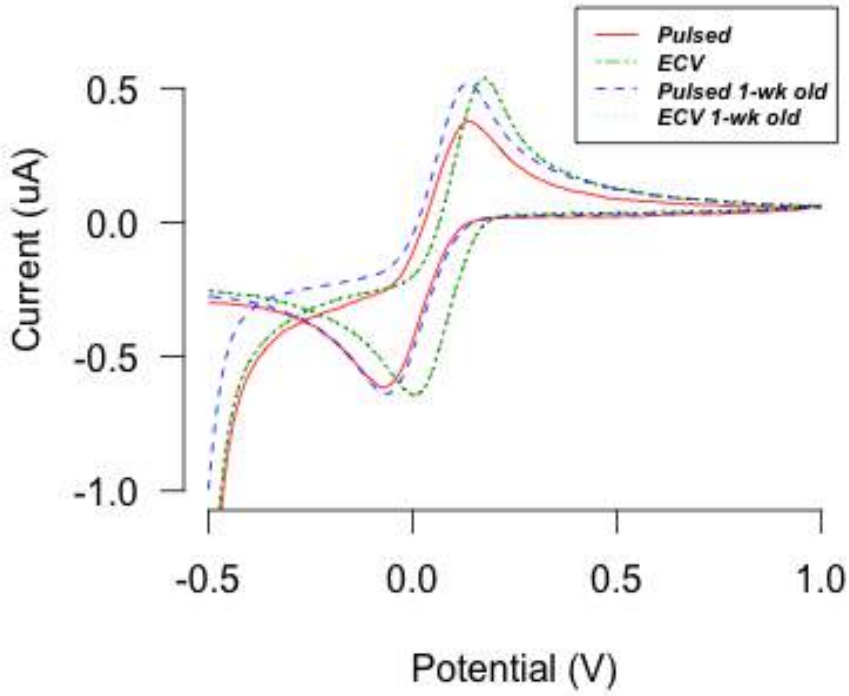

Figure 5.20: Comparison of voltammograms of electrodes prepared using method 3a and 3b in 0.1 mM $K_3[Fe(CN)_6]$.

Table 5.2: Pros and Cons of different Au-deposition protocols applied in this work

	Pros	Cons
LBL deposition	Simple and rapid	Unstable, not reproducible
SAM development	Strong bonding to underneath layer, stable and reproducible	Time consuming, low sensing performance enhancement
Electrodeposition	Acceptable bonding to underneath layer, acceptable sensing performance enhancement, stable and reproducible	Time consuming, No. of cycles depend on the electrode characteristics

5.4 Characteristics of AuNP-coated Gold Electrodes using ECV

Considering the results, the electrodeposition process of AuNP on gold electrode using ECV method was optimized and the focus of the remaining part of this section will be on the characterization of the electrodes modified using this technique.

5.4.1 Electrochemical Behavior

In this work, AuNPs were electrodeposited by ECV starting from $HAuCl_4$ (Method 3a). The successful AuNP formation on the treated electrodes was confirmed by showing a typical CV of gold over the potential range of -0.5 V to +1.2 V in 0.5 M H_2SO_4 solution. (Figure 5.15) This voltammogram shows a single sharp reduction peak at +0.2 V and oxidation peaks at +1.2 V.

5.4.2 Surface Roughness

The increased current noted in further voltammograms confirmed that gold nanoparticles immobilized at the gold interface using this method increased the electrode surface area and facilitate the charge transfer between the AuNPs and the gold electrode. (Figure 5.17)
From the voltammetric responses obtained in $K_3[FeCN_6]$ information regarding the real electrode surface area and its roughness were extrapolated. The diffusion coefficient of the mediator was calculated by performing CV with three different scan rates (0.1, 0.3, 0.5 V/s). The resulting currents were then plotted against the square root of the scan rate and the obtained slope was equal to the diffusion coefficient. In our case, the diffusion coefficient was calculated to be 5e-08 cm^2/s.
Chronocoulometry was then performed to measure the electrical charge passing through the electrode as a function of time. The analysis of the chronocoulometric data was then performed based on the Anson equation. (Equation (5.4))

$$Q = 2.n.F.A.C.D^{(1/2)}.\pi^{(-1/2)}.t^{(1/2)} \tag{5.4}$$

Herein, Q represents the charge (coulombs), n the number of electrons transferred, A the real electrochemical surface area of the electrode (cm^2), F the Faraday's constant (96,485 coulombs/mol), C the concentration of the mediator (mol/cm^3), D the diffusion coefficient of the mediator (cm^2/s) and t time (s).

The slope (a) of the as expected linear plot between Q and square root of time was used to calculate the real electrochemical surface area of the electrode. (Equation (5.5))

$$A = \frac{a}{2.n.F.C.D^{(1/2)}.\pi^{(-1/2)}} \tag{5.5}$$

As expected the real electrochemical surface area of the gold electrodes were calculated to be 0.0784 cm^2, which is 2.3 times greater than the area before electrodeposition (geometric area= 0.0225 cm^2). Based on these results, the roughness factor (ratio of electrochemical surface to geometrical surface) was calculated to be 3.49 (compared to 1.53 in bare sputter deposited Au electrodes before electrodeposition). These results were further confirmed with SEM and AFM.

Electroless gold plating vs. Electrodeposition (ECV)

In another attempt, a group of electrodes were subjected to electroless gold plating. The technique improved the roughness of the surface but failed to improve the sensing properties of the electrodes. This could be explained due to the fact that the deposition of AuNPs on the surface improves the biocompatibility of the surface and results in a 3D structure with higher desire to adsorb certain functional groups. It also improves direct electron transfer from the redox protein to the electrode surface.
WYKO non-contact optical profiler confirms a significant increase in the roughness of the surface following electroless gold plating. (Figure 5.21, 5.22).

5.4.3 Surface Modification

In order to further characterize the morphology of the nanostructured gold film deposits, SEM (Figure 5.23) and AFM (Figure 5.24) analysis was performed. These images also confirmed the considerable increase in the roughness of the surface after electrodeposition and increasing the number of electrodeposition cycles was associated with growing density of deposited nanoparticles.
Figure 5.25 shows typical nanopyramidal structures obtained from different electrodeposition conditions. An increased number of deposition cycles was associated with a significant rise in the density of these nanostructures.
STEM images revealed the formation of nanoclusters of gold nanoparticles with the mean size of 20 nm after the ECV process. (Figure 5.26) This is while as mentioned earlier, the electrochemical characteristics

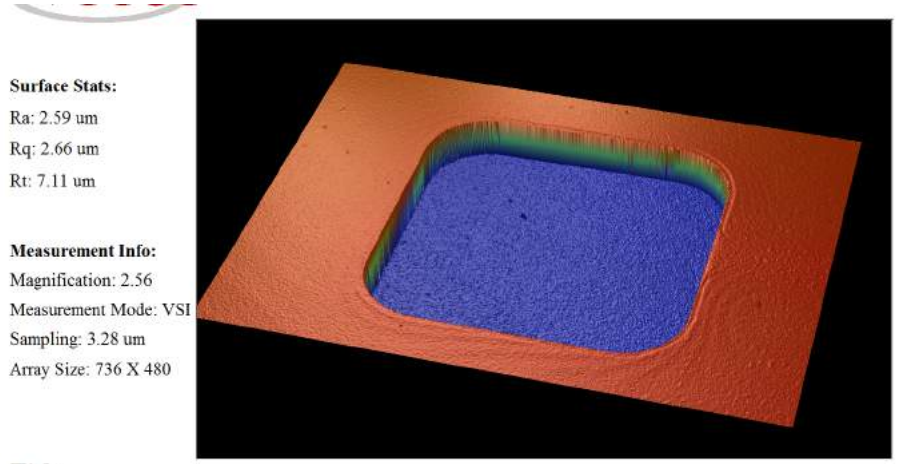

(a)

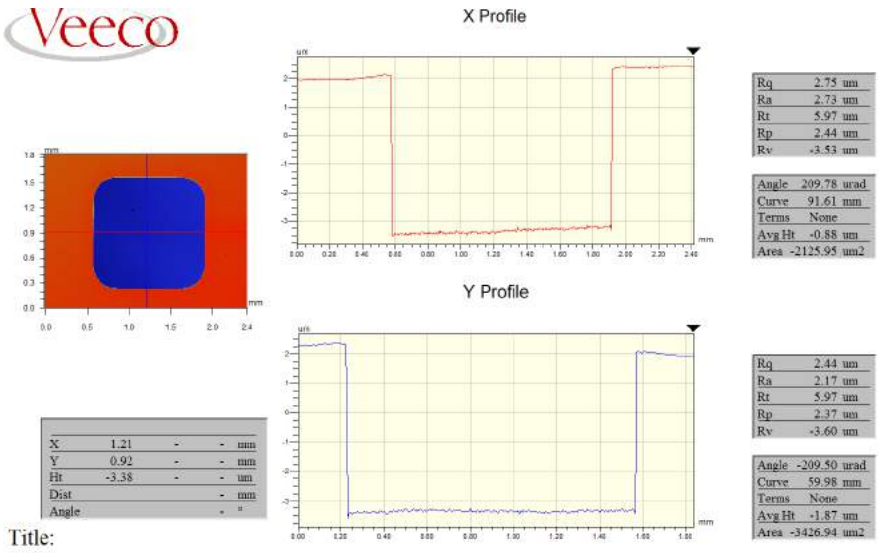

(b)

Figure 5.21: Representative a) three-dimensional image and b) surface profile of bare electrode obtained using Wyko profilometry.

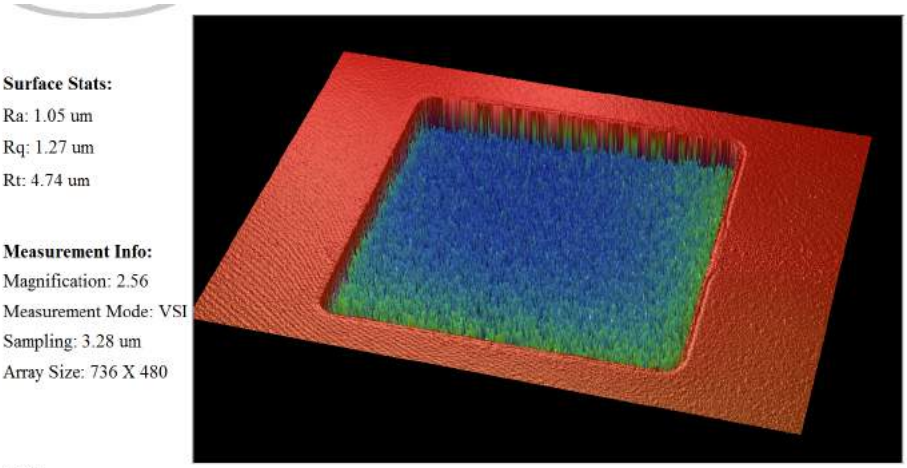

(a)

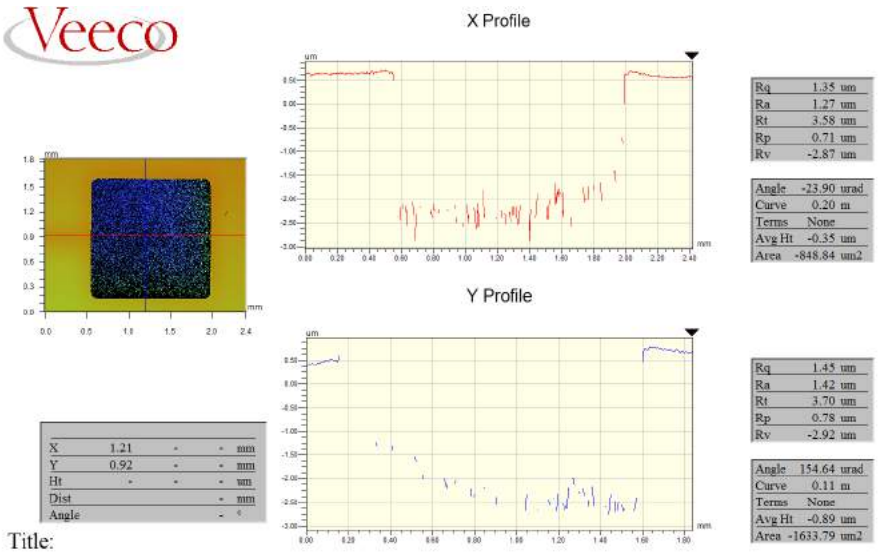

(b)

Figure 5.22: Representative a) three-dimensional image and b) surface profile of electroplated electrode obtained using Wyko profilometry.

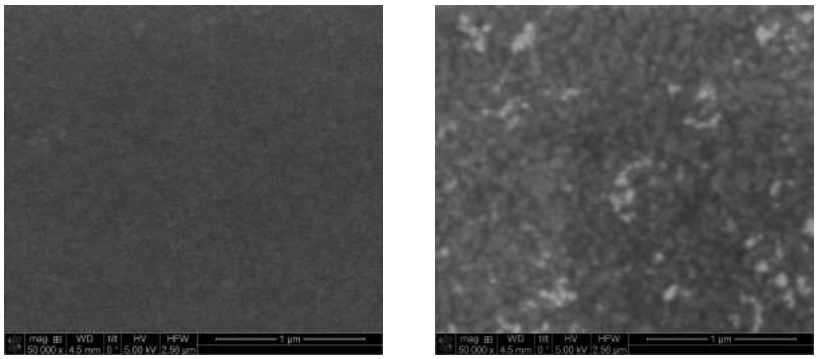

(a) (b)

(c) (d)

Figure 5.23: SEM micrographs of a) bare gold electrode, and gold electrodes after ECV with b) 5 cycles, c) 10 cycles and d) 30 cycles. (For a, b,c, d, scale = 1.0 μm)

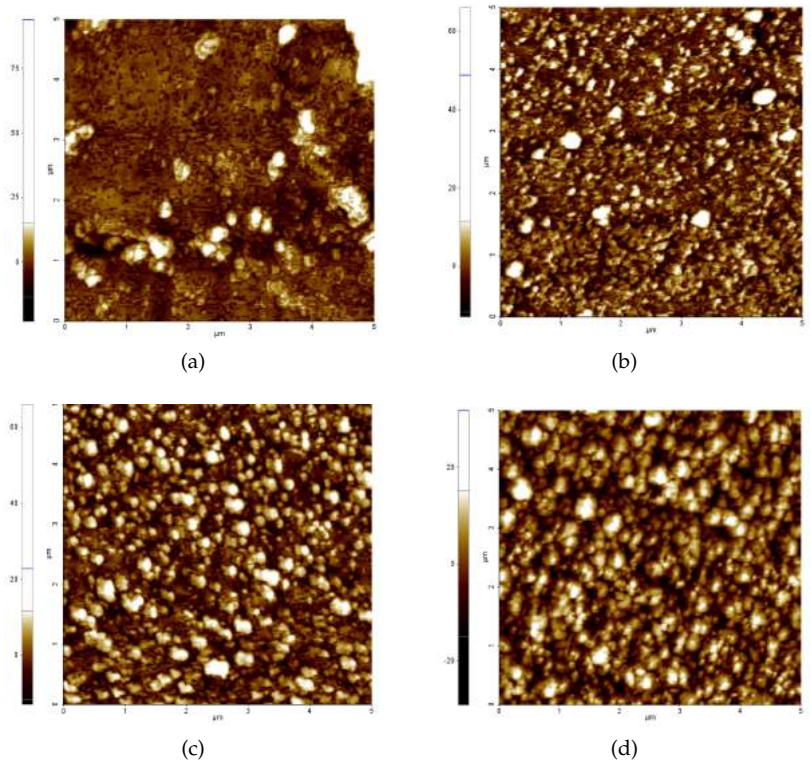

(a) (b)

(c) (d)

Figure 5.24: AFM topography of a) bare gold electrode, and gold electrodes after ECV with b) 5 cycles, c) 10 cycles and d) 30 cycles; 5×5 μm scan size, set point 11 nm

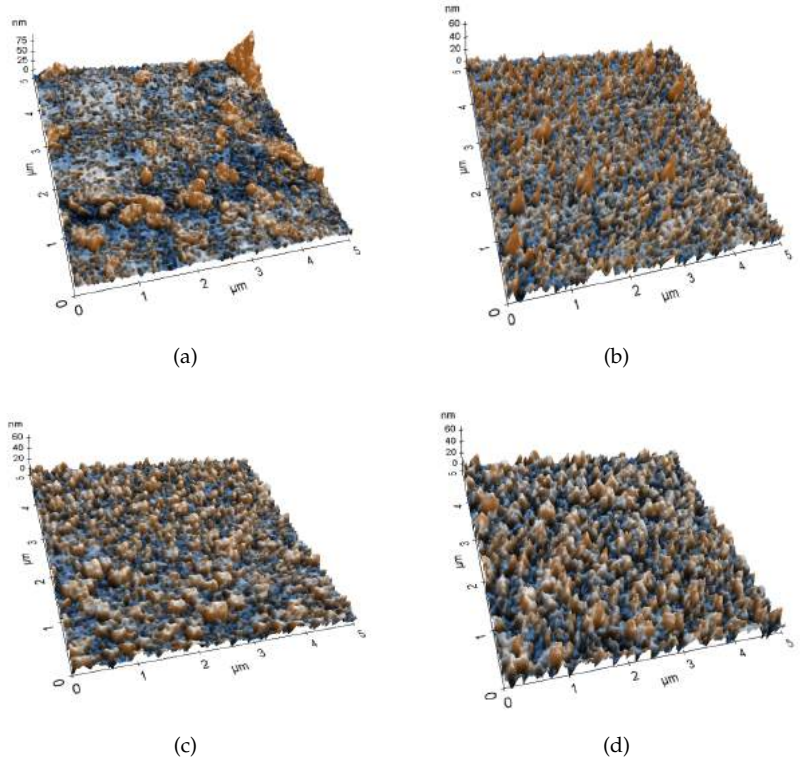

(a) (b)

(c) (d)

Figure 5.25: AFM height images of the surface of a) bare gold electrode, and gold electrodes after CV electrodeposition with b) 5 cycles, c) 10 cycles and d) 30 cycles; 5×5 μm scan size, set point 11 nm

of AuNPs are reported to be strongly size-dependent, and due to geometrical considerations, AuNPs of ~ 20nm lower the probability of proteins finding sterically suitable sites on gold [43]. The quantum effects, originated by d-band electrons of the surface shifted towards the Fermi-level, enables AuNPs to interact in electrocatalytic reactions.

5.4.4 Reproducibility

In order to measure the reproducibility of the as-prepared electrodes, repeatability studies were performed. In this regard peak current in similar CVs performed on a group of electrodes were compared. (Figure 5.27) According to the results, the calculated RSD was (Coefficient of variation= 5.3%), suggesting high likelihood of producing similar electrodes.

5.5 Conclusion

The electrode modified through LBL deposition was unstable and not reproducible. Using SAM and ECV techniques on the other hand, the nanostructures were firmly immobilized on the gold electrode prepared, resulting in an acceptable stability and reproducibility. CV-electrodeposition of AuNP (ECV) causes an observable increase in the peak current of recorded CV curves compared to bare Au electrodes, causing improved electrode kinetics and a reduction in the oxidation potential (thermodynamically feasible reaction). Moreover, electrodes modified using ECV showed better electron transfer rate compared to other studied methods, making them a better candidate for electrochemical sensing purposes.

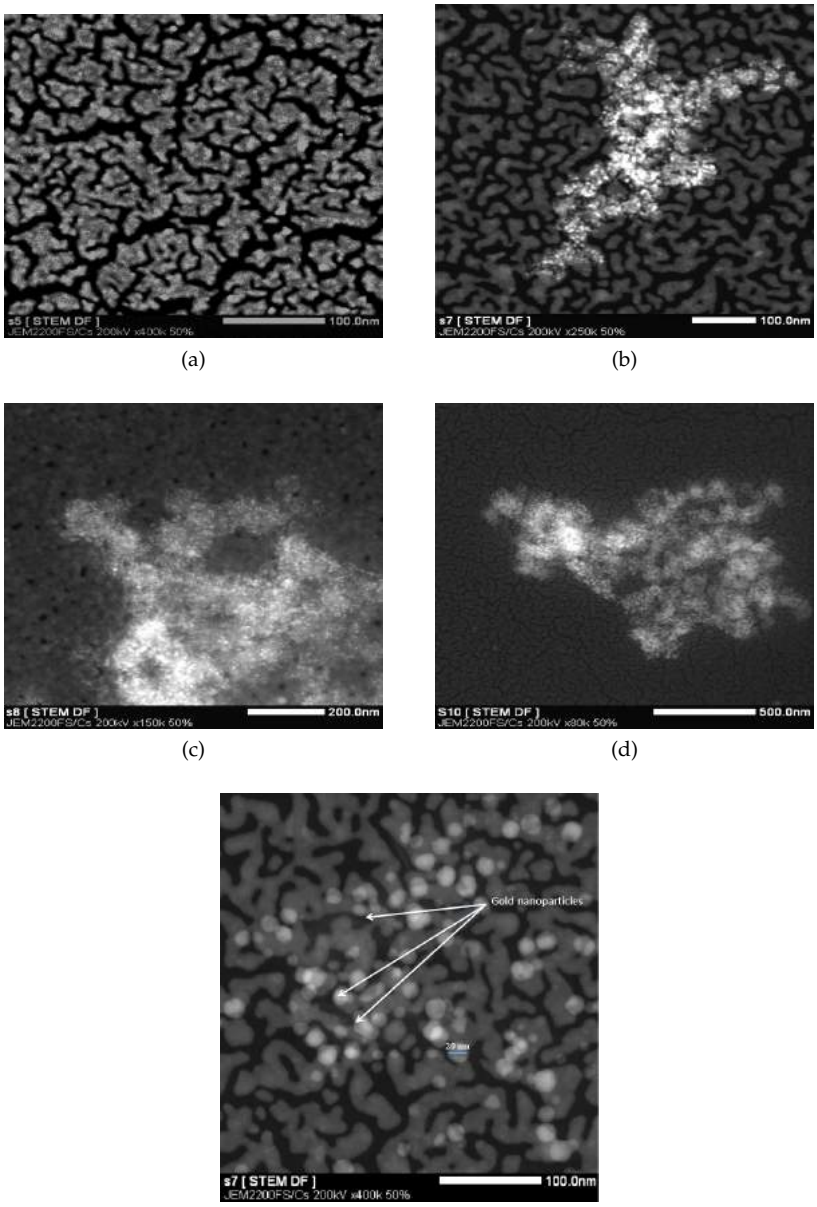

Figure 5.26: STEM results micrographs of a) bare Au TEM grid before ECV electrodeposition by HAADF contrast, and gold electrodes after ECV electrodeposition with b) 5 cycles, c) 10 cycles, and d) 30 cycles, e) Mean size of the produced nanoparticles by HAADF contrast. (For a, b, e, scale = 100 nm; for c, scale = 200 nm; for d, scale = 500 nm)

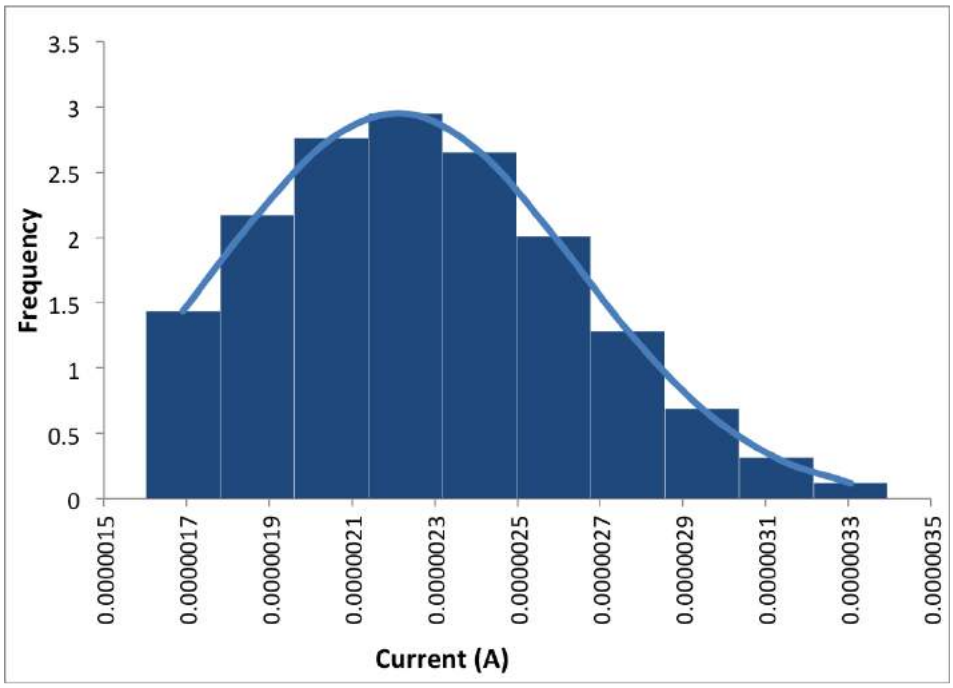

Figure 5.27: Histogram showing frequency distribution of peak currents measured in a group of electrodes prepared using ECV technique.

References

[1] K. Kerman, M. Vestergaard, and E. Tamiya, *Methods in Molecular Biology: Biosensors and Biodetection*. New York: Humana Press, 2009, vol. 504, ch. Electrochemical DNA Biosensors: Protocols for Intercalator-Based Detection of Hybridization in Solution and at the Surface.

[2] M. Ates and A. S. Sarac, "Conducting polymer coated carbon surfaces and biosensor applications," *Prog Org Coat*, vol. 66, no. 4, pp. 337–358, 2009.

[3] F. Lucarelli, G. Marrazza, A. Turner, and M. Mascini, "Carbon and gold electrodes as electrochemical transducers for dna hybridisation sensors," *Biosensors and Bioelectronics*, vol. 19, pp. 515–30, 2004.

[4] U. A. Kirgoz, D. Odaci, S. Timur, A. Merkosi, S. Alegret, N. Besun, and A. Telefoncu, "A biosensor based on graphite epoxy composite electrode for aspartame and ethanol detection," *Anal Chim Acta*, vol. 570, no. 2, pp. 165–169, 2006.

[5] R. Sengupta, M. Bhattacharya, S. Bandyopadhyay, and A. K. Bhowmick, "A review on the mechanical and electrical properties of graphite and modified graphite reinforced polymer composites," *Prog Polym Sci*, vol. 36, no. 5, pp. 638–670, 2011.

[6] X. Cao, Y. Ye, and S. Liu, "Gold nanoparticle-based signal amplification for biosensing," *Anal. Biochem.*, vol. 417, pp. 1–16, 2011.

[7] J. Wang, "Nanomaterial-based amplified transduction of biomolecular interactions," *Small 2005, 1, 1036-1043.*, vol. 1, pp. 1036–43, 2005.

[8] N. Wittenberg and C. Haynes, "Using nanoparticles to push the limits of detection," *Wiley Interdiscip. Rev. Nanomed. Nanobiotechnol.*, vol. 1, pp. 237–254, 2009.

[9] K. Nemani, K. Moodie, J. Brennick, A. Su, and B. Gimi, "In vitro and in vivo evaluation of su-8 biocompatibility," *Mater. Sci. Eng. C.*, vol. 33, no. 7, pp. 4453–4459, 2013.

[10] L. Fischer, M. Tenje, A. Heiskanen, N. Masuda, J. Castillo, A. Bentien, J. Emneus, M. Jakobsen, and A. Boisen, "Gold cleaning methods for electrochemical detection applications," *Microelectron Eng*, vol. 86, pp. 1282–1285, 2009.

[11] M. Noh and I. Tothill, "Development and characterization of disposable gold electrodes, and their use for lead (ii) analysis," *Anal. Bioanal. Chem.*, vol. 386, p. 2095, 2007.

[12] Y. Uludag, Z. Olcer, and M. Sagiroglu, "Design and characterization of a thin-film electrode array with shared reference/counter electrodes for electrochemical detection," *Biosens Bioelectron*, vol. 57, pp. 85–90, 2014.

[13] T. Brulle, W. Ju, P. Niedermayr, A. Denisenko, O. Paschos, O. Schneider, and U. Stimming, "Size-dependent electrocatalytic activity of gold nanoparticles on hopg and highly boron-doped diamond surfaces," *Molecules*, vol. 16, no. 12, 2011.

[14] M. Finot, G. Braybrook, and M. McDermott, "Characterization of electrochemically deposited gold nanocrystals on glassy carbon electrodes," *J Electroanal Chem*, vol. 466, no. 2, pp. 234–241, 1999.

[15] H. Penga, Y. Hua, A. Liua, W. Chena, X. Lina, and X. Yub, "Label-free electrochemical immunosensor based on multi-functional gold nanoparticles–polydopamine–thionine–graphene oxide nanocomposites film for determination of alpha-fetoprotein," *J Electroanal Chem*, vol. 712, pp. 89–95, 2014.

[16] C. Jiang, S. Markutsya, Y. Pikus, and V. Tsukruk, "Freely suspended nanocomposite membranes as highly sensitive sensors," *Nat. Mater.*, vol. 3, pp. 721–728, 2004.

[17] P. Kohl, *Electrodeposition of Gold, in Modern Electroplating*, 5th ed., M. Schlesinger and M. Paunovic, Eds. John Wiley and Sons, Inc., Hoboken, NJ, USA, 2010.

[18] M. Etesami and N. Mohamed, "Catalytic application of gold nanoparticles electrodeposited by fast scan cyclic voltammetry to glycerol electrooxidation in alkaline electrolyte," *Int. J. Electrochem. Sci.*, vol. 6, pp. 4676–4689, 2011.

[19] T. Ling, M. Ahmad, L. Heng, and T. Seng, "The effect of multilayer gold nanoparticles on the electrochemical response of ammonium ion biosensor based on alanine dehydrogenase enzyme," *J Sensors*, 2011.

[20] B. van der Zande, M. Böhmer, L. Fokkink, and C. Schönenberger, "Aqueous gold sols of rod-shaped particles," *Phys Chem B*, vol. 101, pp. 852–854, 1997.

[21] T. Green, "Gold electrodeposition for microelectronic, optoelectronic and microsystem applications," *Gold Bulletin*, vol. 40, no. 2, pp. 105–114, 2007.

[22] M. Mena, P. Sedeno, and J. Pingarron, "A comparison of different strategies for the construction of amperometric enzyme biosensors using gold nanoparticle-modified electrodes," *Anal. Biochem.*, vol. 336, pp. 20–27, 2005.

[23] M. Backman, N. Juslin, and K. Nordlund, "Bond order potential for gold," *EPJB*, vol. 85, p. 317, 2012.

[24] C. Kaulen, M. Homberger, S. Bourone, N. Babajani, S. Karthäuser, A. Besmehn, and U. Simon, "Differential adsorption of gold nanoparticles to gold/palladium and platinum surfaces," *Langmuir*, vol. 30, no. 2, pp. 574–583, 2014.

[25] E. Wurster, A. Elbakry, A. Göpferich, and M. Breunig, "Layer-by-layer assembled gold nanoparticles for the delivery of nucleic acids," *Methods Mol Biol.*, vol. 948, pp. 171–182, 2013.

[26] Y. Xue, H. Zhao, Z. Wu, X. Li, Y. He, and Z. Yuan, "The comparison of different gold nanoparticles/graphene nanosheets hybrid nanocomposites in electrochemical performance and the construction of a sensitive uric acid electrochemical sensor with novel hybrid nanocomposites," *Biosens Bioelectron.*, vol. 29, no. 1, pp. 102–108, 2011.

[27] M. Ottakam Thotiyl, H. Basit, J. Sánchez, C. Goyer, L. Coche-Guerente, P. Dumy, S. Sampath, P. Labbe, and J. Moutel, "Multilayer assemblies of polyelectrolyte-gold nanoparticles for the electrocatalytic oxidation and detection of arsenic(iii)," *J Colloid Interface Sci.*, vol. 383, no. 1, pp. 130–139, 2012.

[28] V. Mani, B. Chikkaveeraiah, V. Patel, J. Gutkind, and J. Rusling, "Ultrasensitive immunosensor for cancer biomarker proteins using gold nanoparticle film electrodes and multienzyme-particle amplification," *ACS nano.*, vol. 3, no. 3, pp. 585–94, 2009.

[29] H. Chen, Y. Wang, Y. Wang, S. Dong, and E. Wang, "One-step preparation and characterization of pdda-protected gold nanoparticles," *Polymer*, vol. 47, pp. 763–766, 2006.

[30] S. Basu, S. Ghosh, S. Kundu, S. Panigrahi, S. Praharaj, and S. Pande, "Biomolecule induced nanoparticle aggregation: Effect of particle size on interparticle coupling," *J Colloid Interface Sci.*, vol. 313, pp. 724–734, 2007.

[31] H. Chen and G. Zhao, "Construction of ionic liquid self-assembled monolayer on gold electrode for hemoglobin modifying and peroxide biosensing," *Int. J. Electrochem. Sci.*, vol. 7, pp. 12 907–21, 2012.

[32] T. Luczak, "Gold and nanogold electrodes modified with gold nanoparticles and meso-2,3-dimercaptosuccinic acid for the simultaneous, sensitive and selective determination of dopamine and its biogenic interferents," *Electroanalysis*, vol. 26, no. 10, pp. 2152–2160, 2014.

[33] T. Luckaz, "Comparison of electrochemical oxidation of epinephrine in the presence of interfering ascorbic and uric acids on gold electrodes modified with s-functionalized compounds and gold nanoparticles," *Electrochim. Acta*, vol. 54, pp. 5863–5870, 2009.

[34] C. Vericat, M. Vela, G. Benitez, P. Carrob, and R. Salvarezza, "Self-assembled monolayers of thiols and dithiols on gold: new challenges for a well-known system," *Chem. Soc. Rev.*, vol. 39, pp. 1805–1834, 2010.

[35] M. Daza Millone, H. Hamoudi, L. Rodriguez, A. Rubert, B. G.A., V. M.E., R. C. Salvarezza, J. E. Gayone, E. A. Sanchez, O. Grizzi, C. Dablemont, and V. A. Esaulov, "Self-assembly of alkanedithiols on au(111) from solution: Effect of chain length and self-assembly conditions," *Langmuir*, vol. 25, pp. 12 945–12 953, 2009.

[36] J. Tour, L. Jones II, D. Pearson, J. J. S. Lamba, T. P. Burgin, G. Whitesides, D. L. Allara, A. N. Parikh, and S. V. Atre, "Self-assembled monolayers and multilayers of conjugated thiols, α, ω-dithiols and thioacetyl-containing adsorbates. understanding attachments between potential molecular wires and gold surfaces," *J American Chemistry Society*, vol. 117, p. 9529, 1996.

[37] H. Ron, S. Matlis, and I. Rubinstein, "Self-assembled monolayers on oxidized metals. 2. gold surface oxidative pretreatment, monolayer properties, and depression formation," *Langmuir*, vol. 14, pp. 1116–1121, 1998.

[38] Y. Tang and P. G. Chen, "Nanoparticle-electrodeposited electrodes used for p-nitrophenol detection in acidic media: Effect of electrodeposition parameters on particle density, size distribution, and electrode performance," *J Chin Chem Soc-Taip*, vol. 58, no. 6, pp. 723–731, 2011.

[39] Y. Takahashi, H. Umino, S. Taura, and S. Yamada, "An electrochemical approach for fabricating organic thin film photoelectrodes consisting of gold nanoparticles and polythiophene," *RCP*, vol. 2, no. 3, pp. 79–81, 2013.

[40] J. Wu, L. Li, B. Shen, G. Cheng, P. He, and Y. Fang, "Polythymine oligonucleotide-modified gold electrode for voltammetric determination of mercury (ii) in aqueous solution," *Electroanalysis*, vol. 22, pp. 479–482, 2010.

[41] B. Park, D. Kim, and D. Yoon, "Surface modification of gold electrode with gold nanoparticles and mixed self-assembled monolayers for enzyme biosensors," *Korean J Chem Eng*, vol. 28, no. 1, pp. 64–70, 2011.

[42] E. AlShamaileh, H. Saadeh, and V. Favry, "Modification of gold surface with gold nanoparticles and cyclohexyl dithiocarbamate as a selective sensor for cysteine," *Journal of Chemistry*, 2013.

[43] N. German, A. Ramanavicius, and A. Ramanaviciene, "Electrochemical deposition of gold nanoparticles on graphite rod for glucose biosensing," *Sensor Actuat B*, vol. 203, pp. 25–34, 2014.

6

Oc & CTX BioSensors: Characteristics and Validation

6.1 Introduction

As mentioned in Chapter 3, while immunoassays have an extensive application in clinical and research areas, the immunosensor concept is yet to be implemented in routine diagnostics [1][2]. There are certain issues in this regard, the most important of which is the coupling chemistry of proteins on surfaces, which is critical for optimal functioning. In other words, the optimal orientation of Ab molecules on the surface is of great importance to obtain a selective and sensitive detection in a reproducible way without affecting its activity [3]. The relative lack of long-term stability of biological molecules is the most serious limitation in commercializing biosensors.
Immobilization methods vary largely based on the surface and protein properties. Ideally, as mentioned earlier, during the process the protein conformation should remain intact so that protein functions are retained. Moreover, the active sites of Ab should be accessible to reaction partners in order to have a high-performance, reproducible assay [4]. This is while once immobilized, biomolecules adsorbed on AuNPs are not free and adopt certain orientation and conformation on the surface [5]. This raises the question of how the activity of an anti-

body is affected by conjugation with a gold particle. Although protein-conjugated gold nanoparticles have been successfully employed as biological markers for decades, instances of total or partial loss of specific activity of a protein upon conjugation have also been reported [6]. Therefore, this chapter deals with the immobilization of two main BTMs (Oc and CTX) on the glass-based gold electrode fabricated as mentioned in Chapter 5 and coated with AuNPs. To our knowledge, a biosensor to assess serum levels of Oc has not been developed before. A step-wise protocol to develop these sensors is explained here.

6.2 Oc Biosensor

6.2.1 Oc

Oc, also known as bone gamma-carboxyglutamic acid-containing protein (BGLAP), is the most abundant non-collagenous protein in bone, comprising 1–2% of the total protein content [7]. It is a small 44-aminoacid long protein (5.8 kDa) synthesized exclusively by osteoblasts (and odontoblasts). The specific glutamyl residues at positions 17, 21 and 24 have a second carboxylate group added to form γ-carboxyglutamyl residues (Gla), which stabilizes the α-helical portion. When Oc meets calcium ions, these active sites (3 Gla residue and 1 Asp) chelate to the ions and Oc folds to a special structure.
Oc is released into the circulation from the matrix during bone resorption and, therefore, its high levels are considered as a marker of bone turnover [8]. Previous studies suggest that serum Oc levels, even in the absence of alkaline phosphatase, is useful in monitoring follow-up changes that currently cannot be assessed with BMD assessment in osteoporosis treatment [9][10]. As mentioned in Chapter 2, Oc is a specific, sensitive and promising marker to be used for better prognosis of osteoporosis and for monitoring response to antiresorptive therapy [11]. (Figure 6.1)

6.2.2 Sensor fabrication process

As mentioned earlier, the glass-based gold electrodes fabricated based on the method explained in Chapter 5 were used. In order to have an AuNP layer on the electrodes that would allow Ab molecules to immobilize on the surface, the ECV technique was used.
The final goal of immobilization strategies is to improve assay sensitivity, specificity, reproducibility, and even application. In this regard, different techniques were modified to form stable and strong bonds

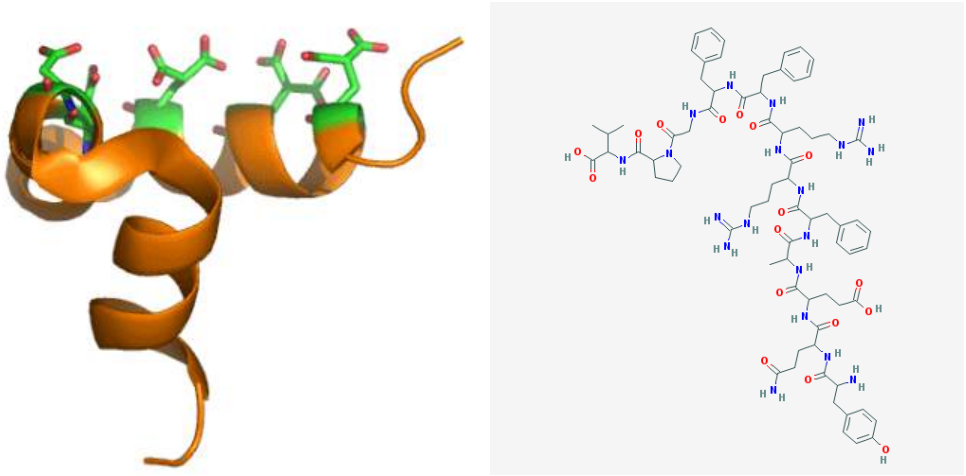

Figure 6.1: 3D and 2D Structure of Oc.

between the protein and the immobilization surface, minimize non-specific adsorption of biomacromolecules, keep the proteins in an active state, and finally orient proteins for unhindered access of binding partners. Consequently, controlled experiments against the standards were performed for verification of the best method and conditions of immobilization of Oc antibody on the gold electrodes. The applied protocols are shown in the flowchart in Figure 6.2. The first two protocols were based on physisorption immobilization, whereas the others were based on covalent attraction between constituents using different cross-linkers.

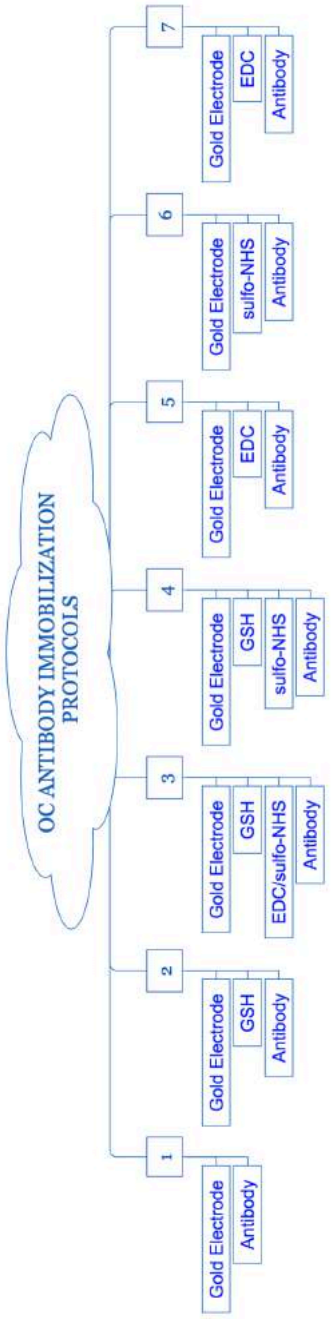

Figure 6.2: Flow chart depicting experimental design for immobilizing antibody on the electrode.

In the first protocol, fragment antigen-binding (Fab) antibody fragments were deposited onto gold via native thiol groups. Passive absorption does not provide permanent attachment of the coating as molecules may desorb from the surface overtime. Proteins may also lose their properties after being absorbed to the surface, caused by changes in tertiary structure or binding of active/Ag to the gold surface rendering it inaccessible. In the second protocol, still the bonding was not strong enough and thus the antibody was washed away during the washing steps.
As for other protocols, covalent coupling using different combinations of EDC and sulfo-NHS was applied. These reactions are not only specific and controllable but also the number of covalent bonds between the surface and Ab can be optimized to help maintain the tertiary structure of the protein.
Here we explain the most complex process (protocol 3), with the maximum number of steps. The other protocols were tested similarly using the same concentrations and incubation times mentioned in this protocol, skipping the non-mentioned materials.
In protocol 3, appropriate amount of a 10 mM solution of GSH was deposited on the gold surface and left to dry at room temperature for an hour [12]. GSH bonds with gold through the formation of an Au-S bond, while providing carboxylate groups for the next layers to react with. A mixture of EDC/sulfo-NHS was used to facilitate the conversion of the carboxylic acid groups of the monolayer to amine groups for subsequent Ab attachment. In this regard, the freshly prepared EDC and sulfo-NHS were mixed with a volume ratio of 1:1 and incubated for 20 min. Appropriate amount of Ab was then added to the solution and incubated for another 60 min. After gently rinsing the prepared surface with distilled water, the electrodes were covered with the solution of EDC/sulfo-NHS/Ab and incubated for 180 min at room temperature.
In order to block the uncoated surface and to minimize nonspecific adsorption of off-target biomolecules and remove non-adsorbed proteins, the surface was gently rinsed. Effective removal of excess EDC/sulfo-NHS after activation is important to prevent protein crosslinking.
Then the unreacted active functional groups were blocked or deactivated by BSA. 20 μl of 0.2% BSA solution in PBS buffer was added for 1 hr. The electrode was then rinsed for 3 min with 0.1 M PBS (Coupling Buffer) and then 0.1M PBS-Tween 20 (Washing Buffer). PBS- Tween 20 is commonly used to minimize the background noise from non-specific binding in bioassays. The electrodes were then shaken to remove excess water.

While DI water and PBS, used as the rinsing reagents in our experiment, are inert, care was taken while applying these solutions to maintain the integrity of the electrode surface as the detachment of the conjugates can be an issue.
The Ab-Ag reaction was then tested by introduction of different concentrations of Ag solution using a fine pipette.

6.2.3 Characteristics of the Oc electrochemical chip

Surface Modification

Successful electrodeposition of gold nanoparticles on the surface and immobilization of antibody on the modified surface was verified by STEM.(Figure 6.3)
To further analyze the chemical composition of different layers, XPS characterization was employed at different steps. In the first step, the XPS signature of the S2p doublet (163,9 - 165,1 eV) was suggestive of the attachment of GSH to the gold surface through the thiol group. The N1s and C1s core level spectrums noted in the successive steps mainly originated from the antibody. The presence of satellite (293 eV) and aromatic (284.3 eV) lines in the XPS spectrum also confirmed the immobilization of the antibody on the surface has been successful.

Electrochemical impedance spectroscopy (EIS)

As mentioned in Chapter 3, EIS is another powerful method, commonly used in electrochemical research, to analyze the electrical resistance of a system. The technique is sensitive to surface phenomena and changes of bulk properties. Therefore it was applied within this work to characterize surface modifications and detect binding events on the transducer surface. The assembly of the layers on the gold electrode surface and the loading of AuNP were confirmed by EIS measurements.
Figure 6.4 shows a Nyquist plot of impedance for the stepwise modification process of the gold electrode. The data was obtained by using 0.1 mM $K_3[Fe(CN)_6]$ and upon application of the biasing potential 0.17 V and 5 mV amplitude in the frequency range of 0.1 Hz to 100 kHz. As already known, the impedance spectra contain a semicircle portion at higher frequencies relating to the electron transfer limited process and a linear part at lower frequencies corresponding to diffusion. The diameter of the semicircles showed the charge transfer resistance rate.
In the EIS measurement, the negatively charged ferri/ferrocyanide couple $[Fe(CN)_6]^{3-/4-}$ was employed as the redox marker for electro-

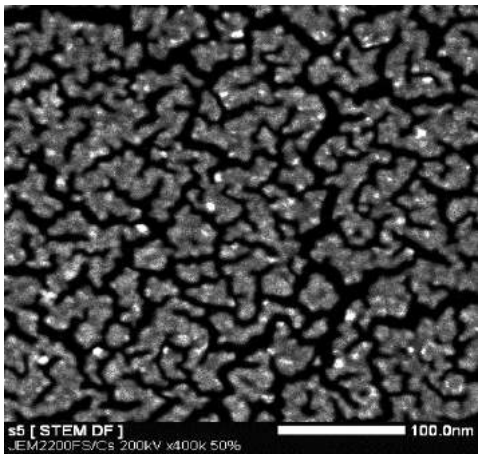

(a)

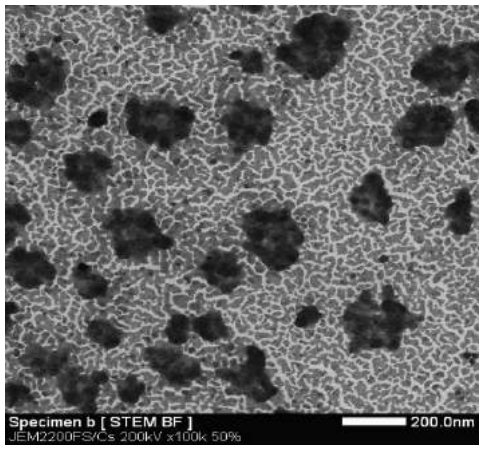

(b)

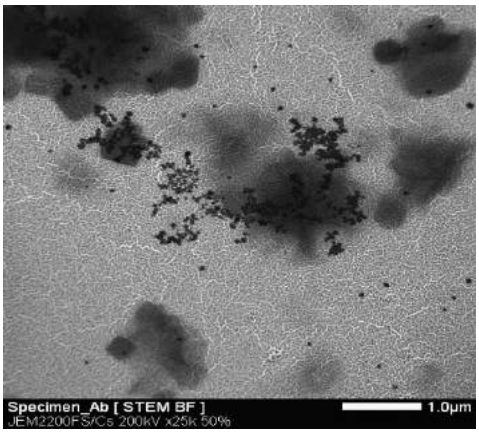

(c)

Figure 6.3: STEM micrographs of a) bare gold nanoparticles by HAADF contrast, b) AuNP-modified gold electrode by BF contrast, c) Ab functionalized gold electrode by BF contrast. (For a, scale = 100 nm; for b, scale = 200 nm; for c, scale = 1.0 μm)

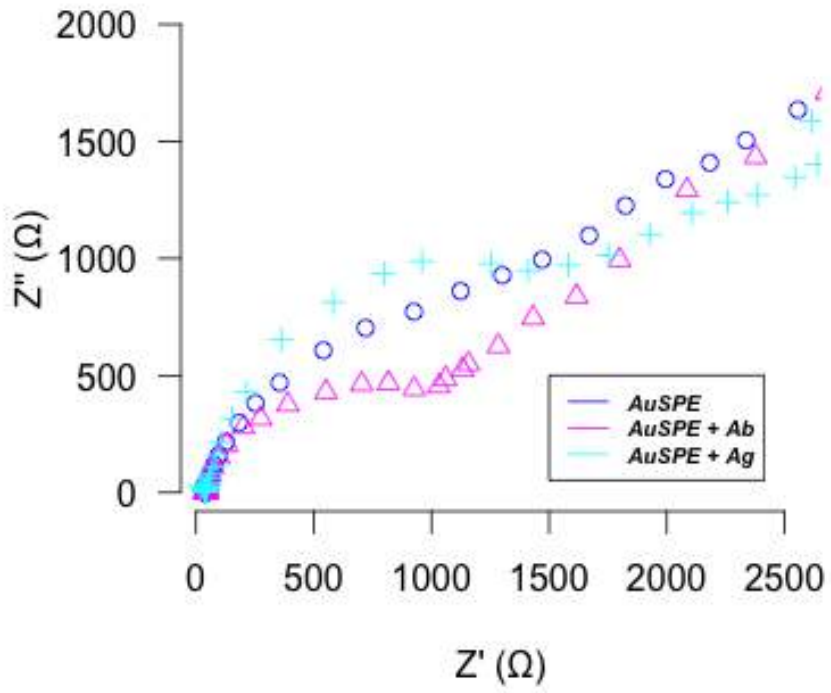

Figure 6.4: EIS results for each modification step (Marine = Gold electrode with gold nanoparticles capped with GSH, Pink = Gold electrode with antibody conjugated gold nanoparticles, Blue = sensor + Ag).

chemical characterization, and thus the diffusion of $[Fe(CN)_6]^{3-/4-}$ and mass loading of the antigen onto the surface of the electrodes have a significant effect on the charge transfer resistance.
As can be seen from the Figure 6.4, the bare electrode produces an almost straight line Nyquist plot with no semicircle domain, implying a diffusion-limited electrochemical process of the redox coupling at the electrode surface. After adding additional layers, a semicircle was noted, indicating the increase of the interfacial charge transfer resistance. Considering the nature of the layers, the changes in this diameter could be explained. Ab binding caused a physical barrier, limiting the access of the redox probe to the electrode. Exposure of Ag generates a further barrier for the electrochemical process, causing a slight increase in the transfer resistance.

6.2.4 Analytical Procedure

Ag concentration against current read during DPV analysis in each protocol was used to calculate and plot linear and logarithmic fit R-squares (degree of fit). The DPV measurements in this work were performed in 0.1 mM $K_3[Fe(CN)_6]$, containing 0.01 M NaCl, applying following parameters: 0.025 V modulation amplitude, 0.05 s modulation time, 0.005 V step potential and voltage range from 0.5 to 1.1 V. The results showed that the immobilization was most effective for sulfo-NHS activation (protocol 4) as it not only followed the decreasing trend suggestive of the inverse correlation of current and Ag concentration, but also had the best R-square.
The stability of the immobilization process was also studied by washing the electrodes with PBS for four times. Again electrodes prepared using protocol 4 showed the best results. In other words, the results showed that the immobilization was most effective for sulfo-NHS activation and that the best results were achieved when carboxylates (-COOH), found on the surface after the deposition of GSH on the gold electrode, were reacted to sulfo-NHS. (Figure 6.5) NHS ester was then reacted with primary amines (-NH2) of the antibody to form amide crosslinks.

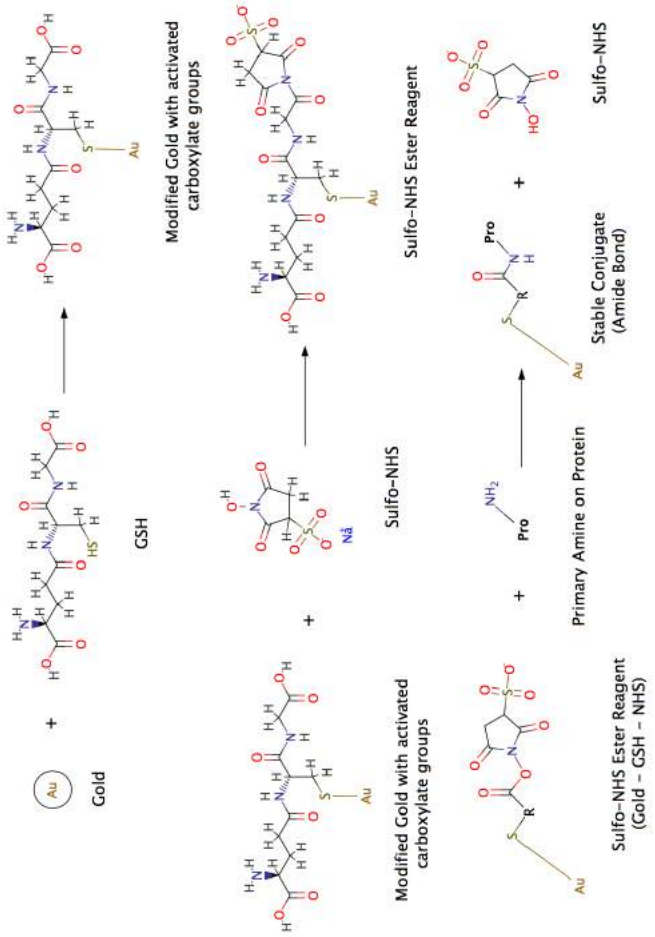

Figure 6.5: Chemical reactions occurring on the surface in different steps.

Afterwards, through plotting the current in that protocol against the diverse concentrations, the calibration curve was formed. As mentioned earlier, as more antigen was introduced onto the surface upon reaction with the immobilized antibody, the redox marker diffusion to the surface of the electrode was hindered due to repulsive interactions. Thus lower current was observed.

Figure 6.6 illustrates the calibration curve plotted using average response of the sensor towards its target, Oc Ag, from experiments performed under the conditions described above.
The calibration curve was generated based on the average value of measurement conducted in triplet set on the sensing interface, which was treated with different amounts of antigen from the lowest to the highest concentrations. Parameters such as lower limits of detection (LLD), upper limits of detection (ULD), and consequently a dynamic range was calculated. Other assessed parameters included limit of detection (LoD) and limit of quantification (LoQ), sensitivity (slope of the gradient), reproducibility (standard deviation divided by the average in percent), tightness of fit (R-square of trend line applied) and behavior (linear, non-linear, etc.).
The LoD and LoQ were calculated using the following equations: (Equation (6.1), (6.2))

$$LoD = \frac{3.3 * \delta}{S} \tag{6.1}$$

$$LoQ = \frac{10 * \delta}{S} \tag{6.2}$$

where δ is the standard deviation of the response and S is the slope of the calibration curve.[13]
Figure 6.7 illustrates the relationship between the blank, LoD and LoQ. For a signal at the LoD, the alpha error (probability of false positive) is small (1 %) [14]. However, the beta error (probability of a false negative) is 50 % for a sample that has a concentration at the LoD, suggesting that the sample could contain an impurity at the LoD, but there is a 50 % chance that the measurement would give a result less than the LoD. At the LoQ, there is minimal chance of a false negative.

The magnitude of electrochemical response current was linearly dependent to the logarithm of Oc concentration with an R square of 0.92 and slope of 0.75 (sensitivity) over the concentration range. The detection limit was calculated to be 0.65 ng/mL. The device had an LoQ of 1.97 ng/mL with a correlation coefficient of 0.99. The sensor was capable of assessing Ag levels in the range of 2.5-90 ng/mL.

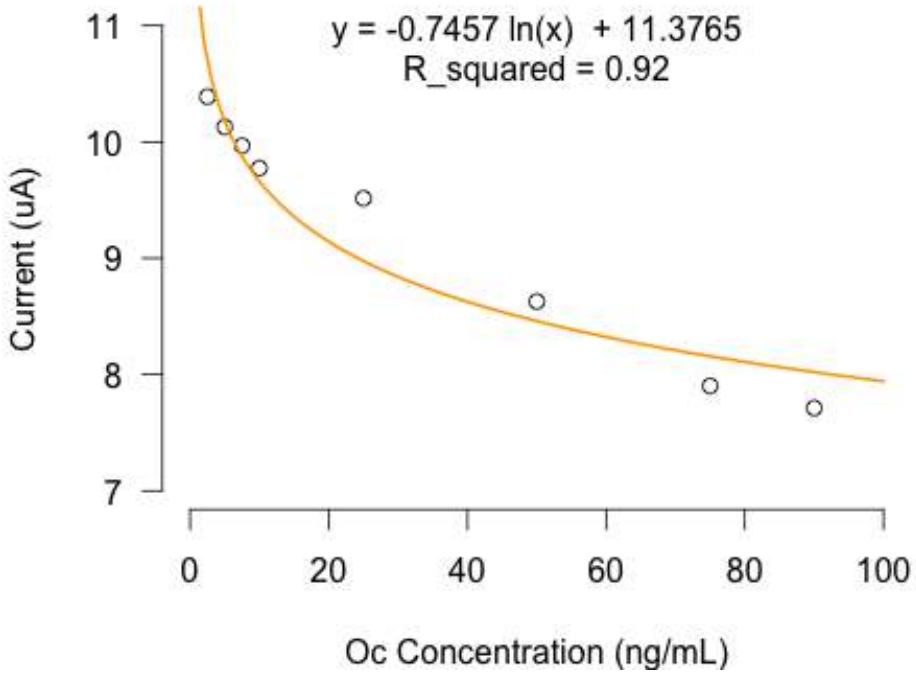

Figure 6.6: Sensor responses to varying Ag concentrations (2.5-90 ng/mL) using protocol 4.

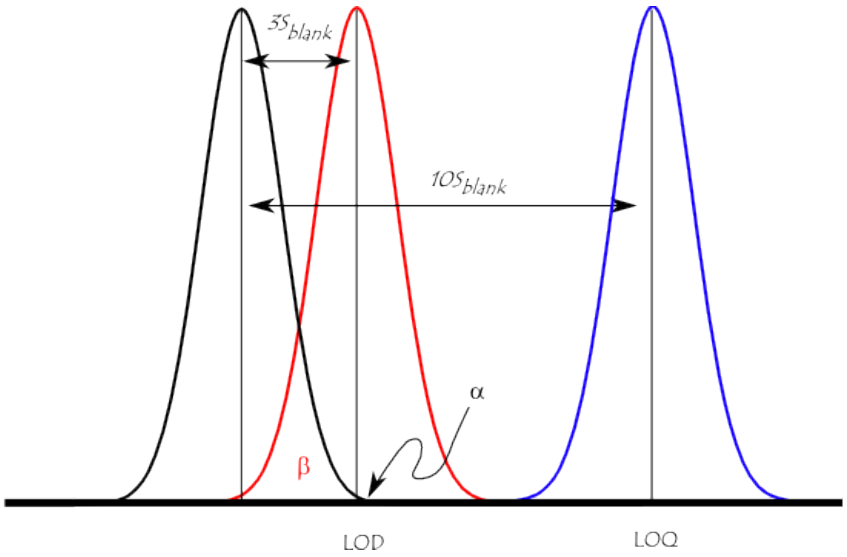

Figure 6.7: Illustration of the concept of LoD and LoQ by showing the theoretical normal distributions associated with blank, LoD, and LoQ level samples..

A schematic illustration of the preparation process of the immunosensor is shown in Figure 6.8.

6.2.5 Real serum measurement

Concentration gradients of serum Oc levels were tested using ECLIA and run against the number read by the sensor for verification. ECLIA is a highly sensitive method for the detection of diverse analytes based on ELISA technology. In this regard, the serum of eight patients whose Oc levels were recently measured using ECLIA was used. Using the trend function in Excel and based on the calibration curve, the concentration of Oc in the tested samples were calculated according to the obtained current. The results were then compared.

According to the results presented in Table 6.1, the coefficients of variation for the ECLIA and Oc sensor were calculated to be 4.4% and 4.48%, respectively.

The correlation between our sensor results and that of ECLIA was also investigated and the results are shown in the correlation and Bland and Altman plots in Figure 6.9. The equation of the trendline in the correlation plot has a slope of 0.97 and R^2 of 0.98. The mean difference between the two methods according to the Bland and Altman plot was

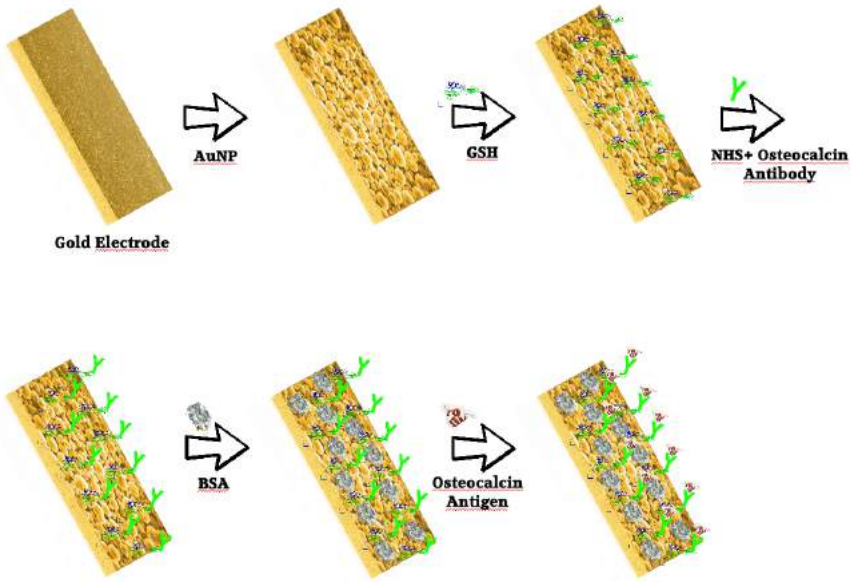

Figure 6.8: A Schematic illustration of the preparation process of the Oc immunosensor.

Table 6.1: Precision of Oc assay using ECLIA and Oc-Sensor.

Serum samples	ECLIA results (ng/mL)	Oc-Sensor results (ng/mL)
1	10.3	10.33
2	15	14.71
3	17.1	17.90
4	26.8	24.35
5	29.8	26.88
6	32.1	29.35
7	33.7	32.11
8	45.5	46.16

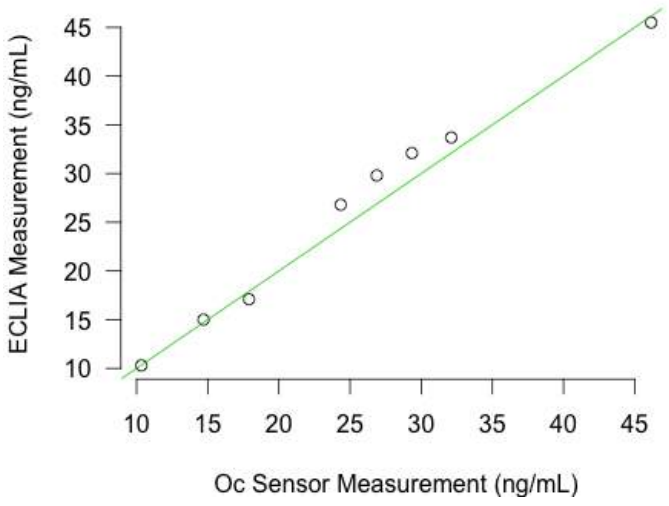

(a)

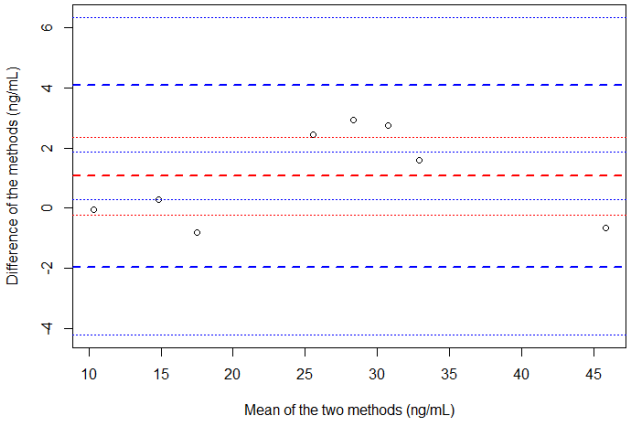

(b)

Figure 6.9: Statistical analysis comparing ECLIA vs. Oc sensor immunoassay a) Correlation plot, b) Bland and Altman plot.

Figure 6.10: PDMS-stamps used for microcontact printing of the antibodies on the electrode surface.

1.06 ng/mL and the 2s limits of the standard deviation (2SD) was 3.03 ng/mL. This indicates that the Oc sensor provides sensitive and specific results of Oc levels in serum [15].

6.2.6 PDMS-Stamps

Previous studies have considered microcontact printing as an effective technique for parallel transfer of material to a surface, making stamping of thousands of microspots of the same molecule simultaneously over areas larger than 1 cm or developing complex protein pattern possible [16] [17]. In order to improve the electrode production approach, we decided to benefit from a combination of hydrophobic and covalent interactions. (Figure 6.10) As described earlier, the simplicity of physisorption makes it a preferred method for immobilizing proteins in early, proof-of-concept experiments. In this regard, we used a PDMS stamp.

The efficacy of the technique, which benefits from an entropically driven interaction and hydrophobic adsorption rather than the formation of chemical bonds, depends on well-known experimental variables such as pH, salt concentration, and temperature. It also requires multiple inking and stamping steps to have discrete pattern of multiple protein species, and according to our experience was not reproducible.

6.3 CTX Biosensor

6.3.1 CTX

Type I collagen accounts for 90% of the organic matrix of the bone, and is subjected to a series of enzymatic and non-enzymatic intra- and extracellular post-translational modifications that may induce bone strength during the normal aging process or on the pace of a disease [18]. Collagen crosslinking is therefore of great importance in determining the biomechanical competence of the bone [19]. Several studies have related the bone content of C-telopeptide (CTX) crosslinks, in part independent of the bone mineral value, with bone strength, suggesting serum CTX as a reference bone resorption marker [20] [21]. In other words, despite the marked effects of circadian variation and other factors such as diet on serum levels of CTX, the marker is reported to be sensitive to short-term changes in bone metabolism.
The first serum CTX assay was a competitive polyclonal antibody ELISA [22] [23]. To overcome the limitations linked to ELISA, several label-free immunosensing biosensor for the detection of CTX levels was developed but never commercialized [24] [25].

6.3.2 Sensor fabrication process

Again, the gold electrodes prepared in Chapter 5 and coated with an AuNP layer using ECV technique were used. The immunosensor was fabricated by the immobilization of antibodies on the gold electrode through EDC/sulfo-NHS covalent-linking.
Firstly, 4 μL of a 10 mM GSH solution was coated on the working electrode and dried at room temperature for 1 hr. After gently rinsing with distilled water, the gold electrodes functionalized with carboxylic groups were incubated in a mixture solution of 400 mM EDC and 100 mM sulfo-NHS and 10 μg/mL CTX for 2.5 hrs. In order to make this solution, EDC and sulfo-NHS (1:1 ratio) were first reacted with each other for 20 min and then CTX Ab was added to the solution and incubated for another 60 min. Subsequently, the electrodes were rinsed to remove the excess antibody complex.
In order to avoid non-specific binding, 10 μL of BSA solution (0.2% m/v in 0.1 M PBS, pH 7.4) was deposited on each electrode for 1 h. Finally, the electrodes were rinsed with 0.1 M PBS and 0.1 M PBS-Tween 20. The electrodes were then shaken to remove excess water. Fully modified electrodes were stored dry until further use with actual antigen samples, but not longer than one day. The electrode carrying the conjugated antibodies were treated carefully as the detachment of the

conjugates can be troublesome if proper handling/pipetting are not employed during washing/blocking steps.

6.3.3 Characteristics of CTX electrochemical chip

Surface Morphology

We used STEM to determine three-dimensional surface morphology of the electrodes after every modification step and to study the interaction between CTX antibody and the electrode surface. STEM images of the fabricated Au nanoparticles on gold surface demonstrated that, the electrodeposition results in surfaces with highly uniform distribution of AuNP of approximately 20 nm in diameter. (Figure 6.11, 6.12, 6.13) As a result, total surface roughness, and thus surface area of the electrode was enhanced. The observation of Ab-functionalized electrodes indicated the affinity of AuNPs to CTX antibody, and the aggregation properties of the antibody complex.
XPS similarly confirmed the successful modification of the electrode surface in every step.

Electrochemical behavior

The AuNP layer enhanced the electrochemical conductivity of the AuNP-modified electrode compared to the bare one, which is related to the increased active surface area of the electrode. (Figure 6.11, 6.12, 6.13) As mentioned in Chapter 5, the real electrochemical surface area of the gold electrodes was 2.3 times greater than the area before electrodeposition, providing a bigger surface for antibody immobilization. In addition, the CV of AuNP-modified electrodes showed a remarkable oxidation peak at 0.142 V and a reduction peak at 0.9 V. This sharp oxidation peak is due to oxide formation and the occurrence of Au stripping. Therefore, the AuNP-modified electrode displayed an advantage for signal amplification.
After the addition of the antibody complex, however, a significant signal reduction in electrical response was noted. This is because of the binding of antibody on the electrode surface which forms a hydrophobic surface that retards the interfacial electron transfer, which will be reflected as reduced electrical response.

6.3.4 Analytical procedure

The fundamental structural unit of an antibody is two identical heavy and light chains interconnected by disulfide bridges. The chains are

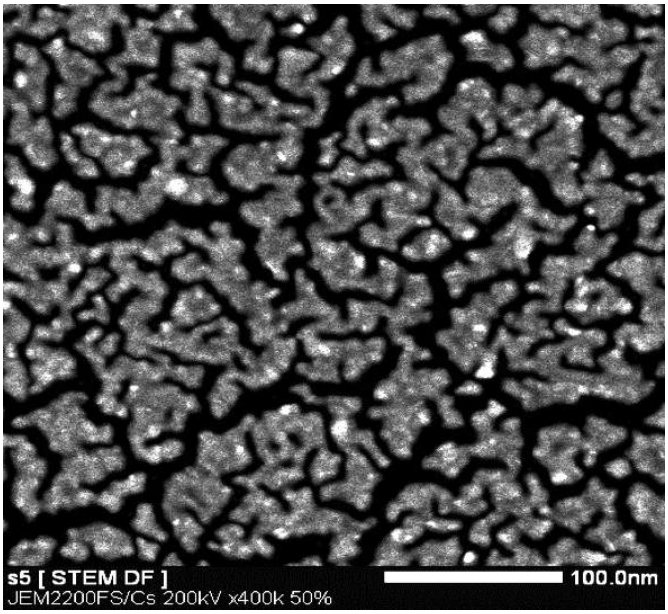

(a)

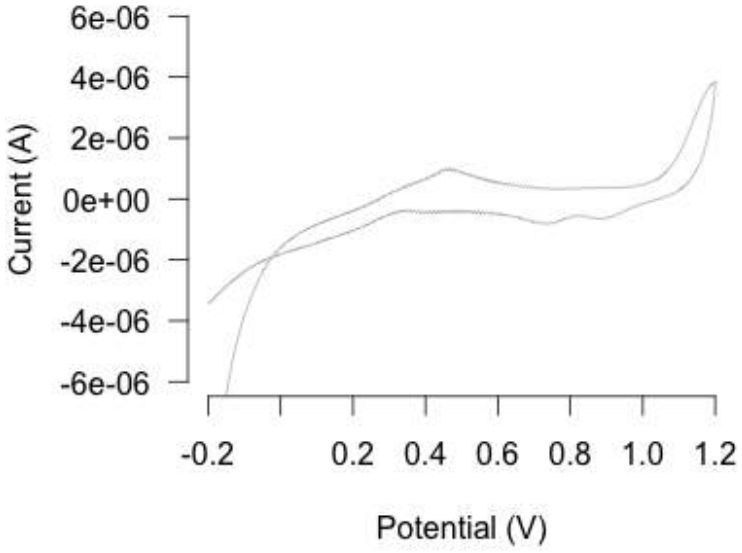

(b)

Figure 6.11: a) STEM micrographs and b) CV of a bare gold electrode.

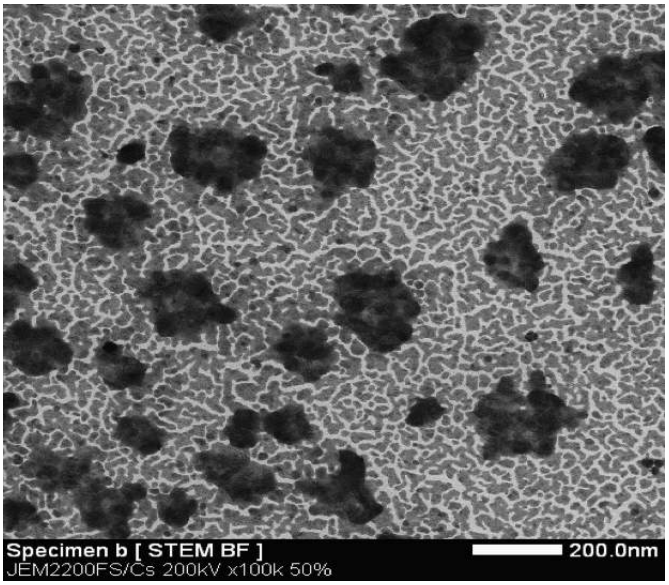

(a)

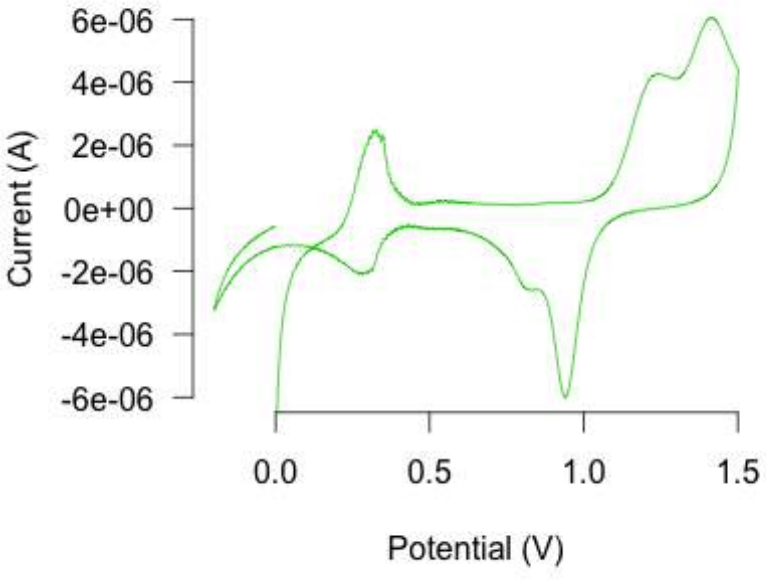

(b)

Figure 6.12: a) STEM micrographs and b) CV of an AuNP-functionalized gold electrode.

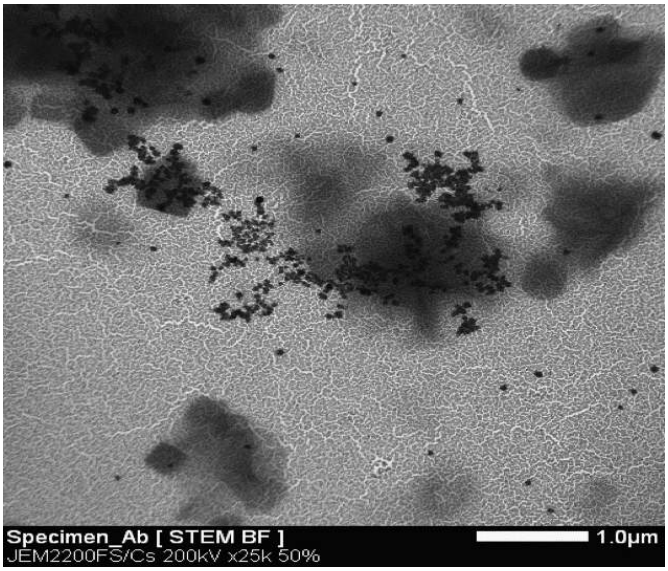

(a)

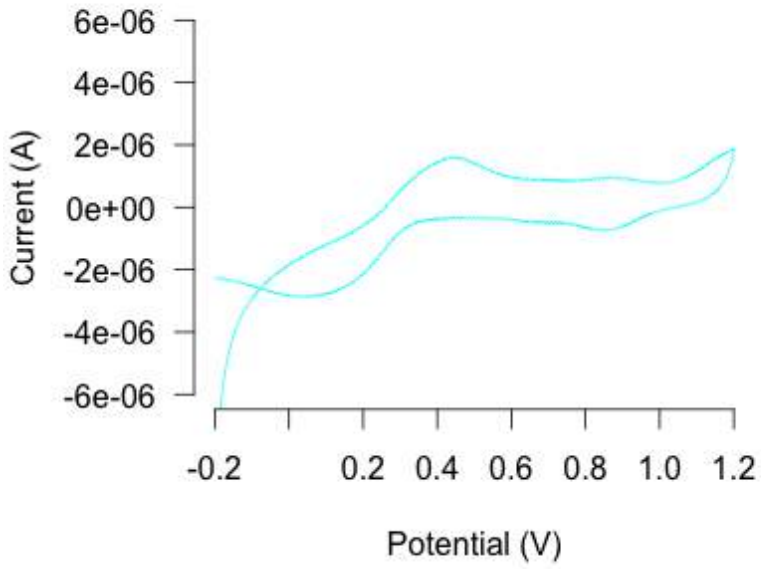

(b)

Figure 6.13: a) STEM micrographs and b) CV of an Ab-functionalized gold electrode.

entirely composed of constant and variable regions, combining one interaction site for the antigen. The conformation of amino acids of antibody in this site determines its antigen binding activity [26]. Several non-covalent bonding, such as van der Waals and non-polar hydrophobic interactions as well as London dispersion attractive and steric repulsion forces contribute to the molecular interactions between the antibody and antigen.

The antibody-antigen reaction on our electrodes was tested by the introduction of Ag solution using a fine pipette. In this regard, concentration gradients of the target, CTX, were prepared and run against the sensor for verification. The concentration against current read during DPV analysis was used to calculate and plot linear and logarithmic fit R-squares (degree of fit).

Under the optimum conditions, the DPV peak current of the immunosensor array for detection of CTX decreased proportionally with the increasing concentration of analytes. (Figure 6.14) A linear response was observed over the logarithm of concentration range (1 - 1000 pg/mL) tested and the activity of the receptor-antigen couple was verified. A slope of 0.004 and a linear regression constant (R^2) of 0.96 was obtained from the response curve. The correlation coefficient was 0.82 and the LOQ was calculated to be 16.5. The limit of detection (LoD) was found to be 5.44 pg/mL, which was much lower than the normal CTX range in plasma (50-450 pg/mL), indicating the sensitivity of the assay.

A schematic illustration of the preparation process of the immunosensor is shown in Figure 6.15.

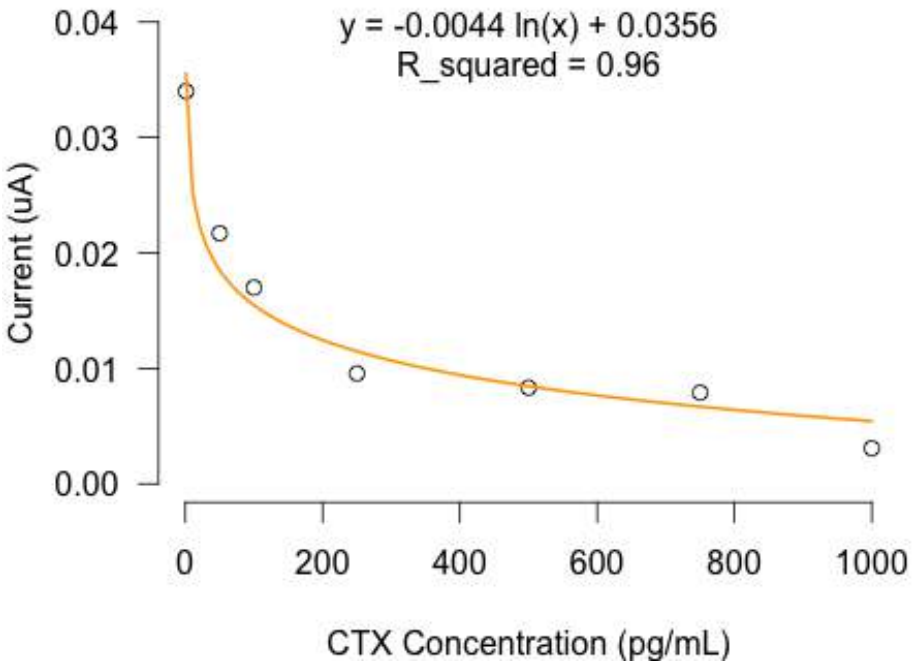

Figure 6.14: Calibration curve of different CTX concentrations using the proposed immunosensor for signal tracing and amplification.

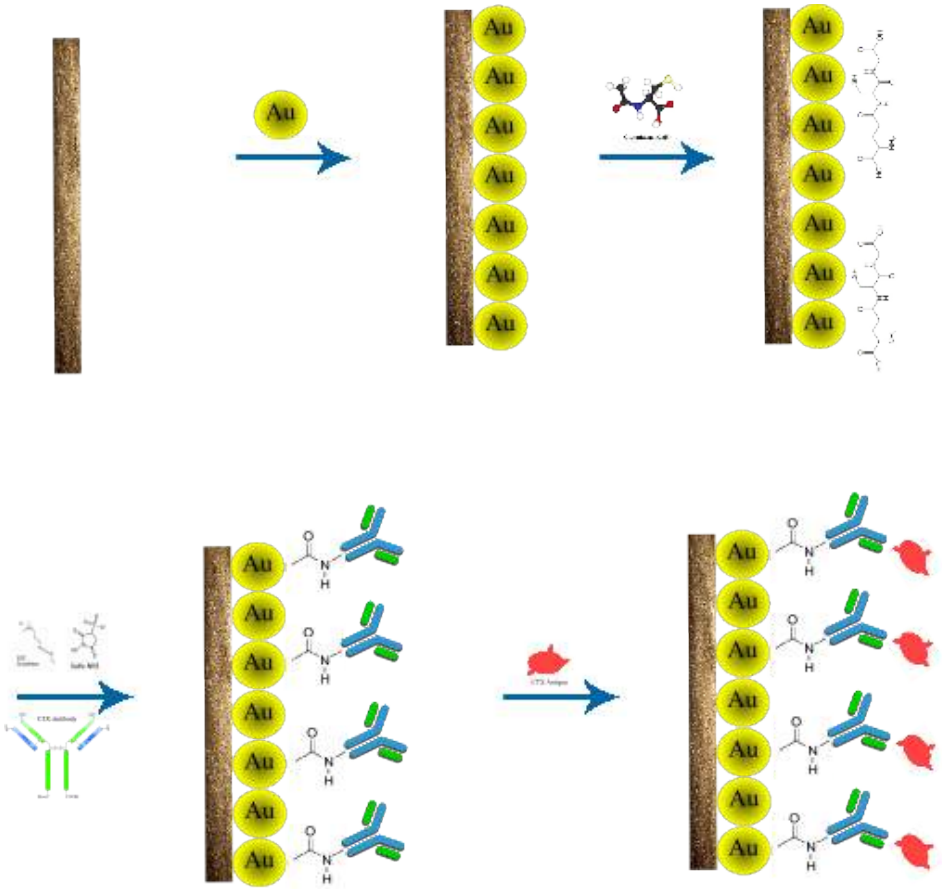

Figure 6.15: Surface preparation is typically made possible by modifying the gold surface by AuNP, leaving carboxyl groups on the surface which in turn can be activated using zero crosslength linkers such as (EDC/NHS), rapidly accepting an antibody and detection can occur under target binding.

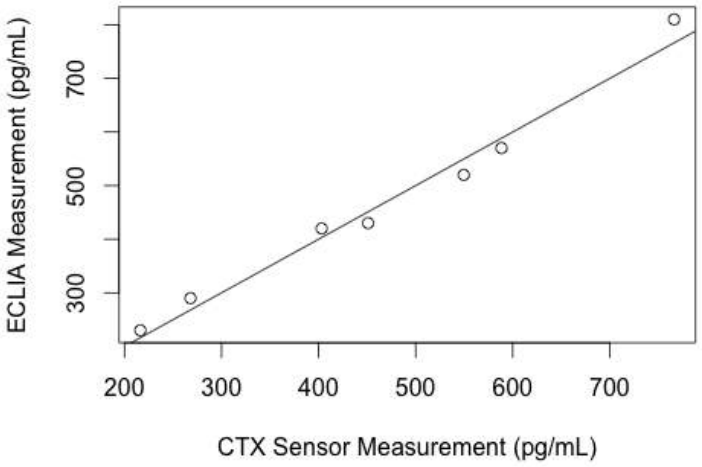

(a)

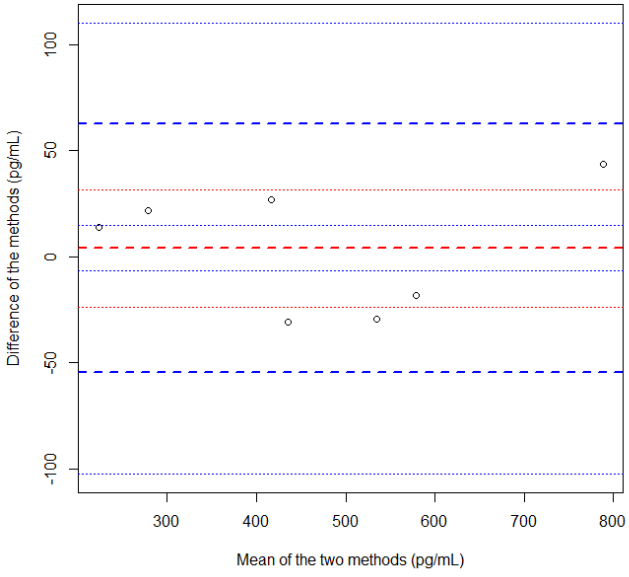

(b)

Figure 6.16: Statistical analysis comparing ECLIA vs. CTX sensor immunoassay a) Correlation plot b)Bland and Altman plot.

Table 6.2: Assay results of clinical serum samples using the proposed and reference (ECLIA) methods.

Serum samples	Proposed method (pg/mL)	Reference method (pg/mL)	Relative error (%)
1	268.02	290	7.58
2	403.13	430	6.25
3	588.43	570	3.23
4	216.38	230	5.92
5	451.03	420	7.39
6	549.55	520	5.68
7	766.34	810	5.39

6.3.5 Real serum measurement

To evaluate the reliability and application potential of the proposed immunoassay method, the assay results of CTX in human serum samples using the proposed method were compared with the reference values obtained by commercial electrochemiluminescent single-analyte tests. In this regard, the serum of seven patients whose CTX levels were recently measured using ECLIA was used. The results are listed in Table 6.2. Acceptable results with relative errors less than 7.58% indicated good accuracy of the proposed method for real sample analysis.
The correlation between our sensor results and that of ECLIA was also investigated and the results are shown in the correlation and Bland and Altman plots in Figure 6.16. The equation of the trendline in the correlation plot has a slope of 0.98 and R^2 of 0.97.

6.4 Optimization

Several factors affect the LoD and thus sensitivity of an assay. Reducing the risk of loss of activity of the antibody upon conjugation and nonspecific binding on exposed gold surfaces plays an important role in this regard. In this immunosensor however we tried to improve direct immobilization of the antibody by modifying the electrode surface by AuNPs and using cross-linkers. Nonspecific binding of antigen on uncovered gold was also resolved by uniform distribution of AuNPs on the whole electrode surface.
Analytical signal also depends on the morphology of the electrode's surface. This is influenced by factors such as surface roughness. As a result, the amount of immobilized antibodies, their proper conjugation to the surface and improved response signal depends on the amount and size of AuNPs deposited on the electrode surface. These are related to the deposition time and scan rate, and were optimized in Chapter 5.
Factors such as the concentration of GSH and Ab as well as the sulfo-NHS:EDC concentration and ratio were studied by a grid experiment where a series of concentrations were tested against each other to obtain the largest signal to noise ratio from the assay. Optimum GSH concentration was found to be 10 mM; 400 mM EDC: 100 mM sulfo-NHS: 10 μg/mL Ab ratio of 1:1:1 were the optimum concentration of the CTX antibody complex. As for Oc, similar concentration of GSH, sulfo-NHS and Ab concentration was used.
The incubation time is another important parameter affecting the analytical performance of the immunoassay. At room temperature, the

DPV response following the antibody complex immobilization increased with the increasing incubation time and then tended to constant values after 2.5 hrs. This showed the saturated binding both between the AuNPs and the antibody.
Similarly, in order to optimize the reaction time, the coupling procedure was repeated each time with a shorter reaction time until the signal change was too low to be detected. An identical procedure was repeated for a range of Ag concentrations in each case. The optimized reaction time, suggestive of saturated binding between the antibody and antigen, was 80s.
As discussed in Chapter 4, temperature had no significant effect on the Ab immobilization and Ag-Ab reaction processes. Thus, to simplify the process, all the steps were performed at room temperature and the optimized incubation time of 2.5 hrs, as calculated in the same chapter, was used.
The highest activity of both Oc and CTX sensors was observed at pH 4.5, in which all the used material (sulfo-NHS, EDC and GSH as well as the antibody) are reported to have the best functionality [27] [28].

6.5 Specificity, Cross-reactivity & Cross-talk

To investigate the specificity and cross-reactivity between analytes and Ab-functionalized surface, the interaction experiments were repeated with constant concentration of the opposite antigen along with PTH. The Oc sensor showed a minimum change from baseline value (<3%) with respects to CTX (100 ng/mL) and PTH (100 ng/mL) as interferents, indicating that the sensor did not interact with CTX or PTH to an appreciable degree over a wide concentration range, which can be attributed to efficient blocking of nonspecific binding sites on gold.(Figure 7.9)

As expected, the CTX immunosensor showed obvious responses only toward its corresponding antigens. Apparently, the cross-reactivity at the array was again negligible (a minimum change of <3% from baseline value). (Figure 7.9)

An excellent immunosensor array must exclude cross talk, which generally results from the diffusion of electroactive indicator produced on one electrode to neighboring electrodes. In this work, as the Ab complex was immobilized on AuNPs, the Ab-antigen reaction would only accumulate on the AuNPs, resulting in a localized stripping reaction at the individual electrode. Hence, the possible cross talk could be well avoided.

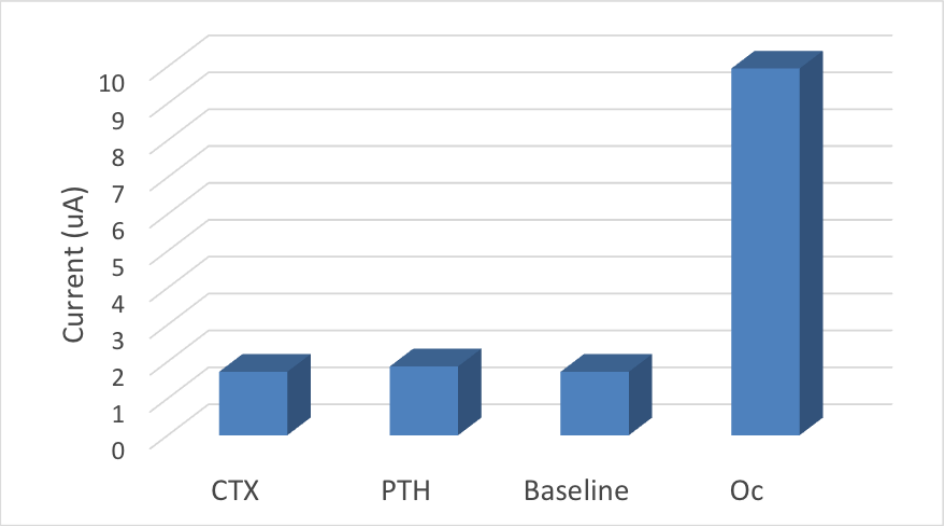

(a)

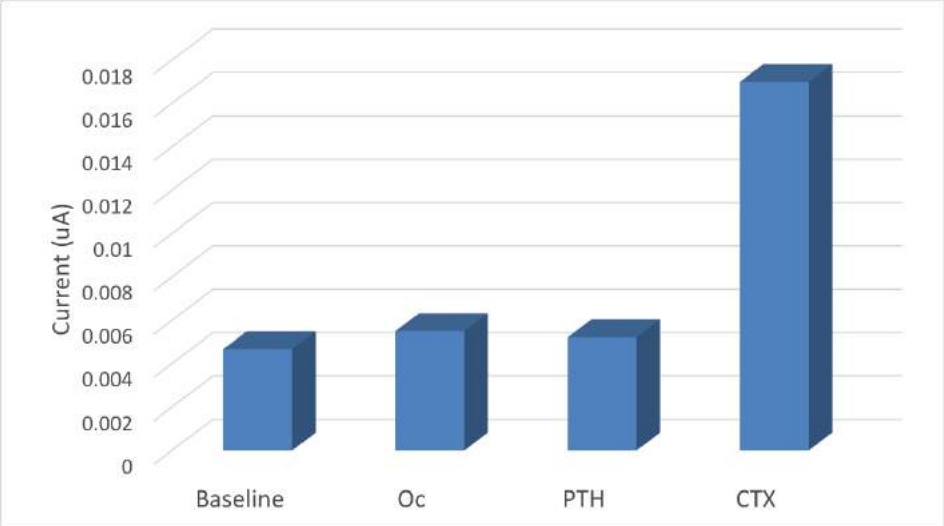

(b)

Figure 6.17: a) Electrochemical response measured for CTX (100 ng/mL), PTH (100 ng/mL) and Oc (100 ng/mL), b) Response measured for CTX sensor incubated with Oc (100 pg/mL), PTH (100 pg/mL) and CTX (100 pg/mL).

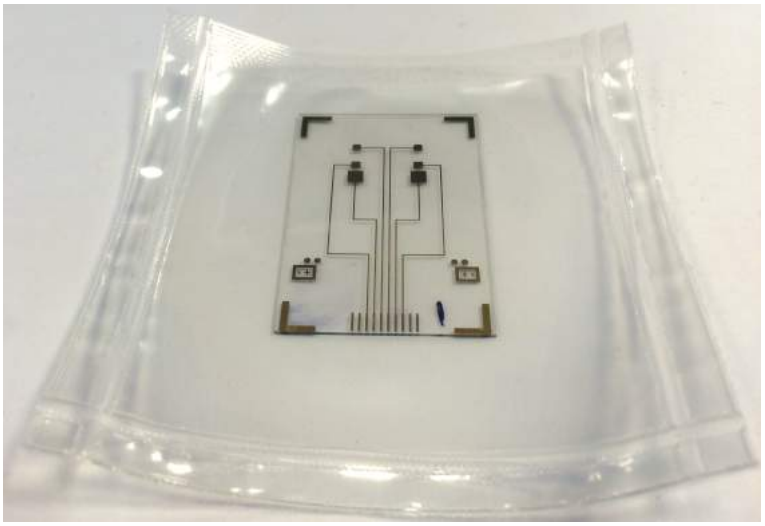

Figure 6.18: Vacuum packed electrode.

6.6 Reproducibility and Stability

The as-prepared immunosensor array could be stored in dry conditions at 4 °C. In this way, over 90% of the initial responses remained for a week of storage. In order to improve the stability, the immunosensors were vacuum packed and kept at room temperature or at 4 °C. The results revealed that the immunosensors lost more than 80% of their response after two weeks of storage, suggesting that vacuum packing alone was not effective in protecting the immunosensor over time. It seems that apart from oxygen, humidity and light can also speed up the degradation process of the modified electrodes.
The interassay precision of the immunosensor was examined based on repeated measurements of two different concentrations of CTX with five immunosensors. The coefficient of variation was 4.1%, indicating that the immunosensor has acceptable stability and reproducibility.

6.7 Conclusion

In this chapter, electrochemical detection method was applied in two different biosensor chips to detect serum levels of CTX and Oc. AuNPs were electrodeposited on gold electrodes to improve the surface area, provide better electron-transfer kinetics, and higher back-

ground charging current. On the AuNP-modified gold electrode, CTX and Oc antibodies were covalently immobilized by crosslinkers and different concentrations of the corresponding antigens were applied for direct determination.
Due to the excellent electrical properties of the as-prepared immunosensor, Oc sensor could detect serum levels of the marker within the range of 2.5-75 ng/mL. Again, the reference value of Oc for adults of both gender is 9-42 ng/mL, suggesting that the sensor can acceptably detect Oc.
Similarly, CTX levels were successfully measured from 1 pg/mL to 1000 pg/mL. This is while the reference value of the marker is as following:

- Males:
  - <18 years: not established
  - 18 - 30 years: 155 - 873 pg/mL
  - 31 - 50 years: 93 - 630 pg/mL
  - 51 - 70 years: 35 - 836 pg/mL
  - >70 years: not established
- Females:
  - <18 years: not established
  - Premenopausal: 25 - 573 pg/mL
  - Postmenopausal: 104 - 1,008 pg/mL

This suggests that the sensor can acceptably detect CTX.
Compared to conventional methods, the proposed electrochemical sensors resulted in selective and sensitive measurement of each of the BTM markers with reduced interference reactions, reduced measurement time, need for less amount of reagent and better stability in a simplified detection system.
The total assay time for these sensors is about 5 min (loading of antigen, incubation time, flushing with PBS and testing). The good correlation between ECLIA and these sensors showed the chips can be used in the clinically relevant range. Moreover, the fact that the initial calibration curve was plotted using pure antigen and the serum tested in the last step also contained other macromolecules suggests the sensor is specific for the antigen and macromolecules present in serum do not affect the results. However, the fact that the Oc Ag used to develop our calibration curve was a full-length protein, while ECLIA was designed to measure N-mid Oc may have affected our results.

References

[1] T. R. Holford, F. Davis, and S. P. Higson, "Recent trends in antibody based sensors," *Biosens Bioelectron*, vol. 34, no. 1, pp. 12 – 24, 2012.

[2] K. Omidfar, F. Khorsand, and M. Darziani Azizi, "New analytical applications of gold nanoparticles as label in ab based sensors," *Biosens Bioelectron*, vol. 43, pp. 336–347, 2013.

[3] E. Katchalski-Katzir, D. Kraemer, and C. Eupergit, "A carrier for immobilization of enzymes of industrial potential," *J Mol Catalysis B: Enzymatic*, vol. 10, pp. 157–176, 2000.

[4] F. Rusmini, Z. Zhong, and J. Feijen, "Protein immobilization strategies for protein biochips," *Biomacromolecules*, vol. 8, p. 1775, 2007.

[5] W. Vastarella, L. Della Seta, A. Masci, J. Maly, M. De Leo, L. Maria Moretto, and R. PIlloton, "Biosensors based on gold nanoelectrode ensembles and screenprinted electrodes," *Int J Environ An Ch*, vol. 87, no. 10-11, pp. 701–714, 2007.

[6] J. La Belle, A. Fairchild, U. Demirok, and A. Verma, "Method for fabrication and verification of conjugated nanoparticle-ab tuning elements for multiplexed electrochemical biosensors," *Methods*, vol. 61, no. 1, pp. 39–51, 2013.

[7] J. Brown, P. D. Delmas, L. Malaval, C. Edouard, M. C. Chapuy, and P. J. Meunier, "Serum bone gla-protein: a specific marker for bone formation in postmenopausal osteoporosis," *Lancet*, vol. 1, pp. 1091–1093, 1984.

[8] K. Nimptsch, S. Hailer, S. Rohrmann, K. Gedrich, G. Wolfram, and J. Linseisen, "Determinants and correlates of serum undercarboxylated osteocalcin," *Ann Nutr Metab.*, vol. 51, no. 6, pp. 563–570, 2007.

[9] S. Atalay, A. Elci, H. Kayadibi, C. Onder, and N. Aka, "Diagnostic utility of osteocalcin, undercarboxylated osteocalcin, and alkaline phosphatase for osteoporosis in premenopausal and postmenopausal women," *Ann Lab Med*, vol. 32, no. 1, pp. 23–30, 2012.

[10] P. Khashayar, H. Aghaei Meybodi, G. Amoabediny, and B. Larijani, "Biochemical markers of bone turnover and their role in osteoporosis diagnosis: A narrative review," *Recent Pat Endocr Metab Immune Drug Discov.*, vol. 9, no. 2, pp. 79–89, 2015.

[11] V. Jagtap, J. Ganu, and N. Nagane, "Bmd and serum intact osteocalcin in postmenopausal osteoporosis women," *Indian J Clin Biochem*, vol. 26, no. 1, pp. 70–73, 2011.

[12] E. Chow, D. Hibberta, and J. Gooding, "Voltammetric detection of cadmium ions at glutathione-modified gold electrodes," *Analyst*, vol. 130, pp. 831–837, 2005.

[13] M. Swartz and I. Krull, *Handbook of Analytical Validation*. CRC Press, Taylor and Francis Group, Boca Raton., 2012.

[14] G. L. Long and J. D. Winefordner, "Linearization of electron capture detector response to strongly responding compounds," *Anal Chem*, vol. 55, no. 7, pp. 713A–724A, 1983.

[15] J. Bartlett and C. Frost, "Reliability, repeatability and reproducibility: analysis of measurement errors in continuous variables," *Ultrasound Obstet Gynecol*, vol. 31, pp. 466–475, 2008.

[16] M. Mayer, J. yang, I. Gitlin, D. H. Gracias, and G. M. Whitesides, "Micropatterned agarose gels for stamping arrays of proteins and gradients of proteins," *Proteomics*, vol. 4, pp. 2366–2376, 2004.

[17] A. Bernard, E. Delamarche, H. Schmid, B. Michel, H. Bosshard, and H. Biebuyck, "Printing patterns of proteins," *Langmuir*, vol. 14, p. 2225, 1998.

[18] P. Garnero, "The contribution of collagen crosslinks to bone strength," *BoneKEy Reports*, vol. 1, p. 182, 2012.

[19] S. Vasikaran, R. Eastell, O. Bruyere, A. Foldes, P. Garnero, A. Griesmacher, M. McClung, H. A. Morris, S. Silverman, T. Trenti, D. Wahl, C. Cooper, J. Kanis, and for the IOF-IFCC Bone Marker Standards Working Group, "Markers of bone turnover for the prediction of fracture risk and monitoring of osteoporosis treatment: A need for international reference standards," *Osteoporos Int*, vol. 22, no. 391-420, 2011.

[20] S. Chubb, "Measurement of c-terminal telopeptide of type i collagen (ctx) in serum," *Clin Biochem*, vol. 45, no. 12, pp. 928–935, 2012.

[21] S. Baim and P. D. Miller, "Perspective: Assessing the clinical utility of serum ctx in postmenopausal osteoporosis and its use in predicting risk of osteonecrosis of the jaw," *J Bone Miner Res*, vol. 24, pp. 561–574, 2009.

[22] M. Bonde, P. Garnero, C. Fledelius, P. Qvist, P. Delmas, and C. Christiansen, "Measurement of bone degradation products in serum using antibodies reactive with an isomerized form of an 8 amino acid sequence of the c-telopeptide of type i collagen," *J Bone Miner Res*, vol. 12, no. 7, pp. 1028–1034, 1997.

[23] C. Rosenquist, C. Fledelius, S. Christgau, B. Pedersen, M. Bonde, P. Qvist, and C. Christiansen, "Serum crosslaps one step elisa. first application of monoclonal antibodies for measurement in serum of bone-related degradation products from c-terminal telopeptides of type i collagen," *Clin Chem*, vol. 44, no. 11, pp. 2281–2289, 1998.

[24] Y.-H. Yun, A. Bhattacharya, N. B. Watts, and M. J. Schulz, "A label-free electronic biosensor for detection of bone turnover markers," *Sensors (Basel)*, vol. 9, no. 10, pp. 7957–7969, 2009.

[25] M. Ramanathan, M. Patil, R. Epur, Y. Yun, V. Shanov, M. Schulz, W. R. Heineman, M. Datta, and P. Kumta, "Gold-coated carbon nanotube electrode arrays: Immunosensors for impedimetric detection of bone biomarkers," *Biosens Bioelectron*, 2016.

[26] A. Killard, B. Deasy, R. O'Kennedy, and M. Smyth, "Antibodies: production, functions and applications in biosensors," *Trends Analyt Chem*, vol. 14, no. 6, pp. 257–266, 1995.

[27] M. Fischer, "Amine coupling through edc/nhs: A practical approach," *Methods Mol Biol.*, vol. 627, pp. 55–73, 2010.

[28] M. Hormozi-Nezhada, E. Seyedhosseinia, and E. Robatjazia, "Spectrophotometric determination of glutathione and cysteine based on aggregation of colloidal gold nanoparticles," *Scientia Iranica*, vol. 19, no. 3, pp. 958–963, 2012.

7
Osteokit Fabrication

7.1 Introduction

Nowadays, considering the limited resources, the use of rapid, cheap, simple-to-operate, disposable, and accurate PoC diagnostics is of great importance and can have a critical impact on clinical decision-making. Although advanced diagnostic technologies, such as polymerase chain reaction (PCR) and ELISA are widely used, their application in developing countries is limited because of the limited availability of laboratory infrastructure, skilled personnel and financial supports [1].
As a result, microfluidic technologies have been widely employed in developing PoC diagnostics and to miniaturize immunoassays to address global health issues because of their potential advantages of low sample and reagent consumption, high throughput and sensitivity, large surface-to-volume ratio, and other benefits related to miniaturization [2]. However, as mentioned in Chapter 3 most microfluidic devices require both complex fabrication processes and external instruments [3]. Several aspects need to be considered while designing a microfluidic device, such as selection of materials, dimensions of the microfluidics devices and fluidic control devices (such as pumps, valves, and mixers).
Some of the materials used for fabrication of microfluidic devices for PoC diagnostics include paper (nitrocellulose or cellulose), glass, sili-

con, plastics (cyclic olefincopolymers or polystyrene), and polycarbonate. Currently, polymers such as PDMS and thermoplastics are most frequently applied to facilitate the translation of microscale systems from simple laboratory tools to commercially marketable products [4]. The latter are more favorable as they allow for the production of dimensionally stable and mechanically robust components while the feature fidelity and integrity are easier to maintain during replication processes [5]. Among thermoplastics, cyclic olefin copolymer (COC), poly (methyl methacrylate) (PMMA), polystyrene, and polycarbonate are frequently used for fabricating microfluidic systems.

Despite the above mentioned advantages, the fabrication of microfluidic channels using these materials requires costly and laboratory intensive cleaning, photolithography, and etching or baking steps in clean room environments. Thus, design iterations to modify the device is labor and resource-intensive [6]. Besides, proper channel enclosure without deforming small features or without clogging of the channel during the bonding process is challenging [7] [8]. Nowadays, the key step to the final integration includes plasma or UV/ozone treatment, thermal fusion, microwave welding, adhesives, surface modification or solvent bonding, which apart from being costly and time-consuming, does not always provide acceptable results [9] [10] [11].

Hot embossing and thermal bonding are currently the methods of choice for fabricating and sealing microfluidic channels in thermoplastic materials [12].These methods allow a relatively fast and easy fabrication of microfluidic devices but they generally need expensive equipment and a cleanroom environment [13].The temperature and pressure applied during these steps also limit the variability of the materials used.

Hot embossing is a popular method for fabricating microfluidic channels in thermoplastic materials. The fabrication process typically starts with a PDMS or epoxy-based master mold, which is made using well-established photolithographic processes [14]. Shrinkage of this master mold and subsequent misalignment are quite common with large, centimeter-order devices [15]. The quality of microfluidic channels during the replication process is also of great importance. During thermal fusion, the polymer is heated to or slightly above its glass transition temperature (Tg), and thus becomes soft and sensitive to heterogeneities in load distribution during the bonding process.

In this chapter we report the design and fabrication of a sensitive multiplexed microfluidic proteomic platform integrated with electrochemical sensing that can easily be translated into a protein biomarker diagnostic. To our knowledge this is the first such device designed as a step toward developing a PoC system for the measurement of several

BTMs.

7.2 System Design and Fabrication

7.2.1 Design and Fabrication of sensor chip

The electrochemical chip was the glass-based gold electrode fabricated in Chapter 5. In brief, it consisted of 6 gold electrodes arranged in a 2 by 3 electrode arrays on a glass. The glass was 25.5*85.5 mm^2, leaving a 25.5*10 mm^2 uncovered area, after assembly of the tape and the COC substrate, for the contact pads to be connected to the read-out circuit using a custom-made PCB. Each gold working electrode (1.5*1.5 mm^2) was placed between one gold pseudo- reference (1.4*1.4 mm^2) and one gold counter electrode (2.5*2.5 mm^2), as depicted in Figure 7.1.

7.2.2 Design and Fabrication of microfluidic manifold

In order to develop a fully operational electrochemical diagnostic prototype, the microfluidic platform consisted of the microchannels and a chamber necessary to expose electrodes in the electrochemical sensor chip to the sample, surface modification solution, and detection probe. All delivered samples and reagents were routed to the waste outlets.
For the fabrication of the microfluidic channel layer, the design of the microfluidic channels was first drawn in a computer-aided design and drafting software (Autodesk, USA). The design was then used to fabricate epoxy molds. Figure 7.2 illustrates the process used to fabricate epoxy (FR-1080)[1] mold from PDMS (Sylgard 184) stamps. The PDMS stamps were themselves fabricated using soft lithography using SU-8 on a silicon wafer, which was itself structured using photolithography. The use of these molds has several advantages. De-molding process after embossing is straight forward without any special mold designs. Moreover, complex structures and topographical features at nano-scale, which cannot be accomplished with a metal mold, can be replicated with such molds [16].

The microstructured epoxy mold was brought into contact with a COC slide placed on a standard 4" * 4" glass slide. A lamination stack consisting of thick metal plates (carrier or tooling plates), pressure distribution material (press pad), thin, polished metal plates (separator plates) and release foil were used to sandwich the epoxy mold and the

[1] This is the main type of epoxy that is generally used for hot embossing applications (up to 135-140 °C).

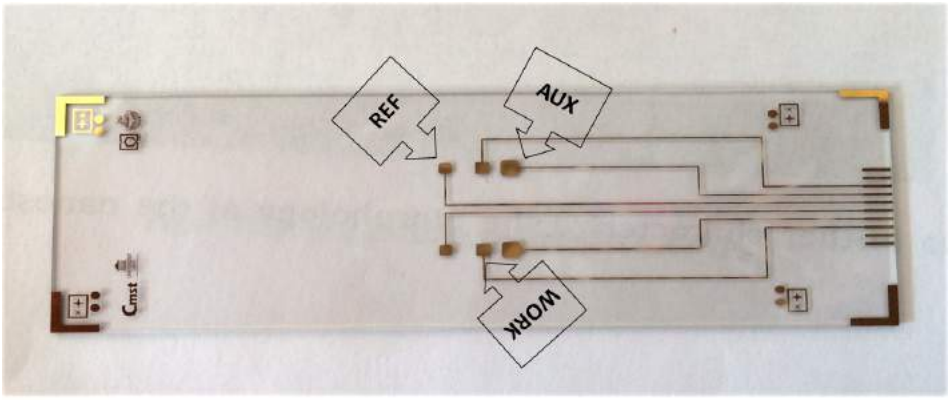

(a)

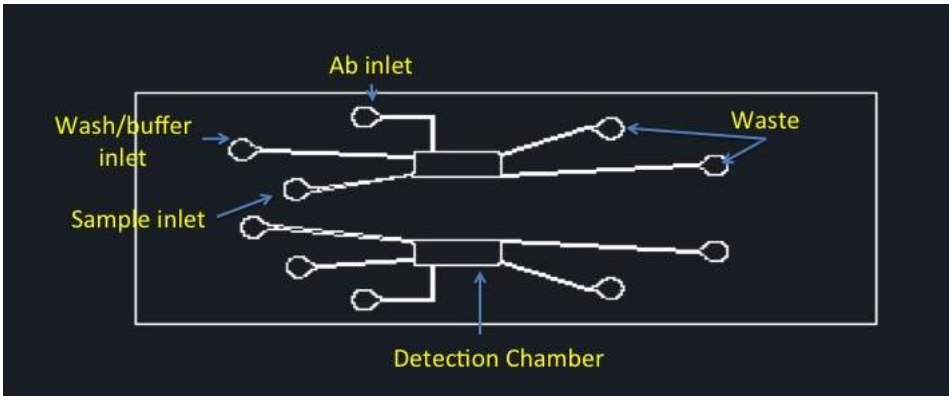

(b)

Figure 7.1: a) Schematics of the electrochemical sensor chip b) Structure of the microfluidic manifold.

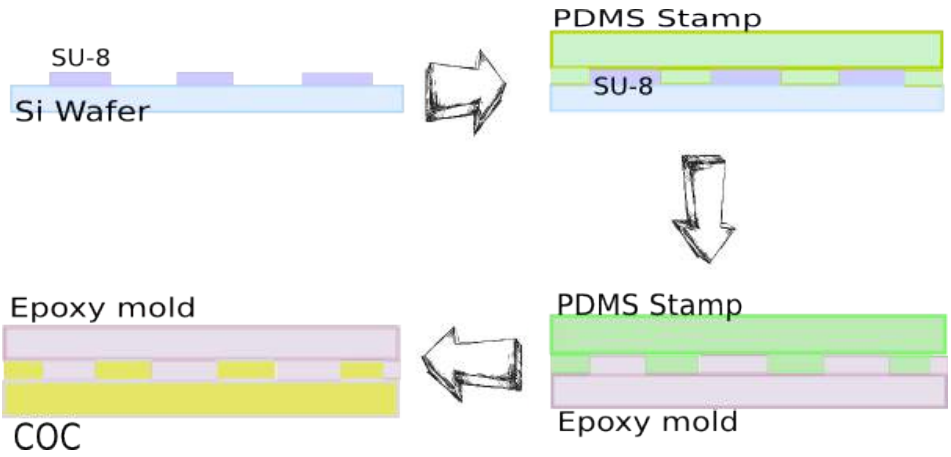

Figure 7.2: Fabrication process of epoxy molds.

COC slide. (Figure 7.3) The assembly was placed in Vacuum Laminating Press (Lauffer RLKV 25),for the hot embossing process applying a load of 3 kN for 5 min at 110 ° C. Vacuum conditions during the entire process prevent trapping of air pockets in the cavities. After solidification of the polymer, the stack was cooled down to room temperature in 6 minutes while maintaining a constant force. Then the assembly was unloaded and the epoxy mold was carefully peeled off from the embossed COC slide to avoid tearing or ripping of the epoxy mold.

As the next step, thermal bonding with Vacuum Laminating Press was used to enclose the open structure of the COC slide replica with a glass slide which also acted as the electrochemical chip (as mentioned in Chapter 6). In this regard, the stack was loaded into the press, and bonded at 3kN and 110 ° C for 10 min and then were cooled to room temperature under the same pressure, then unloaded. The process took 20 minutes. This process was associated with several limitations. (Figure 7.4)

- Some deformation was noted of the fabricated microstructure in the COC.
- The process was time-consuming and the stack assembly was heavy.

Therefore, the microfluidic channels were realized using a double-sided medical grade tape (3M) of 86 μm thickness, which was previously laser machined to generate microchannel structures. The CAD design was used to define the cutting path through the double-sided tape, using a laser beam. Therefore, any modification of the design

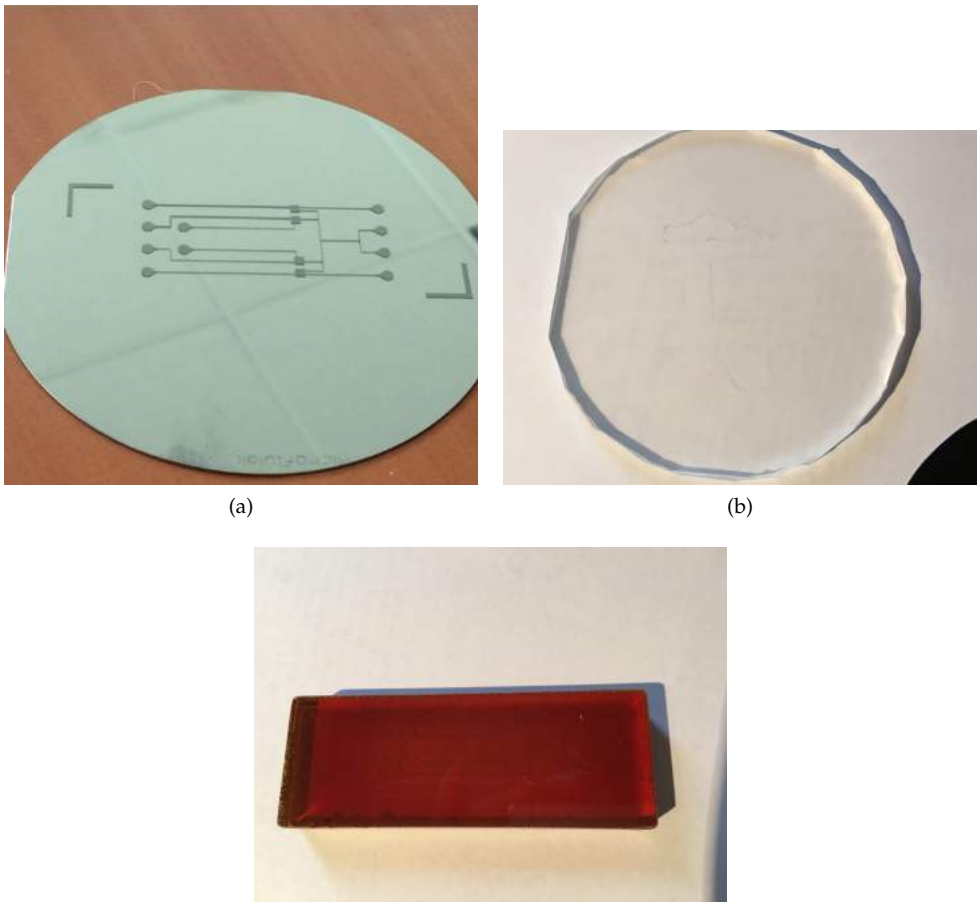

(a) (b)

(c)

Figure 7.3: a) Si Wafer used to fabricate the PDMS stamp. b) PDMS with negative copy of SU-8 master. c) Epoxy mold.

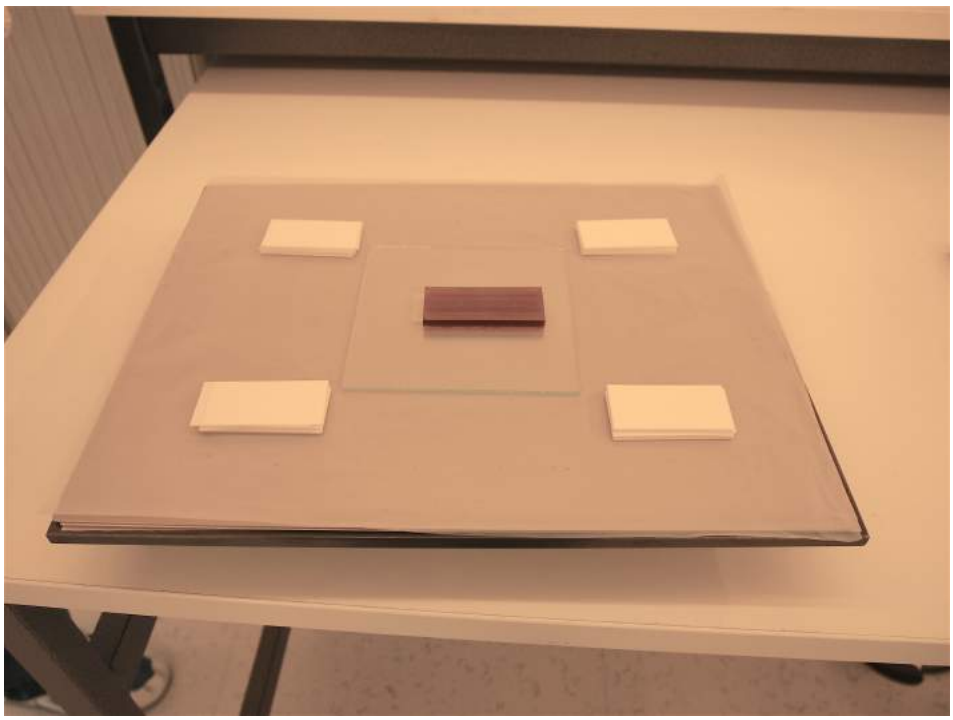

(a)

(b)

Figure 7.4: a) Lamination stack (partially shown). b) Deformed COC after the embossing process.

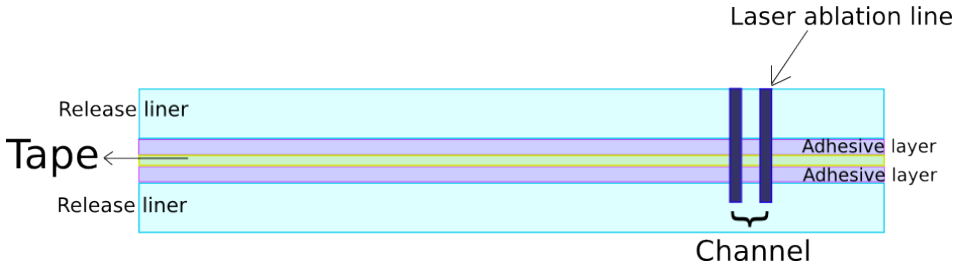

Figure 7.5: Tape was partially cut using laser ablation to facilitate the handling, aligning and assembling process.

is straightforward and easy to implement. Here, a focused 9.6-μm wavelength CO2 laser beam was used to partially cut through the tape at predefined locations to ease handling, aligning and assembling in general. Figure 7.5 shows the cross-section of a partially cut tape. It should be noted that the laser beam spot has a certain diameter (approximately 100 μm), which we compensated for in the CAD design. The patterned tape was then used to integrate the microfluidic manifold, i.e. the COC slide, with the glass sensor chip and aligned using a manual mask aligner (SET MG1410). Using this technique, patterning of COC was not required anymore.

An exploded-view drawing of the three-layer microfluidic manifold with the sensor chip is presented in Figure 7.6. In this regard, the sensor chip (gold electrodes on the glass) acted as the bottom layer. The middle layer (tape) defined the capture/reaction chamber and channels. The topmost layer in the chip serves as the covering for the channels. COC was used as this layer as drilling the I/O holes was much easier in it compared with glass. This layer is a rectangular piece of COC (COC, Topas 8007) (25.5 mm by 75.5 mm, 1 mm thickness) drilled with 1 mm diameter holes that serve as the reservoirs to introduce the sample and buffer solutions as well as to collect the waste. The fluid flows in the microfluidic channels and reaction occurs in the reaction cells where the fluid is exposed to the electrodes on the bottom layer. Figure 7.7 explicitly shows the cross-sectional view of each layer in the chip.

The channels had a width of 200 μm; this is a safe value considering that our studies have shown that 100-μm-channels are wide enough for serum/blood samples to pass through without clogging or sedimentation. The capture/reaction chamber had a width and length of 2.9 mm and 8.9 mm. The height of the channels and chambers were equal to the thickness of the tape (86 μm). Transparency of the injected

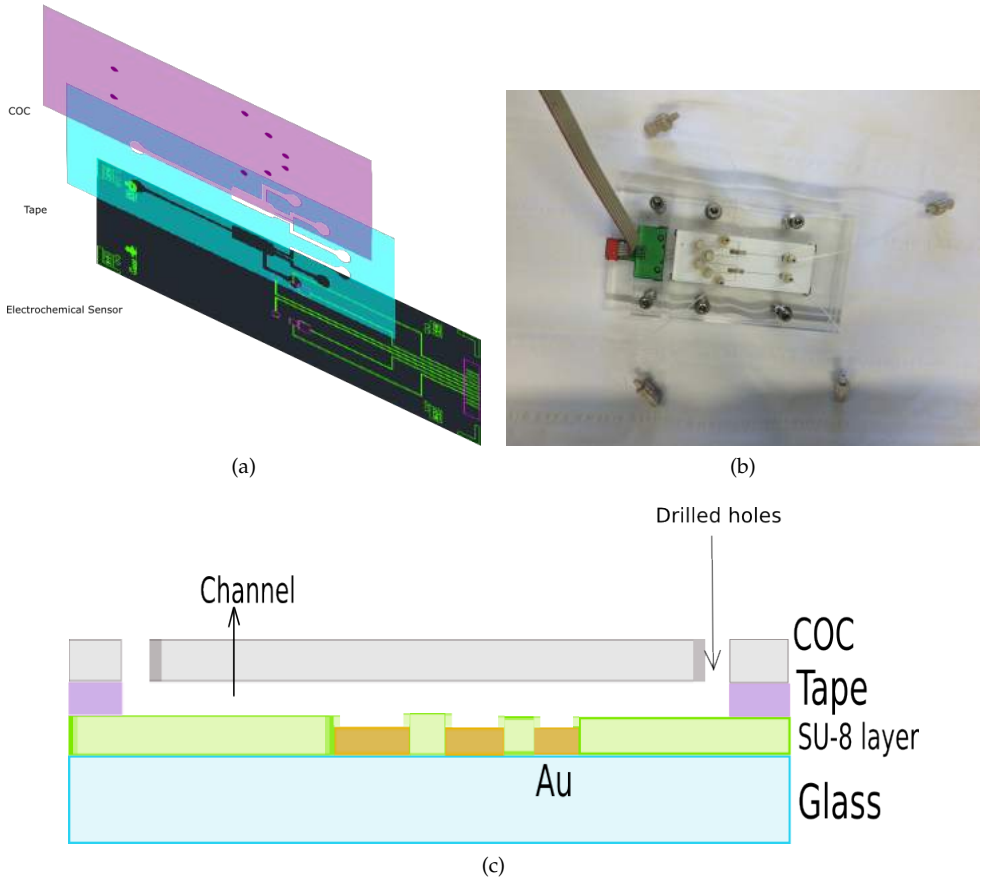

Figure 7.6: Diagram of the microsystem device a) CAD design of each layer, b) Microfluidic device positioned in between 2 PMMA plates, acting as microfluidic chip holder, c) Cross-section of the microfluidic device.

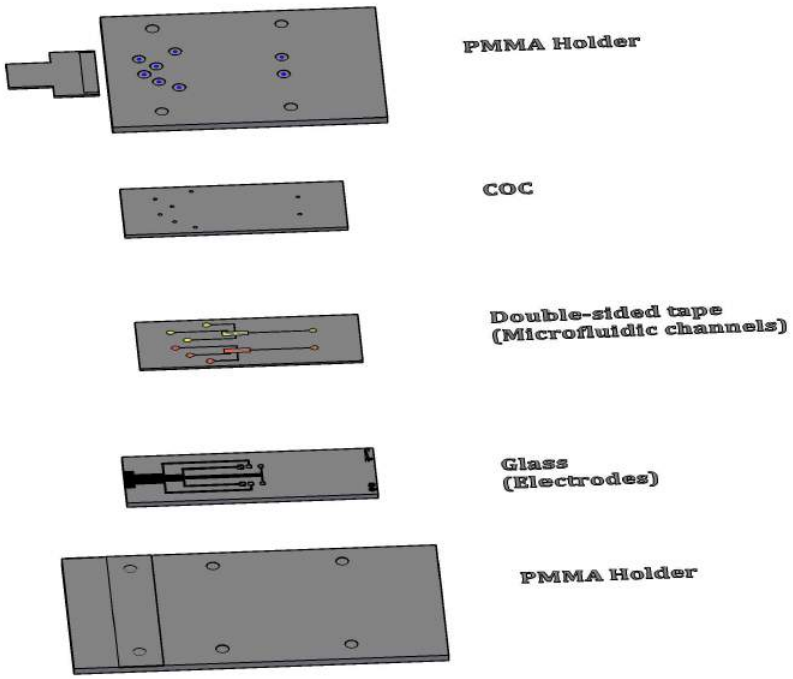

Figure 7.7: Schematic illustration of the build-up of the multilayer microfluidic device and the microfluidic chip holder.

fluids hindered the observation of fluid flow; therefore a blue dye was used to characterize fluid flow profiles in the capture/reaction chamber and channels.
In this approach, each layer is processed as if it was an independent substrate. These are then aligned and bonded to the other layers.

7.2.3 Design and Fabrication of Holder

In order to interface the microfluidic chip with external fluidic and electrical connections, a custom-made holder was designed and fabricated in-house by micro-milling in a 1 mm PMMA sheet and cut out in the dimensions of 65*126 mm^2. The docking station, used to house the chip, functioned as a base with female ports fully integrated into the device to reduce cost and improve reproducibility and reliability of the results [17].
The top PMMA plate includes circular, drilled holes of 1 mm diameter (centered relative to the I/Os) that fit with the corresponding connection ports in the COC. The ports for incorporating fluidic connectors, purchased from LabSmith, were glued to these PMMA holes. These interconnects were chosen because of their small footprint that allowed a high density of fluidic I/O ports and minimal dead volume.
A circular notch of approximately 0.3 mm depth was designed on the inner surface of this plate to place the Viton O-rings (2 mm inner diameter, 4 mm outer diameter, 1 mm thickness), again centered relative to the inlets/outlets. The O-rings were used to provide a leak-free interface between the holder and the inlet and outlets on the COC. Tygon tubing was used to introduce the fluids from a 1 mL Luer-Lok tip, insulin syringe (BD, Franklin Lakes, US). The lower half of the holder is completely featureless. The two sides were tightened together with screws after the assembled device was put in between and aligned by eye.

7.2.4 Assembling and sealing

In order to minimize surface contamination, parts were blown off with high-pressure nitrogen before the assembling step. The assembly of the layers started with removing one of the release liners and bonding the micro-patterned adhesive tape to the COC substrate. A roller was used to avoid the entrapment of air at the interface. Thereafter, the other release liner was removed, and the micro-positioning table and the microscope of a mask aligner system were used to align the COC / tape stack with the glass substrate before bringing them into contact and creating a tight bond. It should be noted that considering

the design, the second part can also be performed manually. This process of stacking - layer, tape, layer, tape - can be repeated as needed to complete the microfluidic device. For the final bonding, the entire assembly was pressed together manually. The microfluidic device was then placed in the custom-made microfluidic chip holder. (Figure 7.6)

7.3 Microfluidic Characteristics

The improvement of detection sensitivity and analysis time has been a key motivation for the development of analytical microsystems [18][19]. Size reduction lowers the consumed reagent and sample volume and also results in portability. It however may compromise the detection limit of the device, especially for low flow rates [20]. This is while the maximum allowed pressure for reliable operation and integrity of the microfluidic device limits the flow rate itself [21]. Therefore, the parameters that contribute to the sensitivity and specificity of the measurements in such devices are as following:

- Successful and functional immobilization of the antibodies on sensor surfaces to perform reagentless detection
- Amplifying reaction signals
- Flawless flow of the solutions in the microchannels during preparation steps and electrochemical process
- Absence of cross talk due to the diffusion of electroactive products from one electrode to a neighboring one causing interference.

7.3.1 Channel Characterization

The dimensions of the resulting microfluidic channels along with the characteristics of the material used to make the microfluidic channels can affect the fluid flow.

Channel Dimension

The narrowest channel, which could be fabricated using the laser-cutting technique, has a width of around 100 μm, because of the laser's beam spot. Therefore the technology is not applicable everywhere, but it offers a cost-effective, simple and accurate solution for several applications.
Figure 7.8 presents the difference in the width of the microfluidic channels seen from the front side and backside of the tape before bonding. The trapezoidal shape of the cross section is typical for microfluidic

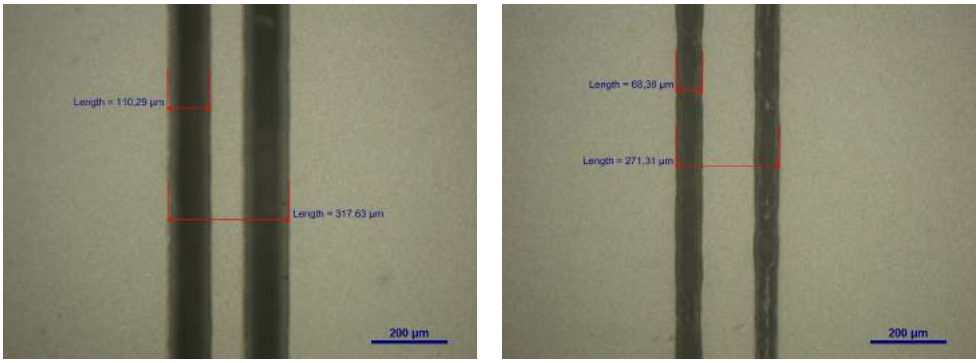

(a) (b)

Figure 7.8: Optical microscope images of the width of a 100 μm wide microchannel before bonding seen from the (a) back and (b) front side of the tape, showing the trapezoidal shape of the microfluidic channels. The dark lines represent the ablated tape.

channels fabricated using laser-cutting and is due to the laser-cutting and can be contributed to the focal plane of the laser beam.(Figure 7.9) Due to the trapezoidal cross-section, the width of the microfluidic channels varied from to 110 ± 5 μm at the top to 65 ± 5 μm at the base of the microfluidic channels.

In order to quantify the uniformity of the cross-sectional geometry of the microfluidic channels along their length, a microfluidic channel was diced along its length at 5 mm intervals and assessed with an optical microscope (Nikon Eclipse LV100) and non-contact optical profiler (WYKO NT3300) to assess its width and height, respectively.[2] (Figure 7.10) The low relative standard deviations confirm the uniformity of the channel dimensions.

Channel Structure

The typical permeability of COC for oxygen is much less than the value observed for other materials popular for the preparation of microfluidic chips [22]. This material property is of great importance as the presence of oxygen in the channel would disturb the reactions and measurements in different ways.

As mentioned earlier, the material used to fabricate michrochannels

[2] As dicing the Glass - Tape - COC at 5 mm intervals was troublesome, COC - Tape - COC was used instead.

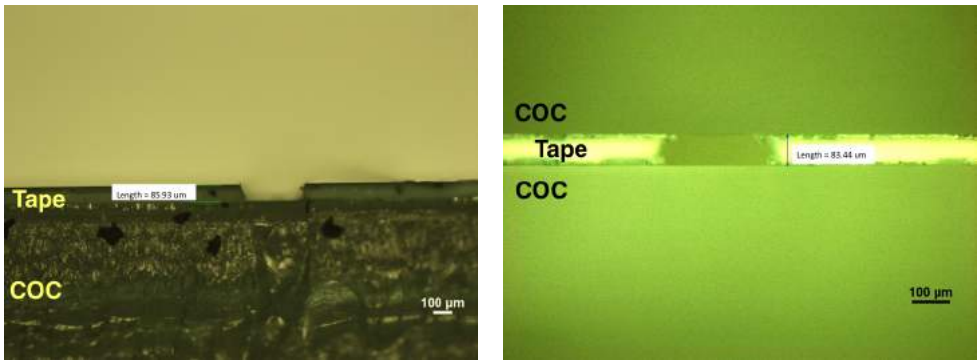

(a) (b)

Figure 7.9: Optical microscope images of the cross-section of a microfluidic channel, showing its height before (COC-Tape) and after bonding (COC-Tape-COC).

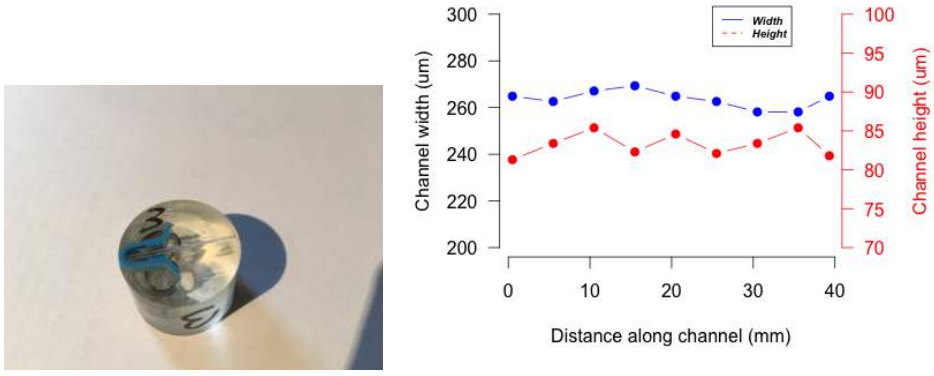

(a) (b)

Figure 7.10: a) Cross-section of the chip, prepared by dicing along the length of the microfluidic channel at 5 mm intervals, b) Channel height and width at 5 mm intervals along the length of a 250μm wide microfluidic channel, measured using an optical microscope and non-contact optical profiler.

should provide proper channel enclosure without deforming small features or clogging the channel during the bonding process [7][8]. To overcome these concerns we used double-sided tape both as glue to bond layers and as channel structure.
One of the main purposes for the fabrication of microfluidic devices with feature size in the micrometer range is to reduce the quantity of the needed sample. In this regard, non-specific adsorption of proteins to channel walls and cross talk to other channels should be prohibited as it may cause unpredictable reduction in the concentration of the assay component and slow its transport rate. As a result, controlled protein adsorption characteristics of the material used in the microchannel structure is of great importance.

Controlled protein adsorption In order to assess the protein adsorption rate in microchannels, the auto fluorescence of different COCs/Cyclic Olefin Polymers (COP), the double-sided tape and polymers to be used as the insulation layer on the immunoelectrode were measured (Chapter 5).
The above mentioned materials were immersed in a 2 mg/mL solution of FITC-Albumin in 0.05 M phosphate buffer (pH 7.0) for 2 hrs and subsequently rinsed with DI water [23]. Thereafter the amount of their protein adsorption capacity was determined by measuring fluorescence (λ_{excit}=495 nm, λ_{emis}=520 nm) in the labeled materials using a fluorescence spectrometer. As it can be seen in Figure 7.11, biocompatible polyimide (PI) was the only material which seemed to adsorb the labeled albumin and thus biocompatible SU-8 was used as the insulation layer instead. The tape, on the other hand, seemed to adsorb negligible amounts of labeled albumin. It was concluded that cross talk is not an issue as the tape and other materials used in the Osteokit had negligible protein adsorption capacity.

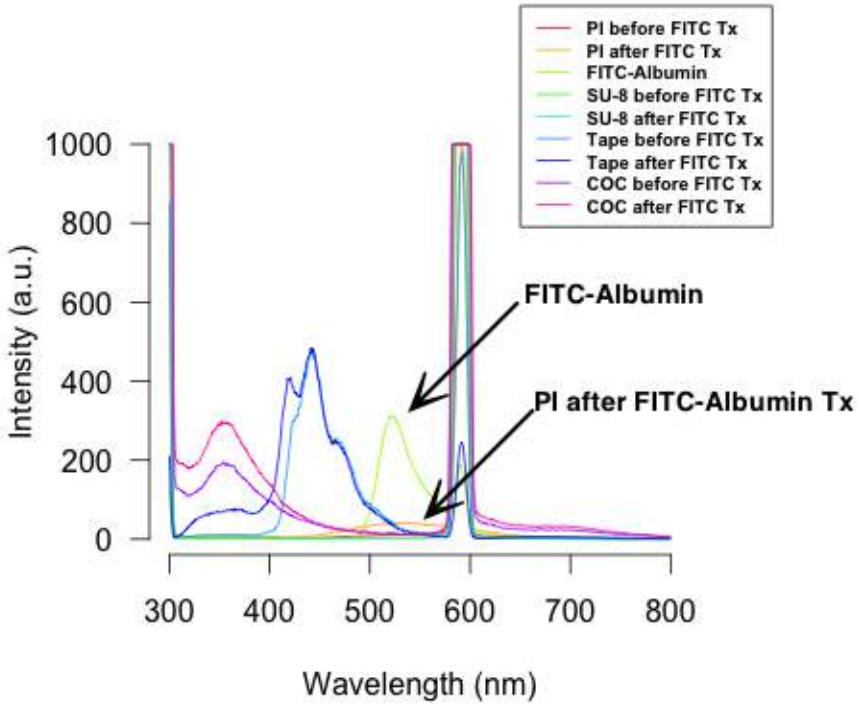

Tx = Treatment

Figure 7.11: Fluorescence emission ratio of different materials to be used in channel fabrication before and after treatment with FITC.

Capture/Reaction Chamber characterization

In general, the detection system in the PoC microfluidic immunoassay devices must have high sensitivity and short response time [24]. There are several parameters that contribute to the sensitivity of the capture/reaction step. These parameters include the area of the electrode surface, flow rate of sample and wash into the capture/reaction chamber, and surface modification step.
Non-optical detection, especially the electrochemical techniques are important for the microfluidic immunoassay as they are highly sensitive, rapid and can be easily integrated by micromachining technology [25]. However, the major disadvantage of this method is the background noise. As mentioned earlier, AuNPs were used for electrode modification because of their excellent acceleration of electron transfer and thus signal amplification and low background noise. It was therefore concluded that AuNPs on the electrodes acted as a powerful multifunctional layer that improved in situ immobilization of antibodies on the electrodes, amplified the measured signals and improved the sensitivity of this electrochemical sensor.
With these parameters in mind, we fabricated a 2.9 * 8.9 mm^2 capture/reaction chamber that was 86μm deep (volume= 2.2 mm^3) to maximize the number of interactions between the agents needed to functionalize the surface as well as target analytes and the functionalized surface.
The special design of the channels along with the application of the chronoamperometry technique to reduce the measurement time and the electrolysis risk also helped overcome the bubble formation concern. It should be noted that in the liquid environment, bubbles are easily generated by electrolysis, and influence the result.

7.3.2 Flow Characterization

For characterizing the fluid flow in the capture/reaction chamber, a colored dye was utilized to visualize the flow of the fluids entering and exiting the capture/reaction chamber. Injecting a colored dye demonstrated the capability of the device to move fluids both through the channels and across different layers over the detection zones. According to our design, the fluid is distributed from an open inlet on the top COC substrate of the device into a single channel, which is connected to an open outlet on the same layer. During this path, it passes over the detection zone, which is located on the bottom glass substrate. If various ports are open, the injected sample can be distributed through different channels to the outlets. This ability to redirect the sample into

multiple detection zones makes it possible to use the microfluidic device for simultaneous measurement of multiple markers in a sample. No leakage was noticed in between adjacent channels.
Transporting liquids from the inlet to the reaction chamber and to the outlet is a key step in the microfluidic immunoassay device. In this project, the fluidic control of the analyte in and out of this chamber was achieved through capillary motion and pressure-driven flow, generated by a syringe pump. The flow behavior mainly depends on the inlet flow rate and thus we tried to introduce liquid into the system with a constant volumetric flow rate. Flow rates higher than 3500 μL/min were observed to be associated with gas bubble introduction into the channels and so were avoided.
Moreover, a wash step was performed at the beginning to ensure the transfer of remaining air in the interconnects, channels and chambers to the outlet. This is because when hydraulic pressure is applied, gas bubbles remaining in the interconnection holes can be trapped in the reaction region during the detection process and cause significant problems by disturbing fluid flow or drying electrodes-on-chip [26].
Liquid movement is also controlled by different fluidic resistance within the parallel channel network. During the experiment, most of the pressurized solution flows into the reaction chamber because the fluidic resistance of other channels, which are filled with air at this point, is higher than that of the reaction chamber. The adopted design was also accountable for reduced back flow and improved flow of the solutions without dead volume formation. This was achieved by computational fluid dynamic (CFD) simulation and testing different designs in the lab.

7.3.3 CFD

All numerical computation presented in this work were performed using COMSOL Multiphysics (Finite Element Method) and Fluent (Finite Difference Method). Simulation was performed for a two-dimensional, incompressible Navier-Stokes flow. A no-slip condition was assumed along the walls of the microchannel and physical values of water (dynamic viscosity: 1.002e-3 cP; density: 1000 kg/m^3) were used in the numerical computation. The effect of the position of the inlet and outlet microchannels and the geometry of the recognition chamber on the flow profile were investigated.
The tests were performed in two states:

- Steady state, where the injection time is estimated to be infinite. This profile studies the velocity and pressure at different points of the microchannel. Both outlets are considered open all through

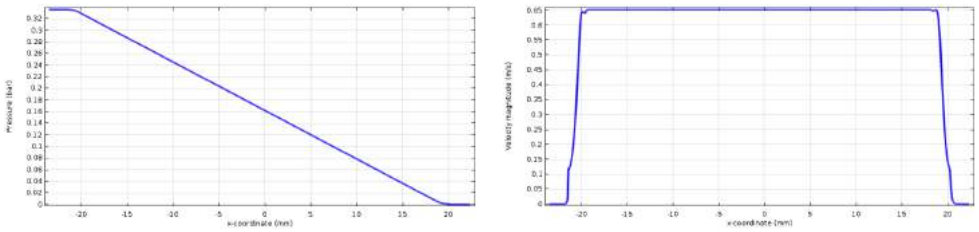

(a) (b)

Figure 7.12: a) Pressure, and b) Velocity change through single microchannel.

the experiments, whereas only one of the inlets is open in each set of tests. As a result, the pressure at the outlet is equal to one atmosphere.

- Transient state, which aims to study the flow profile in the system. In this simulation, the channels are considered to be filled with air before the first injection. A constant flow rate (400 μL/min) is applied to the inlet, pushing the air out of the outlet.

In order to validate the software setup, a single-channel system was used. The pressure drop in the channel is shown in Figure 7.12. As it could be seen, the pressure at the beginning and end of the microchannel are constant and the pressure drop through the channel follows a linear drop. This could be explained by the small size of the fully developed length.

The velocity change through the channel is shown in Figure 7.12. In the inlet, the velocity was minimum and the pressure was maximum. The considerable velocity increase at the beginning of the channel is due to the mass conservation law and the fact that the fluid enters a small channel with a smaller surface area compared to the inlet. Thereafter the velocity remains constant until it reaches the outlet, where a considerable decrease is noted.

When studying the velocity in the microchannel's cross-section, in view of the no-slip condition, the velocity along the walls was observed to be zero and the maximum velocity was reported in the center of the microchannel.(Figure 7.13) The maximum shear stress, on the other hand, was noted on the walls and the minimum in the center of the channel.

The multi-channel network setup was drawn in Gambit software and studied using Fluent. The design was modified in a way that the microchannels and the chamber would be filled completely, the backflow to other inlets is reduced and no dead volume is noted.

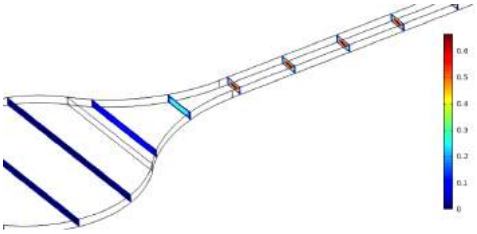

Figure 7.13: Velocity contours in the channel's cross-section.

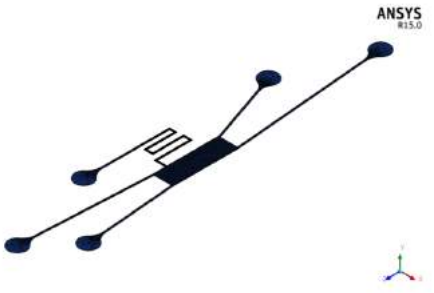

Figure 7.14: Final design of the microfluidic system.

As mentioned earlier, maximum pressure was noted in the inlet. A considerable pressure drop was observed when the fluid entered the chamber, where the pressure became equal to that of the closed inlets. As the outlet pressure was one atmosphere and the pressure in the chamber was higher than the atmosphere pressure, the fluid was guided through the outlet with a negligible back-flow.
It should be noted that in the course of the simulation, dead volumes were identified in the square chamber along with the inlets and outlets, suggesting that the immobilization and washing of the electrodes would not be effective. Based on these observations, a design modification was incorporated, where an additional outlet was added and the angels of the inlets and outlets were changed so that the dead volume was eliminated, the backflow in other inlets was negligible and the fluid flow trajectory, the velocity field and pressure were evenly distributed across the chamber. (Figure 7.14)

Figure 7.15 represents the fluid flow trajectories in the final optimized design. The results showed that the chamber was completely filled after the first second, and thereafter the volume fraction of the fluid remained constant. The system was completely filled after a longer injection time.

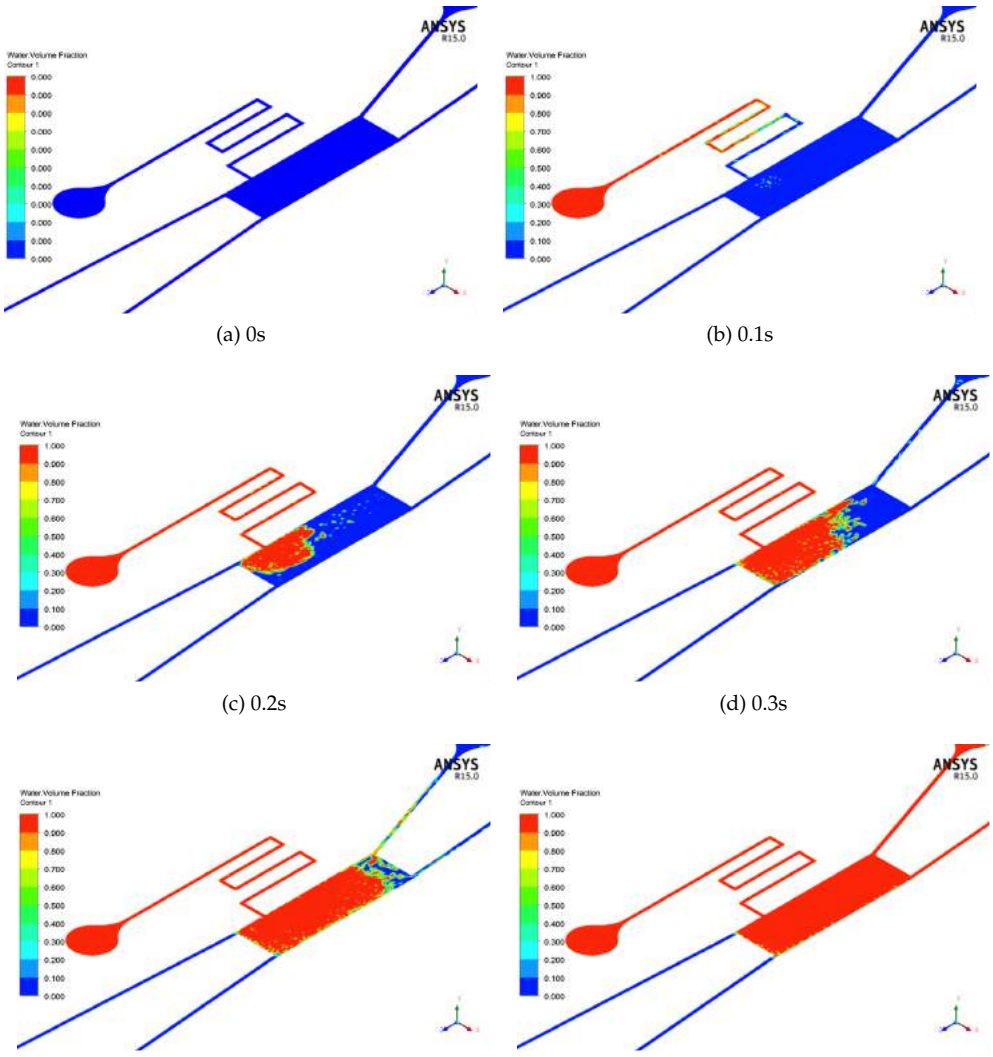

(a) 0s (b) 0.1s

(c) 0.2s (d) 0.3s

(e) 0.4s (f) 1s

Figure 7.15: Fluid flow trajectories in the final design at different time frames

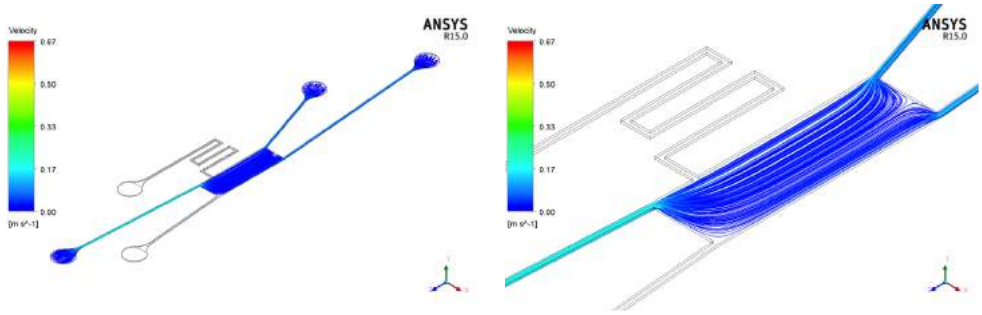

(a) 0s (b) 0.1s

Figure 7.16: Fluid flow trajectories in the chamber.

The maximum Reynolds number was computed to be less than 0.01 confirming laminar flow in the microchannels except for the corners. (Figure 7.16) The reduced shear stress and the turbulent flow observed at the corners of the chamber increased the risk of possible sedimentation, pointing out the need for gentle washing after each steps.

7.3.4 Mechanical Stability

Peel test measurements

To assess the adhesion strength of the tape to either side (i.e. the COC and the glass substrate), a 90° - peel test was performed using a Multipurpose Bondtester (Dage 4000) (Nordson, UK). The test was performed both for a 2.5 cm by 6 cm stripe of tape being bonded to the glass substrate and to the COC substrate. The peeling speed was set at 500 μm/s and the load range at 40 N. After mounting the sample, the sample movement is automatically adjusted to ensure perpendicular peeling force to the surface. The peel strength (N/mm) is calculated by dividing the mean value of the measured peel force (N) in a steady region by the width of the stripe of tape (mm).

The peel test results are visualized by plotting the peel strength versus the elapsed test time. (Figure 7.17) An acceptable adhesion strength of the tape to both the glass substrate (0.18 ± 0.02 N/mm) and the COC substrate (0.21 ± 0.02 N/mm) is shown. (Table 7.1)

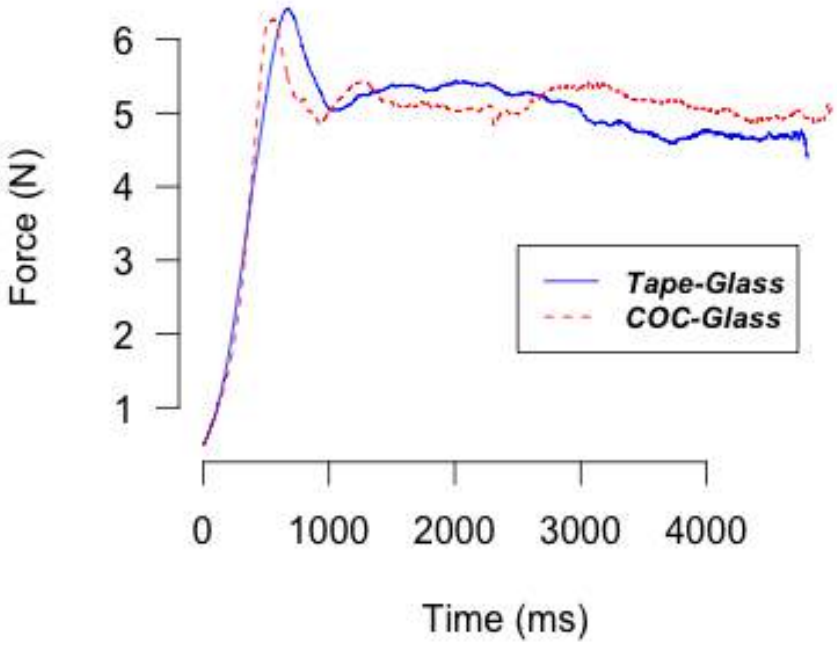

Figure 7.17: Mean peel strength versus elapsed time of the tape on the glass and the COC substrates (Tape width = 25 mm).

Table 7.1: Mean peel force calculated for each stripe of tape bonded to the glass substrate or the COC substrate (Tape width = 25 mm).

	Tape-Glass		Tape-COC	
Test #	Mean peel force (N)	N/mm	Mean peel force (N)	N/mm
1	4.69	0.19	5.69	0.23
2	5.22	0.21	5.19	0.21
3	4.68	0.19	4.81	0.20
4	5.06	0.20	4.92	0.20
5	3.63	0.15	4.44	0.18
6	3.82	0.15	6.12	0.24
7	3.77	0.15	4.74	0.19
8	4.07	0.16	5.60	0.22
9	5.28	0.21	5.32	0.21
10	4.74	0.19	5.47	0.22
11	4.81	0.19	5.38	0.22
Mean ± SD	4.52 ± 0.57	0.18 ± 0.02	5.24 ± 0.46	0.21 ± 0.02

Burst test measurements

In order to measure the pressure at which the microfluidic chip fails, a pressure transducer (CTE9000, First Sensor, Germany) with an error accuracy of 0.2 % over the range of 0 - 16 MPa was connected in-line using Tygon tubing with a syringe pump and a microfluidic chip containing a single channel with an inlet and outlet. (Figure 7.18)
The voltage output of the pressure transducer was monitored using an oscilloscope, and was converted to a pressure value using a calibration curve provided by the manufacturer. Colored dye was pumped through the microfluidic device at different flow rates, starting at 500 μl/min, and the internal pressure buildup was recorded after the voltage demonstrated by the oscilloscope became stable for at least 1 min. As the outlet was open, the pressure at the outlet was considered 1 atmosphere. Taking this in mind, the pressure drop in the channel was calculated.
The burst pressure is defined as the maximum internal pressure recorded prior to device failure due to delamination at the bonding interface or fluidic connections. The burst pressure for each flow rate is the average of 3 measurements.

The burst test showed the ability of the microfluidic device to sustain typical pressure levels when pumping liquids through the microfluidic channels.(Table 7.2)

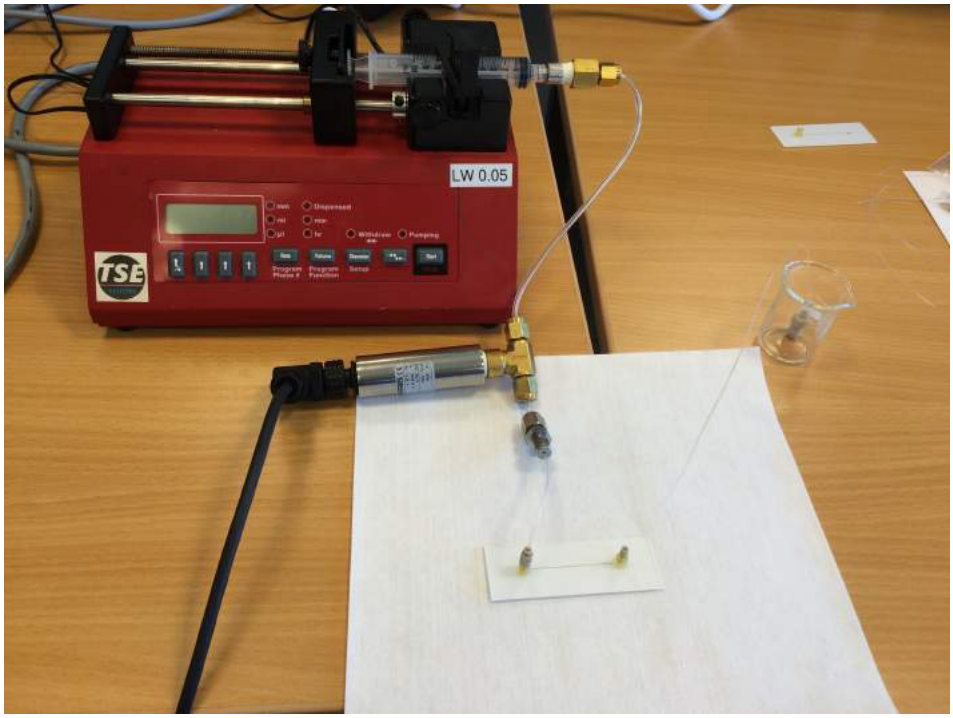

(a)

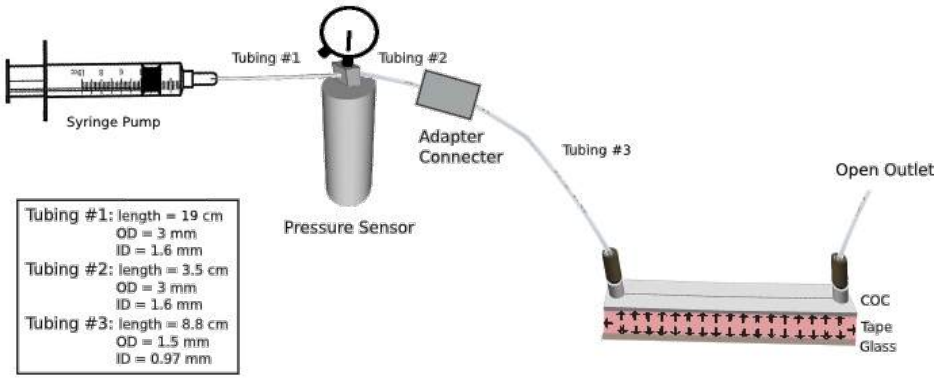

(b)

Figure 7.18: a) Experimental burst test setup, b) Schematic image of the burst test setup.

Table 7.2: Pressure drop calculated for different flow rates. (Calculated using Equation (7.2))

Flow-rate (μL/min)	Pressure at center (bar)	Pressure drop (bar)
0	-	-
200	1.12	0.12
500	1.30	0.29
1000	1.58	0.58
1200	1.70	0.70
1500	1.87	0.87
1700	1.99	0.99
2000	2.17	1.17
2200	2.28	1.28
2500	2.46	1.46
3000	2.75	1.75
4000	3.33	2.33
5000	-	-

The measured pressure at the inlet was in concordance with the pressure calculated theoretically. (Figure 7.19) In a rectangular channel, the equation estimating the pressure drop across the channel is expressed as follows [6]: (Equation (7.2))

$$\Delta P = Q.R = \frac{12 * \mu * Q * l}{h^3 * w(1 - 0.63 * \frac{h}{w})} \tag{7.1}$$

in which Q is the volumetric flow rate of the liquid, R is the fluidic resistance, l is the length of the microfluidic channel (39.3 mm), μ is the viscosity of the fluid (10^{-3} Pa.s), w is the width of the microfluidic channel (0.264 mm), and h is the height of the microfluidic channel (0.0864 mm).
The experimental burst test results showed that inlet flow rates higher than 5000 μl/min may fail either at the point of attachment of the interconnect, or at the interface between the two bonded parts.

Pressure drop in the system was calculated as the following: (Equation (7.1))

$$\Delta P = \frac{8 * \mu * Q * l}{\pi * r^4} \tag{7.2}$$

in which Q is the volumetric flow rate of the liquid (m^3/s), l is the length of the tubing (m), μ is the viscosity of the fluid (10^{-3} Pa.s), r is

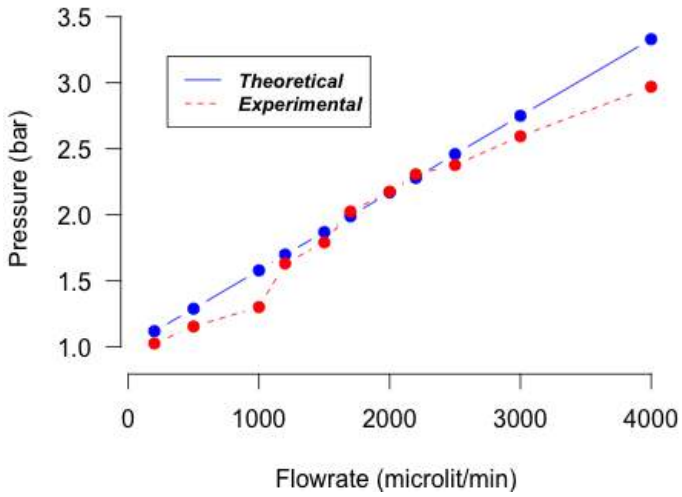

(a)

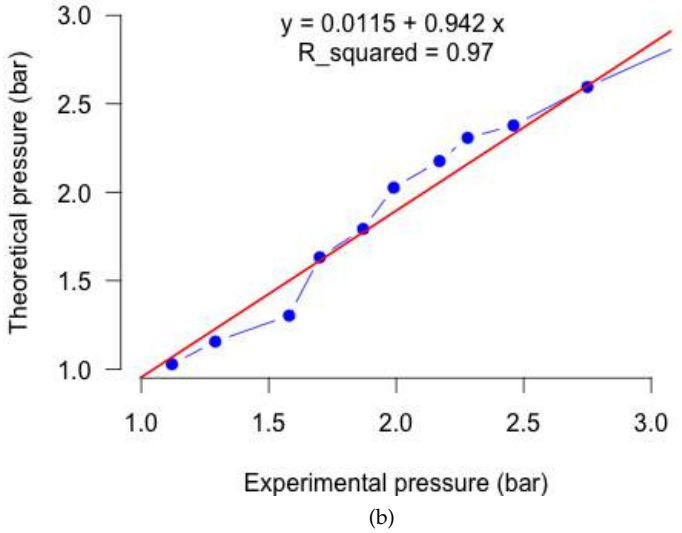

(b)

Figure 7.19: a) Measured vs expected pressure at the inlet for different flow rates. b) Measured vs expected pressure at the inlet.

the radius of the tubing (m).
In order to calculate the highest pressure drop in the system, maximum flow rate (4000 μl/min = 0.06* 10^{-6} m^3/s) tolerated by the channel was used. Using the parameters shown in Figure 7.18, pressure drop was estimated to be 0.93 mbar in tubing 1 and 2 and 6.13 mbar in tubing 3. It could be concluded that the pressure drop in the tubing can be neglected compared to the pressure drop inside the microfluidic channel.

7.4 Conclusion

Currently, developing the microfluidic channels and bonding different layers to each other are the bottlenecks in the rapid prototyping process of microfluidic devices. They considerably prolong the turnaround time between the design of the microchannel layout and the fabrication of the final design. We used a cheap, reliable and rapid method for the fabrication of microfluidic channels using double-sided tapes, enabling not only highly uniform cross-sectional dimensions along the channels but also proper adhesion in hybrid systems, composed of different layers.
Our results showed that the laser-cutting procedure for each sample was performed in 5 min and an additional 5 min was needed for the assembly process. These numbers suggest that the technique is fast and cost-effective compared with the existing microfluidic channel fabrication and bonding techniques. Moreover, modification is not an outlandish task in these devices any more.
The adhesive is shown to have bond strengths that prevent leakage, delamination and channel rupture in the typical pressure range used for microfluidic applications. A further advantage is that the assembly of the different layers does not require any plasma, heat or additional treatments and depending on the required precision of the design, can be performed manually.
This intermediate adhesive layer is therefore believed to solve possible obstacles met during the manufacturing of hybrid devices. In other words, while the microfluidic chip described herein has only two levels, a modified version of the fabrication method can be used in applications requiring a larger number of interconnected tapes across additional layers. It should be added that this fabrication method is scalable to larger platforms as it provides sufficient mechanical strength, is reproducible in form and operation, applicable to a broad range of materials, and capable of being produced with high yields.

References

[1] J. Hua, S. Wang, L. Wanga, F. Lib, B. Pingguan-Murphye, T. Lub, and F. Xua, "Advances in paper-based point-of-care diagnostics," *Biosens Bioelectron*, vol. 54, pp. 585–597, 2014.

[2] W. B. Hawkins KR, "Microfluidic diagnostics for low-resource settings," *Proceedings of the SPIE*, vol. 7593, pp. 75 930L1–L15., 2010.

[3] A. Nilghaz, D. Wicaksono, D. Gustiono, F. Abdul Majid, E. Supriyanto, and M. Abdul Kadir, "Flexible microfluidic cloth-based analytical devices using a low-cost wax patterning technique," *Lab Chip*, vol. 12, pp. 209–218, 2012.

[4] D. Duffy, J. McDonald, O. Schueller, and G. Whitesides, "Rapid prototyping of microfluidic systems in poly(dimethylsiloxane)," *Anal. Chem.*, vol. 70, pp. 4974–4984, 1998.

[5] P. Gu, K. Liu, H. Chen, T. Nishida, and Z. Fan, "Chemical-assisted bonding of thermoplastics/elastomer for fabricating microfluidic valves," *Anal. Chem.*, vol. 83, pp. 446–452, 2011.

[6] S. Mitra and S. Chakraborty, *Microfluidics and Nanofluidics Handbook*. CRC Press/Taylor and Francis, Novato, CA, 2012.

[7] B. Flachsbart, K. Wong, J. Iannacone, E. Abante, R. Vlach, P. Rauchfuss, P. Bohn, J. Sweedler, and M. Shannon, "Design and fabrication of a multilayered polymer microfluidic chip with nanofluidic interconnects via adhesive contact printing," *Lab Chip.*, vol. 6, no. 5, pp. 667–674, 2006.

[8] R. Lin and M. Burns, "Surface-modified polyolefin microfluidic devices for liquid handling," *J. Micromech Microeng*, vol. 15, pp. 2156–2162, 2005.

[9] W. Zhang, S. Lin, C. Wang, J. Hu, C. Li, Z. Zhuang, Y. Zhou, R. Mathies, and C. Yang, "Pmma/pdms valves and pumps for disposable microfluidics," *Lab Chip*, vol. 9, pp. 3088–3094, 2009.

[10] V. Sunkara, D. Park, H. Hwang, R. Chantiwas, S. Soper, and Y. Cho, "Simple room temperature bonding of thermoplastics and poly(dimethylsiloxane)," *Lab Chip*, vol. 11, pp. 962–965, 2011.

[11] G. Mehta, J. Lee, W. Cha, Y. Tung, J. Linderman, and S. Takayama, "Hard top soft bottom microfluidic devices for cell culture and chemical analysis," *Anal. Chem.*, vol. 81, pp. 3714–3722, 2009.

[12] N. Steidle, T. Hahn, C. Bader, M. Schneider, R. Ahrens, M. Worgull, and A. Guber, "Micro and nanostructured microfluidic chip for specific protein immobilization," vol. 128. 17th International Conference on Miniaturized Systems for Chemistry and Life Sciences, 2013.

[13] J. Shah, J. Geist, L. Locascio, M. Gaitan, M. Rao, and W. Vreeland, "Capillarity induced solvent-actuated bonding of polymeric microfluidic devices," *Anal Chem*, vol. 78, pp. 3348–3353, 2006.

[14] J. Steigert, S. Haeberle, T. Brenner, C. Müller, P. Steinert, C.P. Koltay, N. Gottschlich, H. Reinecke, J. Ruhe, and R. Zengerle, "Rapid prototyping of microfluidic chips in coc," *J. Micromech Microeng*, vol. 17, no. 2, 2007.

[15] S. Lee and S. Lee, "Shrinkage ratio of pdms and its alignment method for the wafer level process," *Microsyst Technol*, vol. 14, no. 2, pp. 205–208, 2008.

[16] W. Choi and O. Park, "A soft-imprint technique for submicron-scale patterns using a pdms mold," *Microelectronic Engineering*, vol. 73-74, pp. 178–83, 2004.

[17] D. Figeys, Y. Ning, and R. Aebersold, "A microfabricated device for rapid protein identification by microelectrospray ion trap mass spectrometry," *Anal. Chem.*, vol. 69, no. 16, pp. 3153–3160, 1997.

[18] Z. Zou, J. Kai, M. Rust, J. Han, and C. Ahn, "Functionalized nano interdigitated electrodes arrays on polymer with integrated microfluidics for direct bio-affinity sensing using impedimetric measurement," *Sensor Actuat A-Phys*, vol. 136, no. 2, pp. 518–526, 2007.

[19] J. Mok, M. Mindrinos, R. Davis, and M. Javanmard, "Digital microfluidic assay for protein detection," *Proc Natl Acad Sci U S A*, vol. 111, no. 6, pp. 2110–2115, 2013.

[20] A. Ciftlik and M. Gijs, "A low-temperature parylene-to-silicon dioxide bonding technique for high-pressure microfluidics," *J. Micromech Microeng*, 2011.

[21] Y. Du, C. Chen, M. Zhou, S. Dong, and E. Wang, "Microfluidic electrochemical aptameric assay integrated on-chip: a potentially convenient sensing platform for the amplified and multiplex analysis of small molecules," *Anal Chem.*, vol. 83, no. 5, pp. 1523–1529, 2011.

[22] S. Basrour and L. Robert, "X-ray characterization of residual stresses in electroplated nickel used in liga technique," *Mater. Sci. Eng., A: Struct.*, vol. 288, pp. 270–274, 2000.

[23] K. Hawkins, M. Steedman, R. Baldwin, E. Fu, S. Ghosal, and P. Yager, "A method for characterizing adsorption of flowing solutes to microfluidic device surfaces," *Lab Chip.*, vol. 7, no. 2, pp. 281–285, 2007.

[24] K. Islam, Y. Jang, R. Chand, S. Jha, H. Lee, and Y. Kim, "Microfluidic biosensor for beta-amyloid(1-42) detection using cyclic voltammetry," *J Nanosci Nanotechnol.*, vol. 11, no. 7, pp. 6757–6762, 2011.

[25] D. Grieshaber, R. MacKenzie, J. Voros, and E. Reimhult, "Electrochemical biosensors - sensor principles and architectures," *Sensors*, vol. 8, pp. 1400–1458, 2008.

[26] M. Fuerstman, A. Lai, M. Thurlow, S. Shevkoplyas, H. Stone, and G. Whitesides, "The pressure drop along rectangular microchannels containing bubbles," *Lab Chip.*, vol. 7, pp. 1479–1489, 2007.

8
Osteokit Validation

8.1 Introduction

Unstable immobilization of antibody on the electrode surface as well as nonspecific binding are the main factors that determine the detection limit for an immunoassay [1]. It is known that adsorption of proteins onto bulk metal surfaces leads to their denaturation and loss of bioactivity [2]. Therefore, as mentioned earlier, the gold electrodes were modified with AuNPs to overcome these concerns. The AuNP layer also improved the signals because of their large surface area and efficient electron conducting features. This chapter deals with surface modification of electrodes used in Osteokit and its validation process.

8.2 Immunosensing Process

8.2.1 Pretreatment of Working Electrodes

As mentioned in Chapter 5, in order to coat the working electrode with a gold nanoparticle layer that would allow sufficient immobilization of antibodies (Abs) on the surface in later steps, the ECV technique was used.

8.2.2 Surface Modification of Sensing Interfaces

The sensing chip was then bonded with the microfluidic chip, making the device (Osteokit) ready to use. In subsequent steps, the gold surface was modified for capturing antibodies that, during the assay, bind specifically to the analyte molecules (antigens). (Figure 8.1)
In this regard, the biomarkers were immobilized on the treated surface through covalent binding using cross linkers [3][4]. As mentioned in Chapter 6, the electrodes were first activated by injecting an aqueous solution of 10mM GSH via the loading channel to the reaction chamber and held for incubation for 1 hour. As the next step, the antibody complex was introduced into the reaction chamber through the inlet microchannel until the chamber was filled with the sample. The sample was then allowed to incubate for 2 hrs on the sensor electrodes (static condition). The antibody complex was prepared by incubating the antibodies with cross-linkers (100mM s-NHS for Oc, 400mM EDC/100 mM s-NHS for CTX) for 2.5 hrs in room temperature. The cross-linkers provided covalent attractions between the constituents, facilitating the bonding of the primary amine groups (-NH2) of the antibody to the carboxylic group of GSH to form stable amide bonds.
The active parts of the device were washed between each step with DI to remove unbound fractions. 0.2% (w/v) BSA solution in PBS buffer was then pumped into the microchannel to immerse the treated electrode for 1 hour and block unreacted active functional groups. The assembly was kept at room temperature during all steps and finally rinsed with PBS and then with PBS-Tween 20 thoroughly to remove unbound analytes and other non-specific entities from the electrode surface.

8.2.3 Immunosensing strategy

To investigate the applicability of Osteokit for osteoporosis care, we performed electrochemical immunoassay using fabricated device to measure serum levels of certain BTMs. All experiments were performed within a day to obtain a good sensitivity because the immobilized antibody (Ab) might be degenerated a few days after the electrochemical chip is fabricated.
For this purpose, different concentrations of Oc and CTX were applied on the electrode as the analytes for the sensing test, and the chronoamperometric signals were recorded. The antibody-antigen reaction provides a redox current, which is interpreted by the chronoamperometry. A high quality signal was obtained at + 0.65 V, thus, this potential was taken as the best value for BTM determination.

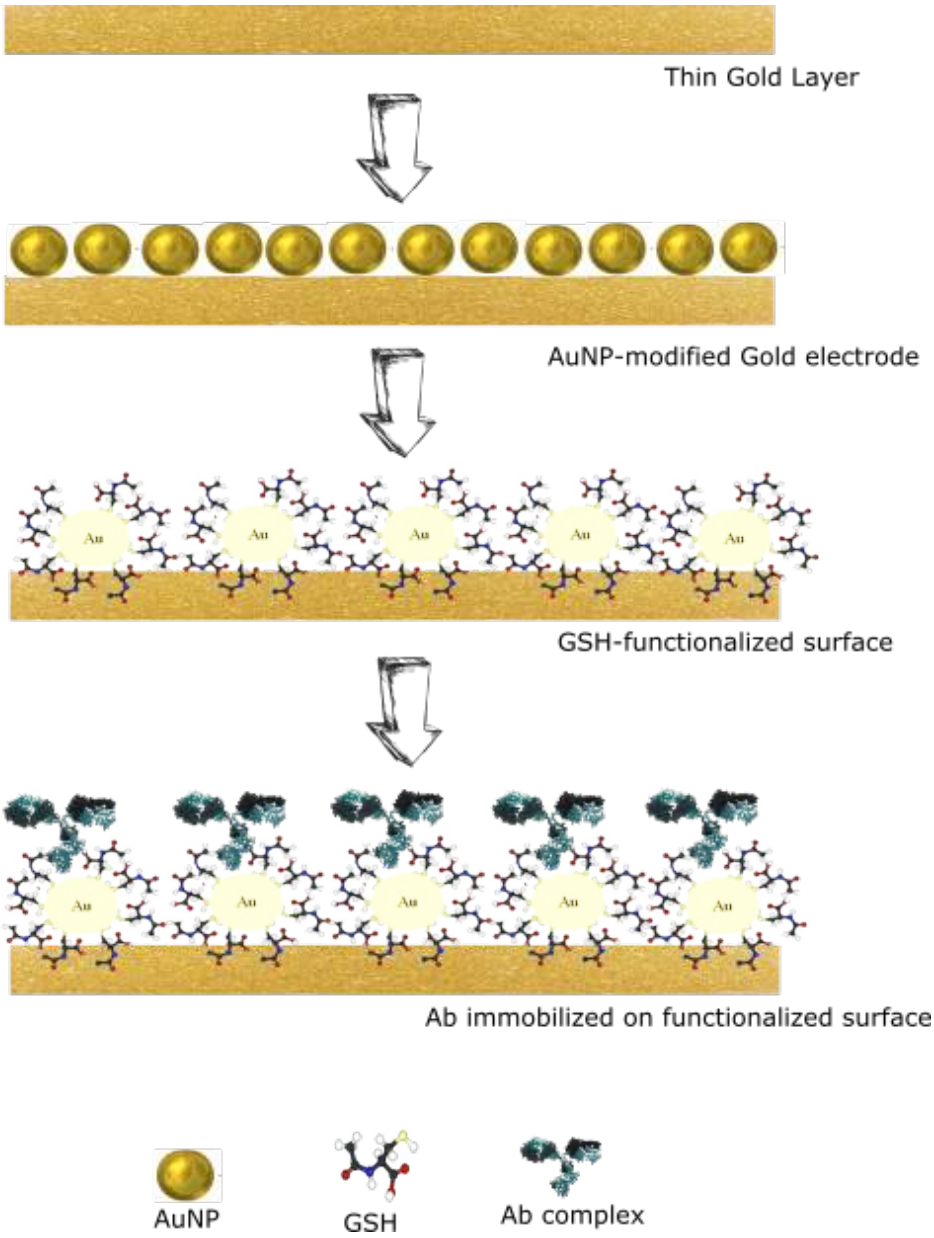

Figure 8.1: A schematic representation of the immunoelectrode fabrication procedure.

In this regard, the microfluidic channels were washed using PBS. Thereafter, the detection solution, $K_3[Fe(CN)_6]$, was then introduced into the reaction chamber to fill the chamber for chronoamperometry measurements (0.1 mM $K_3[Fe(CN)_6]$ as a redox probe, potential of 0.65 V for 15 s). The measured current at 10s (when the status in the microchannel was stabilized) was considered as baseline. Then again, the channels were washed using PBS.

At this step, the desired antigen concentration was injected via the sample channel and left to incubate in the reaction chamber for 5 min. The samples were injected sequentially onto the sensing interface and the signal was recorded. After each measurement, a relatively large amount of buffer solution was injected to wash the analyte sample out and fill the reaction channel.

The electrodes-on-chip were utilized in these steps, and a slightly different offset is reported between the working and reference electrodes in sensors with individualized quasi-reference electrodes, similar to these ones, that will consequently affect the potentials. The measured currents were therefore calibrated based on the baseline current for each electrode to obtain formal potential of the 3-electrode system. In other words, the current ratio was calculated by dividing the current measured after incubating the electrode with the specific concentration of the antigen by the current measured from the same electrode after the Ab-functionalization process.

Thereafter, the average of the ratios calculated from several electrodes incubated with certain antigen concentration was used to develop the calibration curves [1].

The specific bonding between the antibody and antigen helps improve both the sensitivity and selectivity of the assay. In this regard, sample solutions with different concentrations of each antigen were loaded into the corresponding chamber where it reacted with the Ab-functionalized electrode-on-chip. The rate of analyte capture by surface-bound antibodies can be very slow because flow in microfluidic devices is nearly always laminar and mixing occurs only by diffusion. The optimum detection time was established at 5 min. Then, the channel was flushed by passing PBS solutions through the channel twice to ensure complete washing and removal of any unbonded molecules.

[1] Detailed explanation on how the calibration curve was plotted and the data were extracted from the plot is discussed in Chapter 6

8.3 Osteokit characterization

8.3.1 Surface Morphology

Since creating AuNP layer is the first step of surface modification, it is critically important to have a well-dispersed nanoparticle layer with uniform size distribution on the surface. The deposition time and scan rate were therefore properly controlled to assure sufficient deposition and uniform distribution of AuNPs. According to our results, 60 electrodeposition cycles were needed to produce enough uniformly distributed nanoparticles with an average size of about 20 nm to cover the gold electrodes. We used different surface characterization techniques, including SEM, AFM and STEM to characterize the morphology of the as-prepared functionalized electrodes. As it can be seen in Figure 8.2, numerous uniformly distributed nanoparticles were seen on the AuNP-modified gold electrode. After the immobilization of the antibody, these nanoparticles aggregated and became larger in size.

8.3.2 Electrochemical Behavior

The electrochemical behavior of the stepwise fabrication of the electrochemical sensor chip was studied using CV, conducted at a potential range from 0 to 1.2 V at 0.1 V/s. The CV curves on the bare Au, after electrodeposition, and after surface modification with Ab in $K_3[Fe(CN)_6]$ are shown in Figure 8.3. The Au electrode showed well-defined oxidation and reduction behavior of redox moieties Fe(II)/Fe(III) in the electrolyte. The magnitude of response current of the Au electrode was found to increase after the electrodeposition of AuNPs. This suggests the formation of AuNPs, and consequent increased electron transfer rate from the medium to electrode.

When antibodies are immobilized on the working electrode, the conductive area of the working electrode is reduced, the electrical resistance is increased and thus the magnitude of the electrochemical response current is further decreased. This suggests successful immobilization of the antibody on the electrode. Furthermore, compared with bare electrodes, the as prepared AuNPs-based electrode-on-chip showed a 7.5-fold larger current response. This obvious signal enhancement should be attributed to the high loading of AuNPs on the gold electrode.

Later on, the presence of antigens over working electrode resulted in an increase in the double layer capacitance and hence reduced electrochemical behavior of test solution proportional to the concentration of the antigen. This was used as the basis for determination of antigen

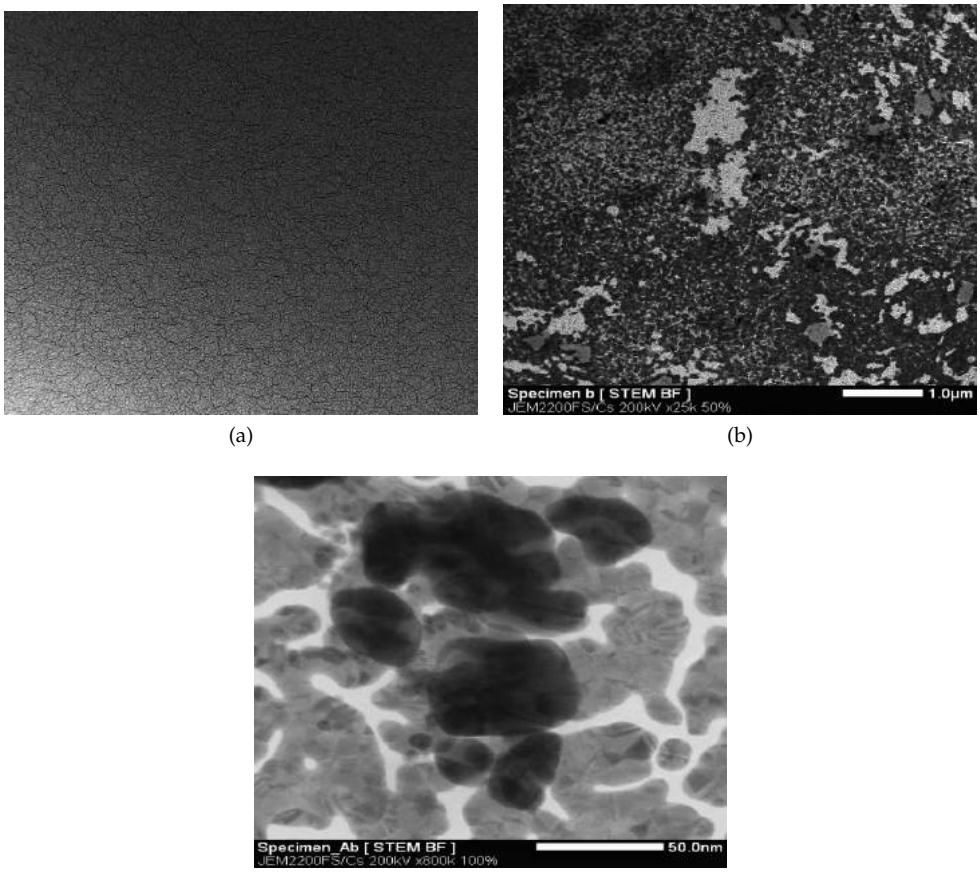

(a) (b)

(c)

Figure 8.2: STEM micrographs of a) bare gold nanoparticles by HAADF contrast, b) AuNP-modified gold electrode by BF contrast, c) Ab functionalized gold electrode by BF contrast. (For a, scale = 1.0 μm; for b, scale = 1.0 μm; for c, scale = 50 nm)

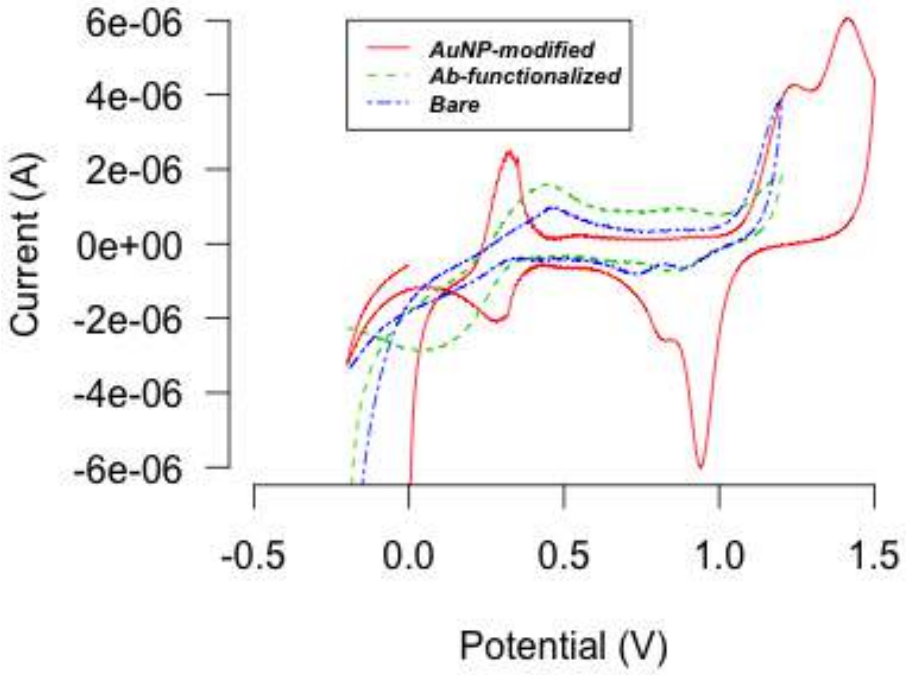

Figure 8.3: CV measurements of bare (green), AuNP-modified (red), Ab-functionalized (blue) electrodes.

concentration.
Incubation time is an important parameter affecting the immunoassay efficacy. DPV studies revealed that the magnitude of current response decreases over time due to the increased binding between antibody and antigen, causing electron transfer resistance. However, no further decrease in current was observed after 5 min, indicating saturated binding of the immunoreaction. Hence, during the electrochemical sensing measurement the electrode-on-chip was incubated with each antigen concentration for 5 min.

8.4 Calibration curve

The electrochemical response of Osteokit was studied as a function of different concentrations of Oc and CTX using chronoamperometry technique under identical experimental conditions (0.1 mM $K_3[Fe(CN)_6]$ as a redox probe, potential of 0.65V for 15s), respectively. (Figure 8.4) It is noted that the sample consumption of this prototype chip device is only 100 μL, which is much less than the traditional methods (10 mL).

The magnitude of response current ratio decreased with increasing antigen concentrations; this is due to the formation of immune-complexes between antibody and antigen resulting in electron charge transfer hindrance at the electrode electrolyte interface. (Figure 8.5) The magnitude of current ratio in the Osteokit with CTX immunoelectrode was linearly dependent to the CTX concentration with an R square of 0.98. The immunoelectrode exhibited a near linear range from 1-1000 pg/mL, at a LoD of 206.7 pg/mL, and LoQ of 626.5 pg/mL, with a correlation coefficient of 0.98.
As for Oc, the Osteokit with Oc immunoelectrode exhibited a near linear relationship between current ratio and logarithmic Oc concentration from 1 to 100 ng/mL (R^2 = 0.93). (Figure 8.5) The LoD was experimentally found to be 1.94 ng/mL. It had a LoQ of 5.89 ng/mL with a correlation coefficient of 0.96.
Osteokit demonstrated a large dynamic range, which is in the order of the physiological concentration of the studied antigens in the serum. Notably, our titration curve revealed an apparent sublinearity at the low end of the dynamic range for both analytes, which could be attributed to the translation of the actual number of antigens captured to the quantity of AuNPs.
In order to improve the results, new immunoelectrodes with larger work area (2.5*2.5 mm^2) were used. The magnitude of response current increased with a power of 10 in the Osteokits with new electrodes.

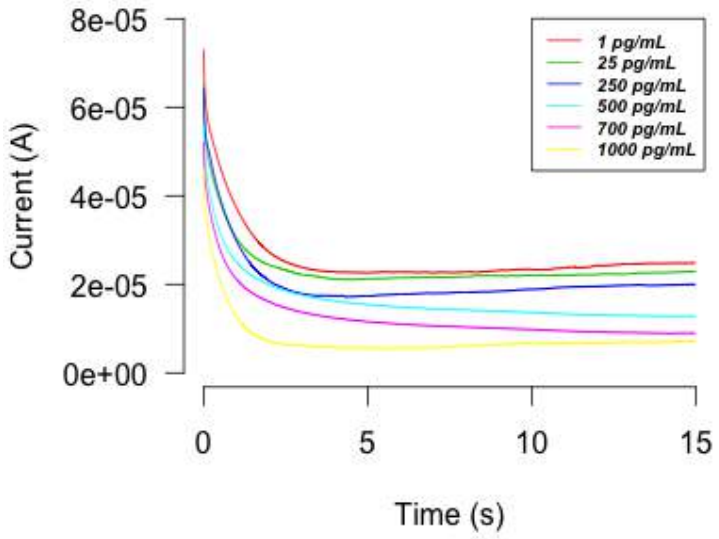

(a)

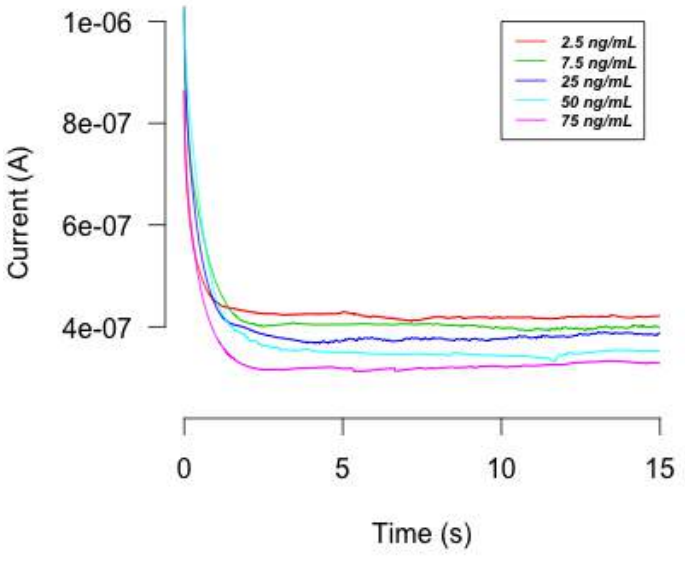

(b)

Figure 8.4: Graphs obtained for the chronoamperometry detection of several concentrations of (a) CTX (b) Oc using the Osteokit.

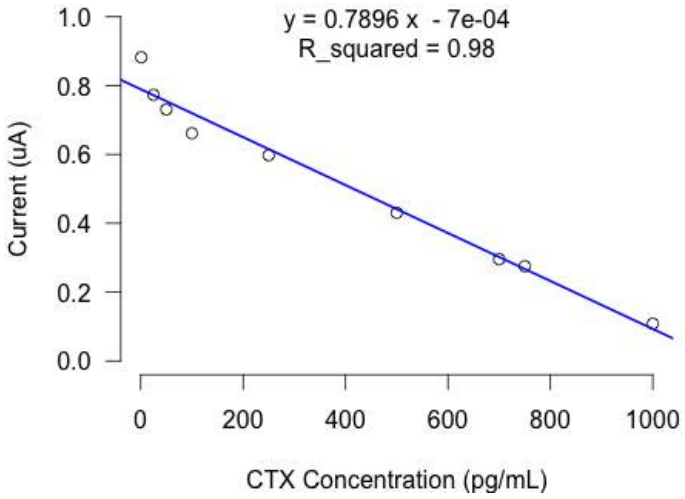

(a)

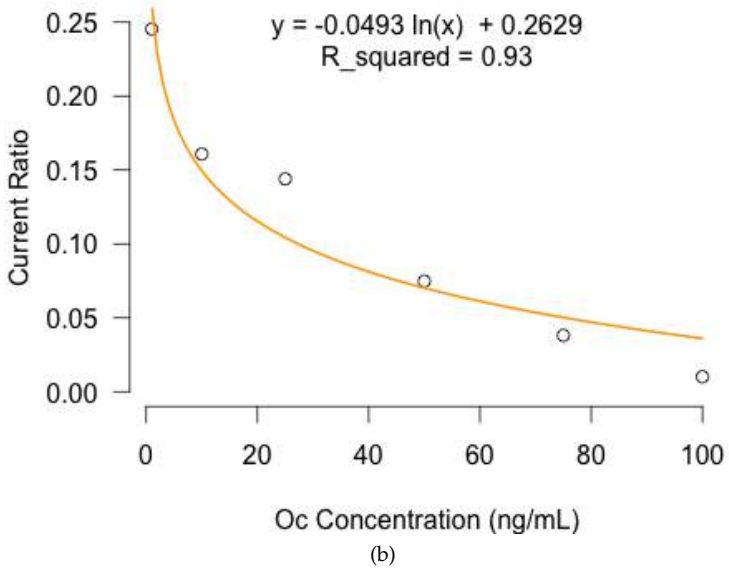

(b)

Figure 8.5: Calibration curve obtained from the electrochemical response studies of Osteokit as a function of a) CTX concentration (1-1000 pg/mL) b) Oc concentration (1-100 ng/mL).

(Figure 8.6) Using the new device, the magnitude of current ratio in the Osteokit with the CTX immunoelectrode was linearly dependent to the logarithmic concentration of CTX with an R square of 0.96. The immunoelectrode exhibited a near linear range from 1-2500 pg/mL, at a LoD of 2.77 pg/mL, and LoQ of 8.40 pg/mL, with a correlation coefficient of 0.91. In other words, increasing the area of the work area significantly improved the results.

8.5 Selectivity and cross-reactivity

Cross-reactivity and selectivity was checked using the same technique reported in Chapter 6. Osteokit showed a minimum change from baseline value (3 -- 5 %) with respect to Oc (100 pg/mL) and PTH (100 pg/mL) as interferents on the CTX immunoelectrode. Similarly there was no remarkable response for CTX (100 ng/mL) and PTH (100 ng/mL) on the Oc immunoelectrode. These results show that Osteokit is selective for both CTX and Oc and no cross-talk occurs between the channels.

8.6 Stability and Repeatability

The sensing interface was used ten times without sacrificing detection efficiency. When the sensing surfaces were regenerated for more tests, the detection of either antigen was not as sensitive as before. This might be a result of losing the activity of the immobilized antibody by repeatedly using the sensing surfaces.
To investigate the stability of the chips, the sensing interfaces were stored at room temperature for a week. Compared with the relative freshly fabricated sensing interfaces, the signal of the conserved sensing interfaces only decreased by 8.1% for Oc and 8.8% for CTX. The small decrease may be ascribed to the partial degradation of the immobilized antibody.
In addition, the results showed a remarkable reproducibility of results, tested by the application of the same concentration of either antigen on different platforms. The results showed that the signal obtained in the respective channels is highly reproducible for both CTX and Oc (RSD lower than 8%), indicating an excellent degree of reproducibility for both detection platforms.

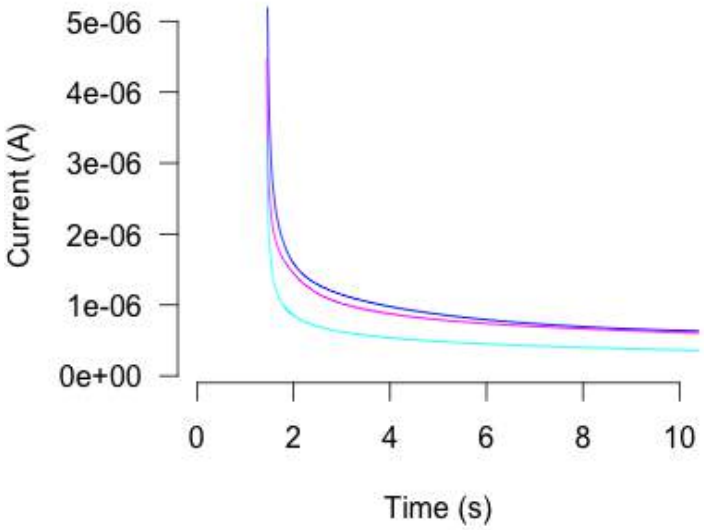

(a)

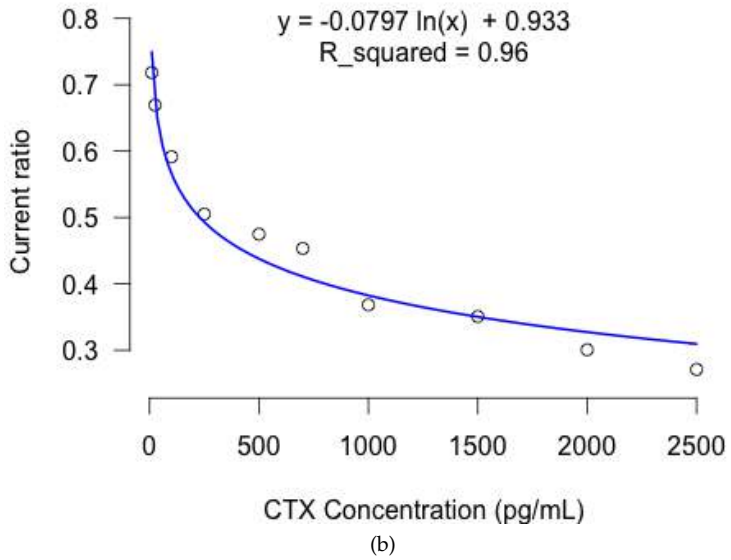

(b)

Figure 8.6: a) Graphs obtained for the chronoamperometry detection of several concentrations of CTX, b) Calibration curve obtained from the electrochemical response studies of Osteokit as a function of CTX concentration (1-2500 pg/mL), using immunoelectrodes with larger work area.

Table 8.1: Precision of Oc and CTX assay using ECLIA and Osteokit.

Oc samples	ECLIA results (ng/mL)	Osteokit results (ng/mL)
1	27.1	22.7
2	30.8	31.9
3	33.1	29.4
4	25	25.4
5	18.9	18.5
6	15.7	10.6
7	36.9	31.1
8	11.3	18.0
9	17.4	13.8
10	39.7	51.1
CTX samples	ECLIA results (pg/mL)	Osteokit results (pg/mL)
1	1250	1021.6
2	1400	1126.8
3	1070	916.9
4	455	416.9
5	325	284.6
6	2480	1145.9
7	816	812.1
8	92	26.9
9	1670	1132.7
10	194	92.2

8.7 Real serum Measurements

To compare the sensitivity of our platform with current gold standard methods, real samples (here, human serum) previously tested with ECLIA were used as analyte [2]. Again, serum of ten patients whose Oc and CTX levels were recently measured using ECLIA was used. Using the trend function in Excel and based on the values of two adjacent points on calibration curve, the concentration of Oc and CTX in the tested samples were calculated according to the obtained current. The results were then compared.

According to the results presented in Table 8.1, the coefficients of variation for the ECLIA and Osteokit were calculated to be 4.6% and 3.7% for Oc, and 6.4% and 7.7% for CTX.

[2]Oc samples were obtained from EMRI laboratory and CTX samples were obtained from UZ Hospital

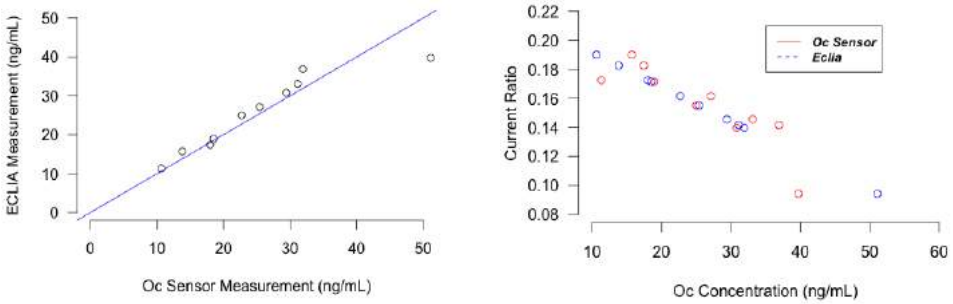

(a) (b)

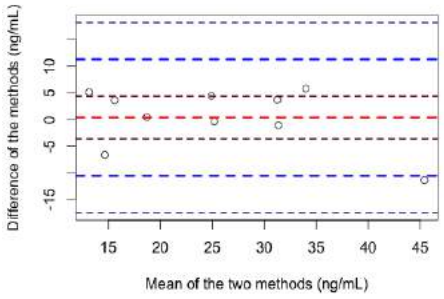

(c)

Figure 8.7: Statistical analysis comparing ECLIA vs. Osteokit in Oc Measurement a,b) Correlation plot, c) Bland and Altman plot.

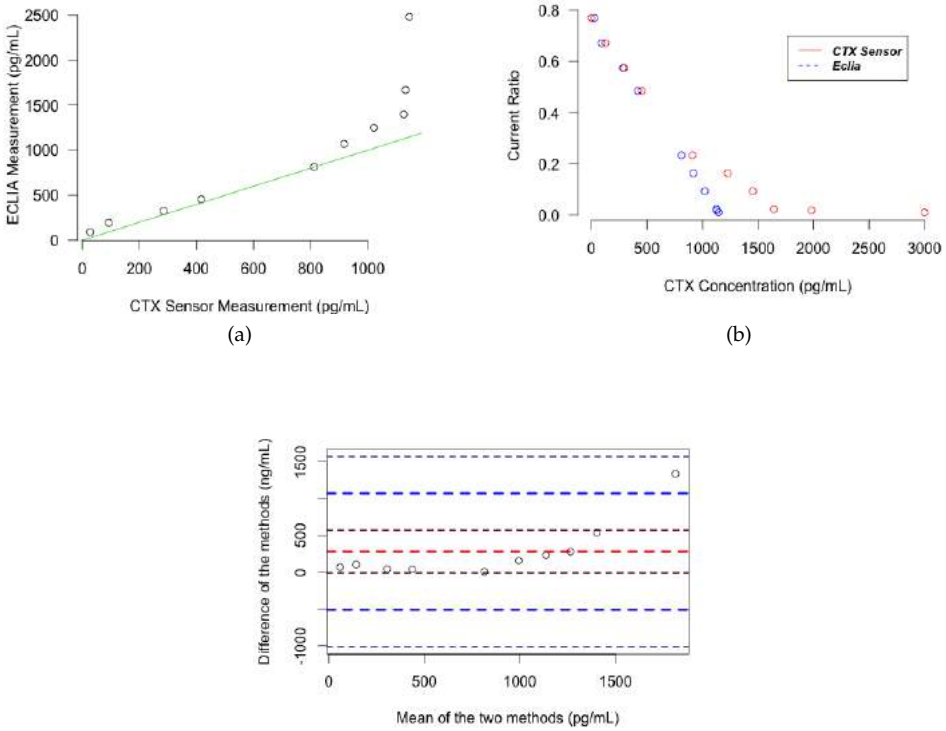

(a) (b)

(c)

Figure 8.8: Statistical analysis comparing ECLIA vs. Osteokit in CTX Measurement a,b) Correlation plot, c) Bland and Altman plot.

The correlation between our sensor results and that of ECLIA was also investigated and the results are shown in the correlation and Bland and Altman plots in Figure 8.7 and 8.8. The R^2 of the trend line in the correlation plot was 0.85 for Oc and 0.87 for CTX. This indicates that Osteokit has an acceptable correlation with ECLIA in measuring both Oc and CTX. However, the results are more acceptable for lower serum levels of CTX. This could be explained due to the fact that the calibration curve was developed for CTX concentrations between 1 - 1000 pg/mL and the ratio for higher concentrations were extrapolated, which is not really accurate. The sublinearity of the curve at the higher concentrations also aggravates the accuracy issues.

8.8 Conclusion

Herein, we presented the development of a microfluidic platform (Osteokit) capable of measuring serum levels of several biomarkers. This platform embodied a unique architecture which enabled low sample volume requirements, short assay time, simplicity of fabrication and use, and low cost instrumentation and at the same time portability, high sensitivity and specificity for the BTMs. The system shortened analytical time, enhanced detection throughput, and decreased detection cost. As a result, in terms of speed and economic expenses, the feasibility of implementation of such diagnostic tests far from the laboratory could be highly pragmatic. Furthermore, we showed this technology to reproducibly be comparable in sensitivity to the current gold standard ECLIA.
The application of an electrode with a larger work area in the Osteokit improved all the results, suggesting that this could be a good start for future works in this field.

References

[1] E. Lempens, B. Helms, and M. Merkx, "Chemoselective protein and peptide immobilization on biosensor surfaces," *Methods Mol Biol.*, vol. 751, pp. 401–420, 2011.

[2] K. Nakanishi, T. Sakiyama, and K. Imamura, "On the adsorption of proteins on solid surfaces, a common but very complicated phenomenon," *J Biosci Bioeng*, vol. 91, no. 3, pp. 233–44, 2001.

[3] J. Křenková and F. Foret, "Immobilized microfluidic enzymatic reactors," *Electrophoresis*, vol. 25, p. 3550, 2004.

[4] B. Brena, P. González-Pombo, and F. Batista-Viera, *Immobilization of Enzymes and Cells. Methods in Molecular Biology*. Springer, 2013, vol. 1051, ch. Immobilization of Enzymes: A Literature Survey.

9
Conclusion and Final Remark

9.1 Main achievements on PhD objectives

The main objective of this work was to develop the first such device to be used in osteoporosis care with enhanced sensitivity and reduced analysis time. In this perspective, we developed an electrochemical biosensor for BTM measurement in a microfluidic chip architecture for identifying individuals at-risk of fracture or monitoring the treatment process in osteoporotic patients. Our platform consisted of two components: a microfluidic control and an electrochemical-sensing module.
This fabrication is advantageous in several aspects.

- First, the modification of gold electrode with Au nanoparticles provided a suitable environment for stable immobilization of BTMs keeping their bioactivity in microreactor environment, and thus supporting high quality and low-background electrochemical sensing.
- Second, the use of highly specific monoclonal antibodies as bioaffinity sensing interface not only improved the selectivity but also allowed the detection with significantly lower amounts of the sample, compared with conventional methods.
- Third, the use of the microchannels provided controlled functionalization of the sensing platform, while preventing possible con-

tamination and cross talk.

- Fourth, the combination of the adhesive tape and the milled holder offered a means to rapidly fabricate prototype devices, which could further be tested and the design refined according to the performances required. In other words, the modular design of the chip allows us to easily modify the microfluidic control module and the electrochemical-sensing module separately.
- Fifth, it could be used as a PoC device without the need for trained personnel.
- Sixth, increased assay speed was another advantage of the current device. While a classical sandwich ELISA typically takes 3-5 h to prepare, this platform can measure biomarkers in minutes, which is especially important in PoC setting.
- And last, compared with the traditional single-analyte immunoassay, the multiplexed microfluidic immunoassay is more efficient in clinical application since it can quantitatively detect a panel of biomarkers with improved diagnostic specificity.

The most attractive feature of this microfluidic device is the ease and accuracy with which it can deliver information on the clinically relevant parameters that a PoC situation would demand. In other words, this platform is simple in design, inexpensive and easy to fabricate, and at the same time offers accurate measurements. Moreover, the use of microfluidic components along with the employment of the electrochemical detection, suggests that the proposed device can be operated as a hand-held device in future. In addition, it should be mentioned that while serum Oc measurement using traditional techniques needs extra attention [1], the current PoC device could overcome these concerns.

9.2 Outlook and Future Work

The means to take strategies that can achieve reliable and robust signal amplification, background signal suppression, or nonspecific binding prevention is essential for improving the analytical performance of a biosensor. With the rapid emergence of nanotechnology and nanoscience, hybrid bio/nanostructure-based signal amplification hold great promise in realizing high sensitivity and selectivity for the

[1] For accurate measurement of serum Oc, blood samples should be collected at a temperature between 20 and 25 °C, then centrifuged within 90 minutes; serum may be stored at -20 °C in plastic tubes for up to 26 weeks. Serum may be thawed and refrozen up to 5 times without significant change in measured serum Oc concentration. [1] [2]

in situ or online detection of biomolecules.
Although this platform has been designed to be adaptable to different types of proteomic assays, initial efforts were focused on the development of a chip to assay two major BTMs, including Oc and CTX. The assay system however could easily be adapted to other biomarkers.
In this regard, the process explained in Chapter 7 was modified for P1NP and the corresponding calibration curve was developed in the same manner. Results showed that the magnitude of current ratio in the Osteokit was linearly dependent to the logarithmic concentration of P1NP with an R square of 0.93. The device exhibited a near linear range from 5-100 μg/mL, at a detection limit of 1.82 μg/mL, and LOQ of 5.51 μg/mL, with a correlation coefficient of 0.90. (Figure 9.1) This is while the reference values for adult male is 22 - 87 μg/L, for premenopausal women is 19-83 μg/L and postmenopausal women is 16-96 μg/L, suggesting that Osteokit can be used to measure P1NP levels.

These results require further validation but may suggest a direction towards which the field of diagnostic biomarkers is moving. Assessing the reproducibility of the results when using real serum and the LSC between Osteokit and ECLIA are needed. Modifying the design in order to measure BTMs in whole blood, using a single inlet for the measurement of all the biomarkers at the same time as well as improving packaging and long-term stability of the electrodes and fabricating a portable read-out are the next steps.
Then, the biosensor must be evaluated in the clinical deployment platform to confirm its performance in predicting or diagnosing the clinical phenotype or outcome of interest as demonstrated in the initial validation phase. It is realistically infeasible to test a large number of patients in this manner due to financial constraints and/or limited availability of patient cohorts. Therefore, the use of prospective-retrospective design and/or biobank samples could be a potential alternative to overcome these obstacles.

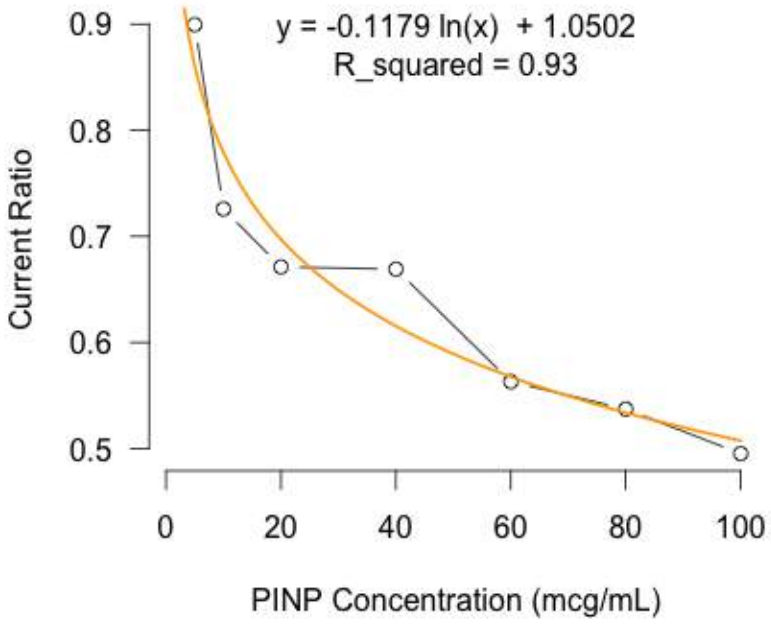

Figure 9.1: Calibration curve obtained from the electrochemical response studies of Osteokit as a function of P1NP concentration (5 - 100 μg/mL).

References

[1] J. Nolla and A. Rozadilla, "The time of blood sampling for osteocalcin determinations," *Ann Rheum Dis*, vol. 49, no. 2, p. 133, 1990.

[2] K. Noonan, M. Kalu, P. Holownia, and J. Burrin, "Effect of different storage temperatures, sample collection procedures and immunoassay methods on osteocalcin measurement," *Eur J Clin Chem Biochem*, vol. 34, no. 10, pp. 841–4, 1996.

A

BTMs and their Characteristics

In the following, a list of most important BTMs and a short description on them is provided. (Table A.1)[1]

Table A.1: Existing bone turnover markers

	Marker 1	Source	Clinical Source	Assay 2
Resorption	NTX	Degradation of bone matrix	Serum or urine	ECLIA, ECA, ELISA
	CTX	Degradation of bone matrix	Serum or urine	ECLIA, ELISA, ICMA
	Dpd/Pyd	Degradation of bone matrix	Urine	HPLC, EIA, CLIA, RIA
	TRAP	Osteoclast	Serum	RIA, ELISA, EIA, Bone-TRAP
	CatK	Osteoclast	Serum	ELISA
	Hyp	Degradation of bone matrix	Urine	ELISA
	BSP	Osteocyte	Serum	ELISA
	OPG	Osteoclast	Serum	ELISA
Formation	Oc	Osteoblast	Serum	ECLIA, RIA, ELISA, IRMA
	BALP	Osteoblast	Serum	Immunoenzymatic Assay, IRMA, ELISA
	P1NP	Newly synthesized bone matrix	Serum	Competitive RAI, ICMA, IRMA
	P1CP	Newly synthesized bone matrix	Serum	RIA, ELISA

1 NTX: Amino terminal telopeptide, CTX: Carboxyterminal telopeptide, Dpd: Deoxypyridinoline, Pyd: Pyridinoline, TRAP: Tartrate-resistant acid phosphatase, CatK: Cathepsin K, Hyp: Hydroxyproline, BSP: Bone sialoprotein, OPG: Osteoprotegerin, Oc: Osteocalcin, BALP: Bone-specific alkaline phosphatase, P1NP: Procollagen type 1 N-terminal propeptide, P1CP: Procollagen type 1 C-terminal propeptide.

2 CLIA: Chemiluminescent Immunoassay, ECA: Enzymatic Colorimetric Assay, ECLIA: Electrochemiluminescence Immunoassay, EIA: Enzyme Immunoassay, ELISA: Enzyme-linked Immunosorbent Assay, HPLC: High-Performance Liquid Chromatography, ICMA: Immunochemiluminescence Assay, IRMA: Immunoradiometric Assay, RAI: Radioimmunoassay.

A.0.1 Bone Resorption Markers

Increased bone resorption induces microarchitectural deterioration of bone tissue, affecting bone strength. Increased bone resorption induces microarchitectural deterioration of bone tissue, affecting bone strength. Most biochemical markers of bone resorption such as urinary total pyridinoline (PYD), urinary free deoxypyridinoline (Dpd), urinary collagen type I cross-linked N- telopeptide (NTX), urinary or serum collagen type I cross-linked C-telopeptide (CTX) are the products of degradation of bone collagen. Non-collagenous proteins such as bone sialoprotein or tartrate- resistant acid phosphatase (TRAP) are also classified in this group.

Type I collagen fragments

Since type I collagen is the main component of the organic matrix of the bone (more than 90%), collagenolytic peptidases in osteoclasts play a critical role in the resorption process [2]. During this process, type I collagen splits into several fragments (the cysteine proteinase and the matrix metalloproteinase (MMP)). These fragments are the most sensitive markers of bone resorption in osteoporosis as they can help estimate the rate of bone degradation.

Cross-linked Telopeptides of type I collagen (CTX) Serum CTX levels follow a circadian rhythm and are reported to be higher in the early morning [3]. After bone degradation, the non-helical regions of type I collagen, the location on which the cross-links bond, are released into the circulation. These products are not reused in the synthesis of new collagen or metabolized in the liver as they are eventually excreted in urine [4]. This marker is shown to significantly predict the risk of hip fracture, independent of bone mass.
C-terminal crosslinking telopeptides generated by metalloproteinase (CTX- MMP), Cross- linked carboxyterminal telopeptide of type I collagen (ICTP), a trimeric cross-link-containing collagen peptide originally isolated by trypsin digestion of human bone collagen, and C-terminal crosslinking telopeptides of type I collagen (CTX), a linear eight amino acid epitope (EKAHDGGR) are the main fragments found on the C-telopeptide end of type I collagen [5]. The CTX epitope, which comprises of a DG- motif susceptible to post- translational modifications, converts to an isomerized form (alpha to beta CTX) during the aging process.
The lysine residue (K) within the CTX epitope also participates in intermolecular cross-links in mature bone. They are also useful in mon-

itoring bone metabolic activity and thus can be used to observe the treatment process in postmenopausal women. Fragments of alpha-CTX containing the sequence AHDGGR (1209-1214) can be measured in urine as well, and is useful to confirm suppressed bone turnover in individuals receiving bone treatments [6]. Elevated urinary levels of native and age- related forms of CTX (alphaL/alphaD CTX ratio) are reported in patients with Paget's disease or osteoporosis. On the other hand, postmenopausal women with low alpha/beta ratio of urinary CTX excretion, suggestive of a low degree of isomerization of type I collagen are at an increased risk of experiencing fracture [7].

N -terminal Crosslinking Telopeptides of type I Collagen (NTX) On the N-telopeptide end, NTX is measured. The measurement of urinary and serum NTX levels reveals the bone resorption rate during the osteoporosis treatment; urinary NTX however is more sensitive and efficient in this regard [8]. Bregenzer et al showed that N-telopeptide levels could be used not only as a tool for osteoporosis screening but also for selecting patients with inflammatory bowel disease at-risk of developing osteoporosis [9]. Chaki et al reported that baseline urinary NTx levels are the most sensitive predictor of bone loss at the lumbar spine region. Another study revealed NTX to be significantly correlated with BMD changes at the femoral neck, but not the spine [10]. NTX, CTX, and ICTP are catabolized to smaller molecules such as Dpd, Galactosyl hydroxylysine (GHYL), hydroxyproline (Hyp). These markers however are no longer widely used [11].

Hydroxyproline (Hyp) Hyp constitutes 12±14% of the total amino acid content of mature collagen. It had long been used as the only marker of bone resorption; this is while significant amounts of urinary Hyp derive from the degradation of the newly synthesized collagen in tissues other than bone and mainly from the diet [12]. Moreover, only 10% of Hyp released during the bone resorption process is excreted in the urine.

Galactosyl hydroxylysine (GHYL) GHYL, the integral parts of bone collagen, are released into the circulation during the degradation of mature collagen. Initially, pyridinium cross- links, pyridinoline (Pyd) and deoxypyridinoline (Dpd) were measured in the urine [12] [13]. Compared with Hyp, Pyd and Dpd have a better accuracy and discrimination power in distinguishing postmenopausal osteoporotic women. The measurement of these two components is not influenced

by the degradation of newly synthesized collagen nor diet. They follow a circadian rhythm and are higher in early morning.

- Pyridinoline (Pyd)
  Pyd levels were reported to be relatively higher in females and individuals with vertebral deformities. [13] It is suggested that Pyd levels have a negative correlation with BMD at lumbar spine and could help differentiate between pre and postmenopausal women.
- Deoxypyridinoline (Dpd)
  Dpd is considered as a useful marker for the diagnosis of osteoporosis and other metabolic bone diseases [14]. While considered as a more specific bone marker than Pyd, Dpd can help predict the risk of vertebral fractures. Urinary excretion of Dpd is positively correlated with histomorphometric parameters of bone resorption.

Tartrate-resistant acid phosphatase isoform 5b (s-TRACP-5b)

The iron-containing enzyme is synthesized by osteoclasts and alveolar macrophages [15]. Its production however is not linked specifically to the osteoclast-mediated collagen degradation, and can be secreted by all active osteoclasts. Enzymes originating from erythrocytes and platelets as well as many other circulating inhibitors affect total TRAP levels [16]. TRACP5b, on the other hand, is a unique indicator of the number of active osteoclasts in the body and, thus a useful indicator of bone resorption. Increased serum levels of TRAP5b is noted in certain diseases such as primary or secondary hyperparathyroidism, Paget's and metastatic bone disease where bone resorption and the number of active osteoclasts is increased [16].

Sclerostin

Sclerostin is a Wnt antagonist produced almost exclusively by osteocytes. Decreased serum sclerostin levels are reported in patients with primary hyperparathyroidism, indicating that sclerostin is down regulated by PTH [17]. Several variables including age and serum levels of hormones such as parathyroid, estradiol, and follicle- stimulating hormone (FSH) influence serum levels of sclerostin in premenopausal women. Sclerostin, on the other hand, plays an important role in postmenopausal osteoporosis [18].

Matrix metalloproteinase (MMP)

The role of MMP in bone has not been completely identified, but several MMPs (the collagenases (MMP-1, -2, -13, and -14) and gelatinases (MMP-2 and MMP-9)) are reported to be involved in collagen degradation in bone tissue [19]. Increased levels of MMP-9 and tissue inhibitors of metalloproteinases (TIMP)-1 and -2 are reported following airways injury in chronic obstructive pulmonary disease (COPD). Bolton et al however showed that the increased levels of circulating MMP-9 in COPD patients was due to the underlying osteoporosis rather than the lung problem [20]. MMP-9, therefore, is considered as an indicator of activated osteoclasts and thus a biomarker of increased bone resorption.

Osteoprotegerin (OPG)

The discovery of the NF-kappa B ligand (sRANKL) signaling system and its decoy receptor osteoprotegerin (OPG) has led to a better understanding of the bone microenvironment. Chiba et al reported that unlike sRANKL, there is a significant positive association between OPG levels and BMD values at lumbar spine in postmenopausal women, suggesting that OPG is a good predictor of osteoporosis in elderly women [21].

Cathepsin K (CatK)

Cathepsin K, the predominant collagenase in osteoclasts, plays an important role in bone resorption [22]. It is suggested that serum levels of CatK may be useful in the diagnosis of chronic bone disorders such as osteoporosis. This comes while Adolf et al failed to show any correlation between CatK and other biomarkers including CTX or BAP, indicating that serum levels of CatK are not suitable for identifying osteoporotic women [23].

Interalpha-Trypsin-Inhibitor Heavy Chain H4 Precursor (ITIH4)

Bhattacharyya et al reported reduced levels of proteolytic fragments of a specific signature fragmentation pattern, ITIH4, in high-turnover patients [24]. They stressed that the plasma kallikrein- sensitive glycoprotein indicates the host's response to increased activity of osteoclasts. The protein can therefore help identify individuals at high risk of fracture.

Dickkopf-related protein1 (DKK1)

DKK1 is a potent Wnt antagonist that specifically blocks Wnt/b-catenin signaling process [25]. The expression of serum Dkk1 is highly but negatively correlated with bone mass at different sites.

A.0.2 Bone Formation Markers

Bone formation markers such as bone-specific alkaline phosphatase, Oc, and serum type I procollagen (C-terminal/N-terminal), can express different phases of osteoblast development and function [26].

Procollagen I extension peptides (s-P1NP)

P1NP follows a circadian rhythm and is higher in early morning [27]. While studying the response to treatment in postmenopausal women who had received teriparatide, P1NP is reported to be the most useful marker. On the other hand, women with high baseline P1NP levels are reported to respond better to bisphosphonate treatment [28].

Procollagen type I C -terminal propeptide (P1CP)

Different studies have shown a significant correlation between serum P1CP levels and the bone formation rate [29]. Unlike P1NP, the clinical application of P1CP in the assessment of metabolic bone diseases is still not clear.

Bone alkaline phosphatase (BALP)

Total alkaline phosphatase (TAP) is a well-known enzyme with an important role in bone formation and mineralization. In adults with normal liver function, approximately 50% of the TAP originates from the liver and 50% from the bones [30]. Other dimeric isoforms of TAP originate from tissues such as intestine, spleen, kidney and placenta.
BALP, an enzyme located on the outer surface of osteoblasts, is one of the most frequently used biochemical markers of bone formation because of its regulatory role in the mineralization of the osteoids. BALP measurement is helpful in diagnosis of bone loss in primary (postmenopausal and senile osteoporosis) and secondary osteoporosis (due to metabolic diseases, renal osteodystrophy, Paget disease and ...) as well as in monitoring antiresorptive therapy [31].

Serum Osteocalcin (Oc)

Oc is the most abundant noncollagenous protein in bone, comprising 1–2% of total protein [32]. The biosynthesis of Oc is regulated by several hormones and growth factors, for instance vitamin K is responsible for its carboxylation. Cathepsin K and matrix metalloproteinases break Oc into smaller fragments during bone resorption. These fragments are rapidly cleared by the kidneys. The vitamin K-dependent hydroxyapatite-binding protein is synthesized only by osteoblasts and odontoblasts, with a small amount being released during matrix resorption. In other words, Oc is a specific indicator of bone formation. According to its circadian rhythm, serum levels of Oc is higher in early morning. Akesson et al showed a 20% lower serum concentration of Oc in women with a previous history of fracture, adding that no such a decline was reported for PICP, ALP, BALP, calcium, phosphate, and albumin [33].

- Undercarboxylated Osteocalcin (ucOc): Impaired g- carboxylation of Oc (ucOc) is reported to be suggestive of both vitamin D and vitamin K deficiency in the elderly [34]. High levels of serum ucOc are linked with a 2- to 3- fold increase in the hip fracture risk, independent of BMD values [35].
- Serum N-terminal Osteocalcin (N-MID Oc): Among BTMs, only the changes in serum N-terminal Oc is significantly correlated with BMD changes after 12 months of Hormone Replacement Therapy (HRT), indicating that the fragment is a suitable predictor for identifying good responders to the treatment [36]. Weng et al reported that the combination of BALP and N-MID are more sensitive than BMD in monitoring osteoporosis treatment [37].

Bone sialoprotein (BSP)

BSP, which accounts for 5-10% of the non-collagenous matrix of the bone, is an important product of active osteoblasts and odontoblasts. It is thus assumed to reflect bone resorption rate in the body [38]. BSP levels are believed to decrease rapidly following intravenous bisphosphonate treatment.

NH2-Terminal pro C-type Natriuretic Peptide (NT proCNP)

Serum levels of NT proCNP, the product of the CNP gene [recently identified in growth plate cartilage (and osteoblasts)], are highly correlated with growth velocity. In other words, NT proCNP reflects the

activity of chondrocytes in growth plate and its levels reduce with corticosteroids use and following hypocaloric diets. The new marker, which was first used to identify responders to growth hormone deficiency (GHD) treatment, is reported to be effective in monitoring the effects of new therapies that improve bone formation in osteoporotic patients [39].

References

[1] P. Khashayar, H. Aghaei Meybodi, G. Amoabediny, and B. Larijani, "Biochemical markers of bone turnover and their role in osteoporosis diagnosis: A narrative review," *Recent Pat Endocr Metab Immune Drug Discov.*, vol. 9, no. 2, pp. 79–89, 2015.

[2] P. Garnero, M. Ferreras, M. A. Karsdal, R. Nicamhlaoibh, J. Risteli, O. Borel, P. Qvist, P. D. Delmas, N. T. Foged, and J. M. Delaissé, "The type i collagen fragments ictp and ctx reveal distinct enzymatic pathways of bone collagen degradation," *J Bone Miner Res*, vol. 18, no. 5, pp. 859–867, 2003.

[3] R. D. Chapurlat, P. Garnero, G. Bréart, P. J. Meunier, and P. D. Delmas, "Serum type i collagen breakdown product (serum ctx) predicts hip fracture risk in elderly women: the epidos study," *Bone*, vol. 27, no. 2, pp. 283–286, 2000.

[4] M. J. Seibel, H. Woitge, C. Scheidt-Nave, G. Leidig-Bruckner, A. Duncan, P. Nicol, R. Ziegler, and S. P. Robins, "Urinary hydroxypyridinium crosslinks of collagen in population-based screening for overt vertebral osteoporosis: results of a pilot study," *J Bone Miner Res*, vol. 9, no. 9, pp. 1433–1440, 1994.

[5] L. O. Chailurkit, B. Ongphiphadhanakul, N. Piaseu, S. Saetung, and R. Rajatanavin, "Biochemical markers of bone turnover and response of bone mineral density to intervention in early postmenopausal women: an experience in a clinical laboratory," *Clin Chem*, vol. 47, no. 6, pp. 1083–1088, 2001.

[6] C. Dane, B. Dane, A. Cetin, and M. Erginbas, "Effect of risedronate on biochemical marker of bone resorption in postmenopausal women with osteoporosis or osteopenia," *Gynecol Endocrinol*, vol. 24, no. 4, pp. 207–213, 2008.

[7] H. Hoshino, M. Takahashi, K. Kushida, T. Ohishi, and T. Inoue, "The relationships between the degree of beta-isomerization of type i collagen degradation products in the urine and aging, menopause and osteoporosis with fractures," *Osteoporos Int*, vol. 9, no. 5, pp. 405–409, 1999.

[8] Y. Abe, H. Ishikawa, and A. Fukao, "Higher efficacy of urinary bone resorption marker measurements in assessing response to treatment for osteoporosis in postmenopausal women," *Tohoku J Exp Med*, vol. 214, no. 1, pp. 51–59, 2008.

[9] N. Bregenzer, P. Erban, H. Albrich, G. Schmitz, S. Feuerbach, J. Schölmerich, and T. Andus, "Screening for osteoporosis in patients with inflammatory bowel disease by using urinary n-telopeptides," *Eur J Gastroenterol Hepatol*, vol. 14, no. 6, pp. 599–605, 2002.

[10] O. Chaki, I. Yoshikata, R. Kikuchi, M. Nakayama, Y. Uchiyama, F. Hirahara, and I. Gorai, "The predictive value of biochemical markers of bone turnover for bone mineral density in postmenopausal japanese women," *J Bone Miner Res*, vol. 15, no. 8, pp. 1537–1544, 2000.

[11] O. S. Donescu, M. C. Battié, T. Videman, J. Risteli, and D. Eyre, "The predictive role of bone turnover markers for bmd in middle-aged men," *Aging Male*, vol. 9, no. 2, pp. 97–102, 2006.

[12] M. J. Seibel, "Biochemical markers of bone turnover: part i: biochemistry and variability," *Clin Biochem Rev*, vol. 26, no. 4, pp. 97–122, 2005.

[13] A. Behre, J. Janott, M. Pfohl, H. Schatz, and A. Pfeiffer, "Clinical value of urinary pyridinium crosslinks as osteoporosis markers: evaluation of a population survey of vertebral osteoporosis," *Med Klin (Munich)*, vol. 96, no. 7, pp. 378–382, 2001.

[14] P. Bettica, L. Moro, S. P. Robins, A. K. Taylor, J. Talbot, F. R. Singer, and D. J. Baylink, "Bone-resorption markers galactosyl hydroxylysine, pyridinium crosslinks, and hydroxyproline compared," *Clin Chem*, vol. 38, no. 11, pp. 2313–2318, 1992.

[15] J. M. Halleen, S. L. Alatalo, A. J. Janckila, H. W. Woitge, M. J. Seibel, and H. K. Väänänen, "Serum tartrate-resistant acid phosphatase 5b is a specific and sensitive marker of bone resorption," *Clin Chem*, vol. 47, no. 3, pp. 597–600, 2001.

[16] B. Habermann, C. Eberhardt, M. Feld, L. Zichner, and A. A. Kurth, "Tartrate-resistant acid phosphatase 5b (trap 5b) as a marker of osteoclast activity in the early phase after cementless total hip replacement," *Acta Orthop*, vol. 78, no. 2, pp. 221–225, 2007.

[17] M.-S. Ardawi, A. Al-Sibiany, T. Bakhsh, A. Rouzi, and M. Qari, "Decreased serum sclerostin levels in patients with primary hyperparathyroidism: a cross-sectional and a longitudinal study," *Osteoporos Int*, vol. 23, no. 6, pp. 1789–1797, 2012.

[18] X.-J. Xu, L. Shen, Y.-p. Yang, F.-r. Lu, R. Zhu, B. Shuai, C.-g. Li, and M.-x. Wu, "Serum sclerostin levels associated with lumbar spine bone mineral density and bone turnover markers in patients with postmenopausal osteoporosis," *Chin Med J (Engl)*, vol. 126, no. 13, pp. 2480–2484, 2013.

[19] G. Dew, G. Murphy, H. Stanton, R. Vallon, P. Angel, J. J. Reynolds, and R. M. Hembry, "Localisation of matrix metalloproteinases and timp-2 in resorbing mouse bone," *Cell Tissue Res*, vol. 299, no. 3, pp. 385–394, 2000.

[20] C. E. Bolton, M. D. Stone, P. H. Edwards, J. M. Duckers, W. D. Evans, and D. J. Shale, "Circulating matrix metalloproteinase-9 and osteoporosis in patients with chronic obstructive pulmonary disease," *Chron Respir Dis*, vol. 6, no. 2, pp. 81–87, 2009.

[21] Y. Chiba, T. Onouchi, T. Ikeda, J. Adachi, Y. Tamura, and T. Horiuchi, "Implications of measuring soluble receptor activators of nuclear factor-kappab ligand and osteoprotegerin in bone metabolism of elderly women," *Gerontology*, vol. 55, no. 3, pp. 275–280, 2009.

[22] Z. Li, M. Kienetz, M. M. Cherney, M. N. G. James, and D. Brömme, "The crystal and molecular structures of a cathepsin k:chondroitin sulfate complex," *J Mol Biol*, vol. 383, no. 1, pp. 78–91, 2008.

[23] D. Adolf, T. Wex, O. Jahn, C. Riebau, W. Halangk, S. Klose, S. Westphal, H. Amthauer, S. Winckler, and S. Piatek, "Serum cathepsin k levels are not suitable to differentiate women with chronic bone disorders such as osteopenia and osteoporosis from healthy pre- and postmenopausal women," *Maturitas*, vol. 71, no. 2, pp. 169–172, 2012.

[24] S. Bhattacharyya, E. R. Siegel, S. J. Achenbach, S. Khosla, and L. J. Suva, "Serum biomarker profile associated with high bone turnover and bmd in postmenopausal women," *J Bone Miner Res*, vol. 23, no. 7, pp. 1106–1117, 2008.

[25] J. S. Butler, D. W. Murray, C. J. Hurson, J. O'Brien, P. P. Doran, and J. M. O'Byrne, "The role of dkk1 in bone mass regulation: correlating serum dkk1 expression with bone mineral density," *J Orthop Res*, vol. 29, no. 3, pp. 414–418, 2011.

[26] P. Garnero and D. P.D, *Biochemical markers of boneturnover in osteoporosis*, K. J. Marcus M, Feldman D, Ed. New York: Academic Press, 2001, vol. 2, no. 459–477.

[27] A. Blumsohn, F. Marin, T. Nickelsen, K. Brixen, G. Sigurdsson, J. González de la Vera, S. Boonen, S. Liu-Léage, C. Barker, R. Eastell, and EUROFORS Study Group, "Early changes in biochemical markers of bone turnover and their relationship with bone mineral density changes after 24 months of treatment with teriparatide," *Osteoporos Int*, vol. 22, no. 6, pp. 1935–1946, 2011.

[28] D. C. Bauer, P. Garnero, M. C. Hochberg, A. Santora, P. Delmas, S. K. Ewing, D. M. Black, and Fracture Intervention Research Group, "Pretreatment levels of bone turnover and the antifracture efficacy of alendronate: the fracture intervention trial," *J Bone Miner Res*, vol. 21, no. 2, pp. 292–299, 2006.

[29] E. F. Eriksen, P. Charles, F. Melsen, L. Mosekilde, L. Risteli, and J. Risteli, "Serum markers of type i collagen formation and degradation in metabolic bone disease: correlation with bone histomorphometry," *J Bone Miner Res*, vol. 8, no. 2, pp. 127–132, 1993.

[30] C. Barbu, A. Roman, R. Rotaru, and S. Fica, "Is there a role for a random measurement of 24-hour urine calcium excretion and serum total alkaline phosphatase in the determination of fracture risk in osteoporotic postmenopausal women?" *Rev Med Chir Soc Med Nat Iasi*, vol. 110, no. 2, pp. 291–294, 2006.

[31] J. Ambroszkiewicz, J. Gajewska, and T. Laskowska-Klita, "Bone alkaline phosphatase: characteristic and its clinical applications," *Med Wieku Rozwoj*, vol. 6, no. 2, pp. 99–110, 2002.

[32] C. M. Gundberg, J. B. Lian, and S. L. Booth, "Vitamin k-dependent carboxylation of osteocalcin: friend or foe?" *Adv Nutr*, vol. 3, no. 2, pp. 149–157, 2012.

[33] K. Akesson, S. Ljunghall, P. Gärdsell, I. Sernbo, and K. J. Obrant, "Serum osteocalcin and fracture susceptibility in elderly women," *Calcif Tissue Int*, vol. 53, no. 2, pp. 86–90, 1993.

[34] S.-M. Kim, K.-M. Kim, B.-T. Kim, N.-S. Joo, K.-N. Kim, and D.-J. Lee, "Correlation of undercarboxylated osteocalcin (ucoc) concentration and bone density with age in healthy korean women," *J Korean Med Sci*, vol. 25, no. 8, pp. 1171–1175, 2010.

[35] P. Vergnaud, P. Garnero, P. J. Meunier, G. Bréart, K. Kamihagi, and P. D. Delmas, "Undercarboxylated osteocalcin measured with a specific immunoassay predicts hip fracture in elderly women: the epidos study," *J Clin Endocrinol Metab*, vol. 82, no. 3, pp. 719–724, 1997.

[36] J. T. Chen, K. Hosoda, K. Hasumi, E. Ogata, and M. Shiraki, "Serum n-terminal osteocalcin is a good indicator for estimating responders to hormone replacement therapy in postmenopausal women," *J Bone Miner Res*, vol. 11, no. 11, pp. 1784–1792, 1996.

[37] X.-M. Weng and J.-P. Pan, "Bone alkaline phosphatase and n-mid osteocalcin in monitoring of osteoporosis treatment with recombinant human parathyroid hormone 1-34," *Zhejiang Da Xue Xue Bao Yi Xue Ban*, vol. 42, no. 5, pp. 578–582, 2013.

[38] J. K. Chen, H. S. Shapiro, J. L. Wrana, S. Reimers, J. N. Heersche, and J. Sodek, "Localization of bone sialoprotein (bsp) expression to sites of mineralized tissue formation in fetal rat tissues by in situ hybridization," *Matrix*, vol. 11, no. 2, pp. 133–143, 1991.

[39] Identification of ntprocnp: A novel biomarker to predict abnormal growth. [Online]. Available: http://pharmalicensing.com/public/outlicensing/view/10462/identification-of-ntprocnp-a-novel-biomarker-to-predict-abnormal-growth

B

Material and Apparatus

B.1 Materials and Reagents

Following items were purchased from Sigma-Aldrich:

- Chloroauric acid ($HAuCl_4 \cdot 3H_2O$)
- sulfo-a-N-hydroxysuccinimide (sulfo-NHS)
- L-Glutathione reduced (GSH)
- trisodium citrate dihydrate (>99%)
- 1, 8-octanedithiol
- poly(diallyldimethylammonium chloride) solution (PDDA , Mw 100,000 200,000)
- potassium hexacyanoferrate (III) ($K_3Fe(CN)_6$)
- Phosphate buffered saline (PBS)
- Bovine Serum Albumins (BSA)
- b-1-ethyl-3-(3-dimethylamonipropyl) carbodiimide (EDC)
- PBS-Tween20
- Albumin-fluorescein isothiocyanate conjugate (FITC-Albumin)

In this work, sulfo-NHS was used instead of NHS as it is more water soluble while showing similar reactivity and specificity.
Carbon (DRP-110) and Gold SPEs (DRP-C223AT) were purchased

from Dropsens (Spain). TOPAS 8007 (COC), supplied by Microfluidic Chipshop (Jena, Germany), was used as the upper layer in the Osteokit. Double-coated polyester diagnostic tape 9965 (3M Medical Specialties, USA) was used. It consists of a 0.05 mm opaque white polyester film coated on both sides with a 0.02 mm neutral pressure sensitive acrylate adhesive and supplied between two clear, 0.05 mm silicone-coated polyester release liners. According to the manufacturer, the tape is bioassay, die cut compatible and printable.
Oc monoclonal antibody (ab13418, ab133612) and full-length Oc protein (ab152231) were purchased from Abcam Co. (UK). Anti-collagen type I antibody (MAB1340) and Human Collagen type I (CC050) were obtained from Merck Chemicals (Belgium). In both cases, monoclonal antibodies were purchased despite their higher price, as they are more specifically detecting one target epitope and binding with an antigen within a mixture of related molecules extremely efficiently, and less likely to cross-react with other proteins. Moreover, compared with polyclonal antibodies, considering their very high homogeneity, in constant experimental conditions, the results are highly reproducible.
PBS was purchased in powder form was used to prepare a working solution of 10 mM phosphate buffer (NaCl 0.138M, KCl 0.0027M), pH 7.4 at 25 °C. PBS and PBS-Tween20 were prepared by dissolving 1 package in 1000 mL of de-ionized (DI) water. PBS was used to prepare the antibody (10 μg/mL) and antigen solutions.
EDC and sulfo-NHS were dissolved in water at 0.4 M and 0.1 M, divided into small aliquots. EDC aliquots were stored at -20 °C, whereas sulfo-NHS was stored at +4 °C.
The clinical serum samples were obtained from the laboratory of the Endocrinology and Metabolism Research Institute, affiliated with Tehran University of Medical Sciences, and the laboratory of the UZ hospital, affiliated with the Ghent University.
All other reagents were of analytical reagent grade and used without further purification. Distilled water was used throughout the experiments. All the experiments were carried out at room temperature.

B.2 Apparatus and Method

All electrochemical experiments were performed using a computer-controlled Dropsens STAT 400 (Dropsens, Spain) in the nanoprobe and Oc biosensor fabrication, and Autolab PGSTAT101 (Metrohm, The Netherlands) for the remaining parts of this work. They were carried out in a solution container, at room temperature (23 °C), using the three-electrode configuration fabricated in Chapter 5. Electroac-

tive substance 0.1 mM $K_3[Fe(CN)_6]$, containing 0.01 M NaCl, and 0.5 M H_2SO_4 were used as electrolyte solutions.
Cyclic voltammogram (CV) and differential pulse voltammogram (DPV), the main electrochemical testing methods used in the experiments, were performed to confirm surface modification changes and to quantify the target molecule concentration at the sample surface. The CV cycles were performed in 0.1 mM $K_3[Fe(CN)_6]$, containing 0.01 M NACl solution from 0.0 V to +1.2 V, at 0.1 V/s scan rate. CV was also used to determine the formal potential of the electrochemical sensor for DPV. The DPV measurements were performed in 0.1 mM $K_3[Fe(CN)_6]$, containing 0.01 M NaCl, applying following parameters: 0.025 V modulation amplitude, 0.05 s modulation time, 0.005 V step potential and voltage range from 0.5 V to 1.1 V.
For the electrodeposition step, external AgCl reference and Pt. gauze (Alfa Aesar Gmbh & Co, Germany) as auxiliary electrode was used. As for the other steps, gold electrodes-on-chip were utilized.
Electrode surface topography as well as the morphology of the Au deposits were measured using Sirion field emission gun scanning electron microscopy (FEG-SEM) (FEI Nova 600 Nanolab Dual-Beam FIB) and atomic force microscopy (AFM). Most high resolution FEG-SEM pictures with magnifications >2.5kx were achieved in "immersion mode" and with the TLD-SE detector (through the Lens Detector). AFM images were acquired on a XE-70 (Park Systems) in non-contact mode (15*15 μm^2) using Nanosensors tm (PPP-NCHR).
Scanning transmission electron microscopy (STEM) (Jeol Zeiss - EM10C JEM-2200FS FEG (S)TEM)- 80 operated under high tension of 200 kV), was used to collect information on the prepared gold nanoparticles and to test for their ability to bind with the proteins. The samples were prepared using a gold (Au) TEM grid purchased from TED PELLA, INC (Sweden). A high angle annular dark field (HAADF) detector was used to distinguish the smallest and dispersed prepared gold nanoparticles from the porous gold substrate. A bright field detector (BF) was used to visualize lager prepared nanoparticles.
X-ray photoelectron spectroscopy (XPS) was performed with an electron spectrometer (SSI-SSX100) to estimate the composition of the surface and confirm successful immobilization in each step.The transmission electron microscopy (TEM) images were obtained with an EM10C 80 KV (Zeiss, Germany) transmission electron microscope. The zeta potential was measured by dynamic light scattering (DLS) (MALVERN Instrument MAL1001767 UK), at a temperature of 25°C and a pH of 7.4. The UV–Vis measurements were carried out on a UV Visible Spectrophotometer SPECORD 250 (Analytik Jena, Germany). Bruker vertex 70 Fourier transform infrared spectroscopy (FTIR) (Ger-

many) was used for further study of the nanoconjugates. A Varian Cary Eclipse fluorescence spectrophotometer equipped with a Varian Cary-block temperature controller was used to assess the protein adsorption capacity of the material.
In order to quantify the uniformity of the cross-sectional geometry of the microfluidic channels along their length, the width and the height of the microfluidic channels were studied at 5 mm intervals using an optical microscope (Nikon Eclipse LV100) and a WYKO NT3300 non-contact optical profiler, respectively.
In order to check the accuracy of the sensor, the electrochemiluminescence immunoassay (ECLIA, Elecsys 2010 autoanalyzer, Roche Diagnostics GmbH, Germany) was used to measure the serum levels of Oc (intra and inter assay coefficients of variation of 1.2-4.0% and 1.7-6.5%, respectively) and CTX (Intermediate precision CV of < 20 %).

C Dissemination

C.1 Research dissemination

C.1.1 Journal papers

A1 Articles

- P. Khashayar, G. Amoabediny, B. Larijani, J. Vanfleteren, "Bone biosensors: knowing the present and predicting the future," *Journal of Micromechanics and Microengineering*, vol. 26, no. 2, 2016. [Online]. Available: http://dx.doi.org/10.1088/0960-1317/26/2/023002
- P. Khashayar, H. R. Aghaei Meybodi, M. Rezai Hemami, A. Keshtkar, H. P. Dimai, B. Larijani, "Vitamin D status and its relationship with bone mineral density in a healthy Iranian population," *Revista Brasileira de Ortopedia (English Edition)*, 2016. [Online]. Available: http://dx.doi.org/10.1016/j.rboe.2015.09.011
- F. Razi, M. Esmaili, E. Nasli Esfahani, P. Yaghmaei, M. Qorbani, Z. Mohammadi, A. Keshtkar, P. Khashayar, B. Larijani, "Bone structure and turnover in postmenopausal women with type 2 diabetes mellitus,"*Menopause*, vol. 23, no. 3, pp. 280-285, 2015. [Online]. Available: http://dx.doi.org/10.1097/GME.0000000000000524

- F. Amininezhad, H. Aghaei Meybodi, M. Qorbani, M. Dini, Z. Mohammadi, P. Khashayar, A. Keshtkar, B. Larijani, "Evaluation of the validity of the FRAX algorithm for predicting risk of osteoporotic fracture in Iran," *Osteologie*, vol. 24, no. 3, pp. 183-186, 2015. [Online].
- A. Keshtkar, O. Tabatabaie, N. Matin, Z. Mohammadi, M. Ebrahimi, P. Khashayar, M. Asadi,"Clinical performance of seven prescreening tools for osteoporosis in Iranian postmenopausal women," *Rheumatology International*, vol. 35, no. 12, pp. 1995-2004, 2015. [Online]. Available: `http://dx.doi.org/10.1007/s00296-015-3286-1`
- A. Keshtkar, P. Khashayar, Z. Mohammadi, K. Etemad, M. Dini, H. Aghaei Meybodi, M. Ebrahimi, F. Razi, M. Ramezani, H. Nabavi, S. Saghafi, H. Sadigh, S. Derakhshan, F. Bayegi, Z. Jouyandeh, M. Hajian, M. Karimi, B. Larijani, "A Suggested Prototype for Assessing Bone Health," *Archives of Iranian Medicine*, vol.18, no. 7, pp. 411-415, 2015. [Online]. Available: `http://dx.doi.org/0151807/AIM.004`.
- A. Keshtkar, M. Ebrahimi, P. Khashayar, Z. Abdollahi, H. Poraram, F. Salehi, Z. Mohammadi, R. Khosrokhavar, B. Larijani, "Community Interventional Trial (CITFOMIST) of Vitamin D Fortified Versus Non-fortified Milk on Serum Levels of 25(OH) D in the Students of Tehran,"*Archives of Iranian Medicine*, vol. 18, no. 5, pp. 272-276, 2015. [Online]. Available: `http://dx.doi.org/0151805/AIM.004`.
- M. Ebrahimi, P. Khashayar, A. Keshtkar, K. Etemad, M. Dini, Z. Mohammadi, H. Ebrahimi, R. Chaman, B. Larijani, "Prevalence of vitamin D deficiency among Iranian adolescents," *Journal of Pediatric Endocrinology & Metabolism*, vol. 27, no. 7-8, pp. 595-602. [Online]. Available: `http://dx.doi.org/10.1515/jpem-2013-0428`.
- S. A. Alavizadeh, M. R. Mohajeri-Tehrani, A. Rostamian, H. R. Aghaei Meybodi, M. Qorbani, A. Keshtkar, S. S. Panahi, F. Rahdari, P. Khashayar, "Prevalence and associated factors of T-score discordance between different sites in Iranian patients with spinal cord injury," *Spinal Cord*, vol. 52, no. 4, pp. 322-326, 2014. [Online]. Available: `http://dx.doi.org/10.1038/sc.2013.143`.
- H. R. Aghaei Meybodi, P. Khashayar, M. Rezai Homami, B. Larijani, "Prevalence of hypertension in an Iranian population," *Renal Failure*, vol. 36, no. 1, pp. 87-91, 2014. [Online]. Available: `http://dx.doi.org/10.3109/0886022X.2013.832315`.
- P. Khashayar, H. R. Aghaei Meybodi, A. Soltani, E. Taheri, M. R.

Homami, R. Heshmat, H. P. Dimai, B. Larijani, "Association between Vitamin D levels and BMI values in an Iranian Population," *Clinical Laboratory*, vol. 60, no. 3, pp. 383-389, 2014. [Online]. Available: http://dx.doi.org/10.7754/Clin.Lab.2013.121033

- A. Keshtkar, Sh. Djalalinia, P. Khashayar, N. Peykari, Z. Mohammadi, B. Larijani, "Iranian Health Research Networks and Vision of Iran by 2025: A Case of Virtual Health Network in EMRI," *Iranian Journal of Public Health*, vol. 42, no. S1, pp. 78-83, 2013. [Online]. Available: http://ijph.tums.ac.ir/index.php/ijph/article/view/4692/4335
- P. Khashayar, R. Heshmat, M. Qorbani, M. E. Motlagh, T. Aminaee, G. Ardalan, Y. Farrokhi-Khajeh-Pasha, M. Taslimi, B. Larijani, "Metabolic Syndrome and Cardiovascular Risk Factors in a National Sample of Adolescent Population in the Middle East and North Africa: The CASPIAN III Study," *International Journal of Endocrinology*, no. 702095, 2013. [Online]. Available: http://dx.doi.org/10.1155/2013/702095
- H. R. Aghaei Meybodi, N. Khalili, P. Khashayar, R. Heshmat, A. Hossein-nezhad, B. Larijani, "Association between reproductive factors and postmenopausal osteoporosis," *Osteologie*, vol. 20, no. 3, pp. 248-251, 2011. [Online].
- P. Khashayar, H. R. Aghaei Meybodi, M. Rezai Homami, M. R. Amini, M. R. Mohajeri-Tehrani, R. Heshmat, B. Larijani, "The Discriminative Value of Various Biochemical Parameters in Detecting Varying Degrees of Vitamin D Deficiency in the Iranian Population," *Clinical Laboratory*, vol. 57, no. 3-4, pp. 163-170, 2011. [Online]. Available: http://clinical-laboratory.de/article/708

A2 Articles

- P. Khashayar, H. A. Meybodi, G. Amoabediny, B. Larijani, "Biochemical Markers of Bone Turnover and their Role in Osteoporosis Diagnosis: A Narrative Review," *Recent Patents on Endocrine Metabolic & Immune Drug Discovery*, vol. 9, no. 2, pp. 79-89, 2015. [Online]. Available: http://dx.doi.org/10.2174/1872214809666150806105433
- B. MehdiKhani, A. Eslami, M. Qorbani, A. Azarkeivan, Z. Mohammadi, P. Khashayar, A. Keshtkar, "Knowledge, attitude, and preventive practice of major thalassemia patients regarding the importance of calcium and Vitamin D," *Journal of Applied Hema-*

tology, vol. 6, no. 1, pp. 13-18, 2015. [Online]. Available: http://dx.doi.org/10.4103/1658-5127.155173

- Sh. Ghafoori, A. Keshtkar, P. Khashayar, M. Ebrahimi, M. Ramezani, Z. Mohammadi, F. Saeidifard, N. Nemati, M. Khoshbin, Solmaz Azizian, Fatemeh Zare, Sara Shirazi, Bagher Larijani, "The risk of osteoporotic fractures and its associating risk factors according to the FRAX model in the Iranian patients: a follow-up cohort," *Journal of Diabetes & Metabolic Disorders*, vol. 13, no.1, pp. 93, 2014. [Online]. Available: http://dx.doi.org/10.1186/s40200-014-0093-2
- Z. Mohammadi, F. Fayyazbakhsh, M. Ebrahimi, M. M. Amoli, P. Khashayar, M. Dini, R. Nezam Zadeh, A. Keshtkar, H. R. Barikani, "Association between vitamin D receptor gene polymorphisms (Fok1 and Bsm1) and osteoporosis: a systematic review," *Journal of Diabetes & Metabolic Disorders*, vol. 13, no.1, pp. 98, 2014. [Online]. Available: http://dx.doi.org/10.1186/s40200-014-0098
- A. Soltani, B. Larijani, P. Khashayar, M. Rezaei Hemami, S. Fakhari, "The Relationship between Anthropometric Parameters and Bone Mineral Density in an Iranian Referral Population," *Acta Medica Iranica*, vol. 52, no. 7, pp. 505-510, 2014. [Online]. Available: http://search.proquest.com/docview/1552012821?pq-origsite=gscholar
- F. Ardeshir Larijani, S. M. Kalantar Motamedi, A. A. Keshtkar, P. Khashayar, Z. Koleini, F. Rahim, B. Larijani, "The Relation between Serum Vitamin D Levels and Blood Pressure: A Population-Based Study," *Acta Medica Iranica*, vol. 52, no. 4, pp. 290-297, 2014. [Online]. Available: *http://search.proquest.com/docview/1536778834?pq-origsite=gscholar*
- B. Heidari, P. Khashayar, M. Rezai Homami, A. Pajouhi, A. Soltani, B. Larijani, "Dual-energy X-ray absorptiometry diagnostic discordance between Z-scores and T-scores in a young Iranian population," *Medical journal of the Islamic Republic of Iran*, vol. 28, pp. 151. [Online]. Available: http://www.ncbi.nlm.nih.gov/pmc/articles/PMC4322344
- B. Shahnazari, A. Keshtkar, A. Soltani, A. Aghamaleki, A. Mansour, B. Matin, Sh. Saghafi, M. Dini, P. Khashayar, B. Larijani, "Estimating the avoidable burden of certain modifiable risk factors in osteoporotic hip fracture using Generalized Impact Fraction (GIF) model in Iran," *Journal Diabetes Metabolic Disorders*, vol.12, no.1, pp.10, 2013. [Online]. Available: http://dx.doi.org/10.1186/2251-6581-12-10

- H. Aghaei-Meybodi, N. Rashidi, M. Montazeri, A. Keshtkar, P. Khashayar, "The Impact of Alendronate on Bone Mineral Density of Osteoporotic Patients," *Acta Medica Iranica*, vol. 51, no. 12, pp. 855-860, 2013. [Online]. Available: `http://search.proquest.com/docview/1498197260?pq-origsite=gscholar`
- F. Fayyazbakhsh, M. Solati-Hashjin, M. A. Shokrgozar, S. Bonakdar, Y. Ganji, N. Mirjordavi, S. A. Ghavimi, P. Khashayar, "Biological Evaluation of a Novel Tissue Engineering Scaffold of Layered Double Hydroxides (LDHs)," *Key Engineering Materials*, vol. 1463, no. 493, pp. 902, 2011. [Online]. Available: `http://dx.doi.org/10.4028/www.scientific.net/KEM.493-494.902`

C.1.2 Others

- A. A. Keshtkar, M. Ranjbaran, H. Soori, K. Etemad, P. Khashayar, M. Dini, B. Larijani, "Is the relationship between individual-and family-levels socioeconomic status with disease different? Analyzing third stage data of IMOS," *Koomesh*, vol. 17, no. 1, pp. 27-36, 2015. [Online].
- Z. Mohammadi, M. Ebrahimi, A. Keshtkar, H. Aghaei Meybodi, P. Khashayar, Z. Jouyande, F. Bayegi, M. Shojaa, M. Ghodsi, Sh. Djalalinia, "Protocol for Systematic Review: Peak Bone Mass Pattern in Different Parts of the World," *Journal of Clinical Research & Bioethics*, vol. 6, no. 2, pp.1, 2015. [Online]. Available: `http://dx.doi.org/10.4172/2155-9627.1000211`
- Z. Mohammadi, A. Keshtkar, F. Fayyazbakhsh, M. Ebrahimi, M. M. Amoli, M. Ghorbani, P. Khashayar, M. Dini, M. Ebrahimi-Rad, B. Larijani, "Prevalence of osteoporosis and vitamin D receptor gene polymorphisms (FokI) in an Iranian general population based study (Kurdistan)(IMOS)," *Medical Journal of The Islamic Republic of Iran*, vol. 29, pp. 238, 2015. [Online]. Available: `http://www.ncbi.nlm.nih.gov/pmc/articles/PMC4715426/pdf/MJIRI-29-238.pdf`
- H. Moazami Goodarzi, B. Larijani, A. Keshtkar, P. Khashayar, "Prevalence and associated factors of T-score discordance between lumbar spine and femoral neck in postmenopausal women: A 11-year IROSTEOPS study," *Iranian Journal of Diabetes and Metabolism*, vol. 13, no. 2, pp. 182-187, 2014. [Online].
- A. Keshtkar, P. Khashayar, S. Saghaf, S. Hezarkhani, S. Sedighi, N. Shahini, M. Aghaei, M. Mekaniki, "Comparing effect of Osteofos versus Alenate on postmenopausal bone mineral density; a

randomized double blind controlled equivalence trial," *Research in Pharmaceutical Sciences*, vol. 7, no. 5, pp. S1005, 2012. [Online].

Under Review

- P. Khashayar, R. Verplancke, D. Schaubroeck, M. De Keersmaecker, A. Adriaens, M. Hosseini, Gh. Amoabediny, B. Larijani, J. Van Fleteren, "Characterization of gold nanoparticle layer deposited on gold electrode by various techniques for improved sensing abilities."
- P. Khashayar, Gh. Amoabediny, B. Larijani, M. Hosseini, R. Verplancke, S. Van Put, J. Vanfleteren, "Rapid prototyping of microfluidic chips using laser-cut double-sided tape for electrochemical biosensors."

Ready to Submit

[1]

- Fabrication and verification of conjugated AuNP-antibody nanoprobe for electrochemical biosensors.
- A highly sensitive electrochemical biosensor based on gold nanoparticles-modified gold electrode for selective determination of serum levels of osteocalcin.
- A highly sensitive electrochemical biosensor based on gold nanoparticles-modified gold electrodes for selective determination of serum levels of CTX.
- A multiplexed microfluidic proteomic platform for bone marker measurement: A proof-of-concept.

C.1.3 Proceedings of international conference

Published

- P. Khashayar, G. Amoabediny, B. Larijani, J. Vanfleteren, "Bone biosensors: Knowing the present and predicting the future," in *Osteoporosis International (World Congress on Osteoporosis, Osteoarthritis and Musculoskeletal diseases, Abstract book)*, vol. 26, no. S1, P. 698, 2015. [Online]. Available: `http://dx.doi.org/10.1007/s00198-015-3060-y`

[1] These articles could not be submitted before the patent is filed

- A. Keshtkar, P. Khashayar, Z. Mohammadi, M. Ebrahimi, B. Larijani, "Efficiency of fortified vitamin D milk in adolescents: The community interventional trial (CITFOMIST)," in *Osteoporosis International (World Congress on Osteoporosis, Osteoarthritis and Musculoskeletal diseases, Abstract book)*, vol. 25, no. S2, P. S362-S362, 2014. [Online]. Available: `http://dx.doi.org/10.1007/s00198-014-2642-4`
- B. Larijani, M. Dini, K. Etemad, M. Ramezani, H. Nabavi, A. Keshtkar, M. Ebrahimi, Z. Mohammadi, P. Khashayar, "Vitamin D status of Iranian adults: A 10-year nationwide study," in *Osteoporosis International (World Congress on Osteoporosis, Osteoarthritis and Musculoskeletal diseases, Abstract book)*, vol. 25, no. S2, P. S362-S363, 2014. [Online]. Available: `http://dx.doi.org/10.1007/s00198-014-2642-4`
- A. Keshtkar, P. Khashayar, K. Etemad, M. Dini, M. Ebrahimi, Z. Mohammadi, E. Taheri, B. Larijani, "Iranian hip fracture registry (IHFR): A basic framework for improving quality of care in patients with osteoporotic fracture," in *Osteoporosis International (European Congress on Osteoporosis and Osteoarthritis, Abstract book)*, vol. 24, no. S1, P. S60-S61, 2013. [Online]. Available: `http://dx.doi.org/10.1007/s00198-013-2312-y`
- A. Keshtkar, A. Avestai, P. Khashayar, R. Heshmat, A. Arabali, N. Abdollahi, M. Ebrahimi, B. Larijani, "Appropriateness of the BMD orders among insured Iranians," in *Osteoporosis International (IOF Regionals, 1st Middle-East and Africa Osteoporosis Meeting, Abstract book)*, vol. 22, no. S5, P. S692-S693, 2011. [Online]. Available: `http://dx.doi.org/10.1007/s00198-011-1743-6`
- A. Keshtkar, A. Avestai, P. Khashayar, R. Heshmat, A. Arabali, N. Abdollahi, P. Pedram, M. Ebrahimi, B. Larijani, "Prevalence of osteoporosis and its risk factors among an Iranian insured population," in *Osteoporosis International (IOF Regionals, 1st Middle-East and Africa Osteoporosis Meeting, Abstract book)*, vol. 22, no. S5, P. S712-S712, 2011. [Online]. Available: *http://dx.doi.org/10.1007/s00198-011-1743-6*
- B. Larijani, A. Keshtkar, H. R. Aghaei, S. Kalantar-Motamedi, P. Khashayar, B. Larijani, "The association between vitamin D serum levels and blood pressure status: An Iranian study," in *Osteoporosis International (IOF Regionals 2nd Asia-Pacific Osteoporosis and Bone Meeting / ANZBMS Annual Scientific Meeting held with the JSBMR, Abstract book)*, vol. 22, no. S4, P. S586-S586, 2011. [Online]. Available: `http://dx.doi.org/10.1007/s00198-011-1717-8`
- F. Larijani, A. A. Keshtkar, H. R. Meybodi, S. Kalantar-Motamedi,

P. Khashayar, B. Larijani, "The association between vitamin D serum levels and blood pressure status: An Iranian study," in*Osteoporosis International(IOF Regionals 2nd Asia-Pacific Osteoporosis and Bone Meeting / ANZBMS Annual Scientific Meeting held with the JSBMR, Abstract book)*, vol. 22, no. S4, P. S586-S586, 2011. [Online]. Available: http://dx.doi.org/10.1007/s00198-011-1717-8

- R. Heshmat, A. Amani, F. Shojaei, P. Khashayar, H. R. Aghaei Meybodi, E. Alijani, "Bone mineral density in female professional athletes," in *Osteoporosis International (1st Asia-Pacific Osteoporosis Meeting, Abstract book)*, vol. 21, no. S5, P. S683-S684, 2011. [Online]. Available: http://dx.doi.org/10.1007/s00198-010-1433-9
- H. R. Aghaei Meybodi, A. Bagheri, A. Soltani, M. M. Tehrani, P. Khashayar, R. Heshmat, B. Larijani, "Effect of high dose versus conventional vitamin D supplement on serum 25(OH)D levels in women with low bone mass," in *Osteoporosis International (1st Asia-Pacific Osteoporosis Meeting, Abstract book)*, vol. 21, no. S5, P. S744-S744, 2011. [Online]. Available: http://dx.doi.org/10.1007/s00198-010-1433-9
- P. Khashayar, H. R. Aghaei Meybodi, M. Rezaei Homami, R. Heshmat, B. Larijani, "The correlation of biochemical markers and osteoporosis risk in an Iranian population," in *Osteoporosis International (IOF World Congress on Osteoporosis/10th European Congress on Clinical and Economic Aspects of Osteoporosis and Osteoarthritis, Abstract book)*, vol. 21, no. S1, P. 215-215, 2010. [Online]. Available: http://dx.doi.org/10.?1007/?s00198-010-1313-3
- P. Khashayar, H. R. Aghaei Meybodi, M. Rezai Homami, R. Heshmat, B. Larijani, "The Prevalence of Osteoporosis in an Iranian Population," in *Journal of Clinical Densitometry*, vol.13, no. 1, pp. 112, 2010. [Online]. Available: http://dx.doi.org/10.1016/j.jocd.2010.01.022

Accepted

- P. Khashayar, F. Razi, E. Nasli Esfehani, A. Keshtkar, B. Larijani, "Association between metabolic syndrome and bone mineral density: The IMOS study," in *Osteoporosis International (IOF World Congress on Osteoporosis, Osteoarthritis and Musculoskeletal Diseases)*, 2016.
- P. Khashayar, M. Ebrahimi, H. Ebrahimi, M. Raji, M. Dini, K. Etemad, Z. Mohammadi, A. Keshtkar, B. Larijani, "Curing Osteoporosis Care: New Strategies for Quality Improvement," in

Osteoporosis International (IOF World Congress on Osteoporosis, Osteoarthritis and Musculoskeletal Diseases), 2016.

- P. Khashayar, M. Ebrahimi, H. Ebrahimi, M. Raji, M. Dini, K. Etemad, Z. Mohammadi, A. Keshtkar, B. Larijani, "Quality of Osteoporosis Care in an Iranian Population," in *Osteoporosis International (IOF World Congress on Osteoporosis, Osteoarthritis and Musculoskeletal Diseases)*, 2016.
- P. Khashayar, A. Keshtkar, A. Ziaee, B. Larijani, "Awareness of osteoporosis among Iranian female head of household," in *Osteoporosis International (IOF World Congress on Osteoporosis, Osteoarthritis and Musculoskeletal Diseases)*, 2016.

C.1.4 Patent

- Multiplexed microfluidic proteomic platform. [In the Filing Process]